# Replacement of Homogeneous Acids in the Conversion of meta-Phenylenediamine to Resorcinol by Heterogeneous Analogues

*by*

*Bryan Brack BSc. Eng. (Chem.)*



Submitted to the University of Cape Town in fulfillment of the requirements for the degree of

**DOCTOR OF PHILOSOPHY**

Department of Chemical Engineering
University of Cape Town
Rondebosch
Cape Town
South Africa

June 2001

# Replacement of Homogeneous Acids in the Conversion of meta-Phenylenediamine to Resorcinol by Heterogeneous Analogues

**Bryan Brack**

**Department of Chemical Engineering, University of Cape Town**

**June 2001**

## Abstract

The liquid phase synthesis of resorcinol from meta-phenylenediamine in the presence of heterogeneous solid acids instead of the patented mineral acids offers a solution to the extremely corrosive properties of these mineral acids at reaction temperature (200-275°C). The presence of acids is required for the transformation of meta-phenylenediamine with water to resorcinol. The thermodynamic analysis showed that acids are required as reagents to drive the otherwise thermodynamically unfavourable reaction forward. With mineral acids the rate of reaction is proportional to the hydronium-ion concentration. The mineral acid strength and the acid concentration determine the extent of production of side-products.

The synthesis was performed in the presence of aluminosilicates (H-USY, H-Beta, H-ZSM-5 and H-silica-alumina) or zirconium phosphates. Temperature programmed desorption studies were used to determine the number of acid sites and acid site strength. To evaluate the adsorption strength of the relevant compounds, liquid-phase adsorption studies were conducted at low temperatures with the intention of predicting the heat of competitive adsorption at reaction temperature. This method, however, is not viable since the heterogeneous analogues act as 'concentrating vessels' resulting in the determination of the heat of physisorption rather than chemisorption.

High resorcinol yields can be obtained in the presence of the heterogeneous analogues, albeit at higher reaction temperatures. The crystal structure of zeolites H-Beta and H-USY is destroyed while that of H-ZSM-5 is retained. Comparison of the reaction rate constants with the zeolite crystal diameter shows that the true reaction rate constant when using mineral acids ~ Beta ($d_{crystal}$<0.3μm) > ZSM-5 ($d_{crystal}$~0.5μm) > USY ($d_{crystal}$~0.5μm) >> ZSM-5 ($d_{crystal}$=1-5μm). Since the reaction rate constants of Beta are comparable to those of the mineral acids, it might be concluded that all Brønsted acids within H-Beta are utilised equally. For aluminosilicates with small crystallite sizes the $NH_3$ produced per Brønsted acid site is greater than one, thus indicating some catalytic activity.

The swelling property of layered zirconium phosphates enhances the accessibility of meta-phenylenediamine onto its surface acid sites. However, the zirconium phosphates are not as stable as H-ZSM-5 since leaching of phosphate groups into solution occurs at relatively low temperatures (225°C). Zirconium phosphates could be reused several times if the spent solid is kiln calcined at 400°C. Of the zirconium phosphates used during the investigation, the γ-form is preferred.

I hereby declare that this submission is my own work and that, to the best of my knowledge and belief, it contains no material previously published or written by another person nor material which has been accepted for the award of any other degree or diploma of the university or other institute of higher learning, except where due acknowledgement has been made in the text

## Acknowledgements

Thanks are due to my supervisors A./Prof. Eric van Steen and Dr Dave Gammon for all their assistance and guidance without which this thesis would not have been possible. Also many thanks to Prof. Cyril O'Connor for his time and effort in commenting on previously submitted manuscripts. Many thanks to Dr Klaus Möller, A./Prof. Jack Fletcher for their input. I wish to express my appreciation to the Catalysis Research Unit, and also thank the FRD, AECI and other sponsors of the Catalysis Research Unit at UCT.

A special thanks to Michael Claeys and all the fellow students for not only imparting their knowledge but also valued friendship. Special thanks also to the guys of the Fine Chemicals Catalysis sub-unit: Uwe Wilkenhöner, Gillian Moon and Palali Motsoestoe. Thanks to the organisers Natasha Ristic and Heiko Manstein as well as the LINUX people Warwick Duncan, Peter Schwan and Michael Halhead. I like to also thank and acknowledge the contributions received by the numerous other people constituting the chemical engineering department for their friendship and assistance.

I express my appreciation to the administrative help received from Pam and Lorna. My gratitude also goes to the laboratory assistance of Helen, Maria, Shireen and Gary for all their hard work. Thanks also to the technical support received from Peter Dobias, Joachim Macke, Granville de la Cruz, Bill Randall and Craig Ballfour.

I would especially like to thank my parents, Erich and Margrit, and my sister Sandra for their love, encouragement and affection. A deep sense of gratitude goes to my parents for their financial and motivational support throughout my stay here at UCT. All I have achieved is a tribute to them.

A special thank-you also to Melanie Buwalda for her support, love and understanding, and especially for putting up with me through all the times when the task of completing a PhD thesis seemed impossible.

# SYNOPSIS

Resorcinol is an important building block in the pharmaceutical, adhesion and dye industry. A number of different processes for the production of resorcinol are available with each synthesis route having intrinsic advantages and disadvantages that differ from one process to another.

A viable route to resorcinol in South Africa is via meta-dinitrobenzene due to the large-scale production of nitrobenzene from benzene. Since meta-dintrobenzene is formed as a side-product during the production of nitrobenzene and is hydrogenated quite easily, the acid hydrolysis of MPDA to resorcinol will be considered during this investigation. MPDA is converted to resorcinol via the intermediate meta-aminophenol (MAP) in the presence of an acid **HA**:

$$\mathbf{MPDA} + \mathbf{H_3O^+} + \mathbf{A^-} \rightleftharpoons \mathbf{MAP} + \mathbf{NH_4^+A^-} \quad (rxn\ 1)$$

$$\mathbf{MAP} + \mathbf{H_3O^+} + \mathbf{A^-} \rightleftharpoons \mathbf{Resorcinol} + \mathbf{NH_4^+A^-} \quad (rxn\ 2)$$

The industrial synthesis of resorcinol from MPDA can be carried out in an autoclave in the presence of water and mineral acids at temperatures ranging between 200°C to 275°C. The water serves as a reactant as well as a solvent. The mineral acids used are ammonium bisulphate, phosphoric acid or sulphuric acid. It is known that mineral acids such as $H_2SO_4$ are highly corrosive, and polymerisation and condensation reactions do occur, leading to resin formation.

From studies with the mineral acids, i.e. $H_2SO_4$ ($pK_a$ = -2 at 25°C) (98w/w%), $H_3PO_4$ ($pK_a$ = 2.12 at 25°C) (85w/w%), and $(NH_4)H_2PO_4$ p.a. ($pK_a$ = 7.4 at 25°C), it is deduced that the rate of reaction is directly proportional to the hydronium ion concentration, which is primarily dependent on the ionisation constant of the mineral acids. No resorcinol is produced from MPDA without the addition of a mineral acid. Since ammonia is a stronger base than the reactant MPDA, the catalytic conversion of MPDA to resorcinol is unfavourable. This is confirmed by means of a thermodynamic study, which predicts that ammonium-salt formation during the course of the reaction is vital to drive the reaction forward towards acceptable yields of resorcinol.

From reaction studies with mineral acids, it is found that the mineral acid strength as well as the acid concentration inside the autoclave determines the extent of the production of polymeric ethers. Mineral acids having an ionisation constant greater than that of hydronium ions are hygroscopic at high concentrations and lead to the production of ethers, thereby yielding water molecules. Traces of dimers comprising aryl-groups bonded by –NH– links (3,3'-diamino-diphenylamine and 3-hydroxy,3'-amino-diphenylamine) are observed, which are hydrolysed further to MAP or resorcinol.

There is an incentive to replace these corrosive and environmentally hazardous mineral acids with solid acids that would also ease the separation process. In addition, the use of zeolite would be expected to suppress condensation and polymerisation reactions. This would occur if the transition-state of the condensation is too bulky to fit into the pores or if the condensation products cannot diffuse out of the pores of the zeolites and the reverse reaction occurs. Therefore, aluminosilicates H-ZSM-5 (Si/Al = 13), H-ZSM-5 (Si/Al = 22), H-Beta (Si/Al = 14.4), H-USY (Si/Al = 5.6) and amorphous H-silica-alumina (Si/Al = 6.9) with different pore diameters and pore architectures are investigated. Reactions are carried out at 225°C, 275°C and 300°C. The aluminosilicates are characterised before and after the reaction at 300°C by means of $NH_3$ temperature programmed desorption ($NH_3$–TPD), thermogravimetric desorption (DT-TGA), $N_2$–BET, X-Ray Diffraction and SEM. The $NH_3$–TPD study and TGA on water are also used to determine the respective heats of desorption of strongly adsorbed ammonia and water by varying the temperature ramping rate. To evaluate the strengths of interaction of MPDA, MAP and resorcinol with the aluminosilicates, liquid phase adsorption studies are conducted at low temperatures (30°C, 50°C and 70°C) with the intention of predicting the heat of competitive adsorption (solute: either MPDA, MAP or resorcinol; solvent = $H_2O$). This method, however, is not viable since zeolites act as 'concentrating vessels' resulting in the determination of the heat of physisorption rather than chemisorption.

At lower temperatures, all zeolites apart from H-USY (~9mol% resorcinol yield) show a decrease in the mass balance, which is attributed to the strong adsorption of MPDA. At higher temperature, drastic increases in resorcinol yields are observed, although only small increases are observed for H-USY (~25%) and H-ZSM-5 (Si/Al = 13) (~3%). Comparison of X-Ray Diffraction and $N_2$-BET data before and after the reaction show the extent of destruction of the zeolite framework structure as follows: USY ≈ silica-alumina > Beta > ZSM-5; the USY structure collapses totally and ZSM-5 structure is retained. Comparison of the reaction rate constants with the zeolite crystal diameter shows that for all zeolites the dominant part of the reaction occurs on the more external surface acid sites. The true reaction rate constants when using mineral acids ≈ Beta ($d_{crystal}$ < 0.3μm) > ZSM-5 (Si/Al = 22, $d_{crystal}$ = ca. 0.5μm) > USY ($d_{crystal}$ ≈ 0.5μm) >> ZSM-5 (Si/Al = 13, $d_{crystal}$ = 1 - 5μm). Since the true reaction rates of Beta are comparable to those of the mineral acids, all the Brønsted acid sites within H-Beta are utilised equally as with the mineral acids. Not all acid sites on USY and ZSM-5 seem to have the same activity. The reactions with H-Beta and H-ZSM-5 (Si/Al = 22) returned turnover numbers (moles $NH_3$ produced / moles acid sites) greater than 1, which is attributed to the existence of an equilibrium between ammonia adsorbed on the aluminosilicate, in the bulk solution and in the autoclave headspace. With a suitable reactor design (low silica/alumina H-ZSM-5 with small crystal size) and carrying out the reaction at temperatures greater than 300°C, the removal of ammonia from the headspace is possible and likely to improve the overall turnover number.

In addition to the aluminosilicates, the layered compounds α-zirconium phosphate (α-$Zr(HPO_4)_2 \cdot H_2O$) and γ-zirconium phosphate (γ-$Zr(PO_4)(H_2PO_4) \cdot 2H_2O$) are investigated as heterogeneous solid acids for the conversion of MPDA to resorcinol. The layered zirconium phosphate compounds consist of fixed ionogenic phosphate groups on macromolecular planes, which resemble the structure of ortho-phosphoric acid. In contrast to aluminosilicates, the ability of the zirconium layers to swell in the presence of amines (MPDA) allows for easy access of the MPDA molecules to an active site. Some zirconium phosphates samples are kiln treated (400°C) prior to their reaction to test their thermal and chemical stability. Reactions with the zirconium phosphates and their 400°C kiln-treated α- and γ-zirconium phosphates are carried out at 225°C and 275°C. The zirconium phosphates are characterised before and after reaction by means of DT-TGA, $N_2$–BET, X-Ray Diffraction, FT-IR and SEM. Unsuccessful attempts are also made by means of liquid phase adsorption (30°C, 50°C and 70°C) to evaluate the strength of interaction of MPDA, MAP and resorcinol with the Brønsted acids on the zirconium phosphates (solute: either MPDA, MAP or resorcinol; solvent = $H_2O$). The spent zirconium phosphates samples are further characterised by regenerating and reusing them in a second reaction.

At 225°C, slight leaching of phosphate groups into solution is observed with the α-zirconium phosphate samples undergoing a slow transformation to $(NH_4)Zr_2(PO_4)_3$ (ca. 8% after 25hours). The leaching and transformation processes are greater at higher temperatures. The acid sites on γ-zirconium phosphates interact with the MPDA more readily than those on α-zirconium phosphates. The true reaction rate of γ-zirconium phosphate ($d_{layer}$ = 12.20Å) is comparable to the reactions with mineral acids, while those of α-zirconium phosphates ($d_{layer}$ = 7.55Å) are generally slower. The rate constants for α-zirconium phosphates are found to be a function of the interlayer distance, interlayer attraction forces and Brønsted acid strength. The turnover number calculated for the hydrolysis of MPDA to resorcinol in the presence of zirconium phosphates is ~0.6 mole $NH_3$ produced per mole acid sites, showing that this reaction can hardly be classified as catalytic. However, γ-zirconium phosphate could be reused several times (3$^{rd}$ cycle at 275°C leads to a resorcinol yield ~ 70% after 25hours) if the spent solid is kiln calcination at 400°C. Notwithstanding the zirconium phosphates' limited capacity as regenerable reagents, this is a positive factor in favouring their use as an alternative to the traditional homogeneous routes.

# Table of Contents

Page

Declaration ..... i
Acknowledgements ..... iii
Synopsis ..... iv
Table of Contents ..... vii
List of Figures ..... xiii
List of Tables ..... xx
Publications to date from this thesis ..... xxiii
Nomenclature ..... xxiv
Glossary ..... xxix

**1. INTRODUCTION** ..... 1

**2. LITERATURE REVIEW AND PROPOSALS** ..... 3

**2.1 RESORCINOL PRODUCTION** ..... 3
2.1.1 Processes for Synthesis of Resorcinol ..... 3
2.1.1.1 Comparison of industrial processes ..... 5
2.1.1.2 Benzene disulfonation ..... 6
2.1.1.3 Hydroperoxidation of diisopropylbenzene ..... 7
2.1.1.4 Resorcinol from δ-ketocarboxylic acid esters ..... 8
2.1.1.5 Oxidative dehydrogenation of cyclohexanone ..... 10
2.1.1.6 Hydrolysis of hydrogenated m-dinitrobenzene ..... 11
2.1.1.7 General overview of processes ..... 13

2.1.2 Conversion of MPDA to Resorcinol ..... 15
2.1.2.1 Thermodynamics regarding transformation of MPDA to resorcinol ..... 15
2.1.3 Overall Reaction Pattern for Transformation of MPDA ..... 23
2.1.4 Homogeneous Reagents ..... 25
2.1.5 Problems / Proposals ..... 27

**2.2 ZEOLITES** ..... 30
2.2.1 Zeolite Pore Structure ..... 31
2.2.1.1 Structure of ZSM-5 ..... 32
2.2.1.2 Structure of a faujasite ..... 33
2.2.1.3 Structure of zeolite Beta ..... 34
2.2.2 Acidity of Zeolites ..... 37
2.2.3 Interaction of Water with Zeolites ..... 40
2.2.4 Dealumination of Zeolites ..... 42
2.2.5 Adsorption of Ammonia ..... 44
2.2.6 Adsorption of Organic Compounds ..... 45
2.3.7 Use of Zeolites for MPDA to Resorcinol ..... 46

**2.3 ZIRCONIUM PHOSPHATES** ..... 49
2.3.1 Zirconium Phosphate Structures ..... 49
2.3.1.1 Structure of $\alpha$-$Zr(HPO_4)_2 \cdot H_2O$ ..... 52
2.3.1.2 Structure of $\gamma$-$Zr(PO_4)(H_2PO_4) \cdot 2H_2O$ ..... 54
2.3.2 Adsorption / Intercalation Processes ..... 57
2.3.2.1 Intercalation into $\alpha$-$Zr(HPO_4)_2 \cdot H_2O$ ..... 61
2.3.2.2 Intercalation into $\gamma$-$Zr(PO_4)(H_2PO_4) \cdot 2H_2O$ ..... 65
2.3.3 Chemical and Thermal Properties ..... 66
2.3.3.1 Chemical and thermal properties of $\alpha$-$Zr(HPO_4)_2 \cdot H_2O$ ..... 67
2.3.3.2 Chemical and thermal properties of $\gamma$-$Zr(PO_4)(H_2PO_4) \cdot 2H_2O$ ..... 69

**3. EXPERIMENTAL** ..... 71

**3.1 REAGENTS** ..... 71

**3.2 SOLID CHARACTERISATION** ..... 72

3.2.1 Elemental Analysis ..... 72

3.2.2 Solid Structure and Morphology ..... 73

3.2.2.1 X-ray diffraction (XRD) ..... 73

3.2.2.2 Scanning electron microscopy (SEM) ..... 73

3.2.3 Thermal Stability ..... 74

3.2.4 Acidity of Solids ..... 74

3.2.4.1 Ammonia temperature programmed desorption (TPD) Method ..... 74

3.2.4.2 Temperature programmed desorption (TPD) of 4-methyl-quinoline ..... 77

3.2.4.3 Adsorption strength of water on aluminosilicates ..... 79

3.2.4.4 FT-IR acidity determination ..... 80

3.2.4.5 Adsorption study ..... 80

3.2.5 Surface Area and Pore Volume of Solids ..... 82

**3.3 REACTOR CONFIGURATION AND EXPERIMENTAL PROCEDURE** ..... 83

3.3.1 Reaction Studies ..... 83

3.3.1.1 Homogeneous reactions ..... 85

3.3.1.2 Heterogeneous reactions ..... 85

2.3.1.3 Data evaluation ..... 87

3.3.2 Liquid Sample Analysis ..... 89

3.3.2.1 HPLC sample preparation ..... 89

3.3.2.2 HPLC analysis ..... 89

**3.4 ERROR ANALYSIS** ..... 84

**4. RESULTS AND DISCUSSION** ..... 91

**4.1 REACTOR RAMPING / HEATING PROFILES** ..... 91

**4.2 REACTIONS IN ABSENCE OF ACIDS** ..... 92

**4.3 REACTIONS USING MINERAL ACIDS** ..... 93

4.3.1 Reactions with Sulphuric Acid ..... 93

4.3.2 Reactions with Phosphoric Acid ..... 97

4.3.3 Reactions with Ammonium-Dihydrogen Phosphate ..... 99

4.3.4 Observations Regarding use of Mineral Acids ..... 101

**4.4 REACTIONS WITH ALUMINOSILICATES** ..... 103

4.4.1 Characterisation of Uncalcined Aluminosilicates ..... 103

4.4.2 Characterisation of Calcined Aluminosilicates ..... 104

4.4.2.1 Structure and morphology ..... 104

4.4.2.2 Adsorption strength of water on rehydrated aluminosilicates ..... 108

4.4.2.3 Strength of adsorption of $NH_3$ on aluminosilicates ..... 110

4.4.2.4 Quantification of external acid sites of ZSM-5 samples . 113

4.4.2.5 Pore volume analysis ..... 115

4.4.2.6 Adsorption studies of solutes on zeolites ..... 117

4.4.3 Heterogeneous Reactions using Aluminosilicates ..... 133

4.4.3.1 Reactions with H-USY ..... 133

4.4.3.2 Reactions with H-Beta ..... 139

4.4.3.3 Reactions with H-ZSM-5 (Si/Al = 13) ..... 146

4.4.3.4 Reactions with H-ZSM-5 (Si/Al = 22) ..... 149

4.4.3.5 Reactions with silica-alumina ..... 152

4.4.3.6 Reactions with γ-alumina ..... 153

4.4.4 Characterisation of spent Aluminosilicates ..... 154

4.4.4.1 Structure and morphology ..... 154

4.4.4.2 Pore volume analysis ..... 157

**4.5 REACTIONS WITH ZIRCONIUM PHOSPHATES** ..... 162

4.5.1 Characterisation of Zirconium Phosphates ..... 162

4.5.1.1 Thermogravimetric differential analysis ..... 163

4.5.1.2 Structure and morphology ..... 167

4.5.1.3 Adsorption of solutes on zirconium phosphates ..... 173

4.5.2 Heterogeneous Reactions using Zirconium Phosphates ..... 181

4.5.2.1 Reactions with previously uncalcined zirconium phosphates ..... 182

4.5.2.2 Reactions with regenerated zirconium phosphates ..... 189

4.5.3 Characterisation of Zirconium Phosphates after Reaction ..... 191

4.5.3.1 Structure and morphology ..... 191

**4.6 COMPARISON OF MINERAL ACID AND SOLID REAGENTS / CATALYSTS** ..... 199

4.6.1 Reaction Mechanism and Model Development ..... 199

4.6.1.1 Proposed reaction mechanism for homogeneous acids ..... 199

4.6.1.2 Proposed mechanism for heterogeneous acids ..... 200

4.6.1.3 Development of reaction model ..... 201

4.6.1.4 Inclusion of reactor ramping / heating profiles into the rate equation ..... 203

4.6.2 Modelling of Homogeneous Reactions ..... 204

4.6.3 Homogeneous Acids versus Aluminosilicates ..... 210

4.6.4 Aqueous Acids versus Zirconium Phosphates ..... 218

**4.7 OUTLOOK FOR REPLACEMENT OF HOMOGENEOUS ACIDS WITH HETEROGENEOUS ANALOGUES** ..... 222

4.7.1 Reactions with Homogeneous Acids ..... 222

4.7.2 Reactions with Aluminosilicates ..... 222

4.7.3 Reactions with Zirconium Phosphates ..... 224

**5. CONCLUSIONS AND RECOMMENDATION** ..... 225

**REFERENCES** ..... 231

**APPENDICES**

**Appendix-A: Adsorption from Solution** ..... 249

**Appendix-B: Chemical and Physical Data of Reaction Compounds** ..... 264

**Appendix-C: Derivation of Response Factors** ..... 272

**Appendix-D: Worked Example for evaluating Adsorbed Concentration** ..... 275

**Appendix-E: Determination of Response Factors for 3,3'-Diamino-Diphenylamine and 3-Hydroxy-3'-Amino-Diphenylamine** ..277

**Appendix-F: Correction of observed Sample Concentration** ..... 281

**Appendix-G: Reaction Data using Mineral Acids** ..... 286

**Appendix-H: Adsorption Data of Solutes onto Zeolites** ..... 289

**Appendix- I: Reaction Data using Aluminosilicates** ..... 293

**Appendix-J: Adsorption Data of Solutes onto Zirconium Phosphates** ..298

**Appendix-K: Reaction Data using Zirconium Phosphates** ..... 302

## LIST OF FIGURES

Page

Figure 2.1 Classification of directing effects for substituents [redrawn from McMurry, 1992] ..... 4

Figure 2.2 Process for the production of resorcinol via benzene disulfonation ..... 7

Figure 2.3 Process for the production of resorcinol via diisopropyl-benzene ..... 8

Figure 2.4 Process for the production of resorcinol from acetone and acrylic acid ..... 10

Figure 2.5 Process for the production of resorcinol from benzene via the oxidative dehydrogenation of cyclohexanone ..... 11

Figure 2.6 Process for the production of resorcinol via benzene nitration ..... 13

Figure 2.7 Equilibrium conversion of MPDA (A) and molar yields of resorcinol (B) at different temperatures and initial water to MPDA mole ratios (2100:1; 100:1; 20:1) for the gas phase catalytic conversion of MPDA to resorcinol (Reaction 2.19) ..... 18

Figure 2.8 Equilibrium conversion of MPDA (A) and molar yield of resorcinol (B) at different temperatures and pressures (0.5atm, 1.0atm, 2.0atm) for the conversion of MPDA to resorcinol in the gas phase with the transformation of solid phosphoric acid to ammonium-dihydrogen phosphate (Reaction 2.20). Molar ratio of water to MPDA ≥ 20 ..... 19

Figure 2.9 Equilibrium conversion of MPDA (A) and molar yield of resorcinol (B) for the catalytic conversion of MDPA in aqueous phase (Reaction 2.24) ..... 23

Figure 2.10 Overall simplified reaction mechanism for hydrolysis of MPDA to produce resorcinol [developed at AECI Ltd. (South Africa)] ..... 24

Figure 2.11 Illustration of ZSM-5 zeolite pore dimensions of the straight channel system (A) and the sinusoidal channel system (B) [Meier *et al.*, 1996]. Illustration (C) depicts the intersecting straight and sinusoidal channel system of ZSM-5 zeolite [ Meier *et al.*, 1978] ..... 33

Figure 2.12 Pore dimensions (A) giving access to a supercage of the faujasite structure (B) that is built up by sodalite cages (C) [Meier *et al.*, 1996] ..... 34

Figure 2.13 Front (A) and side view (B) of the centrosymmetrical, tertiary structural building unit of zeolite Beta. A second, perpendicular 6-ring is added to create an object with left-handed (C) and right-handed (D) symmetry. (Al and Si atoms, solid circles; O atoms, open circles) [Treacy and Newsam, 1988] ..... 35

Figure 2.14 Zeolite Beta structures A, B and C with the plane [100] illustrated on the left and the [010] projection shown on the right ..... 36

Figure 2.15 Formation of Brønsted acid site centres via the thermal treatment of the ammonium exchanged aluminosilicates ..... 37

Figure 2.16 Illustration of different types of Brønsted acid sites found within a zeolite [redrawn from Sauer, 1989] ..... 39

Figure 2.17 Illustration of the adsorption of water onto a bridged hydroxyl group (Structure I) by either hydrogen bonding of the water molecule (Structure II) or the formation of a hydronium ion that screens the framework aluminium species (Structure III) [Marchese *et al.*, 1993] ..... 41

Figure 2.18 Schematic representation for the dealumination of a protonated zeolite [Beyerlein *et al.*, 1997] ..... 43

Figure 2.19 Possible adsorption of aniline (A) and phenol (B) onto a zeolite Brønsted acid site [Venuto, 1994] ..... 46

Figure 2.20 Schematic illustration of some definitions and important characteristics of layered zirconium phosphates [redrawn from Alberti and Costantino, 1996] ..... 50

Figure 2.21 Idealised crystal structure of α-zirconium phosphate with solid lines illustrating one of the cavities created by arrangement of the layers; protons and water molecules are omitted [Clearfield and Costantino, 1996] ..... 52

Figure 2.22 Schematic projection perpendicular to the crystal axis c, showing negatively charged atoms of two facing sides of adjacent layers forming zeolitic cavities, with each cavity accommodating one water molecule. Shaded and open circles respectively refer to oxygen atoms lying above and below the intermediate plane [redrawn from Alberti and Costantino, 1974 and 1984] ..... 53

Figure 2.23 (a) Representation of layered γ-$Zr(PO_4)(H_2PO_4)\cdot 2H_2O$ viewed down the *b*-axis with water molecules being omitted [Clearfiled and Costantino, 1996]; (b) Polyhedral presentation of the γ-zirconium phosphate structure down

the *a*-axis, illustrating the hydrogen bonds between the water molecules and the hydroxyl groups (dashed lines) [Poojary *et al.*, 1995] ..... 56

Figure 2.24 Simplistic schematic illustration of intercalation of neutral molecules into the interlayer region of a lamellar solid with ideally rigid layers [redrawn from Alberti and Costantino, 1996] ..... 59

Figure 2.25 Simplistic schematic illustration of 'moving boundary' concept during intercalation into the interlayer region of a lamellar solid with ideally flexible layers [redrawn from Alberti and Costantino, 1996] ..... 60

Figure 2.26 Schematic depiction of n-alkyl-monoamine, e.g., butylamine, double layers being formed within $\alpha$-$Zr(HPO_4)_2 \cdot H_2O$ at maximum amine loading [Clearfield and Tindwa, 1977] ..... 62

Figure 2.27 Common orientations of n-alkyl-monoamines in the interlayer region of $\alpha$-$ZrP(HPO_4)_2 \cdot H_2O$: (a) alkyl chain axis parallel to the layer plane; (b) monolayer of extended molecules; (c) bilayer of extended molecules [Clearfield Costantino, 1996] ..... 63

Figure 3.1 Simplified schematic of the apparatus used for ammonia and 4-methyl-quinoline temperature programmed desorption studies ..... 78

Figure 3.2 Schematic of high-pressure batch reactor ..... 84

Figure 4.1 225°C, 250°C, 275°C and 300°C heating profiles of the Parr autoclave charged with 350ml water and 10g solid acid ..... 91

Figure 4.2 Concentration versus time (init. MPDA conc. = 26.4mmol/L) at (A) 225°C (init. $H_2SO_4$:MPDA mole ratio = 3.39); (B) 225°C (init. $H_2SO_4$:MPDA = 6.77); and (C) 275°C (init. $H_2SO_4$:MPDA = 3.38) ..... 94

Figure 4.3 Yield versus time (init. MPDA conc. = 26.4mmol/L) profiles for 3,3'-diamino-diphenylamine (x) and 3-hydroxy,3'-amino-diphenylamine (●) for reactions at (A) 225°C (init. $H_2SO_4$:MPDA molar ratio = 3.39); (B) 225°C (init. $H_2SO_4$:MPDA = 6.77); and (C) 275°C (init. $H_2SO_4$:MPDA = 3.38) ..... 96

Figure 4.4 Concentration versus time (init. MPDA conc. = 26.4mmol/L) with an initial $H_3PO_4$ to MPDA mole ratio of 6.77 and reaction temperature set at (A) 225°C and (B) 275°C respectively ..... 97

Figure 4.5 Yield versus time plots (init. MPDA conc. = 26.4mmol/L) for 3,3'-diamino-diphenylamine (x) and 3-hydroxy,3'-amino-diphenylamine (●) for reactions with an initial $H_3PO_4$ to MPDA molar ratio of 6.77 and temperatures: (A) 225°C and (B) 275°C ..... 98

Figure 4.6 Concentration-time plots (initial MPDA conc. = 26.4mmol/L) for reaction temperatures (A) 225°C (init. $(NH_4)H_2PO_4$:MPDA mole ratio = 6.76) and (B) 275°C (init. $(NH_4)H_2PO_4$:MPDA = 6.63); (◆), (■) and (Δ) respectively denote the species MPDA, MAP and resorcinol ..... 99

Figure 4.7 Yield-time plots (init. MPDA conc. = 26.4mmol/L) for 3,3'-diamino-diphenylamine (x) and 3-hydroxy,3'-amino-diphenylamine (●) for reactions at (A) 225°C (init. $H_2SO_4$:MPDA molar ratio = 3.39); (B) 225°C (init. $H_2SO_4$:MPDA = 6.77); and (C) 275°C (init. $H_2SO_4$:MPDA = 3.38)..... 101

Figure 4.8 XRD patterns of USY, Beta, ZSM-5 (Si/Al = 13) and ZSM-5 (Si/Al = 22) using Cu-Kα radiation and step size = 0.1°..... 105

Figure 4.9 Electron micrographs of USY..... 106

Figure 4.10 Electron micrographs of Beta..... 106

Figure 4.11 Electron micrographs of ZSM-5 (Si/Al = 13)..... 107

Figure 4.12 Electron micrographs of ZSM-5 (Si/Al = 22)..... 107

Figure 4.13 TGA and DTA curves of relevant aluminosilicates with ramping rate set at 10°C/min ($N_2$-flowrate equals 30ml(NTP)/min) ..... 108

Figure 4.14 $NH_3$-TPD spectra of silica-alumina, ZSM-5 (Si/Al = 13), Beta and USY (ca. 0.25g (hydrated), 63ml(NTP)/min helium, 10°C/min) ..... 111

Figure 4.15 4-Methyl-quinoline TPD spectra of ZSM-5 (Si/Al = 22) (top curves) and ZSM-5 (Si/Al = 13) (bottom curves), (1.0g, 100ml(NTP)/min He, 10°C/min, *m/e* = 78). The experiment is repeated to check its reproducibility; compare dashed boxes (A) and (B)..... 114

Figure 4.16 Pore size distribution of silica-alumina (×), H-USY (□), H-Beta (◆), H-ZSM-5(Si/Al=13) (Δ) and ZSM-5(Si/Al=22) (•)..... 117

Figure 4.17 Adsorption-equilibrium data for aqueous MPDA on USY, Beta and ZSM-5 (Si/Al = 13) at 30°C (◆), 50°C (□), 70° (Δ) and 90°C (×). ..... 118

Figure 4.18 Adsorption-equilibrium data with the focus primarily on the initial slopes of the adsorption isotherms of aqueous MPDA on (A) H-USY, (B) H-Beta and (C) H-ZSM-5 (Si/Al = 13) at 30°C (♦), 50°C (■), 70° (Δ) and 90°C (×) ..... 122

Figure 4.19 Adsorption-equilibrium data for aqueous MAP on USY, Beta and ZSM-5 (Si/Al = 13) at 30°C (♦) and 70° (Δ) ..... 125

Figure 4.20 Adsorption-equilibrium data with the focus primarily on the initial slopes of the adsorption isotherms of aqueous MAP on (A) H-USY, (B) H-Beta and (C) H-ZSM-5 (Si/Al = 13) at 30°C (♦) and 70° (Δ) ..... 128

Figure 4.21 Adsorption-equilibrium data for aqueous resorcinol on USY (■), Beta (+) and ZSM-5 (Si/Al = 13) (O) at 70° ..... 130

Figure 4.22 Adsorption-equilibrium data for aqueous ammonia on USY (■), Beta (+) and ZSM-5 (Si/Al = 13) (O) at 70° ..... 131

Figure 4.23 Concentration profiles of MPDA (◆), MAP (■) and resorcinol (Δ) (given as mole percent of organic compounds relative to the initial moles of MPDA) versus reaction time over zeolite USY at temperatures (A) 225°C, (B) 275°C and (C) 300°C ..... 135

Figure 4.24 Yield profiles of 3,3'-diamino-diphenylamine (x) and 3-hydroxy,3'-amino-diphenylamine (●) versus reaction time over zeolite H-USY at temperatures (A) 225°C, (B) 275°C and (C) 300°C. ..... 138

Figure 4.25 Concentration profiles of MPDA (◆), MAP (■) and resorcinol (Δ) (given as mole percent of organic compounds relative to the initial moles of MPDA) versus reaction time over zeolite H-Beta at temperatures (A) 225°C, (B) 275°C and (C) 300°C ..... 140

Figure 4.26 Yield profiles of 3,3'-diamino-diphenylamine (x) and 3-hydroxy,3'-amino-diphenylamine (●) versus reaction time over zeolite H-Beta at temperatures (A) 225°C, (B) 275°C and (C) 300°C ..... 144

Figure 4.27 Concentration profiles of MPDA (◆), MAP (■) and resorcinol (Δ) versus reaction time over ZSM-5 (Si/Al = 13) at (A) 225°C, (B) 275°C and (C) 300°C ..... 147

Figure 4.28 Concentration profiles of MPDA (◆), MAP (■) and resorcinol (Δ) versus reaction time over H-ZSM-5 (Si/Al = 22) at 300°C ..... 150

Figure 4.29 Concentration-time profiles of MPDA (◆), MAP (■) and resorcinol (Δ) versus reaction time over H-exchanged

silica-alumina at 300°C ..... 152

Figure 4.30 XRD patterns of spent and recalcined USY, Beta, ZSM-5 (Si/Al = 13) and ZSM-5 (Si/Al = 22) applying Cu-Kα radiation with step size equal to 0.1° ..... 155

Figure 4.31 Electron micrographs of USY (left) and Beta (right) after reactions at 300°C ..... 156

Figure 4.32 Electron micrographs of ZSM-5 (Si/Al = 13) (left) and ZSM-5 (Si/Al = 22) (right) after reaction at 300°C ..... 157

Figure 4.33 Pore size distribution of spent USY (□), Beta (♦), ZSM-5 (Si/Al=13) (Δ), silica-alumina (×) and ZSM-5 (Si/Al=22) (•)..... 159

Figure 4.34 TGA and DTA curves of relevant zirconium phosphates with ramping rate set at 1°C/min ($N_2$-flowrate = 30ml(NTP)/min) ..... 163

Figure 4.35 XRD-spectra of α-ZrP400, α-ZrP, γ-ZrP400 and γ-ZrP using Cu-Kα radiation and step size = 0.1° ..... 168

Figure 4.36 FT-IR spectra of the original α-zirconium phosphate recorded at ambient temperature, 180°C and 400°C ..... 169

Figure 4.37 FT-IR spectra of the original γ-zirconium phosphate recorded at ambient temperature, 180°C and 400°C ..... 170

Figure 4.38 Scanning electron micrographs of α-ZrP (left) and α-ZrP400 (right)..... 172

Figure 4.39 Scanning electron micrographs of γ-ZrP (left) and γ-ZrP400 (right)..... 173

Figure 4.40 Adsorption-equilibrium data for aqueous MPDA on α-ZrP (♦), α-ZrP400 (Δ), γ-ZrP (■) and γ-ZrP400 (x) at 70°C..... 175

Figure 4.41 Correlation of the measured solution pH versus the MPDA concentration (T = 70°C) after removal of adsorbents α-ZrP (♦), α-ZrP400 (Δ), γ-ZrP (■) and γ-ZrP400 (x) from the bulk solution..... 177

Figure 4.42 Adsorption-equilibrium data for aqueous MAP on α-ZrP (♦), α-ZrP400 (Δ), γ-ZrP (■) and γ-ZrP400 (x) at 70°C..... 179

Figure 4.43 Adsorption-equilibrium data for aqueous resorcinol on α-ZrP (♦), α-ZrP400 (Δ), γ-ZrP (■) and γ-ZrP400 (x) at 70°C..... 181

Figure 4.44 Concentration profiles of MPDA (♦), MAP (■) and resorcinol (Δ) versus reaction time with (A) α-ZrP, (B) α-ZrP400, (C) γ-ZrP and (D) γ-ZrP400; (- - -): mole balance of the organic compounds found in solution. (Reaction temperature = 225°C) ..... 183

Figure 4.45 Yield profiles of 3,3'-diamino-diphenylamine (x) and 3-hydroxy-3'-amino-diphenylamine (●) versus reaction time with (A) α-ZrP, (B) α-ZrP400, (C) γ-ZrP and (D) γ-ZrP400 (Reaction temp. = 225°C) ..... 187

Figure 4.46 pH of solution (without solid) as a function of reaction time for α-ZrP (◆), α-ZrP400 (Δ), γ-ZrP (■) and γ-ZrP400 (x). The reaction temperature is 225°C ..... 188

Figure 4.47 Concentration profiles of MPDA (◆), MAP (■) and resorcinol (Δ) versus reaction time with (A) γ-ZrP(batch no. E0906) and (B) γ-ZrP(batch no. G05-7); (- - -): mole balance of the organic compounds found in solution. (Reaction temperature = 225°C) ..... 189

Figure 4.48 XRD-spectra of (A) α-ZrP, (B) α-ZrP400, (C) γ-ZrP and (D) γ-ZrP400 before the first reaction, after the first reaction at 225°C and after the second reaction at 225°C. Symbol '1' illustrates the appearance of a new phase $(NH_4)Zr_2(PO_4)_3$ or $(H_3O)Zr_2(PO_4)_3$ ..... 192

Figure 4.49 XRD-spectra of (A) α-ZrP, (B) α-ZrP400, (C) γ-ZrP and (D) γ-ZrP400 after the first reaction at 275°C and after the second reaction at 275°C, clearly illustrating the formation of the new phase $(NH_4)Zr_2(PO_4)_3$ or $(H_3O)Zr_2(PO_4)_3$ ..... 193

Figure 4.50 FT-IR spectra of (A) α-ZrP, (B) α-ZrP400, (C) γ-ZrP and γ-ZrP400 before the first reaction and after the second reaction at 275°C ..... 196

Figure 4.51 Electron micrographs of spent α-ZrP (left) and α-ZrP400 (right) after second reaction at 275°C ..... 198

Figure 4.52 Electron micrographs of spent γ-ZrP (left) and γ-ZrP400 (right) after second reaction at 275°C ..... 198

Figure 4.53 Proposed mechanism for the formation of MAP from MPDA (A) and for the formation of resorcinol from MAP (B) in the presence of mineral acids ..... 200

Figure 4.54 Proposed mechanism for the conversion of MPDA to MAP over a heterogeneous acid reagent / catalyst. The electron donating effect of the second amine group on the intermediate aromatic nucleus has been ignored ..... 201

# LIST OF TABLES


Page

Table 2.1 Manufacturing processes for resorcinol ..... 5

Table 2.2 Summary of advantages and disadvantages of available process routes towards resorcinol ..... 14

Table 2.3 Calculated equilibrium constants ($K_a$) and heat of reactions ($\Delta h_{rxn}$) at 25°C for Reactions 2.19 and 2.20 in gaseous phase ..... 16

Table 2.4 Calculated equilibrium constants ($K_a$) and heat of reactions ($\Delta h_{rxn}$) at 25°C for Reactions 2.24 and 2.25 in liquid phase ..... 21

Table 2.5 Acidity constants for species in aqueous solution at 25°C [Shriver *et al.*, 1994] ..... 27

Table 2.6 Channel systems of some commonly known zeolites [Venuto, 1994] ..... 32

Table 3.1 Error analysis ..... 90

Table 3.2 Error analysis of reaction work ..... 90

Table 4.1 Observed weight loss at 450°C of relevant aluminosilicates ..... 104

Table 4.2 Heat of desorption of water on the aluminosilicates by the method of Cventanovic and Amenomiya ..... 109

Table 4.3 Heat of desorption of $NH_3$ on the aluminosilicates by the method of Cventanovic and Amenomiya ..... 112

Table 4.4 Surface area and pore volume data for silica-alumina, H-USY, H-Beta, H-ZSM-5 (Si/Al = 13), H-ZSM-5 (Si/Al = 22) ..... 116

Table 4.5 Comparison of MPDA adsorption capacity observed during liquid phase adsorption with the number of acid sites and BET pore volumes ..... 119

Table 4.6 Comparison of the adsorption capacity during liquid phase adsorption of MAP and MPDA on relevant zeolites ..... 126

Table 4.7 Comparison of the adsorption capacity during liquid phase adsorption of MAP and MPDA on relevant zeolites ..... 132

Table 4.8 XRD determined change in crystallinity after reaction at 300°C relative to that before reaction ..... 156

Table 4.9 Surface area and pore volume data for spent silica-alumina, USY, Beta, ZSM-5 (Si/Al = 13) and ZSM-5 (Si/Al = 22) ..... 158

Table 4.10 Comparison of $S_{BET}$ surface area, and selective pore volume data of spent silica-alumina, USY, Beta, ZSM-5 (Si/Al = 13) and ZSM-5 (Si/Al = 22) ..... 160

Table 4.11 Observed weight loss at 180°C and 400°C of α- and γ-zirconium phosphates ..... 165

Table 4.12 *d*-Spacing and relative intensities of the X-ray powder patterns of α-ZrP and γ-ZrP as well as the 400°C calcined equivalents α-ZrP400 and γ-ZrP400 ..... 167

Table 4.13 Comparison of resorcinol yields (reaction temperature = 225°C) and solution pH's measured after 25h reaction time during the first set of reactions with those measured during the second set of reactions where the regenerated zirconium phosphate is used ..... 190

Table 4.14 Determination of the time period to be subtracted from the observed reaction time to account for the ramping period ..... 204

Table 4.15 Water autoprotolysis constants and first and second dissociation constants of phosphoric and sulphuric acid at relevant temperatures ..... 205

Table 4.16 Prediction of the hydronium ion concentration [*AS*] at different temperatures and ammonia concentrations relevant to the modelling of the homogeneous reactions ..... 206

Table 4.17 Rough evaluation of rate constants for the conversion of MPDA to resorcinol in the presence of mineral acids $H_2SO_4$, $H_3PO_4$ and $(NH_4)H_2PO_4$ ..... 207

Table 4.18 Comparison of activation energies of $H_2SO_4$, $H_3PO_4$ and $(NH_4)H_2PO_4$ ..... 209

Table 4.19 Evaluation of rate constants for the conversion of MPDA to resorcinol in the presence of aluminosilicates H-USY, H-Beta, H-ZSM-5 (Si/Al = 13), H-ZSM-5 (Si/Al = 22) and silica-alumina ..... 213

Table 4.20 Comparison of runs in the presence of zeolites at 300°C with their respective crystallite sizes and external acid concentrations ..... 216

Table 4.21 Comparison of true rate constants $k_1$ and $k_2$ in the presence of $H_3PO_4$ with reactions conducted in the presence of aluminosilicates ..... 217

Table 4.22 Rough evaluation of rate constants for the conversion of MPDA to resorcinol in the presence of zirconium phosphates α-ZrP, α-ZrP400, γ-ZrP and γ-ZrP400 ..... 218

Table 4.23 Comparison of true rate constants $k_1$ and $k_2$ in the presence of $H_3PO_4$ with reactions conducted in the presence of zirconium phosphates ..... 220

Table 4.24 Cost of selected aluminosilicates ..... 223

# PUBLICATIONS TO DATE FROM THIS THESIS

*Journal Publications:*

B. Brack, D.W. Gammon and E. van Steen, "Synthesis of resorcinol from meta-phenylenediamine in the presence of zeolites", *Journal of Molecular Catalysis A: Chemical*, 154 (1999) 73-83.

B. Brack, D.W. Gammon and E. van Steen, "Synthesis of resorcinol from meta-phenylenediamine in the presence of zirconium phosphates", *Microporous and Mesoporous Materials*, 41 (2000) 149-159.

*Patent Publications*

B. Brack, E.W.J. van Steen, D.W. Gammon, T.J. Khaile, C.M. Jungmann and L.J. van Rensburg, "Synthesis of resorcinol", SA-Patent ZA98/6640, 1998.

*Conference Snapshot Presentations (Poster):*

B. Brack, D.W. Gammon and E. van Steen, "Synthesis of resorcinol from meta-phenylenediamine in the presence of zeolites and zirconium phosphates", Chemical Engineering R&D Abstract Programme, Cape Town, South Africa, 22 October 1999.

B. Brack, D.W. Gammon and E. van Steen, "Synthesis of resorcinol from meta-phenylenediamine in the presence of zeolites and zirconium phosphates", Catalysis Conference CATSA, Rustenburg, South Africa, 31 October till 2 November 1999.

# NOMENCLATURE

Symbols and constants that are defined and used locally are not included here.

| | |
|---|---|
| $a_i$ | activity of $i$-th component |
| $A_s$ | total surface area |
| $AS$ | acid sites |
| $C$ | concentration |
| $C_p$ | heat capacity |
| $d$ | diameter (zeolites) or interlayer distance (zirconium phosphates) |
| $E_a$ | activation energy |
| $f$ | fugacity |
| $FW$ | formula weight |
| $F$ | flow rate of carrier gas |
| $G$ | (molar) Gibbs free energy of (refer to subscript or superscript) |
| $H^{ex}$ | excess partial molar enthalpy |
| $I$ | intensity |
| $k$ | rate constant |
| $K$ | equilibrium constant |
| $K_a$ | equilibrium constant defined according to system |
| $\tilde{K}_a$ | equilibrium constant; according to Equations A.24 and A.25 |
| $m$ | mass (defined locally) |
| $n_i^e$ | surface excess of $i$-th component; moles |
| $n_{i,o}{}^s$ | surface phase capacity of pure component $i$; moles |
| $n_i^s$ | total number of moles of the $i$-th component in the surface phase |
| $n^o$ | total number of moles in the adsorption system |
| $N$ | number of moles |
| $P$ | pressure or molar pressure |
| $r$ | ratio of two components |
| $S$ | entropy or molar entropy |

| | |
|---|---|
| $S_{BET}$ | surface area determined using BET isotherm |
| $t$ | time |
| $T$ | temperature |
| $T_r$ | reduced temperature |
| $U$ | molar internal energy |
| $v_i$ | volume fraction of $i$-th component |
| $V$ | volume or molar volume |
| $w$ | weight |
| $w_i$ | partial molar area occupied by the $i$-th component |
| $W$ | molar work |
| $x_i$ | mole fraction of $i$-th component |
| $X$ | conversion |
| $y$ | mole fraction (gas) |
| | |
| $\beta$ | linear heating rate |
| $\chi$ | Flory interaction parameter |
| $\varepsilon_{ij}$ | binary interaction parameters between $i$-th and $j$-th components |
| $\phi_i$ | volume fraction of $i$-th component |
| $\gamma_i$ | activity coefficient of $i$-th component |
| $\pi$ | heterogeneity parameter |
| $\theta$ | coverage |
| $\rho$ | density |
| $\sigma$ | interfacial tension |
| $\Delta G$ | change in Gibbs free energy (refer to subscript or superscript) |
| $\Delta h$ | change in heat of (refer to subscript or superscript) |
| $\Delta H$ | change in heat of (refer to subscript or superscript) |
| $\Delta S$ | change in entropy of (refer to subscript or superscript) |
| $\Gamma_2^e$ | surface excess of the i-th component per mass adsorbed |

**Subscripts**

| | |
|---|---|
| *a* | adsorption |
| *ad* | adsorption |
| *Al* | aluminium Species |
| *aq* | aqueous |
| *des* | desorption |
| *ext* | external |
| *f* | formation |
| *g* | gas phase |
| *HA* | mineral acid |
| *i* | *i*-th component |
| *j* | *j*-th component |
| *l* | liquid |
| *lc* | layer charge |
| *loc* | local |
| *m* | maximum |
| *max* | maximum |
| *MAP* | meta-aminophenol |
| *MPDA* | meta-phenylenediamine |
| *o* | initial or pure component |
| *RES* | resorcinol |
| *rxn* | reaction |
| *s* | solid phase |
| *w* | water |
| *vap* | vaporisation |

### Superscripts

| | |
|---|---|
| $l$ | liquid / bulk phase |
| $L$ | liquid phase |
| $o$ | standard (pure component) |
| $phys$ | physisorbed |
| $prot$ | protonated |
| $s$ | solid / adsorbed phase; or partial |
| $V$ | vapour phase |
| $vap$ | vapourisation |
| $rxn$ | reaction |

### Constants

| | |
|---|---|
| $R$ | universal gas constant; 8.314 J/(mol K) |
| $N_A$ | Avogadro's constant; $6.022 \cdot 10^{23}$ 1/mol |
| $k$ | Boltzmann's constant; $1.381 \cdot 10^{-23}$ J/mol |
| $q$ | electronic charge; $1.6022 \cdot 10^{-19}$ C |



### Abbreviations

| | |
|---|---|
| AA | Atomic Adsorption Spectroscopy |
| BET | Brunauer, Emmett and Teller isotherm |
| DTA | Differential Thermal Analysis |
| EFAl | Extra Framework Aluminium |
| FT-IR | Fourier Transform Infra-Red |
| GC | Gas Chromatography |
| GCMS | Gas Chromatography with Mass Spectrometer as Detector |
| HTD | High Temperature Desorption |
| HPLC | High Pressure Liquid Chromatography |

| | |
|---|---|
| HY (USHY) | Zeolite Y (ultrastable) |
| I.D. | Inner Diameter |
| IR | Infra-Red |
| LTD | Low Temperature Desorption |
| MAP | meta-Aminophenol |
| MPDA | meta-Phenylenediamine |
| MS | Mass Spectrometer |
| m.a.s | magic angle spinning |
| NASICON | Sodium Super-Ionic Conductor |
| NTP | Normal Temperature Pressure |
| NMR | Nuclear Magnetic Resonance |
| SEM | Scanning Electron Microscopy |
| TCD | Thermal Conductivity Detector |
| TGA | Thermogravimetric Analysis |
| TPD | Temperature Programmed Desorption |
| USP | United States Pharmacopoeia |
| XRD | X-Ray Diffraction |
| | |
| α-ZrP | α-Zirconium Phosphate, $\alpha$-$Zr(HPO_4)_2 \cdot H_2O$ |
| α-ZrP400 | Calcined α-ZrP at 400°C for 12hours |
| γ-ZrP | γ-Zirconium Phosphate, $\gamma$-$Zr(PO_4)(H_2PO_4) \cdot 2H_2O$ |
| γ-ZrP400 | Calcined γ-ZrP at 400°C for 12hours |

## Glossary

| | |
|---|---|
| basal spacing | distance between barycentres of two adjacent sheets |
| d-spacing | see basal spacing |
| E-factor | mass ratio of by-products relative to desired product |
| Gallery height | actual distance between two lamella (free distance) |
| lamella | planar macromolecular sheet |
| interlamellar distance | see basal spacing |
| interlayer distance | see basal spacing |
| Interlayer region | free space between two adjacent layers |

# Chapter 1

## Introduction



Discovery consists of seeing what everybody has seen and thinking what nobody has thought

(Albert Szent-Györgyi)

# 1. INTRODUCTION

Resorcinol forms an important building block in the pharmaceuticals, adhesion and dye industries [Dressler, 1994]. The available resorcinol synthesis routes are either highly energy intensive, capital intensive, safety hazardous or may include a multitude of stages that result in difficult removable isomers and co-products. The resorcinol synthesis route conducive to South Africa is that from meta-dinitrobenzene. The South African explosives industry produces large amounts of nitrobenzene from benzene. In the presence of a nickel catalyst, the meta-dinitrobenzene can quite easily be catalytically hydrogenated to meta-phenylenediamine. Thereafter, the purified meta-phenylenediamine (MPDA) can be converted to resorcinol in the presence of water and a suitable promoter. The promoters comprise of mineral acids of which ammonium-bisulphate, phosphoric and sulphuric acid are amongst the most commonly used [Greco, 1968 - 1972]. Although side reactions, especially condensation reactions, do occur, high resorcinol yields (>95%) can be obtained in the presence of mineral acids. The mineral acids tend to be highly corrosive at the required reaction temperatures (in excess of 200°C), making the process capital intensive.

The objective of this study is to replace the corrosive and hazardous homogeneous mineral acids previously required for the MPDA hydrolysis with heterogeneous solid acids that posses localised acid sites. The heterogeneous acids considered are aluminosilicates (e.g., zeolites) and zirconium phosphates. The pore structure of the zeolites is thought to aid in suppressing condensation reactions. This might occur if the transition-state for the condensation is too bulky to fit into the pores and/or if the condensation products cannot diffuse out of the pores of the zeolites and the reverse reaction occurs. Heterogeneous acids would also ease the separation process since no acid neutralisation and precipitation steps would be required.

# Chapter 2

## Literature Review and Proposals



The simplest schoolboy is now familiar with truths
for which Archimedes would have sacrificed his life
(Ernest Renan)

# 2. LITERATURE REVIEW AND PROPOSALS

## 2.1 RESORCINOL PRODUCTION

Resorcinol (1,3-dihydroxybenzene) and resorcinol-based resins are primarily used in the tire and rubber industries to enhance the adhesion between reinforcing materials and rubber. It is used in the manufacture of wood adhesive resins and forms an important building block for the production of pharmaceuticals and ultraviolet absorbers. Resorcinol is also required as a starting material for the preparation of dyes [Varagnat, 1981; Dressler, 1994]. The estimated world-wide manufacturing capacity of resorcinol is around 30 000 tons per year [Krumenacker *et al.*, 1995] and the world price of resorcinol in November 2000 was averaged at 17.60$ per kg USP grade resorcinol (6.60$/kg technical grade resorcinol) [n.n., 2000].

Although, resorcinol is a sought after chemical, its synthesis route has not evolved since the 1980's and still relies heavily on stoichiometric reactions. Since the hydroxyl substituent on a benzene ring is ortho- and para-directing, the meta-isomer can only be obtained from benzene in an indirect way. For example, the hydroxylation of phenol using TS-1 type catalysts with hydrogen peroxide yields hydroquinone and catechol but not resorcinol (<0.5%) [Romano *et. al*, 1990]. Consequently, the commercially feasible production of resorcinol depends on the yield and selectivity of a meta-precursor that can then be converted to resorcinol. Catalytic processes for the production of resorcinol are available, although these processes are greatly dependent on the market value of the co- and/or by-products formed [Fellmann *et al.*, 1991].

## 2.1.1 PROCESSES FOR SYNTHESIS OF RESORCINOL

Figure 2.1 illustrates that the high yields of meta-disubstituted products can only be achieved via the aromatic nitration or the aromatic sulfonation processes. These processes are based on the primary $-NO_2$ or $-SO_3H$ substituents on the benzene ring being strongly meta-directing. Meta-directors exert their directing influence because they deactivate the meta-position less than they deactivate the ortho- and para-position. Highly concentrated acids are required to sulfonate or nitrate the benzene ring since the reactivity of the mono-substituted equivalent is less than that of benzene. This translates into vast amounts of base required to neutralise the acid medium after reaction, which results in mineral salts as by-products. The very corrosive properties of sulfuric acid or nitric acid make these processes also capital intensive due to high maintenance costs on the reactors.



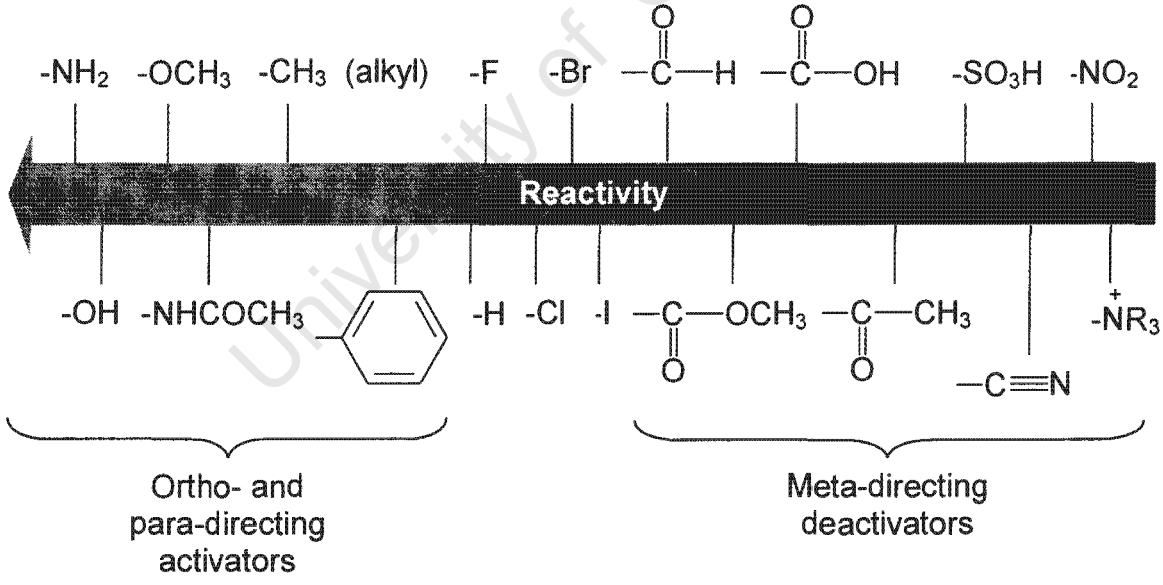


**Figure 2.1** Classification of directing effects for substituents [redrawn from McMurry, 1992].

Catalytic 1,3-substitution reactions on the benzene ring can be achieved using meta-directing organic substituents, e.g., an acyl substituent. Nevertheless, the

selectivity towards meta-directed compounds would not be as pronounced as observed for the nitro and sulfonate groups. Therefore, larger amounts of ortho and para disubstituted benzene molecules are produced as by-products. This leads to large capital expenditures for the overall process due to separation units required to purify the desired product.

The main route for the industrial synthesis of resorcinol is the alkaline fusion of meta-benzenedisulfonic acid, whereas the hydroperoxidation of diisopropyl-benzene is primarily adopted in Japan [Krumenacker *et al.*, 1995]. Other patented processes exist and are presented in Table 2.1. Apart for the δ-keto-acid route, all other resorcinol processes require benzene as a starting material.

**Table 2.1 Manufacturing processes for resorcinol**

| Process | References |
|---|---|
| Alkaline fusion of m-benzenedisulfonic acid | [Allen, 1976] |
| Hydroperoxidation of diisopropylbenzene | [Varagnat, 1981] |
| Dehydrogenation of cyclised δ-ketocarboxylic acid esters | [Meyer *et al.*, 1979; Greco, 1982] |
| Oxidative dehydrogenation of cyclohexanone | [Fellmann *et al.*, 1991] |
| Hydrolysis of hydrogenated m-dinitrobenzene | [Greco, 1972] |



### 2.1.1.1 COMPARISON OF INDUSTRIAL PROSESSES

A convenient way of comparing the different chemical processes for the manufacture of resorcinol on an environmental and economic level is given by the E-factor, which is defined as the mass of by-products formed per mass of products produced [Sheldon, 1996]. The theoretical E-factor is based on the inverse of the atom selectivity as follows:

$$\text{Theoretical E-factor} = \frac{1}{\text{Atom Selectivity}} - 1 \qquad \textbf{2.1}$$

The atom selectivity is calculated by dividing the molecular weight of the desired product by the summated molecular weights of all products formed as given by the stoichiometric equation. The true E-factor, however, is greater than the theoretical one since the general plant efficiencies are far from perfect and unwanted side-reactions do occur. Additionally, only limited information is given regarding neutralisation steps.

### 2.1.1.2 BENZENE DISULFONATION

The first step involves the reaction of benzene with fuming sulphuric acid to form meta-benzenedisulfonic acid (Reaction 2.2). The acid medium is then neutralised with NaOH [Varagnat, 1981] or $Na_2SO_3$ [Allen, 1967] to produce a disulfonate sodium salt (Reaction 2.3). The caustic salt is further treated with dry caustic soda at 350°C to eliminate the sulfonic acid group to produce sodium resorcinate and sodium sulfite (Reaction 2.4). Resorcinol is then extracted with sulphuric acid (Reaction 2.5). Based on m-benzenedisulfonic acid, the resorcinol yield is around 94% [Varagnat, 1981]. This commercial process is energy intensive due to the drying step. In addition, the use of concentrated sulphuric acid and caustic soda makes the process very capital intensive [Fellmann *et al.*, 1991]. The theoretical E-factor (mass by-products / mass resorcinol) for the overall process equals 4.56.



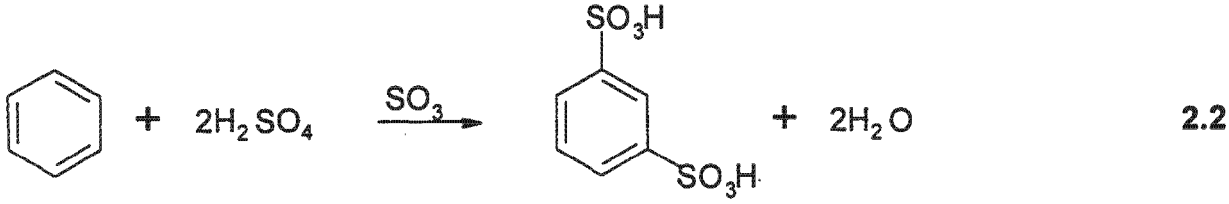


**2.2**

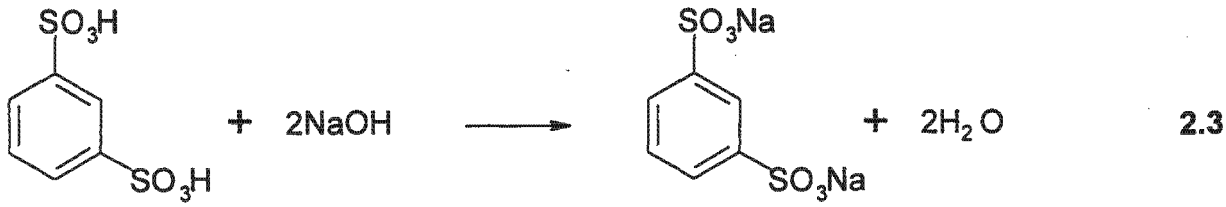


**2.3**

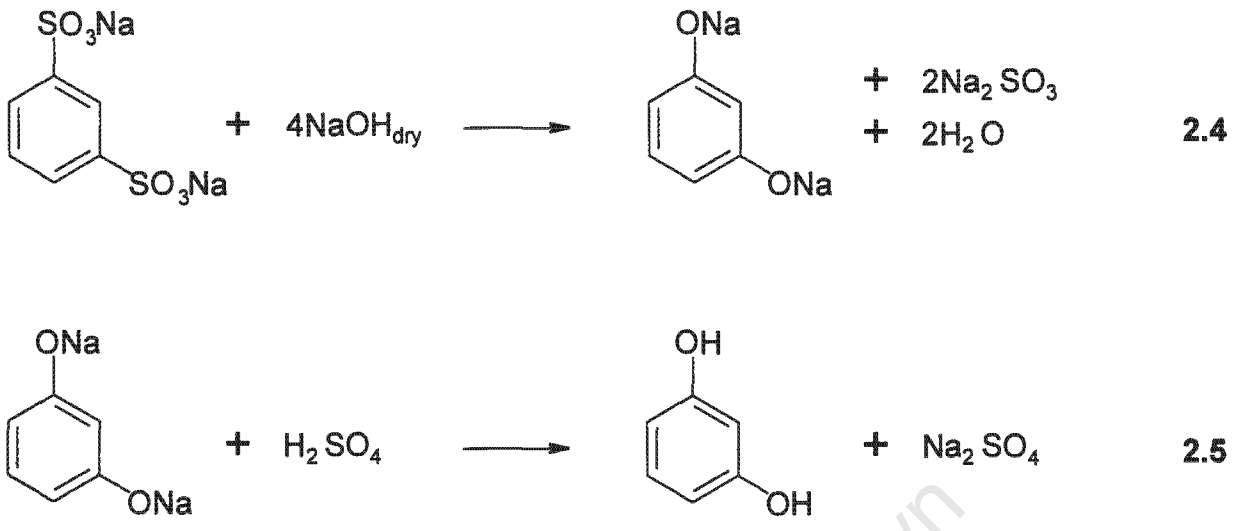


**Figure 2.2** Process for the production of resorcinol via benzene disulfonation.



### 2.1.1.3 HYDROPEROXIDATION OF DIISOPROPYLBENZENE

A process primarily adopted in Japan is that of the diisopropylbenzene route to resorcinol. The liquid phase Friedel-Craft alkylation of benzene by propylene is carried out over a variety of heterogeneous acid catalysts (Reaction 2.6). Zeolites are the most commonly used acids with the zeolite structure influencing the selectivity of the meta to para ratio [Kaeding, 1984]. The para-isomer and the other propylated species (e.g., cumene) formed must be removed and recycled so that high yields of the pure meta-product is obtained. The meta-diisopropyl-benzene is oxidised in air to obtain the di-hydroperoxide (Reaction 2.7). Hydrogen-peroxide can be used to prevent the formation of alcohol side-products [Wu, 1987]. Acid cleavage of the di-hydrogenperoxide yields acetone and resorcinol (Reaction 2.8). Acetone in the presence of hydrogen peroxide, however, forms sensitive explosive compounds that create safety hazards.

Since the addition of propylene is not a very selective reaction, separation processes have to be employed to purify the desired meta-intermediate from the para-isomer, cumene, and propylene. The economic viability of the process itself is very dependent on the co-products formed [Fellmann *et al.*, 1991]. The theoretical E-factor (mass by-products per mass resorcinol) equals 1.05.

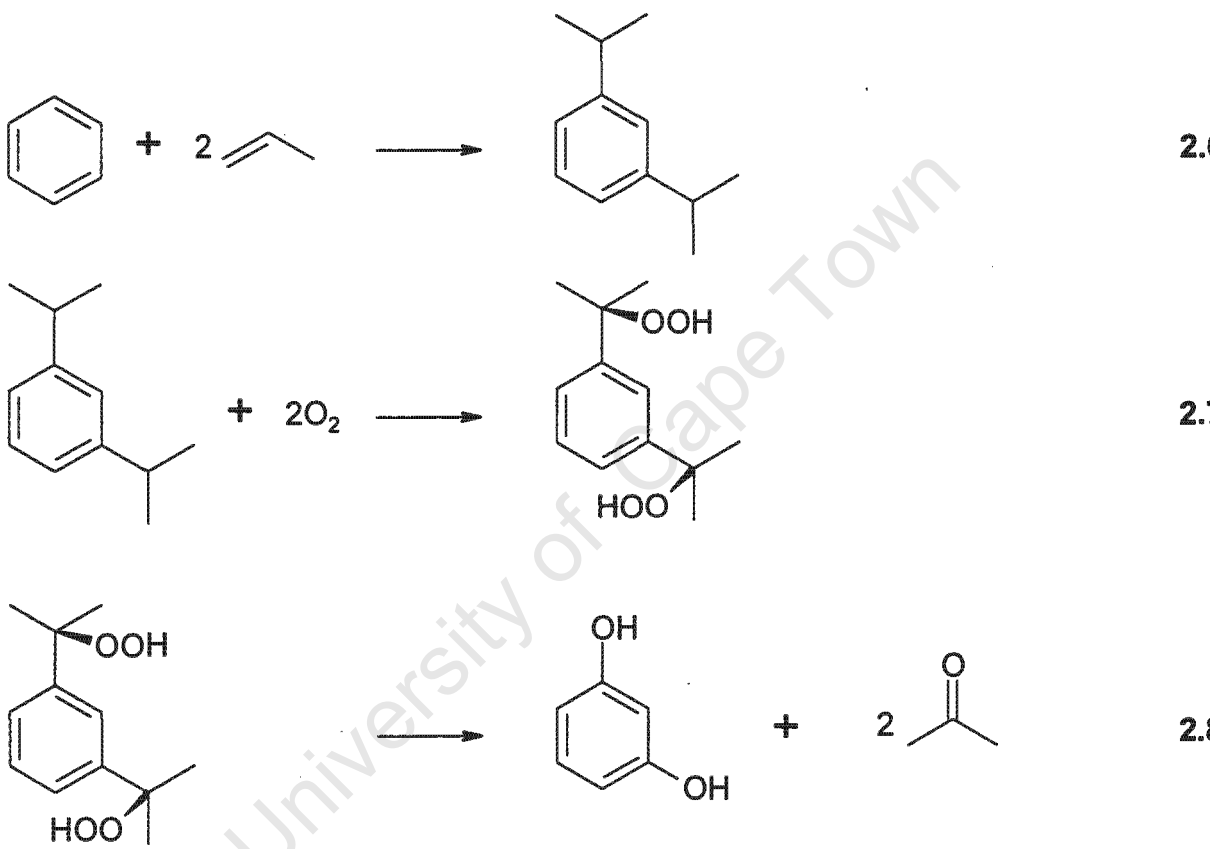




**Figure 2.3** Process for the production of resorcinol via diisopropylbenzene.

### 2.1.1.4 RESORCINOL FROM δ-KETOCARBOXYLIC ACID ESTERS

Manufacturing resorcinol from acetone and acrylic acid emerged as a viable route due to the low cost of the raw materials. Acrylic acid is first reacted with an alcohol to obtain an ester in the presence of an acid catalyst (Reaction 2.9). The δ-ketocarboxylic-acid ester is then obtained upon reacting the acrylic ester with

acetone in the presence of a cyclic lower alkyl secondary amine such as methyl-β-pyrrolidin-1-yl propionate [Meyer *et al.*, 1979]. The Michael addition is a liquid phase reaction, carried out between 170°C and 250°C (Reaction 2.10). Depending on the process, Reaction 2.11 can be carried out in one or two steps. The one step production of resorcinol from the δ-ketocarboxylic acid involves a gas phase reaction in the presence of a hydrogen/nitrogen carrier and a two-component catalyst consisting of thorium-on-carbon and platinum/chrome-oxide-on-alumina [Müller *et al.*, 1979]. Separation difficulties and the impractical reactivation of the very expensive catalyst make this process unfavourable [Fellmann *et al.*, 1991]. The two step process involves a gas phase reaction of the keto-carboxylic acid ester to a cyclic intermediate (3-hydroxy-2-cyclohexene-1-one) in the presence of toluene and an activated carbon catalyst [Greco, 1982]. Since the keto-carboxylic acid ester is soluble in toluene and the cyclic intermediate is immiscible in toluene, the presence of toluene increases the conversion of ester and eases the separation process. The second step involves a liquid-phase dehydrogenation of the 3-hydroxy-2-cyclohezene-1-one intermediate to resorcinol. The dehydrogenation is carried out in a pressurised CSTR at 170°C using isopropyl-alcohol as a solvent, palladium-on-carbon as catalyst and a nitrogen purge stream to remove the formed hydrogen [Greco, 1982]. Although the theoretical E-factor (mass by-products / mass resorcinol) in Figure 2.4 equals 0.18, the value gives an incorrect interpretation of the selectivity of the process due to prevalent side-reactions.




**2.9**


**2.10**

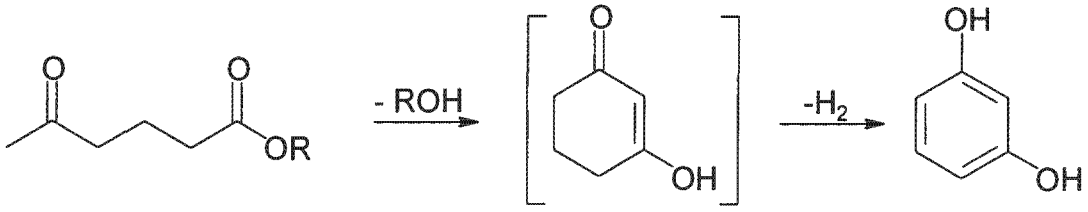


2.11

**Figure 2.4** Process for the production of resorcinol from acetone and acrylic acid.

### 2.1.1.5 OXIDATIVE DEHYDROGENATION OF CYCLOHEXANONE

A further process to resorcinol is via the oxidative dehydrogenation of cyclohexanone [Fellmann *et al.*, 1991]. Many routes to cyclohexanone or 2-cyclohexenone are available [Fellmann *et al.*, 1991]. One of the possible routes to cyclohexanone (Reaction 2.12) is given by first hydrogenating gaseous benzene over a platinum catalyst to form cyclohexane ($150^{\circ}C < T < 400^{\circ}C$; $0.5MPa < P < 5MPa$). Subsequently, liquid cyclohexane is oxidised in the presence of an oxygen containing gas to produce a mixture of cyclohexanone and cyclohexanol ($120^{\circ}C < T < 190^{\circ}C$). After separating the cyclohexanone from the mixture, the cyclohexanol can be dehydrogenated catalytically over a platinum catalyst back to cyclohexanone [Van de Mond *et al.*, 1981].

The next step involves the oxidative dehydrogenation of cyclohexanone with oxygen to form 2-cyclohexen-1-one (Reaction 2.13). The liquid phase reaction uses acetic acid as a solvent and the catalyst employed consists of a mixture of soluble Pd(II) and Cu(II) complexes. During the reaction, the Cu(II), however, transforms itself to cuprous oxide [Theissen, 1971]. The addition of water to 2-cyclohexen-1-one over, e.g., Amberlyst 15, yields 3-hydroxycyclohexanone (Reaction 2.14). The selectivity to the desired product is ca. 100% [Fellmann *et al.*, 1991]. Resorcinol is thus obtained from 3-hydroxycyclohexanone by employing the same method as described previously (see Reaction 2.11). This

process requires a considerable amount of steps. Purifying the product after each reaction tends to be very capital intensive. Nevertheless, many of the intermediates are valuable and therefore this could be a viable route to resorcinol. According to Figure 2.5, the theoretical E-factor (mass by-products / mass resorcinol) equates to 0.50.

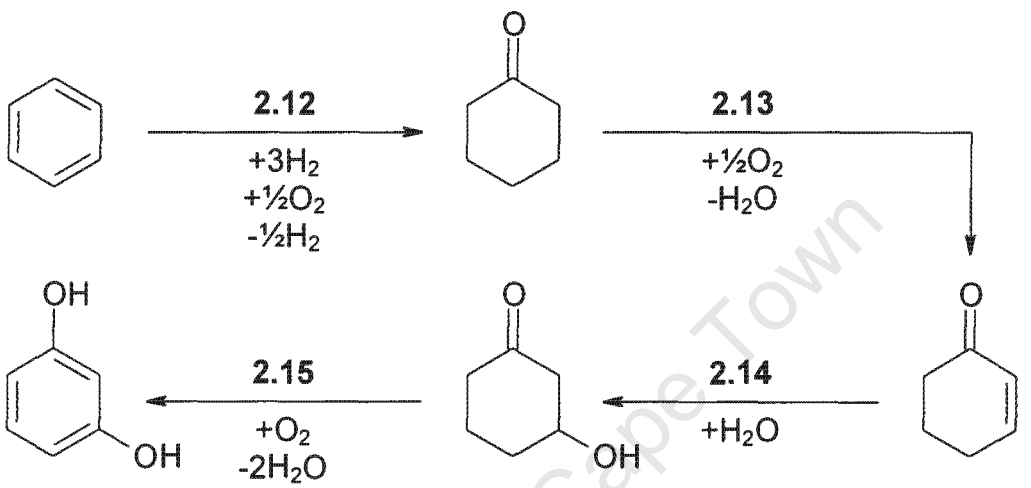


**Figure 2.5** Process for the production of resorcinol from benzene via the oxidative dehydrogenation of cyclohexanone.



### 2.1.1.6 HYDROLYSIS OF HYDROGENATED m-DINITROBENZENE

Treating benzene with a mixture of concentrated nitric and sulphuric acid yields meta-dinitrobenzene (Reaction 2.16). After neutralising the strongly acidic solution with a base, the meta-dinitrobenzene is recovered. The formation of large quantities of salt and the production of other isomers makes the nitration process very expensive [Fellmann *et al.*, 1991]. Using a mixture of a mononuclear aromatic hydrocarbon and a lower aliphatic alcohol as a solvent, the meta-dinitrobenzene is hydrogenated to meta-phenylenediamine over a nickel catalyst (Reaction 2.17). A substantially pure meta-phenylenediamine is obtained keeping the reaction temperature under 100°C and the corresponding pressure at 400psig [Greco, 1972].

Hydrolysing the meta-phenylenediamine (MPDA) using ammonium-bisulphate, sulphuric or phosphoric acid yields the desired resorcinol. As shown in Reaction 2.18, the hydrolysis proceeds via the intermediate meta-aminophenol (MAP) [Greco, 1968] with water serving as a reactant and solvent for both consecutive reactions. The reaction is typically performed in liquid phase in an autoclave applying a reaction temperature between 170°C and 250°C [Greco, 1972].

For the industrial production of resorcinol to be feasible, the mass percent of MPDA to water should lie between 5 and 15 percent. The reaction is considered unprofitable if the MPDA mass percent is below 5% [Greco, 1968]. A solution of more than 15 mass percent MPDA may lead to possible reactor blockages since the probability of polymerisation increases. Furthermore, corrosion of the equipment becomes more problematic since more concentrated acids are required. The reactor itself should not be constructed using stainless steel or monel metal since the presence of acids lead to the added production of metal/amine complexes that enhance the formation of resins [Greco, 1968]. Resorcinol is extracted from the reaction mixture using ether. The dissolved resorcinol in ether is then distilled. The theoretical E-factor (mass by-products / mass resorcinol) equals 3.07.



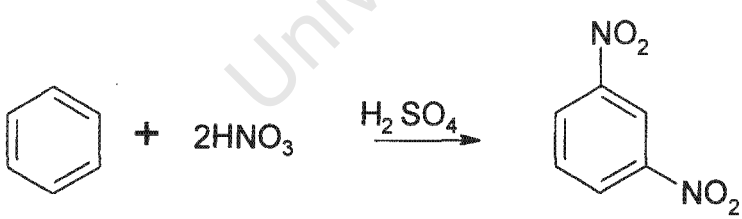


**2.16**

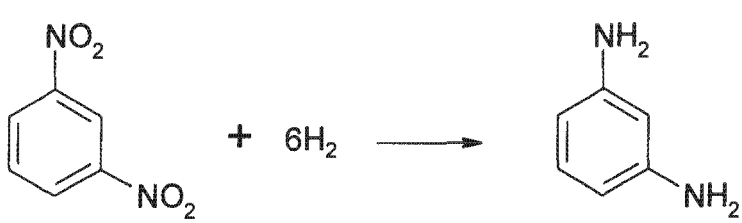


**2.17**

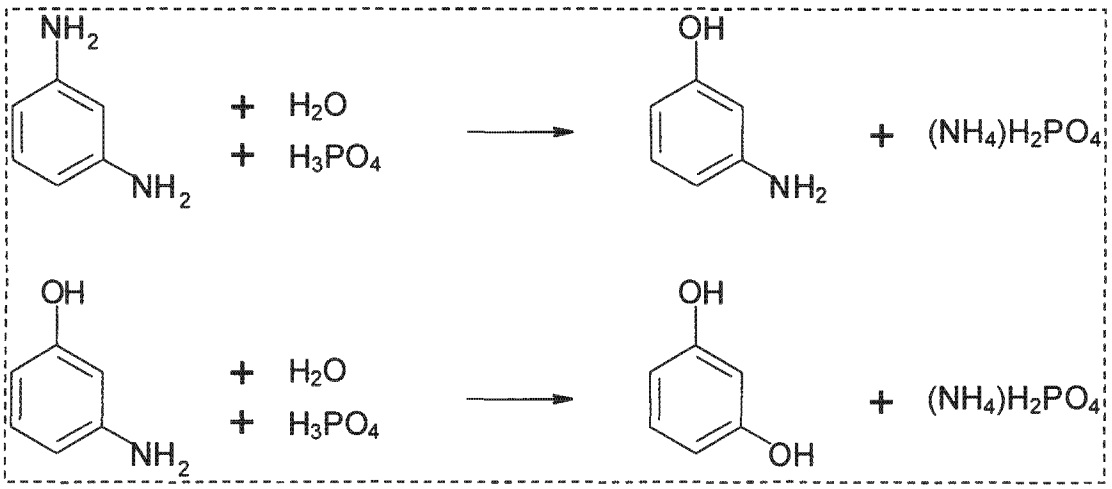


2.18

**Figure 2.6** Process for the production of resorcinol via benzene nitration.



### 2.1.1.7 GENERAL OVERVIEW OF PROCESSES

Table 2.2 shows that no direct route from a bulk chemical towards resorcinol is available. All process routes considered require 3 or 4 reaction steps. Process-routes making use of heterogeneous catalysis, i.e., the hydroperoxidation of diisopropylbenzene, the oxidative dehydrogenation of cyclohexanone or via cyclisised δ-ketocarboxylic acid esters, are efficient as shown by the relatively low theoretical E-factors. The catalytic routes are not 100% selective. The side-products often need to be removed after each reaction to prevent the formation of a diverse array of chemical products further downstream. The side-product formation has not been included in the theoretical E-factor.

Side-products often have similar physical properties as the desired product resulting in large separation expenses being incurred due to initial capital investments and operating expenses. If the side-products have commercial value the separation costs may be recovered. Catalyst deactivation can also offset the viability of a particular catalytic route. The irreversible poisoning of certain catalysts and the formation of side-products invariably leads to an E-factor larger than predicted by the theoretical E-factor.

Larger theoretical E-factors are calculated for the synthesis of resorcinol via the benzene disulfonation and the hydrolysis of hydrogenated m-dinitrobenzene route. The true E-factors should be considerably larger than those calculated in Table 2.2, since for example, the extraction of resorcinol from an acid solution would also require the neutralisation of the excess mineral acids. Newer technology, however, enables the recovery of the bulk of the unspent sulphuric acid via the formation of gaseous $SO_3$. Consequently, the direct removal of sulphuric acid from a reaction mixture gives it an advantage over, for example, phosphoric acid. Further disadvantages of the usage of mineral acids are their corrosive nature that can lead to larger capital expenditures and their hazardous make-up that is not easily contained in the advent of a spillage.

**Table 2.2 Summary of advantages and disadvantages of available process routes towards resorcinol**

| Reaction Process | No. React. Steps | Theoretical E-factor | Remarks |
|---|---|---|---|
| Benzene disulfonation | 4 | 4.56 | • Capital intensive due to corrosion of materials of construction<br>• Energy intensive; drying Na-salt product<br>• Formation of additional salts during separation |
| Hydroperoxidation of diisopropylbenzene | 3 | 1.05 | • Side-reactions; large separation expenses<br>• Explosion hazards |
| Cyclisation of δ-keto-carboxylic acid esters | 3 - 4 | 0.18 | • Separation difficulty; many separation stages<br>• Impractical reactivation of expensive catalyst |
| Oxidative dehydrogen-ation of cyclohexanone | 4 | 0.50 | • Side Product formation<br>• Capital and Energy In-tensive; purification of product after each reaction step |
| Hydrolysis of hydrogen-ated m-dinitrobenzene | 3 | 3.07 | • Capital Intensive due to materials of construction<br>• Formation of additional salts during separation |

## 2.1.2 CONVERSION OF MPDA TO RESORCINOL

Within the South African context the manufacture of resorcinol via meta-phenylenediamine is a viable option due to the production of large quantities of meta-dinitrobenzene. The compound is co-produced during the manufacture of nitrobenzene, which is an intermediate for the production of explosives. The manufacturing process of nitrobenzene / meta-dintrobenzene is in itself a very environmentally unfriendly, capital and energy intensive process. The benzene nitrification reaction will not be investigated in this study, although studies have been reported to make this process more environmentally friendly [Vassena *et al.*, 1999].

### 2.1.2.1 THERMODYNAMICS REGARDING TRANSFORMATION OF MPDA TO RESORCINOL

Simplistic thermodynamic equilibrium calculations between reaction temperatures of 150°C and 350°C have been performed for both gaseous and liquid phase systems. For both phases, calculations have been performed with and without the presence of a mineral acid. According to Reaction 2.18, phosphoric acid is arbitrarily chosen as the mineral acid, although the use of ammonium-bisulfate or sulphuric acid gives similar results. It is important to note that the conversion of MPDA to resorcinol occurs via meta-aminophenol (MAP) (see Reaction 2.18).

The chemical and physical data for the relevant components are given in APPENDIX-B. Inadequate information on MAP necessitates estimation techniques (group contribution method; Van Krevelen and Chermin, 1952) being used for determining the properties of MAP [Perry *et al.*, 1984]. Using this method, it follows that in essence the thermodynamic properties of MAP may be obtained by averaging the properties of MPDA and resorcinol. The latter route is thus chosen.

**(i) Gas phase equilibrium**

Reaction 2.19 displays the gaseous conversion of MPDA to resorcinol in the presence of a catalyst. Reaction 2.20, however, illustrates the set of reactions if a heterogeneous reagent is used, with the reasonable assumption that phosphoric acid and its corresponding salt do not undergo any phase changes and remain solid throughout the reaction.

$$MPDA_{(g)} + H_2O_{(g)} \longrightarrow MAP_{(g)} + NH_{3(g)}$$
$$MAP_{(g)} + H_2O_{(g)} \longrightarrow Resorcinol_{(g)} + NH_{3(g)} \qquad \textbf{2.19}$$

$$MPDA_{(g)} + H_2O_{(g)} + H_3PO_{4(s)} \longrightarrow MAP_{(g)} + NH_4H_2PO_{4(s)}$$
$$MAP_{(g)} + H_2O_{(g)} + H_3PO_{4(s)} \longrightarrow Resorcinol_{(g)} + NH_4H_2PO_{4(s)} \qquad \textbf{2.20}$$

**Table 2.3 Calculated equilibrium constants ($K_a$) and heat of reactions ($\Delta h_{rxn}$) at 25°C for Reaction 2.19 and 2.20 in gaseous phase.**

| | | $K_a$ at 25°C | $\Delta h_{rxn}$ at 25°C (J/mol) |
|---|---|---|---|
| Reaction 2.19 | $MPDA_{(g)} \rightarrow MAP_{(g)}$ | 6.91E-4 | 1.30E4 |
| | $MAP_{(g)} \rightarrow Resorcinol_{(g)}$ | 6.91E-4 | 1.30E4 |
| Reaction 2.20 | $MPDA_{(g)} \rightarrow MAP_{(g)}$ | 1.17E9 | -1.02E5 |
| | $MAP_{(g)} \rightarrow Resorcinol_{(g)}$ | 1.17E9 | -1.02E5 |

Table 2.3 gives the calculated equilibrium constants and heat of reactions at 25°C for Reaction 2.19 and 2.20, respectively. For each reaction system considered, the equilibrium constant and the heat of reaction in proceeding from MPDA to MAP is identical to that of MAP to resorcinol. This is caused as a result of estimating the properties of MAP by averaging the properties of MPDA and resorcinol. The catalytic conversion of MPDA to resorcinol (see Reaction 2.19 in

Table 2.3) is predicted to be endothermic ($\Delta h_{rxn} > 0$) , and the very low equilibrium constants signify an unfavourable forward reaction at 25°C. Since the reaction is endothermic, the conversion of MPDA should improve with increasing temperature. In contrast to Reaction 2.19, the presence of a heterogeneous reagent, e.g., $H_3PO_{4(s)}$ in Reaction 2.20, results in a highly exothermic reaction with a very large equilibrium constant at 25°C. For Reaction 2.20 a decrease in the equilibrium constant is expected with increasing temperature. The heat of reaction, $\Delta h_{rxn}$, calculated at 25°C is assumed to be temperature independent to obtain a first estimate on the equilibrium constants at higher temperatures (see Equation 2.21).

$$\ln\frac{K_a(T_2)}{K_a(298K)} = -\int_{298K}^{T_2}\frac{\Delta h_{rxn}(T)}{RT^2}dT \qquad \textbf{2.21}$$

A low enough operating pressure is chosen for the ideal gas law to become applicable. Therefore, the equilibrium constants, $K_a$, are given by Equations 2.22 and 2.23 for Reactions 2.19 and 2.20, respectively. The extent of each of the reactions is given by $X$. Subscripts *1* and *2* respectively refer to reactions MPDA → MAP and MAP → resorcinol. The term $W$ represents the number of moles of water added initially to 1 mole of MPDA. Values chosen for $W$ are 20, 100, and 2100 to give Water to MPDA ratios of 20:1, 100:1 and 2100:1.

$$K_{a,1} = \frac{(X_1 - X_2)(X_1 + X_2)}{(1 - X_1)(W - X_1 - X_2)} \quad \text{and} \quad K_{a,2} = \frac{X_2(X_1 + X_2)}{(X_1 - X_2)(W - X_1 - X_2)} \qquad \textbf{2.22}$$

$$K_{a,1} = \frac{(X_1 - X_2)(W + 1 - X_1 - X_2)}{(1 - X_1)(W - X_1 - X_2)}\frac{1atm}{p} \quad \text{and} \quad K_{a,2} = \frac{X_2(W + 1 - X_1 - X_2)}{(X_1 - X_2)(W - X_1 - X_2)}\frac{1atm}{p} \qquad \textbf{2.23}$$

According to Equation 2.22, the equilibrium extent of Reaction 2.19 is pressure independent. Equation 2.22 clearly illustrates the strong dependence of the extent of the reaction on the initial water to MPDA mole ratio. The increasing equilibrium conversion with increasing water to MPDA mole ratios for Reaction

2.19 is depicted in Figure 2.7. Subtracting the equilibrium resorcinol yields from the equilibrium MPDA conversion reveals that a considerable amount of MAP should be expected. For water to MPDA mole ratios of 20:1 and 100:1 the ratio of resorcinol to MAP is ca. 1:1. For large water to MPDA mole ratios, i.e., 2100:1, the ratio of resorcinol to MAP at equilibrium is between 4 (at 150°C) and 11 (at 330°C). Thus, the catalytic production of resorcinol in the gas phase with a high yield requires very large water to MPDA mole ratios and high temperatures to prevent excessive separation and purification costs. Nevertheless, the large excess of water required during reaction would render the process uneconomical.

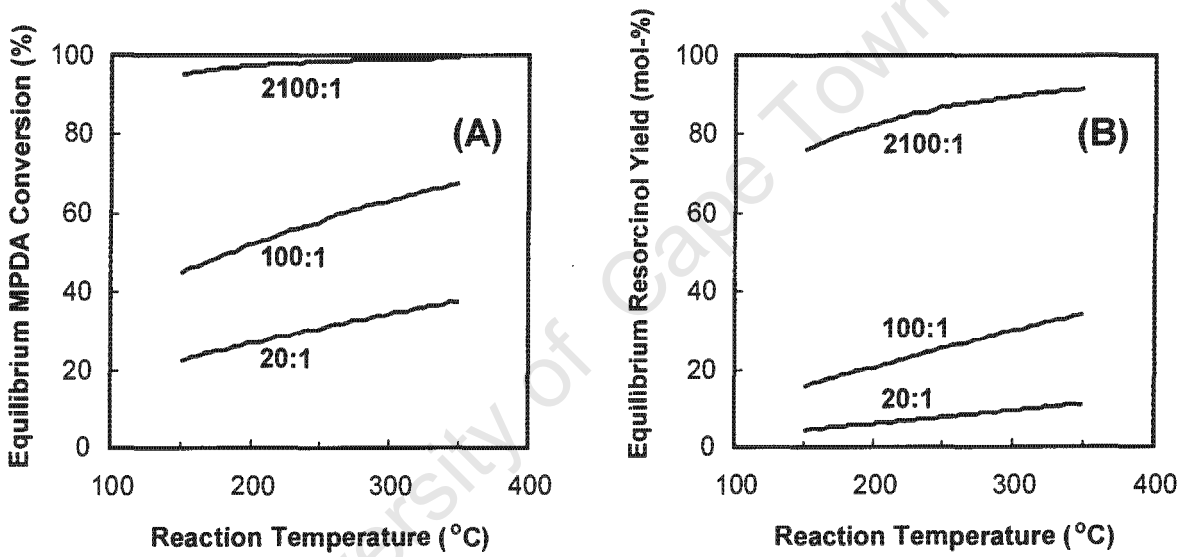


**Figure 2.7** Equilibrium conversion of MPDA (A) and molar yield of resorcinol (B) at different temperatures and initial water to MPDA mole ratios (2100:1; 100:1; 20:1) for the catalytic gas phase conversion of MPDA to resorcinol (Reaction 2.19).

The gaseous conversion of MPDA in the presence of a heterogeneous reagent, i.e., $H_3PO_4$ (Reaction 2.20), is pressure dependent as expressed by Equation 2.23. Consequently, increasing the reaction pressure leads to an increase in the resorcinol yield. Figure 2.8 illustrates the MPDA equilibrium conversion and expected equilibrium resorcinol yields at various temperatures for reaction pressures of 0.5atm, 1.0atm and 2.0atm. The moderate pressures are chosen to

ensure that the ideal gas law may still be assumed applicable. A negligible improvement in the resorcinol yield of Reaction 2.20 is obtained when increasing the water to MPDA mole ratio from 20:1 to 2100:1. Therefore, the expressions given by Equation 2.23 may be simplified by assigning a large number to $W$, thereby setting $(W+1-X_1-X_2)/(W-X_1-X_2)$ equal to 1. The new simplified expressions for Equation 2.23 are used to generate Figure 2.8.

Figure 2.8 clearly shows an increase in the extent of the reaction with increasing pressure. Furthermore, it can be seen that the resorcinol yield becomes thermodynamically limited at high temperatures (T > 300°C).

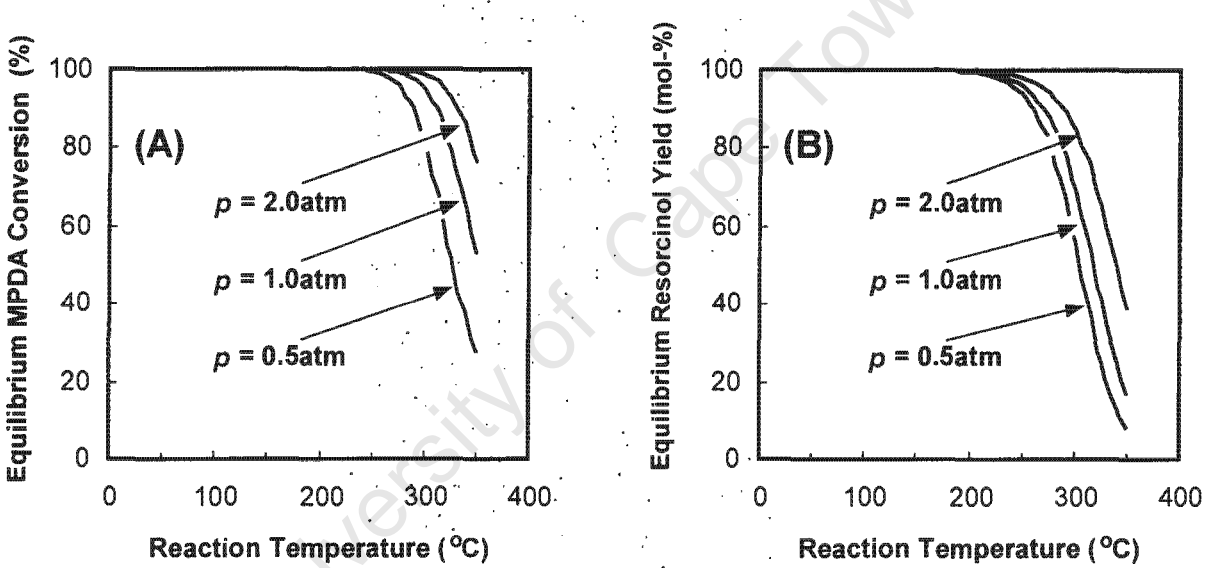


**Figure 2.8** Equilibrium conversion of MPDA (A) and molar yield of resorcinol (B) at different temperatures and pressures (0.5atm, 1.0atm, 2.0atm) for the conversion of MPDA to resorcinol in the gas phase with the transformation of solid phosphoric acid to ammonium-dihydrogen phosphate (Reaction 2.20). Molar ratio of water to MPDA ≥ 20.

**(ii) Liquid phase equilibrium**

Reaction 2.24 displays the conversion of MPDA to resorcinol in the liquid phase and in the absence of any co-reacting substances. Since the reaction occurs in dilute solutions, the magnitude of the hydrolysis of the solutes needs to be estimated. This is done by extrapolating the constants for hydrolysis given at low temperatures (see APPENDIX-B) by means of the van't Hoff equation. Of all relevant components, the extent of hydrolysis of ammonia is the largest at room temperature. Establishing the equilibrium constants at 20°C, 30°C and 50°C for the reaction $NH_{3(aq)} + H_2O \Leftrightarrow NH_4^+{}_{(aq)} + OH^-{}_{(aq)}$ by making use of the constants for hydrolysis given in APPENDIX-B and knowing the ionisation constant of water at 25°C = $10^{-14}$, the extent of hydrolysis of aqueous ammonia at 300°C is estimated to be <1% for a water to $NH_{3(aq)}$ ratio of 21000. It is, nevertheless, understood that the ionisation constant of water at 300°C is $10^{-11.406}$ (see APPENDIX-B) and thus the estimated extent of hydrolysis of $NH_{3(aq)}$ is not entirely justifiable. However, for the sake of simplicity, the aqueous ammonia formed during the reaction is assumed not to hydrolyse to $NH_4^+$ and $OH^-$.

$$MPDA_{(aq)} + H_2O_{(l)} \longrightarrow MAP_{(aq)} + NH_{3(aq)}$$
$$MAP_{(aq)} + H_2O_{(l)} \longrightarrow Resorcinol_{(aq)} + NH_{3(aq)} \qquad \textbf{2.24}$$

Reaction 2.25 shows the conversion of MPDA to resorcinol in the presence of a mineral acid, i.e., $H_3PO_4$. The solution is assumed to be dilute enough for the $H_3PO_{4(aq)}$ (25°C < T < 350°) to fully dissociate solely into $H^+$ and $H_2PO_4^-$ ($pK_a$ of $H_3PO_{4(aq)}$ at 25°C = 2.12; Shriver *et al.*, 1994). The same assumption is applied for ammonium-dihydrogen phosphate. The formation of di- and tri-ammonium phosphate salts is assumed to be negligible.

$$MPDA_{(aq)} + H_2O_{(l)} + H^+{}_{(aq)} + H_2PO_4^-{}_{(aq)} \longrightarrow MAP_{(aq)} + NH_4^+{}_{(aq)} + H_2PO_4^-{}_{(aq)}$$
$$MAP_{(aq)} + H_2O_{(l)} + H^+{}_{(aq)} + H_2PO_4^-{}_{(aq)} \longrightarrow Resorcinol._{(aq)} + NH_4^+{}_{(aq)} + H_2PO_4^-{}_{(aq)} \qquad \textbf{2.25}$$

Table 2.4 gives the calculated equilibrium constants and heat of reactions at 25°C for Reactions 2.24 and 2.25, respectively. The Gibbs free energy and the heats of formation for the organic components in the aqueous state could not be found in literature and thus the liquid heats and free energies of formation are estimated by means of the Peng-Robinson equation [Sandler, 1989]. The heat of formation of $NH_{3(aq)}$ at 25°C is given in APPENDIX-B and the free energy of formation of $NH_{3(aq)}$ at 25°C for very dilute solutions is estimated from the constant for hydrolysis to be equal to -26570J/mol. The free energies of formation for $NH_4^+$ and $OH^-$ ions are given in APPENDIX-B.

**Table 2.4 Calculated equilibrium constants ($K_a$) and heat of reactions ($\Delta h_{rxn}$) at 25°C for Reaction 2.24 and 2.25 in liquid phase.**

| | | $K_a$ at 25°C | $\Delta h_{rxn}$ at 25°C (J/mol) |
|---|---|---|---|
| Reaction 2.24 | $MPDA_{(aq)} \rightarrow MAP_{(aq)}$ | 1.80E-3mol/L | 2.01E4 |
| | $MAP_{(aq)} \rightarrow Resorcinol_{(aq)}$ | 1.77E-3mol/L | 2.03E4 |
| Reaction 2.25 | $MPDA_{(aq)} \rightarrow MAP_{(aq)}$ | 3.36E6 | -3.24E4 |
| | $MAP_{(aq)} \rightarrow Resorcinol_{(aq)}$ | 3.32E6 | -3.22E4 |

Similar to the reaction carried out in the gaseous phase, the conversion of aqueous MPDA to resorcinol in the absence of any co-reaction mineral salt (Reaction 2.24) is endothermic ($\Delta h_{rxn}>0$). In the presence of $H_3PO_4$ (Reaction 2.25), the liquid phase hydrolysis of MPDA becomes exothermic ($\Delta h_{rxn}<0$). The molar extent of reaction for very dilute systems, i.e., water to MPDA mole ratio = 2100, in Reaction 2.24 and 2.25 respectively is calculated by assuming the aqueous species to be in a 1molal ideal solution as shown in Equations 2.26 and 2.27. The activity coefficients of the organic compounds for the solute-solute interactions are assumed to be approximately equal. The extent of the reaction is given by $X$. Subscripts $1$ and $2$ respectively refer to reactions MPDA → MAP and

MAP → resorcinol. The term $W$ represents the number of moles of water added initially to 1 mole of MPDA. Values chosen for $W$ are 2100 and 100 to give water to MPDA ratios of 2100:1 and 100:1. Although water to MPDA ratios of 100:1 would not satisfy the assumption of a dilute solution, it has been included for the sake of completeness. In the presence of phosphoric acid, the amount of water present is unimportant as long as the ratio given by the activity coefficients does not deviate too strongly from unity. The term $A$ in equation 2.27 represents the number of moles of phosphoric acid initially added to the MPDA. Since 2mole $H_3PO_4$ is required to convert 1mole of MPDA to resorcinol, values chosen for $A$ are greater than 2. The equilibrium constant for a certain reaction temperature is calculated using Equation 2.21 and assuming a constant heat of reaction, $\Delta h_{rxn}$, given in Table 2.4.

$$K_{a,1} = \frac{(X_1 - X_2)(X_1 + X_2) * 1000}{(1 - X_1) * W * 18} \quad \text{and} \quad K_{a,2} = \frac{X_2(X_1 + X_2) * 1000}{(X_1 - X_2) * W * 18} \qquad \textbf{2.26}$$

$$K_{a,1} = \frac{(X_1 - X_2)(X_1 + X_2)}{(1 - X_1)(A - X_1 - X_2)} \quad \text{and} \quad K_{a,2} = \frac{X_2(X_1 + X_2)}{(X_1 - X_2)(A - X_1 - X_2)} \qquad \textbf{2.27}$$

According to Equation 2.26 and Figure 2.9 the equilibrium extent of Reaction 2.24 is strongly dependent on the initial water to MPDA mole ratio. Essentially, the same general observations hold true for the MPDA conversion in the aqueous phase as for the gaseous phase. Nevertheless, for the same water to MPDA mole ratios, i.e., 2100:1, a lower equilibrium MPDA conversion and resorcinol yield is obtained for the aqueous phase than for the same reaction in the gaseous phase. Since the heat of reaction in Equation 2.21 has been taken as a constant, alterations of solute-solute activity coefficients for the case when the initial water to MPDA mole ratio equals 100:1 would not lead to any improvement in the accuracy in predicting the equilibrium extent of the reaction.

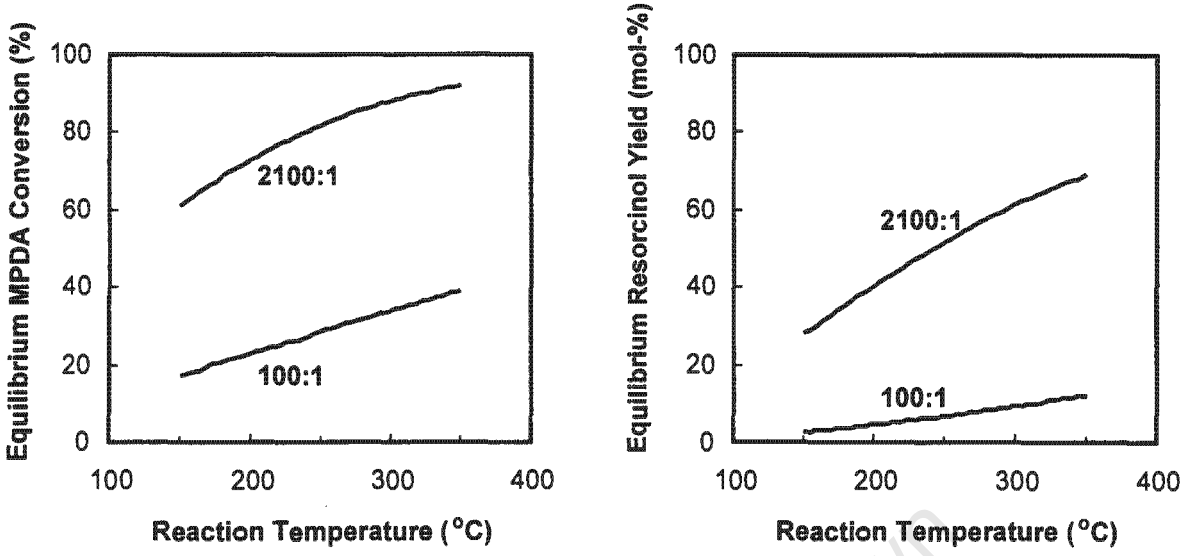


**Figure 2.9** Equilibrium conversion of MPDA (A) and molar yield of resorcinol (B) for the catalytic conversion of MPDA in aqueous phase (Reaction 2.24).

Reaction 2.25 goes essentially to completion if the initial $H_3PO_{4(aq)}$ to $MPDA_{(aq)}$ (dilute solutions) is 2 with the resorcinol yield at 150°C equalling 99.5% and at 350°C equalling 97.8%. Any initial $H_3PO_{4(aq)}$ to $MPDA_{(aq)}$ value greater than 2 results in an increase in the equilibrium resorcinol yield. A similar phenomenon is observed when assuming the phosphoric acid and its corresponding ammonium salt to remain a ***solid*** throughout the reaction. Thus, the equilibrium resorcinol yield should also approach 100% in the presence of a heterogeneous polyphosphate reagent.

## 2.1.3 OVERALL REACTION PATTERN FOR TRANSFORMATION OF MPDA

Apart for the hydrolysis of MPDA being a set of consecutive reactions with resorcinol being formed via the intermediate MAP, ample side-reactions in the form of polymerisation reactions can occur. A simplified version of possible poly-

merisation reactions is illustrated in Figure 2.10. Analogous reactions not shown in Figure 2.10 would in effect result in a vast array of dimerisation and polymerisation side products with the aryl-groups being bonded by –NH– or –O– bridges.

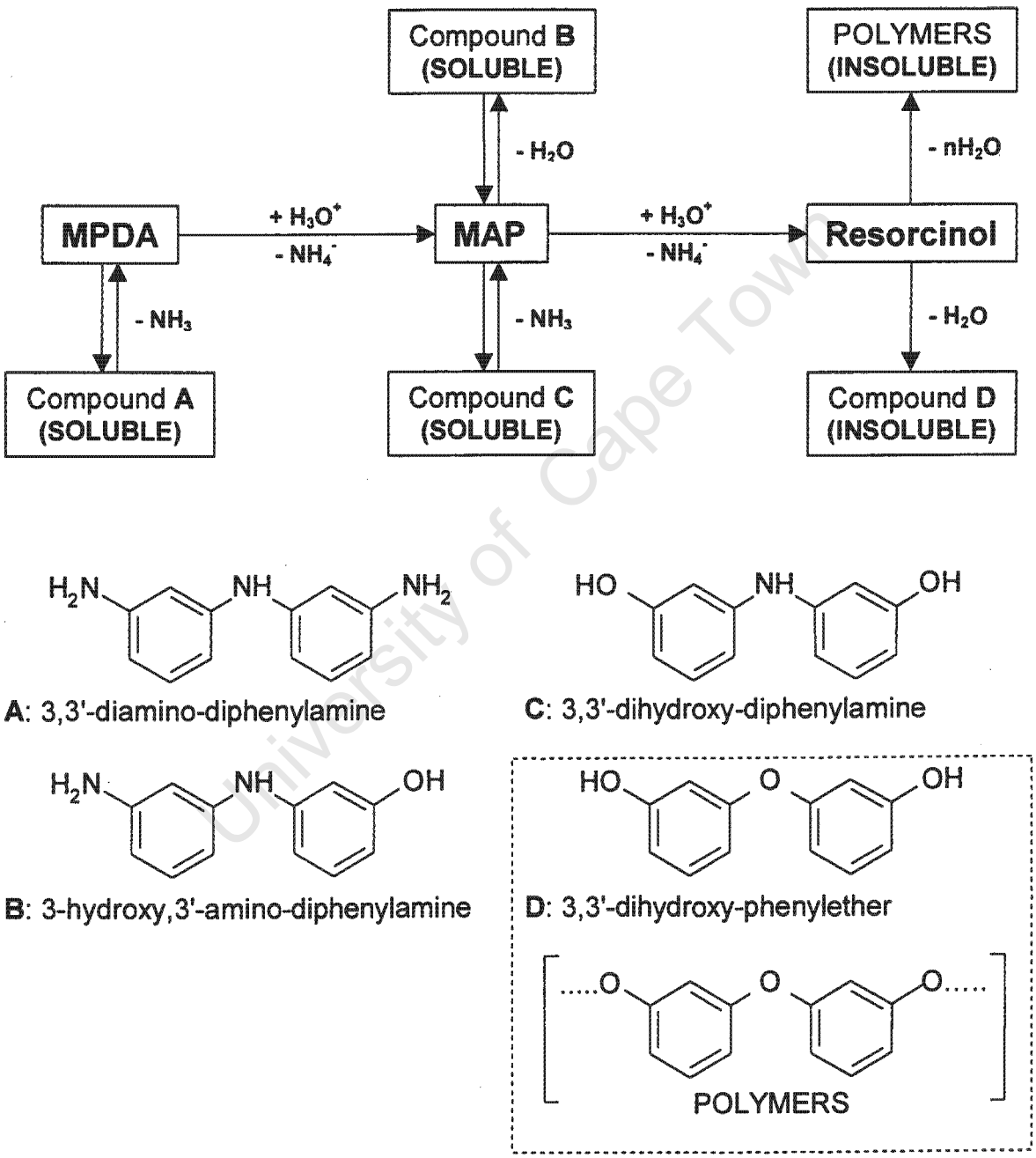


**Figure 2.10** Overall simplified reaction mechanism for hydrolysis of MPDA to produce Resorcinol [developed at AECI Ltd. (South Africa)].

The ether formation is found to be essentially irreversible. In addition, ethers are far less soluble in water than the polyphenylene-amines. The diphenylamines can undergo acid cleavages to form hydroxylated benzenes. Thus, the reaction mechanism illustrated in Figure 2.10 is not entirely correct since the breaking of the -NH- links is more likely to occur via acid hydrolysis than it being reversible.

## 2.1.4 HOMOGENEOUS REAGENTS

First attempts to produce resorcinol from aqueous MPDA in the presence of mineral acids such as hydrochloric acid, stannous chloride and sulphuric acid were carried out at the end of the 19$^{th}$ century [Greco, 1968]. All the experimental conditions resulted in low yields of resorcinol in admixture with substantial amounts of tarry resins. This observation came to no surprise, since the difunctional properties of resorcinol, MPDA as well as the intermediate product meta-aminophenol (MAP) allows for the polymerisation to various resins to take place in the presence of strong acids and bases. This route was abandoned until Greco [1968-1972] furthered the investigation by using sulphuric acid, phosphoric acid and ammonium bisulphate.



**Sulphuric acid**: Resorcinol can be produced in significant amounts when operating the autoclave within a certain temperature range (180°C – 230°C). At temperatures above 250°C sulphuric acid is transformed into an oxidising agent due to the formation of $SO_2$ [Musso, 1967]. The reaction, however, must not go to completion and the removal of resorcinol from solution needs to take place before any substantial polymerisation, i.e., etherification, of resorcinol can occur. The mole ratio of MPDA to sulphuric acid needs to be kept between 1.2 and 2.2 to ensure satisfactory conversion of MPDA and the neutralisation of sulphuric acid to lower the rate of resorcinol polymerisation. The optimum resorcinol yield (~75%) is obtained employing a 1.8 $H_2SO_4$ to MPDA mole ratio and keeping the reaction temperature at 220°C [Greco, 1968].

**Phosphoric acid**: Unlike sulphuric acid, the mole ratio of phosphoric acid to MPDA is no longer critical as long as enough acid is available to ensure complete conversion of MPDA. High resorcinol yield (~95%) is obtained by maintaining the reaction temperature between 170°C and 250°C. This was ascribed to the unique feature of phosphoric acid, i.e., only the primary hydrogen in phosphoric acid is strong enough and the formed dihydrogen ammonium phosphate salt can act as an inhibitor in the formation of resorcinol polymers [Greco, 1969].

**Ammonium bisulphate**: The MPDA hydrolysis can also be carried out by contacting the MPDA with at least four moles ammonium bisulphate per mole of MPDA in aqueous solution and temperatures of 200°C to 300°C [Greco, 1972]. The formed salt $(NH_4)_2SO_4$ can be regenerated to ammonium bisulphate by heating the salt melt to 310°C – 450°C [Young, 1978]. Similar to phosphoric acid, minor quantities of polymers are produced.

By comparing the ionisation constants (see Table 2.5) of the mineral acids used by Greco [1968 – 1972], it is clearly illustrated that the acid strength is a major criterion for generating resorcinol in high yields. The stronger the acid, the larger the expected driving force towards resorcinol due to the acid-base reaction that involves the formation of ammonium ions (see Reaction 2.18). Acids with low $pK_a$ values also tend to be become more hydrophilic [Shriver *et al.*, 1994]. Depending on the $H_2SO_4$ concentration towards the end of the MPDA to resorcinol reaction, the hydrophilic property of the sulphuric acid leads to the transformation of resorcinol to polymer ethers since a maximum of one water molecule is liberated per two –OH functional groups. Since the $pK_a$ values of ammonium-bisulfate and phosphoric acid are greater than zero, the ether formation from resorcinol should not occur. Consequently, the statement made by Greco [1969] that the formed $(NH_4)H_2PO_4$ when using $H_3PO_4$ acts as an inhibitor during the formation of resorcinol polymers is incorrect.

**Table 2.5 Acidity constants for species in aqueous solution at 25°C [Shriver *et al.*, 1994]**

| Acid | HA | $A^-$ | $K_a$ | $pK_a$ |
|---|---|---|---|---|
| Sulphuric | $H_2SO_4$ | $HSO_4^-$ | $10^2$ | -2 |
| Hydronium ion | $H_3O^+$ | $H_2O$ | 1 | 0.0 |
| Hydrogensulphate ion | $HSO_4^-$ | $SO_4^{2-}$ | $1.2 \times 10^{-2}$ | 1.92 |
| Phosphoric | $H_3PO_4$ | $H_2PO_4^-$ | $7.5 \times 10^{-3}$ | 2.12 |
| Dihydrogenphosphate ion | $H_2PO_4^-$ | $HPO_4^{2-}$ | $4 \times 10^{-8}$ | 7.4 |

Furthermore, the mineral acid used for the conversion of MPDA to resorcinol should not be able to act as an oxidising agent. Thus, acids like $HNO_3$ are unsuitable since MPDA, a known antioxidant, is oxidised readily. The use of $H_2SO_4$ above 250°C presents a similar scenario due to the transformation of $H_2SO_4$ to $SO_2$, which is also an oxidising agent.



## 2.1.5 PROBLEMS / PROPOSALS

From the information gathered out of literature, the MPDA acid hydrolysis reaction to resorcinol are solely conducted in the aqueous phase using water as a reactant and solvent. Typical mineral acids considered are $H_2SO_4$, $H_3PO_4$ and $(NH_4)HSO_4$ with which resorcinol of high yields can be obtained (200°C - 300°C) [Greco, 1968 - 1972]. The simplistic equilibrium studies performed on the acid hydrolysis of aqueous MPDA in the liquid phase in the presence of $H_3PO_4$ (see Section 2.1.3) reveal that in the absence of any polymerisation side-reactions very high resorcinol yields are attainable (99.5% at 150°C; 97.8% at 350°C). If the mineral acids are, however, excluded from the reaction mixture, appreciable equilibrium resorcinol yields are only attainable for highly dilute solutions, as shown in Figure 2.9. Even with the initial water to MPDA ratio equal to 2100:1, the resorcinol yield in the absence of any mineral acid at 350°C is ca. 69% in admixture with the intermediate MAP (23%) and the reagent MPDA (8%).

Therefore, a purely catalytic conversion of MPDA to resorcinol renders itself uneconomical. By comparison of Figure 2.7 and 2.8, a similar conclusion can be derived for the conversion of MPDA to resorcinol in the gas phase.

Nevertheless, the use of mineral acids poses many economical and environmental disadvantages. The mineral acids considered for the hydrolysis of MPDA to resorcinol are highly corrosive at reaction temperature (200°C - 300°C) making the process quite capital intensive. Since MPDA in solution with mineral acids leads to the added production of metal/amine complexes when exposed to stainless steel or monel metal, the autoclave reactor cannot be constructed from the usual metal of choice. Instead, alternative metals are required that often result in greater capital expenditures. Separation and drying of the neutralised mineral acid from the reaction product solution is energy intensive and requires for the disposal of the inorganic salt by-product. The corrosive nature of mineral acids may also pose work-environmental disadvantages due to its inconvenient handling ability in the case of spillage, etc.



The use of water insoluble, large surface area heterogeneous acids could rectify the above-mentioned shortcomings experienced with mineral acids and may serve as a replacement for the aqueous mineral acids. Since the acid sites are confined to a heterogeneous surface, the acid corrosion of construction materials and the formation of metal/amine complexes are unlikely. Additionally, solid acids ease and simplify the separation processes in that no neutralisation and drying steps are required. Solid acids also present safer handling than liquid mineral acids [Venuto, 1994].

The objective of the investigation is to replace the corrosive and hazardous homogeneous mineral acids previously required for the MPDA hydrolysis with a regenerable / reusable, heterogeneous acid such as aluminosilicates (e.g. zeolites) and zirconium phosphates. Thereby, the theoretical E-factor calculated for the MPDA hydrolysis reaction improves from 2.09kg by-products per kg

resorcinol when using $H_3PO_4$ to just 0.31kg ammonia per kg resorcinol in the presence of a truly regenerable solid reagent. The pore structure of the zeolites is thought to aid in suppressing the condensation side reactions by exerting control over the reaction selectivity.

## 2.2 ZEOLITES

Zeolites are three-dimensional crystalline aluminosilicates consisting of arrays of corner-sharing $SiO_4$– and $AlO_4$–tetrahedra linked via the oxygen atoms. The aluminosilicate framework is built up by sharing all vertices of the $SiO_4$– or $AlO_4$–tetrahedra so that the ratio O/(Si + Al) = 2. The occurrence of $Al^{3+}$ in place of $Si^{4+}$ in an aluminosilicate renders a net negative charge on the zeolite framework. An additional cation, such as $H^+$, $Na^+$, or $½Ca^{2+}$, is therefore required to neutralise the negative charge created by each Al atom replacing a Si atom. Consequently, the unit cell formula can be represented by:

$$M_{x/n}[(AlO_2)_x(SiO_2)_y] \cdot wH_2O \qquad \text{[Flanigen } et\ al.\text{, 1991]} \qquad \textbf{2.28}$$

where $n$ represents the valency of cation M. The term M is generally a Group I or Group II ion, although other cations can also balance the negative charge created by the presence of Al in the structure. The variables $x$ and $y$ depict the total number of tetrahedra per unit cell and $w$ corresponds to the number of water molecules sorbed per unit cell within the intercrystalline void [Breck, 1974]. The number of $AlO_4$–tetrahedra that can be incorporated into the zeolite structure can vary considerably. However, according to the Löwenstein's empirical rule the Si/Al ratio is always greater than 1 since the $AlO_4$–tetrahedra has to be linked to four $SiO_4$–tetrahedra [Haber, 1981].

Crystalline aluminosilicates, i.e., zeolites, have an open structure with regular apertures of molecular dimensions, thereby allowing only molecules into their pore structure that are smaller in diameter. Different arrangements of the $SiO_4$– and $AlO_4$–tetrahedra allow the formation of large varieties of zeolite structure types with uniform cavities and unique differential sizes and shapes. Since each zeolite variety is defined by a crystal structure, the cages, pores and channel sizes are highly regular and of precise dimensions.

Apart from the aforementioned cations required to neutralise the negatively charged aluminosilicate framework, small guest molecules such as water are also accommodated within the zeolite structure, as illustrated in Formula 2.28. The presence of water in the zeolite structure allows for cations to be easily exchanged with those in the surrounding solution, e.g., $NH_4^+$. The ability for zeolites to act as ion-exchangers and as molecular sieves of great thermal stability allows for their use in shape-selective heterogeneous catalysis. By choosing a corresponding ion-exchanger the adsorptive and catalytic properties of the zeolite is modified. Therefore, fully incorporating $NH_4^+$ ions into the zeolite structure by ion-exchange followed by subsequent thermal decomposition of $NH_4^+$ into $NH_3$ results in the remaining protons screening the negative charge on the $AlO_4^-$ tetrahedra. Thereby, Brønsted acid centres [Haber, 1981] are formed, which can be useful for the heterogeneous synthesis of resorcinol from meta-phenylenediamine. Since the presence of water within the zeolite structure is important for the formation of resorcinol from meta-phenylenediamine, zeolites with low Si/Al ratios are chosen due to their strongly polar anionic frameworks. The protons screening the framework aluminium thus create strong local electrostatic fields that interact with highly polar molecules such as water.



## 2.2.1 ZEOLITE PORE STRUCTURE

Zeolites are subdivided into small-, medium- and large-pore zeolites, depending on the number of tetrahedral $SiO_4$– and $AlO_4$–members required for creating the largest pore aperture. Small pore zeolites with 8-membered ring channels sorb only linear molecules such as n-paraffins and primary alcohols. These zeolite structures, commonly consist of large cages with access only through the 8-membered rings. The pore channel systems of 10-membered rings such as ZSM-5 are of uniform dimension in the absence of any cage structures. The structures of the Beta zeolite and that of the Faujasite zeolites such as X and Y zeolites are large pore zeolites, consisting of 12-membered rings, able to sorb larger

molecules [Venuto, 1994]. Key structural properties for some of the zeolites are described in Table 2.6.

**Table 2.6 Channel systems of some commonly known zeolites [Venuto, 1994]**

| Molecular Sieve Type | Structure type code | Ring size of channels | Pore size of largest channel (Å) | Channel system dimensionality |
|---|---|---|---|---|
| ***Small pore*** | | | | |
| Linde Type A | LTA | 8-8-8 | 4.1 | 3 |
| Erionite | ERI | 8-8-8 | 3.6 x 5.1 | 3 |
| ***Medium* pore** | | | | |
| ZSM-5 | MFI | 10-10-10 | 5.3 x 5.6 | 3 |
| ZSM-22 | TON | 10 | 4.4 x 5.5 | 1 |
| ***Large pore*** | | | | |
| Faujasite/X/Y | FAU | 12-12-12 | 7.4 | 3 |
| Beta | BEA | 12-12 | 7.6 x 6.4 | 3 |
| Mordenite | MOR | 12-8 | 6.5 x 7.0 | 2 |



### 2.2.1.1 STRUCTURE OF ZSM-5

ZSM-5 crystallises predominantly with orthorhombic symmetry [Meier *et al.*, 1996], although monoclinic symmetries have also been observed [De Vos Burchart *et al.*, 1993]. The framework of ZSM-5 contains two perpendicularly intersecting 10-ring channel systems that form a three dimensional network. The one channel system is straight running parallel to the [010] plane with near-circular (5.3 x 5.6Å) pore openings, while the other sinusoidal channel system is parallel to the [001] plane with elliptical openings (5.1 x 5.6Å). This is illustrated in

Figure 2.11. At the intersection of the two channels, a free volume of ca. 9Å diameter is created. This larger volume may be significant in catalysis in terms of product selectivity as well as catalyst deactivation [Derouane and Vedrine, 1980; Derouane, 1980].

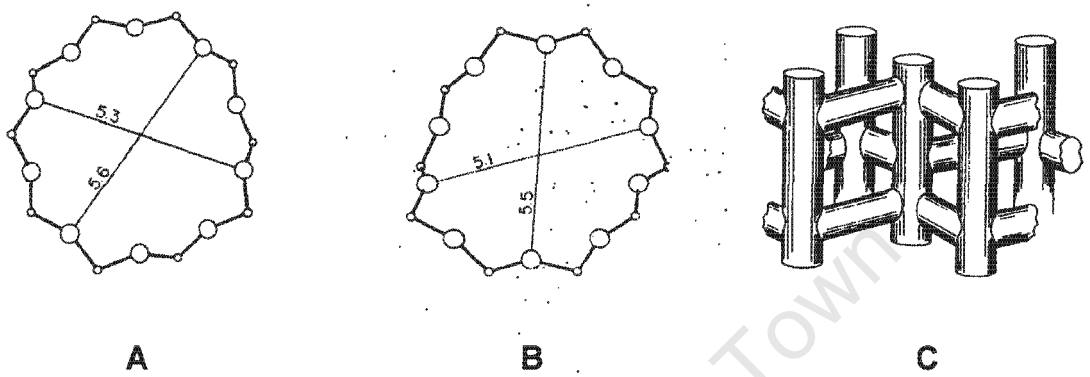


**Figure 2.11** Illustration of ZSM-5 zeolite pore dimensions of the straight channel system (A) and the sinusoidal channel system (B) [Meier *et al.*, 1996]. Illustration (C) depicts the intersecting straight and sinusoidal channel system of ZSM-5 zeolite [Meier *et al.*, 1978].



### 2.2.1.2 STRUCTURE OF A FAUJASITE

The faujasite zeolites crystallise with cubic symmetry [Meier *et al.*, 1996]. The pore channel system of the zeolite consists of a very open, three-dimensional network made up of sodalite units or cages (see Figure 2.12C) that are linked together via their hexagonal faces by hexagonal prisms as illustrated in Figure 2.12B. This arrangement produces supercages of roughly spherical dimensions with a diameter equalling 11.4Å. Access to these supercages is restricted by 7.4Å pore openings. Typically, one supercage is able to accommodate 5.4 benzene molecules at 25°C [Venuto, 1994]. The sodalite cages and the hexagonal prisms make up a small-pore system that gives access to only small molecules such as water and ammonia.

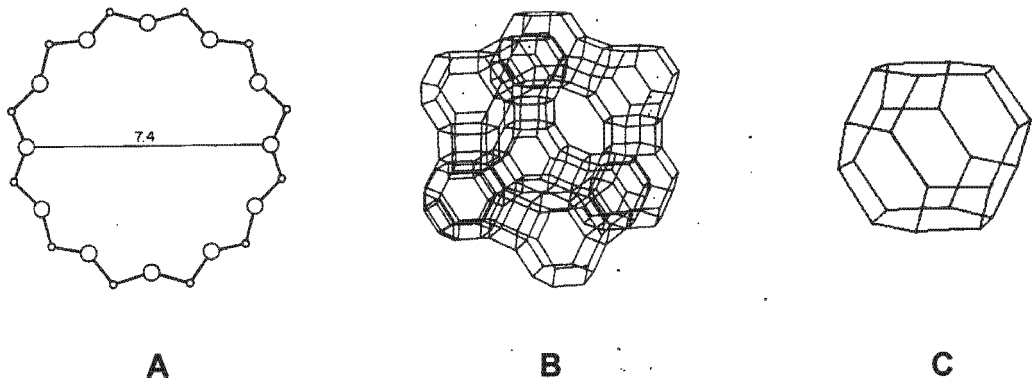


**Figure 2.12** Pore dimensions (A) giving access to a supercage of the faujasite structure (B) that is built up by sodalite cages (C) [Meier *et al.*, 1996].



### 2.2.1.3 STRUCTURE OF ZEOLITE BETA

Zeolite Beta is a large pore zeolite containing a fully three-dimensional 12-membered ring pore system, opening into channels [Ratnasamy *et al.*, 1989]. Zeolite Beta crystallises in both tetragonal and monoclinic symmetry. Due to the channel system of zeolite Beta, molecules that are able to penetrate the 12-ring channel openings can subsequently interact with all acid sites present within the pore structure of the zeolite [Higgins *et al.*, 1988].

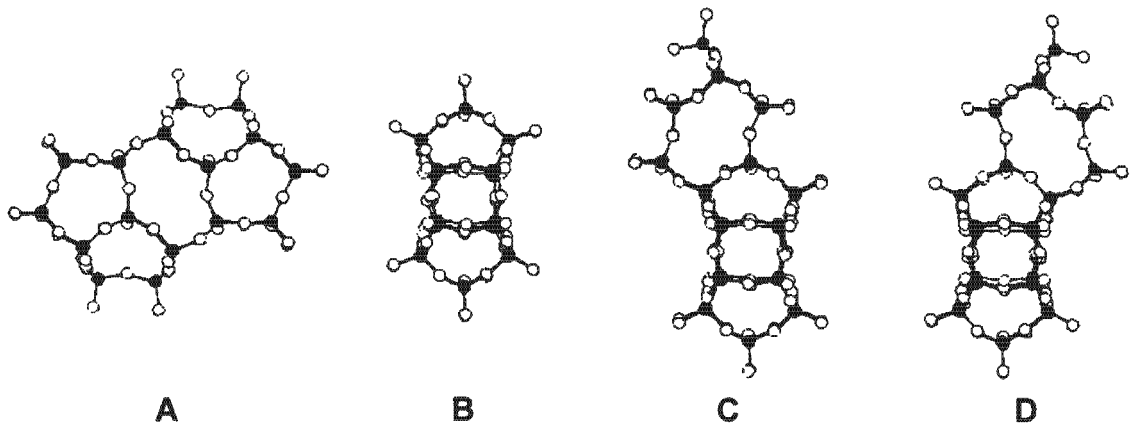


**Figure 2.13** Front (A) and side view (B) of the centrosymmetrical, tertiary structural building unit of zeolite Beta. A second, perpendicular 6-ring is added to create an object with left-handed (C) and right-handed (D) symmetry. (Al and Si atoms, solid circles; O atoms, open circles) [Treacy and Newsam, 1988].

The framework of zeolite Beta consists of intergrown hybrids of three distinct but closely related structures that are arranged in layers [Treacy and Newsam, 1988]. All three structures are constructed from the same basic structural building unit as illustrated in Figure 2.13. Figure 2.14 shows the three possible morphologies (Polymorph A, B and C) obtained by different arrangements of the centrosymmetrical tertiary building unit (Figure 2.13A). The three polymorphs in Figure 2.14 are revealed by simultaneously observing the left- or right-handed arrangement of the 6-ring along the [100] and the [010] projections; with structures B and C representing an enantiomorphic pair. The 12-membered ring channels along these two projections are identical and linear [Higgins *et al.*, 1988] with the pore size corresponding to 7.6 x 6.4Å [Meier *et al.*, 1996]. The framework structure of zeolite Beta is, however, disordered along the [001] plane due to stacking faults arising because of successive layers having to interconnect in either a left- or right-handed fashion, and both modes of linkage occur with almost equal probability [Treacy and Newsam, 1988]. Nevertheless, a large sorption capacity of about 0.2ml/g is maintained. The third 12-membered ring

channel along the [001] projection is nonlinear with pore dimensions equal to 5.5 x 5.5Å [Meier, *et al.*, 1996].

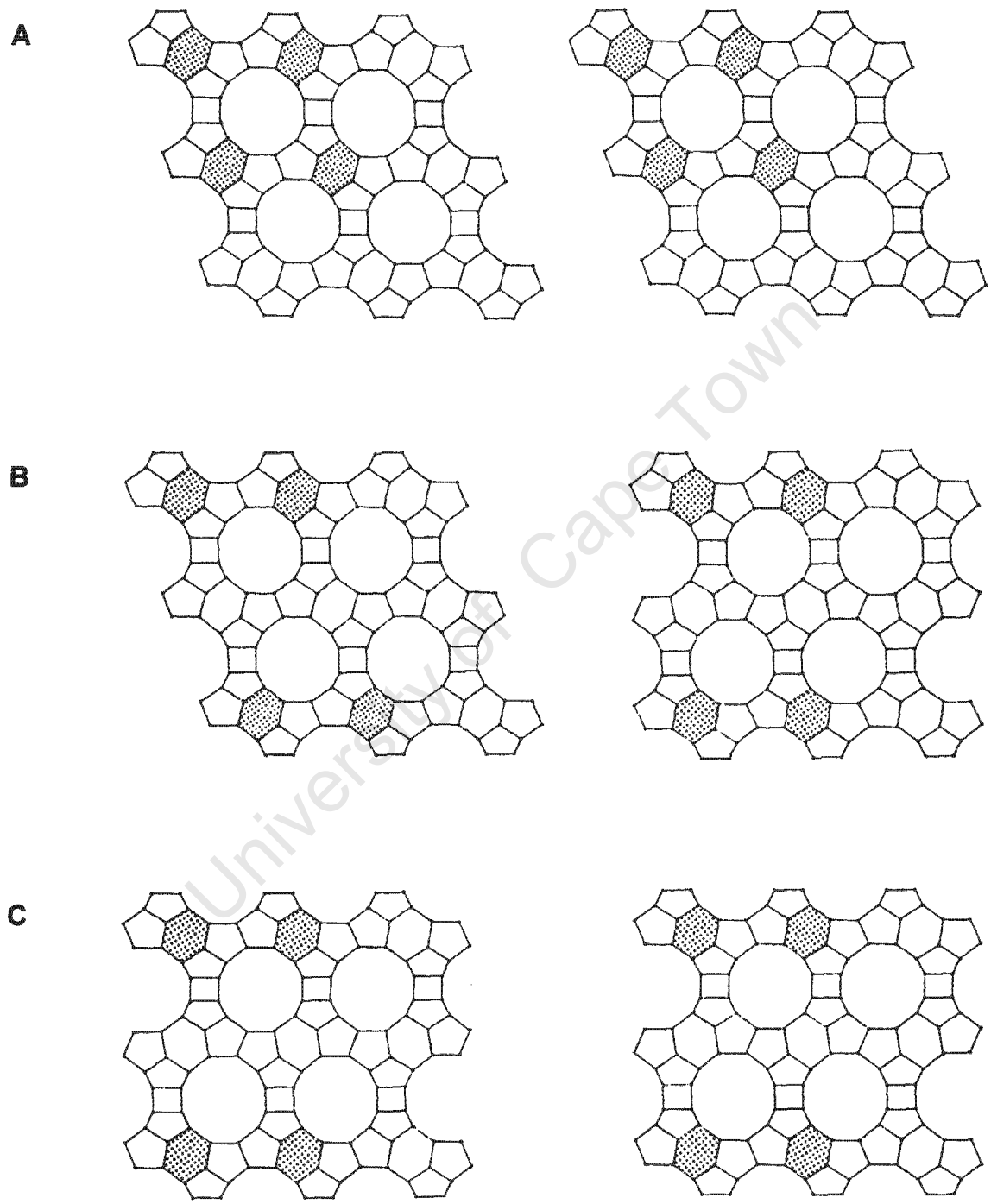




**Figure 2.14** Zeolite Beta structures A, B and C with the plane [100] illustrated on the left and the [010] projection shown on the right.

## 2.2.2 ACIDITY OF ZEOLITES

The electrical imbalance between the metal oxygen stoichiometry due to the substitution of Al in the silicon-oxygen structure is countered by the presence of a cation. This is clearly seen in Figure 2.15, where some $Si^{4+}$ of the neutral $SiO_2$ molecular sieve structure is selectively substituted with framework $Al^{3+}$. Due to the incorporation of $Al^{3+}$ the overall zeolite framework becomes negatively charged which needs to be compensated by metal cations or protons that respectively constitute Lewis- or Brønsted-acid sites. Zeolites are usually synthesised in the sodium-form. Brønsted acidity is created by ion-exchanging the sodium with ammonia followed by a 400-500°C calcination in order to obtain the proton form as illustrated below.

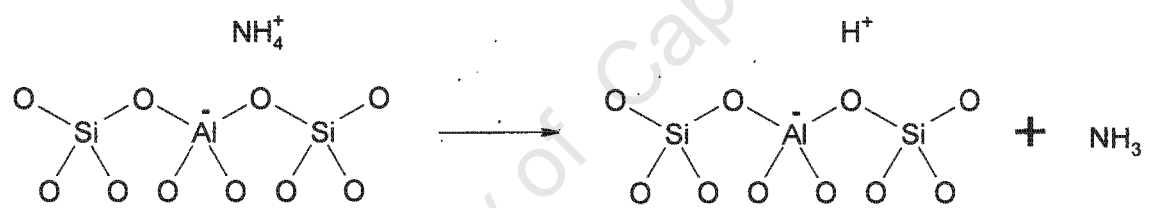


**Figure 2.15** Formation of Brønsted acid site centres via the thermal treatment of the ammonium exchanged aluminosilicate.

Intuitively, the O-H bonds in Figure 2.15 are thought to be of an ionic nature since the cations neutralising the zeolite framework charge are readily ion-exchanged. However, strong evidence exists that the hydroxyl groups in zeolites possess predominantly covalent characteristics [Kazansky, 1991]. The proton attached to the oxygen atom connecting the neighbouring silicon and aluminium atoms result in the formation of a three-coordinate oxygen atom, creating relatively weak OH bonds [Van Santen, 1994]. Therefore, the protonic acid centres formed in Figure 2.15 are classified as very strong Brønsted acid centres, comparable to 98% $H_2SO_4$ [Venuto, 1994].

The Brønsted acid strength is dependent on a number of factors such as the aluminium concentration, location and distribution of the aluminium species as well as the overall zeolite framework. Kazansky [1994] observed that the covalent OH interaction-energy varies little with acidity and concluded that the acid strength is mainly dependent on the stabilisation of the negative charge left on the aluminosilicate framework upon deprotonation. The proximity of the aluminium tetrahedra largely affects the lattice stability. It is shown that if the $AlO_4$–tetrahedra are separated by at least two $SiO_4$–tetrahedra, no significant framework destabilisation should occur [Dempsey, 1974]. Based on IR measurements, Barthomeuf [1980] established that for Si/Al ratios greater than 6, the $AlO_4$–sites may be assumed to be adequately separated provided that these negative aluminium centres are evenly dispersed throughout the crystal. Van Santen [1994] observed that the dominant effect controlling the OH bond-strength depends on the proton concentration with the strength of the Brønsted acidity increasing with decreasing proton concentration. The proton concentration can be altered by either maintaining a low framework aluminium concentration or by poisoning some Brønsted acid sites with sodium, thus changing them into Lewis acid sites, which provide additional stability to the framework.

The stability of the overall zeolite structure also affects the strength of the acid sites. Since the framework of ZSM-5 is more stable than Beta or Faujasite Y, the acid strength of the framework hydroxyls are expected to be greatest in ZSM-5 [van Santen, 1994]. The acid strength of the bridging hydroxyl groups is found to be in following order: ZSM-5 > Beta > Y, derived by observing the shift in the relevant O-H frequency upon adsorption of benzene [Hedge *et al.*, 1989]. Similar observations are made with $NH_3$-TPD [Katada *et al.*, 1997]. The lower acid strength is also partially a result of the lower Si/Al ratios observed for H-Beta and H-Y zeolites. The Si/Al ratio of the ZSM-5 zeolite structure ranges between ca. 20 and 8000 while that of Beta and the Faujasite is below 20, with the Si/Al ratio of Faujasites approaching 1 [Venuto, 1994]. A further reason for the greater framework stability of ZSM-5 is explained by the even distribution of the $AlO_4$–

tetrahedra throughout the structure [Dempsey, 1974; van Santen, 1994]. Thus, the Brønsted acid sites in the ZSM-5 structure are chemically homogeneous, regardless of the Si/Al ratio [Topsoe *et al.*, 1981], consisting primarily of Si(1Al) and Si(0Al) [Fyfe *et al.*, 1984]. Regarding the ZSM-5 structure, the Si(2Al) are generally only observed for Si/Al<10 with the probability for one framework aluminium atom to be in an Al-O-Si-O-Al arrangement being less than 5% [Brunner, 1989].

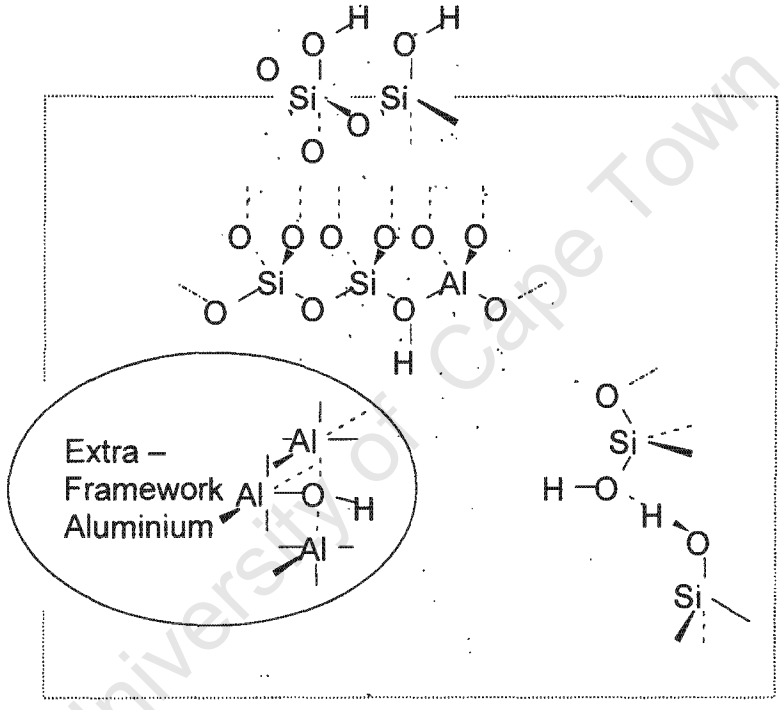


**Figure 2.16** Illustration of different types of Brønsted acid sites found within a zeolite [redrawn from Sauer, 1989]

Demonstrated in Figure 2.16 are the different types of hydroxyl groups encountered within a zeolite structure. The schematic view of a zeolite microcrystallite illustrates the nonacidic SiOH terminal hydroxyl groups found on the outer surface and bridged acidic SiOH observed on the walls of the micropores [Woolery *et al.*, 1986; Brunner *et al.*, 1989; Sauer, 1989]. Evidence is also presented for the formation of weakly acid AlOH groups due to the formation

of extra-framework or non-framework aluminium species. The thermal activation of $NH_4$-zeolite under mild conditions leads to the formation of isolated octahedrally coordinated extra-framework alumina. These species are typically found in the supercages of H-USY and the channel intersections for the case of H-ZSM-5. Protonated zeolite Y also contain isolated tetra-coordinated extra-framework aluminium species within their sodalite cages [Beyerlein *et al.*, 1997; Campbell *et al.*, 1996].

The effect of non-framework aluminium species on the development of strong Brønsted acid sites in protonated zeolites is shown to be of importance. Nevertheless, the interaction of framework and non-framework aluminium is not well understood. There are suggestions, that the freed framework aluminium species interact with some of the Si-O-Al to form Lewis sites in much the same way as the Group I and II cations, thus providing added stability to the zeolite crystal structure [Beyerlein *et al.*, 1997]. Therefore, according to Van Santen [1994], the acid strength of the remaining Brønsted acid sites should increase, as is generally observed. The enhancement of the activity of the zeolite is thus explained on the basis of an interaction of Brønsted acid sites with that of Lewis sites due to the extra-framework aluminium (EFAl) species.



## 2.2.3 INTERACTION OF WATER WITH ZEOLITES

The adsorption of water on Brønsted acid sites of zeolites has been studied extensively by means of powder neutron diffraction [Smith, 1996], IR [Pelmenschikov, 1993] and $^1H$ NMR [Haase, 1994] spectroscopic analyses as well as quantum chemical ab initio techniques [Haase, 1994; Krossner, 1996]. Although the formation of aqua-oxonium ions ($H_3O^+ \cdot H_2O$) are observed for water being adsorbed onto dehydrated HY zeolites, the presence of hydronium ions on strongly acidic H-ZSM-5 has been the subject of some dispute [Marchese, 1993].

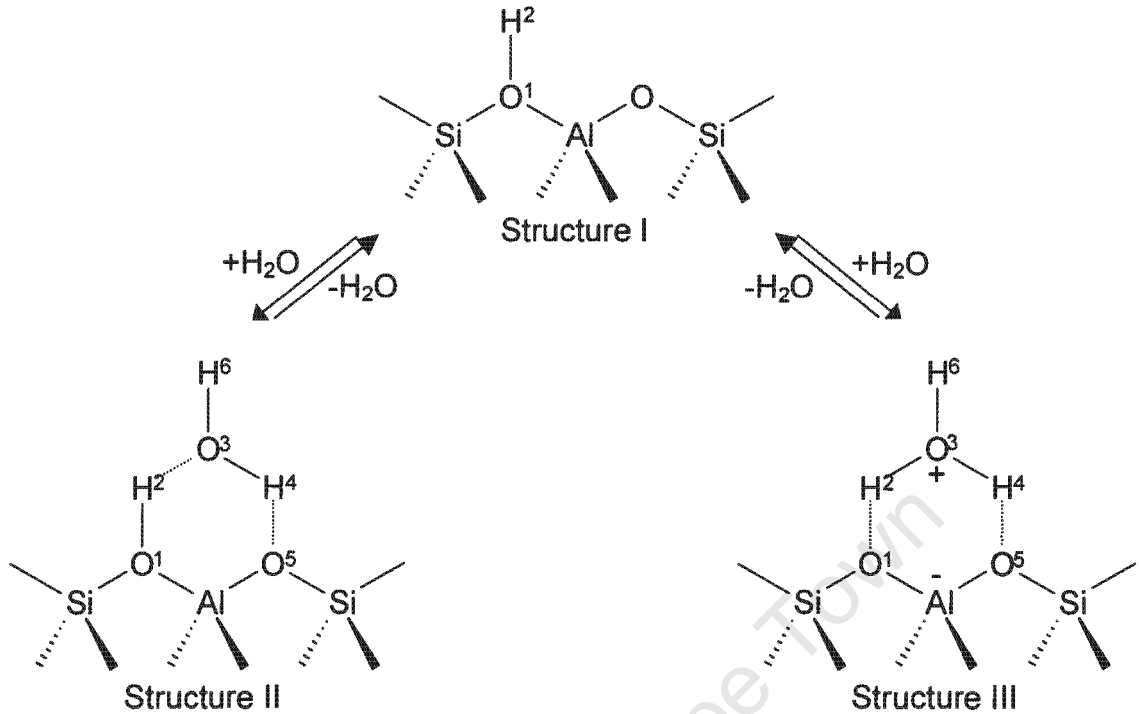


**Figure 2.17** Illustration of the adsorption of water onto a bridged hydroxyl group (Structure I) by either hydrogen bonding of the water molecule (Structure II) or the formation of a hydronium ion that screens the framework aluminium species (Structure III) [Marchese *et al.*, 1993].

Depicted in Figure 2.17 are two possible adsorption structures for water. Structure II in Figure 2.17 illustrates a neutral water molecule being attached to the Brønsted acid site via two hydrogen bonds. Structure III shows the manner in which the adsorbed water molecule is protonated and thus coordinated via two protons to the negatively charged zeolite framework site. Nevertheless, recent interpretations of spectroscopic data and computational studies tend to suggest that hydrogen bonded water molecules have to be present to assist in the stability of the oxonium structure [Krossner, 1996]. Therefore, the formation of oxonium species [$H_3O^+ \cdot nH_2O$] is only possible for higher water loadings [Haase, 1994]. Chen [1978] observed that principally four water molecules adsorb onto each tetrahedrally coordinated aluminium site within the zeolite Mordenite. This

implies that the oxonium structure could consist of one hydronium and 3 hydrogen bonded water molecules. Further observations revealed that if the $SiO_2/Al_2O_3$ ratio is below 10, the framework aluminium concentration is high enough such that the whole crystalline void volume is occupied by water [Chen, 1978]. It is likely that at low water coverage, only very strongly hydrogen-bonded water complexes prevail on the Brønsted acid site with hydronium ions themselves being absent [Pelmenschikov, 1993].

Apart for the phenomena observed for the oxonium water complexes, water molecules also interact with other polar sites residing within the zeolite cavities. Such sites include silanol groups (≡SiOH) that are quite often created by zeolite defects. The concentration of extra framework aluminium species also affects the amount of water attracted to the zeolite structure [Chen, 1978; Campbell,1996]. Experimental work conducted on H-ZSM-5 involving $^{18}O$-exchange with bridging oxygen in liquid water at 95°C suggests that Si-O-Si and Si-O-Al bridges cleave under rather mild conditions [Von Ballmoos and Meier, 1982].

Water does, however, not interact with the homopolar (≡Si-O-Si≡) bonds [Chen, 1976] since these bonds are hydrophobic. This implies that the hydrophobicity of a zeolite is dependent on the Si/Al ratio since high Si/Al ratios result in more (≡Si-O-Si≡) bonds. For example, zeolites such as H-Y, which typically has a low Si/Al ratio, has many Brønsted acid sites with hydronium ions more readily formed. In contrast, zeolite H-ZSM-5 that normally has less framework aluminium generally presents itself as being of a more hydrophobic nature [Marchese, 1993].

## 2.2.4 DEALUMINATION OF ZEOLITES

Water has a significant influence on the dealumination of framework aluminium sites leading to the formation of extra-framework aluminium species (EFAl). This influences the stability of the zeolite framework [Brunner *et al.*, 1989]. Although

the Brønsted acid activity and framework stability is increased upon mild steaming at moderate temperatures, serious breakdown of the zeolite structure occurs upon severe steaming and very high temperatures. This is shown during extensive studies for ZSM-5 [Brunner *et al.*, 1989; Campbell *et al.*, 1996] and Faujasite Y [Wang *et al.*, 1991] zeolites.

Engelhardt *et al.* [1983] observed that only aluminium atoms associated with $NH_4^+$ and $H^+$ cations (and not $Na^+$) can be removed by hydrolysis from the zeolite framework. Wang *et al.* [1991] showed that the migration of the extra framework aluminium species (EFAl) to the outer surface of the zeolite crystal is only possible in the presence of water. Therefore, water can play a significant role in the destabilisation of the zeolite crystal structure. The expulsion of Al atoms from framework T-sites is given in Figure 2.18. In a second step, the vacancies created by the expulsion of Al from the lattice are refilled to a large extent by Si atoms migrating from the collapsed portion of the crystal. Although there is only limited consensus regarding the mechanism of the Si replacement / 'healing' process, it is generally agreed that if this 'healing' did not occur the entire crystal would collapse prematurely. This would not correspond to the observed phenomena, which amongst others include a shrinking unit cell size and increasing hydrothermal stability [Beyerlein *et al.*, 1997].

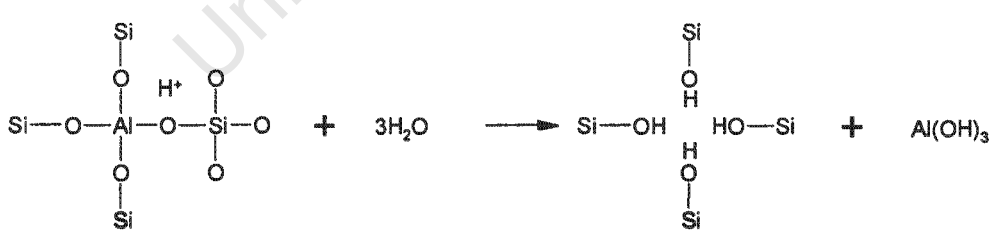


**Figure 2.18** Schematic representation for the dealumination of a protonated zeolite [Beyerlein *et al.*, 1997].

From extensive kinetic work by Wang *et al.* [1991] on the dealumination of the Faujasite Y zeolite, the rate law governing the removal of framework aluminium is found to be 1$^{st}$ order. Two distinct periods of dealumination are observed, namely

an initial one in which dealumination is rapid and a second one in which dealumination is slow. The first period (Equation 2.29) would correspond the dealumination of the protonic zeolite and the second period (Equation 2.30) to that of the zeolite exchanged cationic aluminium species. Correspondingly, Equation 2.30 describes the rate of dealumination of USY (Ultra Stable Y) zeolites for a given temperature (Kelvin) and water vapour pressure (kPa) with $N_{Al}$ representing the number of framework aluminium tetrahedra. The time is expressed in hours:

$$\frac{-dN_{Al}}{dt} = 0.6e^{-2400/T} N_{Al} p_w^{0.5} \qquad \textbf{2.29}$$

$$\frac{-dN_{Al}}{dt} = 10.5e^{-8350/T} N_{Al} p_w \qquad \textbf{2.30}$$



## 2.2.5 ADSORPTION OF AMMONIA

Since ammonia itself is a base, it readily neutralises (poisons) the strong Brønsted acid sites. Chemisorption also occurs on Lewis acid sites, however, the strength of the adsorption depends on the type of cation present at the bridging Si-O-Al oxygen. For instance, Warawdekar and Rajadhyaksha [1987] noticed that the acid strengths measured for various cation exchanged zeolite Y show the following trend: NaHY > CuNaY > CrNaY > CaNaY > NaY. Ammonia interacts less strongly with the surface silanol (Si-OH) groups because of the weak Brønsted acidity realised on silanol hydroxyl groups. The adsorption strength of ammonia onto the silanol groups is comparable to ammonia adsorbing on a sodium exchanged zeolite [Topsoe *et al.*, 1981].

## 2.2.6 ADSORPTION OF ORGANIC COMPOUNDS

The larger molecular diameter of meta-phenylenediamine (MPDA), meta-aminophenol (MAP) and resorcinol prevents these molecules from accessing certain parts of the zeolites, e.g., the sodalite cages in faujasites. Even the 5.3 x 5.6Å aperture of the medium pore zeolite structure of ZSM-5 could not accommodate the organic compounds if it were not for a certain degree of structural flexibility. Dessau [1980] concluded on the basis of available sorption data at 20°C that molecules having minimum elliptical cross-sections greater than 6.4 x 6.9Å would be excluded from the interior of ZSM-5 zeolites. Based on the findings of Dessau [1980], the organic compounds relevant to this study should be able to access the ZSM-5 channel structure since the molecular size of MPDA is calculated at 6.6 x 4.8Å. Since the ZSM-5 zeolite structure needs to adapt to the incoming meta-substituted benzene structures, the configurational diffusivities of these molecules are expected to be relatively low. In liquid phase adsorption stripping the incoming molecule off its hydrating water needs to be taken into account when considering the uptake of the organic molecule from aqueous solutions in zeolites.

Strong adsorption of benzene onto the surface of large-pore zeolites has been documented [Venuto, 1994]. Hopkins [1973], and Freeman and Unland [1978] observed that the adsorption of benzene onto Lewis acid sites is stronger than on the hydroxyl groups. Meta-phenylenediamine (MPDA), meta-aminophenol and resorcinol have the tendency to adsorb end-on via the polar –OH and $–NH_2$ functionalities rather than the $\pi$ electron system of the aromatic nucleus as observed for benzene [Warawdekar and Rajadhyaksha, 1987]. The basic nature of the $–NH_2$ group results in very strong interactions with the acid sites (see Figure 2.19A). Some aminobenzenes, such as aniline, tend to adsorb even more strongly onto the zeolite surface than ammonia [Katada *et al.*, 1997]. Infrared spectroscopic studies conducted on the adsorption of phenol onto Brønsted acid sites at 300°C led Katada *et al.* [1997] to suggest that phenol (–OH groups)

adsorbs onto non-acidic sites such as oxygen anions, since the IR adsorption bands depicting the acid hydroxide frequencies were unaffected by the adsorption of phenol. According to Katada *et al.* [1997], the acidity of phenol allows it to adsorb onto oxygen anions. Nevertheless, these findings are contradictory to the ideas of Parton *et al.* [1988], suggesting that the phenol taken up from aqueous solution interacts so strongly with the Brønsted acid sites of H-ZSM-5 (Si/Al = 19) that pore mouth-blockages occur at ambient temperature. It is also postulated that phenol, a weak acid, is being weakly adsorbed perpendicularly to the zeolite surface by H-bonding at a neighbouring site via its hydroxyl group as shown in Figure 2.19B [Venuto, 1994]. Phenolic compounds generally desorb above 204°C [Venuto and Wu, 1966].

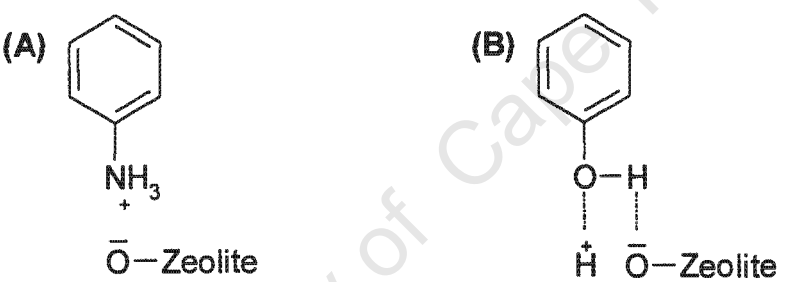


**Figure 2.19** Possible adsorption of aniline (A) and phenol (B) onto a zeolite Brønsted acid site [Venuto, 1994].



## 2.2.7 USE OF ZEOLITES FOR MPDA TO RESORCINOL

Based on the thermodynamic investigation in Section 2.1.2.1, the adequate conversion of MPDA to resorcinol is only possible in the presence of a co-reacting reagent (acid) that ensures the removal of ammonia from the reaction fluid and serves as a thermodynamic driving force towards the formation of resorcinol. Consequently, for the conversion of MPDA to resorcinol, zeolites can only be employed as heterogeneous reagents and not as catalysts. The very strong Brønsted acid sites present on the aluminosilicates have already been compared to that of 98% $H_2SO_4$ [Venuto, 1994]. This results in the very strong

adsorption of ammonia (see Section 2.2.5) and amine functional groups (see Section 2.2.6). If upon adsorption of MPDA onto a Brønsted acid site via the -$NH_2$ functional group the MPDA is converted in the presence of a water nucleophile to a phenolic compound, the resulting ammonia would remain chemisorbed while the weak heat of adsorption of the formed phenolic compounds (see Section 2.2.6) constitutes their removal from the heterogeneous surface into the bulk solution. Thus, the reaction temperature needs to be high enough to ensure the adequate ease of desorption of the phenolic compounds while at the same time preventing the removal of the chemisorbed ammonia.

Although the preferred adsorption interaction between the relevant compounds and the zeolite Brønsted or cationic acid sites occur via the polar –OH and –$NH_2$ functionalities, the adsorption options for these aromatic nuclei are considerably enhanced since the 'flat' adsorption via the benzene $\pi$-electrons is also possible [Venuto, 1994]. The resulting ability for the aromatic nuclei to act as either an electrophile or a nucleophile allows for bimolecular reactions to take place. Additionally, the catalytic activity for bimolecular reactions is strongly dependent on relatively high acid site concentration to ensure a high concentration of reactants in the pores of the zeolites that favour these types of reactions [Feast and Lercher, 1996]. Enhanced activities have been reported [Warawdekar and Rajadyaksha, 1996] for H-zeolites partially exchanged with Group I, II and transition metal (multicationic) species. The zeolite facilitates nucleophilic substitution of aromatics by electron withdrawal from the aromatic ring via coordination on the metal cations [Freeman and Unland, 1978]. The manner in which the aromatic compound interacts with the acid sites is also highly dependent on the temperature [Venuto, 1994].

Ensuring the presence of water within the zeolite structure tends to be vital for the successful hydrolysis of MPDA to product resorcinol since water serves as a reactant as well as a solvent, thus preventing the zeolites from serving as a pure host-lattice or organic compound concentrating "vessel". Therefore, in the

presence of a suitable solvent, less side-reactions should occur in the liquid phase. As mentioned in Section 2.2.3, the hydrophilic nature of a zeolite depends on maintaining a low framework Si/Al ratio. The leaching and migration of aluminium species from the zeolite framework can result in the formation of extra-framework alumina-species and Lewis acid sites. The formed species could promote the formation of diphenyl-compounds since the commercial formation of diphenylamine (from aniline) is carried out in the vapour phase employing an alumina or silica-alumina catalyst [Warawdekar and Rajadhyaksha, 1987]. Consequently, investigations into reactions with MPDA and high surface area γ-alumina are required to check for possible polymerisation side-reaction. An amorphous silica-alumina catalyst will also be employed for the conversion of MPDA to resorcinol to identify whether a crystalline zeolite pore structure has any effect on the shape selectivity towards resorcinol in preventing dimerisation or polymerisation side-reactions.

## 2.3 ZIRCONIUM PHOSPHATES

Zirconium phosphates are layered compounds, consisting of covalently bonded planar macromolecules, known as lamellae, that are held together by van der Waals bonds between the adjacent layers. Similar to aluminosilicates, the framework of zirconium phosphates is negatively charged with counterions, e.g., $H^+$ and $Na^+$, balancing the fixed charges present within the zirconium phosphates. Whereas the fixed charges present in aluminosilicates originate by the isomorphous substitution of $Si^{4+}$ with $Al^{3+}$, the localised fixed charges present on the zirconium phosphate layers are due to ionogenic phosphate groups attached to the planar macromolecule [Alberti and Costantino, 1996]. Since the fixed ionogenic phosphate groups on the macromolecular plane are essentially constituents of mineral ortho-phosphoric acid, it would be intuitive that, like with phosphoric acid, resorcinol of high yield and selectivity is produced in the presence of zirconium phosphates. The ability for zirconium phosphate layers to swell should allow for easy access of the incoming MPDA molecule to an active site. Zirconium phosphates are also regarded as being thermally stable and highly water insoluble compounds, which further assists in justifying their successful use as heterogeneous acids for the hydrolysis of MPDA to resorcinol.



### 2.3.1 ZIRCONIUM PHOSPHATE STRUCTURES

The structures of the two most frequently studied layered zirconium phosphates are that of $\alpha$-$Zr(HPO_4)_2{\cdot}H_2O$ and $\gamma$-$Zr(PO_4)(H_2PO_4){\cdot}2H_2O$. Both types of zirconium phosphates are crystalline compounds, comprising of planar macromolecules that are packed and held together via van der Waals forces between the adjacent layers. As illustrated in Figure 2.20, the distance between the barycentres of two adjacent macromolecular sheets or lamellae is known as the 'd-spacing', 'interlamellar distance', 'interlayer distance', interlayer spacing' or 'basal spacing'. The 'gallery height' or the 'free distance' refers to the distance

between two adjacent macromolecular sheets or lamellae, obtained by subtracting the layer thickness from the interlayer distance. The space between the layers is called the 'interlayer region' [Alberti and Costantino, 1996].

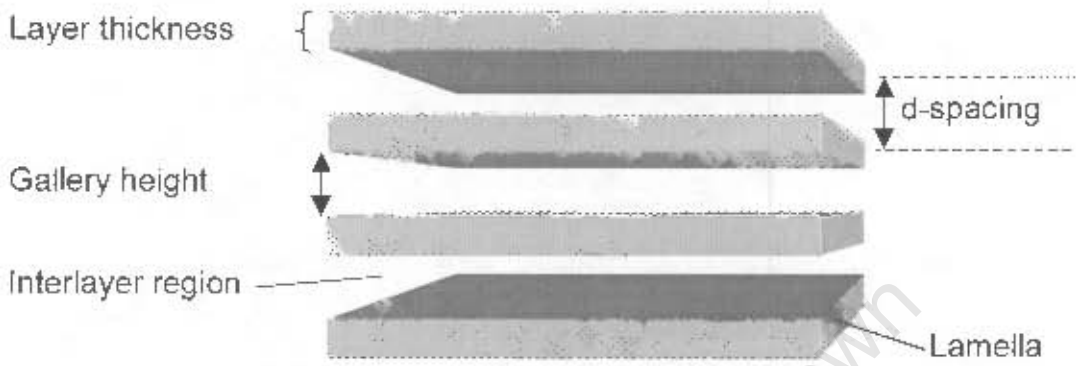


**Figure 2.20** Schematic illustration of some definitions and important characteristics of layered zirconium phosphates [redrawn from Alberti and Costantino, 1996]

The total surface area $A_s$ (area per gram) of a layered compound is easily calculated from Equation 2.31 [Alberti and Costantino, 1996]. Depending on the chosen dimensions of the unit cell, $M_c$ represents the formula weight of the unit cell (g/mol); *ab* the lamellar surface area of one side of the unit cell; and $n$ the number of such sites exposed to the interlayer region. $N_A$ is the Avogadro constant.

$$A_s = \frac{N_A(ab)^* n}{M_c} \qquad \textbf{2.31}$$

Since the total surface area cannot be determined by $N_2$-BET due to the contraction of the interlayer distance upon degassing, Equation 2.31 is vital for determining the surface area of layered compounds. Clearfield and Djuric [1978] observed that the crystallinity of zirconium phosphates is related to the measured

BET surface area, with highly crystalline $\alpha$-$Zr(HPO_4)_2 \cdot H_2O$ samples giving a surface area of $2.4 m^2/g$ as a result of only the outermost lamellae being exposed towards $N_2$ adsorption. The surface area of low crystalline samples is approximately 72 to $237 m^2/g$. For structures with unknown cell parameters, the total surface area may be estimated by means of the density, $\rho$, and the interlayer distance, $d$, of the layered compound [Alberti and Costantino, 1996]:

$$A_s = 2 * (\rho d)^{-1} \qquad \textbf{2.32}$$

The homogeneous distribution of active sites within zirconium phosphates allows for the accurate determination of the area available per active site, also known as the 'free area':

$$\text{free area} = \frac{A_s * FW}{a * N_A} \qquad \textbf{2.33}$$

where $FW$ is the molecular formula weight and $a$ the number of equivalents of active sites per $FW$. The 'free area' is important for the adsorption as well as the reaction study determining the maximum amount of guest molecules able to intercalate or adsorb. Generally, if the size of the guest molecules is larger than the 'free area' of the active sites, a full stoichiometric intercalation is not achieved.

A further important parameter is the 'layer charge density', $\rho_c$, describing the number of elementary charges per unit surface area, with $C$ presenting the number of electrons per one Coulomb charge.

$$\rho_c = (\text{free area})^{-1} * C \qquad \textbf{2.34}$$

### 2.3.1.1 STRUCTURE OF $\alpha$-$Zr(HPO_4)_2 \cdot H_2O$

Crystalline layered $\alpha$-$Zr(HPO_4)_2 \cdot H_2O$ was first synthesised by Clearfield and Stynes [1964] by boiling amorphous zirconium phosphate gel in concentrated phosphoric acid (10 – 12mol/L) for several days. Clearfield and Smith [1969] solved the monoclinic crystal structure of $\alpha$-$Zr(HPO_4)_2 \cdot H_2O$ using single-crystal diffraction data. However, the preparation of high-quality $\alpha$-$Zr(HPO_4)_2 \cdot H_2O$ crystals via the HF direct precipitation method allowed for the refinement of the $\alpha$-zirconium phosphate structure yielding cell dimensions: $a$ = 9.060Å, $b$ = 5.297Å, $c$ = 15.414Å and $\beta$ = 101.71°, space group $P2_1/n$ [Troup and Clearfield, 1977]. Accordingly, the interlayer distance equals 7.55Å with the formula weight per unit cell $M_c$ equalling 4 times the molecular formula weight $FW$. The unit cell volume (725.7Å$^3$) is calculated with the density equalling 2.78g/cm$^3$ (Equations 2.31 and 2.32).

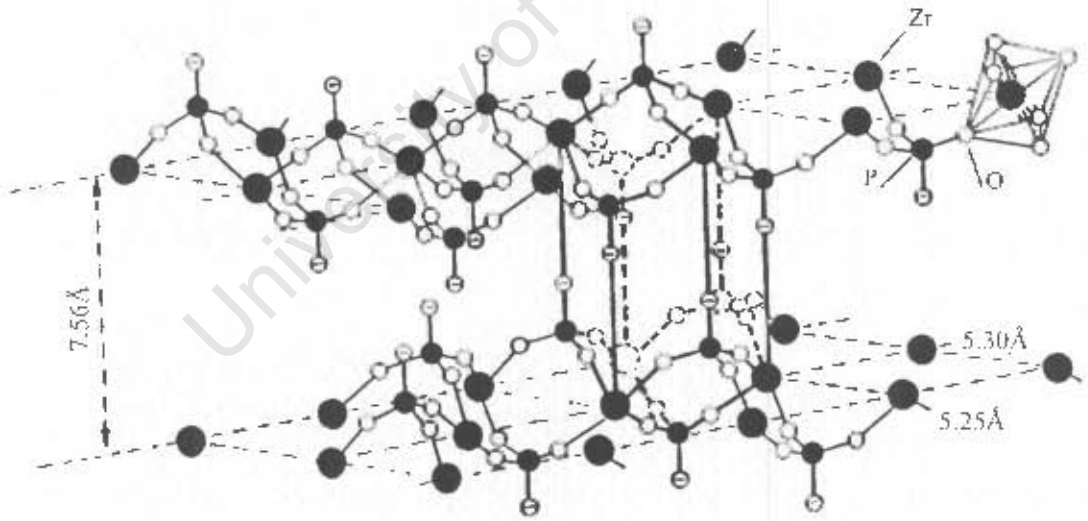


**Figure 2.21** Idealised crystal structure of $\alpha$-zirconium phosphate with solid lines illustrating one of the cavities created by arrangement of the layers; protons and water molecules are omitted [Clearfield and Costantino, 1996].

The layer structure of $\alpha$-$Zr(HPO_4)_2 \cdot H_2O$ consists of zirconium atoms lying above and below (± 0.25Å) the mean plane [Clearfield, 1984] and are bridged by tetrahedral $PO_3(OH)$ phosphate anions. The phosphate groups are situated alternately above and below the metal plane, with three oxygen atoms of each phosphate group being linked to three zirconium atoms. Consequently, each zirconium atom is surrounded by a slightly distorted octahedron of oxygen atoms belonging to six different phosphate groups. The fourth oxygen per phosphate group bears a negative charge that is balanced by an ion-exchangeable proton with the resulting acid OH group pointing towards the nearest neighbouring layer.

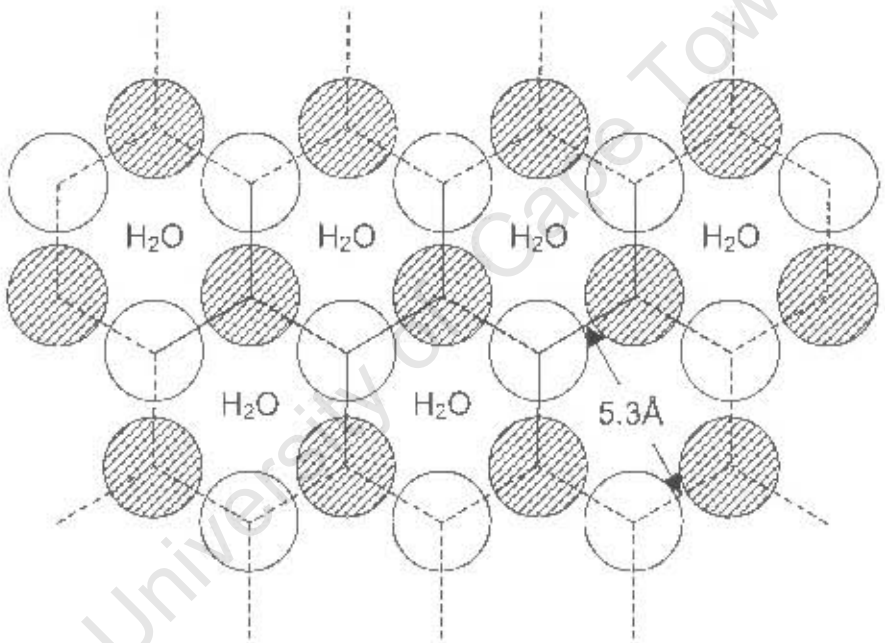


**Figure 2.22** Schematic projection perpendicular to the crystal axis c, showing negatively charged oxygen atoms of two facing sides of adjacent layers forming zeolitic cavities, with each cavity accommodating one water molecule. Shaded and open circles respectively refer to oxygen atoms lying above and below the intermediate plane [redrawn from Alberti and Costantino, 1974 and 1984].

Adjacent layers are displaced relative to one another, producing a stacking arrangement where the phosphorus atom of one layer is placed directly above

the zirconium atom in the layer below [Clearfield and Smith, 1969]. Consequently, as shown in Figure 2.22, the negatively charged oxygen between facing sides of two adjacent layers form an intermediate plane with the oxygen anions being arranged in a hexagonal fashion. Stacking of the layers, as illustrated in Figure 2.21, leads to the formation of small cavities that are interconnected by windows whose maximum diameter is 2.64Å [Troup and Clearfield, 1977], thus preventing molecules of diameters greater than 2.64Å from entering the interlayer region. In essence, the number of these small cavities corresponds to the number of zirconium atoms. Each cavity accommodates one hydration water molecule with the water being hydrogen bonded to three of the acid phosphate groups on the same layer. The water molecules interact with three adjacent phosphate groups, accepting two hydrogen bonds and giving a third one. The other proton on the water points into the cavity of an adjacent layer and undergoes no hydrogen bonding. Thus, the layers are only weekly held together by dispersion forces. α-Zirconium phosphate, unlike other clays, does not undergo infinite swelling when suspended in water. Troup and Clearfield [1977] ascribed this to the strong binding of the layers to the high degree of crystallite perfection. However, Dyer and Leigh [1972] attributed this phenomenon to the very high lattice charge or layer charge density, $\rho_L$ = $4.12*10^{14}e^{-}/cm^2$ [Alberti and Costantino, 1996]. Application of Equation 2.31 yields a lamellar surface area of $965m^2g^{-1}$. The corresponding 'free area' associated with each =P-OH group equals $24.0Å^2$ (Equation 2.33). The total / maximum ion exchange capacity for $\alpha$-$Zr(HPO_4)_2{\cdot}H_2O$ is 6.64mequiv. per gram, which is slightly less in the presence of impurities [Clearfield, 1993].

### 2.3.1.2 STRUCTURE OF $\gamma$-$Zr(PO_4)(H_2PO_4){\cdot}2H_2O$

The preparation of a second planar macromolecule, termed γ-zirconium phosphate, having the same chemical composition as $\alpha$-$Zr(HPO_4)_2{\cdot}H_2O$ but

different structure was first reported by Clearfield *et al.* [1968]. The synthesis of crystalline γ-zirconium phosphate involves a water soluble zirconyl salt in the presence of a mono-substituted dihydrogenphosphate, which upon refluxing for several days, yields a mono-substituted γ-zirconium phosphate salt [Alberti *et al.*, 1989]. The hydrogen form of γ-zirconium phosphate is then obtained by ion exchange. On the basis of solid-state $^{31}P$ magic-angle spinning MAS NMR spectroscopy [Clayden, 1987] and studies performed on isostructural titanium phosphate [Christensen *et al.*, 1990] the correct structural formula, i.e., γ-$Zr(PO_4)(H_2PO_4)\cdot 2H_2O$, is suggested. Therefore, the monoclinic γ-zirconium phosphate crystals consists of $PO_4^{3-}$ groups in which all the oxygen atoms are bonded to zirconium atoms as well as $H_2PO_4^-$ groups in which only two of the oxygen atoms bond to the zirconium atoms with the other two oxygen atoms bearing two acidic protons. The failure to produce γ-zirconium phosphate crystals large enough for X-ray structure determination required the use of X-ray powder diffraction resulting in slight deviations within the reported literature. The most recently accepted unit cell parameters for γ-$Zr(PO_4)(H_2PO_4)\cdot 2H_2O$ are: $a$ = 5.386Å, $b$ = 6.636Å, $c$ = 24.806Å and $\beta$ = 98.70° [Clearfield and Costantino, 1996], space group $P2_1$ and $n$ = 4 [Poojary *et al.*, 1995]. Therefore, the interlayer distance equals 12.20Å, the unit cell volume = 876.4Å$^3$ and density = 2.43g/cm$^3$. The free area surrounding each $P(OH)_2$ group on the surface of the layers equals 35.7Å$^2$, i.e., 17.8Å$^2$ if the free area is associated with each OH group on the plane. Consequently, the total lamellar surface area corresponds to 674m$^2$/g. The maximum ion exchange capacity equals 6.27mequiv./g and the layer charge density $\rho_{ic}$ is 5.60e$^-$/cm$^2$.

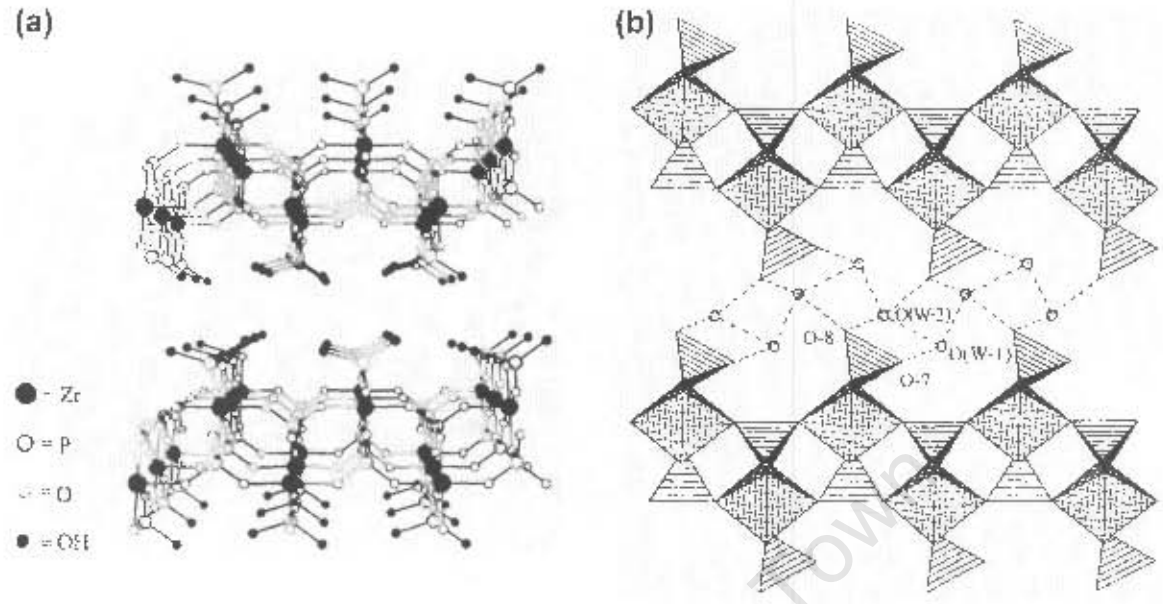


**Figure 2.23** (a) Representation of layered γ-$Zr(PO_4)(H_2PO_4)\cdot 2H_2O$ viewed down the *b*-axis with water molecules being omitted [Clearfield and Costantino, 1996]; (b) Polyhedral presentation of the γ-zirconium phosphate structure down the *a*-axis, illustrating the hydrogen bonds between the water molecules and hydroxyl groups (dashed lines) [Poojary *et al.*, 1995].

A detailed structural view is given in Figure 2.23, illustrating the octahedrally co-ordinated zirconium atoms that are surrounded by oxygen atoms originating from the $PO_4^{3-}$ and $H_2PO_4^-$ phosphate tetrahedra. All four oxygen of the $PO_4^{3-}$ group bridge across zirconium atoms with one set of bridges running parallel to the *a*-axis and another parallel to the *b*-axis, thereby joining all the zirconium atoms, setting up the raw framework structure. The central phosphate atoms within the framework phosphate group, i.e., $PO_4^{3-}$ group, are positioned alternately ca. 0.65A above and below the mean plane of a particular layer. In turn, the zirconium atoms are located ca. 1.6Å sequentially above and below the mean plane. Thus, the framework phosphate tetrahedra are sandwiched between the zirconium octahedra. The $H_2PO_4^-$ group is located on the outer periphery of the

layer utilising two of its oxygen to bridge across zirconium atoms in the *a*-direction. The other two oxygen extend into the interlamellar region, each oxygen bonded to one ion-exchangeable proton [Poojary *et al.*, 1994]. Figure 2.23(b) illustrates the manner in which the two different water molecules, i.e., W1 and W2, are hydrogen bonded towards the POH groups and towards one another, producing a zigzag chain of water molecules that runs between the dihydrogenphosphate groups. Consequently, unlike for $\alpha$-$Zr(HPO_4)_2 \cdot H_2O$, hydrogen bonds exist between the layers of $\gamma$-$Zr(PO_4)(H_2PO_4) \cdot 2H_2O$. Illustrated in Figure 2.23(b) are two four-membered rings created by hydrogen bonding. The one ring involves O(7), O(8), O(W1) and O(W2); and the other ring consists of O(8), O(W2), O(W1) and O(W2). O(7) and O(8) denote the charged oxygen present on the $H_2PO_4^-$; O(W1) and O(W2) refer to the respective oxygen residing within the water molecules [Poojary, 1995].

## 2.3.2 ADSORPTION / INTERCALATION PROCESSES

The acid sites situated between layers and on the exterior surfaces of the zirconium phosphates allow for the adsorption of Brønsted bases. The term 'intercalation' commonly refers to the adsorption of components onto acid sites positioned within the interlayer region of the zirconium phosphates. Consequently, intercalation involves the ***reversible*** insertion of guest species into the interlayer region of the zirconium phosphate host. Although the interlayer distance between a layered zirconium phosphate host changes upon intercalation of guest molecules, the macromolecular layered structure is retained [Alberti and Costantino, 1996]. The advantage of using layered compounds as opposed to the rigid 3 dimensional aluminosilicates for the hydrolysis of resorcinol from MPDA is the accommodation of larger molecules in zirconium phosphates, due to an increase in the interlayer distance. This may result in greater access of reactant MPDA onto active P-(OH) sites. The initial separation of the layers during the intercalation process requires work to overcome the

dispersion binding energy. Therefore, only if the energy for intercalation is large enough will it be possible for the layers to move apart. From the first law of thermodynamics, a change in the internal energy, $dU$, for the interlayer solution is given by

$$dU = TdS - pdV + \sum G_i^s dn_i^s + dW_p \qquad 2.35$$

The partial molar Gibbs free energy and the number of moles of species $i$ are given by $G_i^s$ and $n_i$, respectively. The additional expression, $W_p$, is the work done in spreading the layers of the zirconium phosphates to overcome the surface electrostatic forces that hold the macromolecular zirconium phosphate sheets together [Granquist and McAtee, 1963]. Since the intercalation process in layered zirconium phosphates occurs discontinuously, the term 'activation energy' is often used in literature, which generally refers to the minimum energy required for increasing the gallery height by a certain distance to allow for a particular intercalation process to occur.

The driving force for the spreading of the layers essentially involves electrostatic energetics that are created between the Brønsted acid sites and the neutral polar molecules present in the bulk solution. Apart for the electrostatic considerations, also entropic considerations are of some importance as well as stripping the incoming molecules of its hydration water. Whether or not neutral molecules will be allowed into the interlayer region of the zirconium phosphate would depend firstly on their molecular size as well as on the interlayer region of the zirconium phosphate. The spreading of the layers and the diffusion of proton accepting neutral molecules into the interlayer region of the zirconium phosphates depends on the chemical potential difference that is created between the proton rich interlayer region and the aqueous solution. This should be large enough to overcome the minimum work required in spreading the layers. Consequently, the more basic Brønsted bases (e.g., amines) in solution lead to a greater potential difference between the interlayer region and the bulk solution, and the more likely

the spreading of the macromolecular sheets becomes. The minimum work implies that the interlayer distance is minimally increased. This typically occurs when the molecules diffuse flat and parallel into the layers. Thus, the initial rate of amine uptake is slow, but after a definite induction time due to spreading of the layers, a considerable increase in the rate of uptake may occur. If the $xy$ area of the parallel oriented molecules is larger than the free area associated with each active site, not all the acid sites have been protonated and if the potential difference between the interlayer region and the solution is enough for another increase in the interlayer distance, more molecules will be able to adsorb. An increase in the interlayer distance allows for the mode of adsorption to change from a parallel orientation to a more upright position, thereby reducing any steric hindrance [Alberti and Costantino, 1984]. The maximum number of molecules able to intercalate is thus dependent on the number of active sites present and also the number of basic Brønsted functional groups situated on the incoming molecule. The molecular dimensions of the intercalate is also of importance, since this could lead to steric hindrances, as well as the chemical stability of the acid sites themselves which could lead to hydrolysis of the phosphate groups. The rigidity or flexibilty of the macromolecular layers also determines the manner in which the intercalation proceeds [Alberti and Costantino, 1996]. The two extremes are schematically illustrated in Figures 2.24 and 2.25.



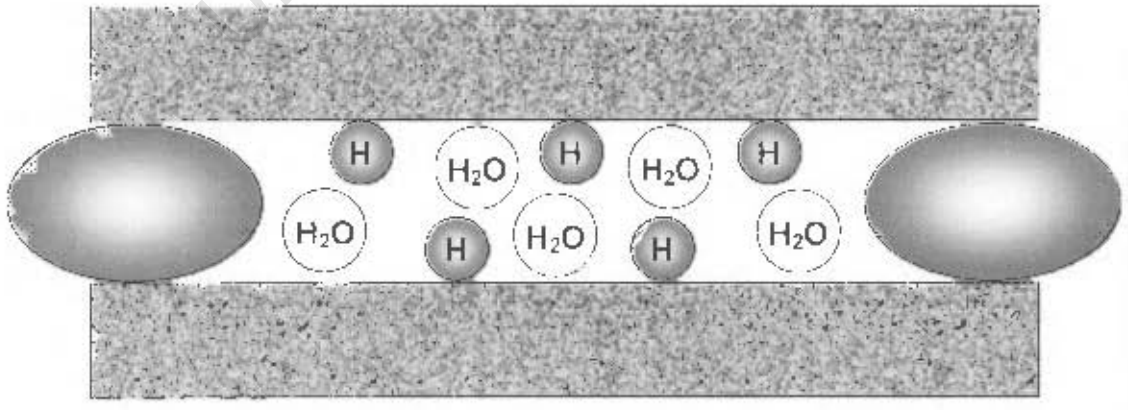


**Figure 2.24** Simplistic schematic illustration of intercalation of neutral molecules into the interlayer region of a lamellar solid with ideally rigid layers [redrawn from Alberti and Costantino, 1996].

The rigidity of the layers play an important role during the intercalation process since for highly ***rigid*** lamellae (see Figure 2.24) the enlargement of the whole interlayer region must occur, even by the insertion of only a few guest molecules. Consequently, the energy required for the initial penetration of the molecules into the interlayer region has to be large enough to enlarge the whole interlayer region at the same time. As soon as the final interlayer distance has been acquired during the initial intercalation of molecules, no more energy is needed for the enlargement and the rate of adsorption should increase considerably. The energy requirement in separating the layers is proportional to the attraction between adjacent layers, with the attraction being a function of the layer charge density $\rho_{fc}$ and the interlayer distance [Alberti and Costantino, 1996].

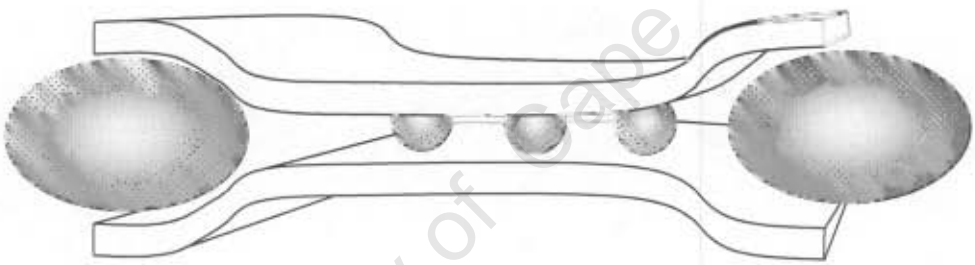

**Figure 2.25** Simplistic schematic illustration of 'moving boundary' concept during intercalation of neutral molecules into the interlayer region of a lamellar solid with ideally flexible layers [redrawn from Alberti and Costantino, 1996].



During the intercalation process of guest molecules into solids with ideally ***flexible*** layers, only the exterior portion of the interlayer region must be forced to expand, resulting in the coexistence of smaller and larger interlayer distances. Thus, there is the formation of a phase boundary between the intercalated and non-intercalated zones of the interlayer region. The phase boundary facilitates further penetration of guest molecules. As the intercalation process proceeds, the phase boundary moves towards the centre of layers. Since the initial enlargement is limited to only the external portion of the interlayer region, the

initial energy required is less than that necessary for systems with rigid layer systems. However, during the process of intercalation, integral work $\int dW_p$ has to be done in spreading the layers. The number of degrees of freedom at constant temperature and pressure is zero and thus the intercalation process must take place at constant composition of the external solution. This implies that for aqueous solutions, intercalation will occur when the pH of the external solution remains constant and the solution pH will only change once the original phase has been completely converted into the new intercalating phase [Alberti and Costantino, 1996; Costantino *et al.*, 1986].

### 2.3.2.1 INTERCALATION INTO $\alpha$-$Zr(HPO_4)_2 \cdot H_2O$

The zirconium atoms within $\alpha$-zirconium phosphates are situated nearly in a plane with only phosphate groups connecting the zirconium atoms, suggesting that the lamellae of $\alpha$-$Zr(HPO_4)_2 \cdot H_2O$ should be relatively flexible. Thus $\alpha$-zirconium phosphate may be visualised as a solid consisting of layers approaching that of a flexible layered solid. Bending of the layers therefore occurs at a distance very close to the intercalating guest molecules (see Figure 2.25) and organic compounds intercalate by the 'moving boundary' model. In this way, the full intercalation of an organic base results in a progressive saturation of active sites with discontinuous changes in the basal spacing until the fully intercalated phase is obtained. Generally, the number of phases formed corresponds to the number of different orientations that the guest molecules may assume during the formation of the fully intercalated phase. It may occur that before a given phase has been fully transformed into another, a new intercalate phase begins to form at the edge of the crystallite, resulting in more than two phases co-existing [Costantino *et al.*, 1986]. Similar behaviours are also observed upon desorption of the guest molecules or thermal dehydration of $\alpha$-zirconium phosphate.

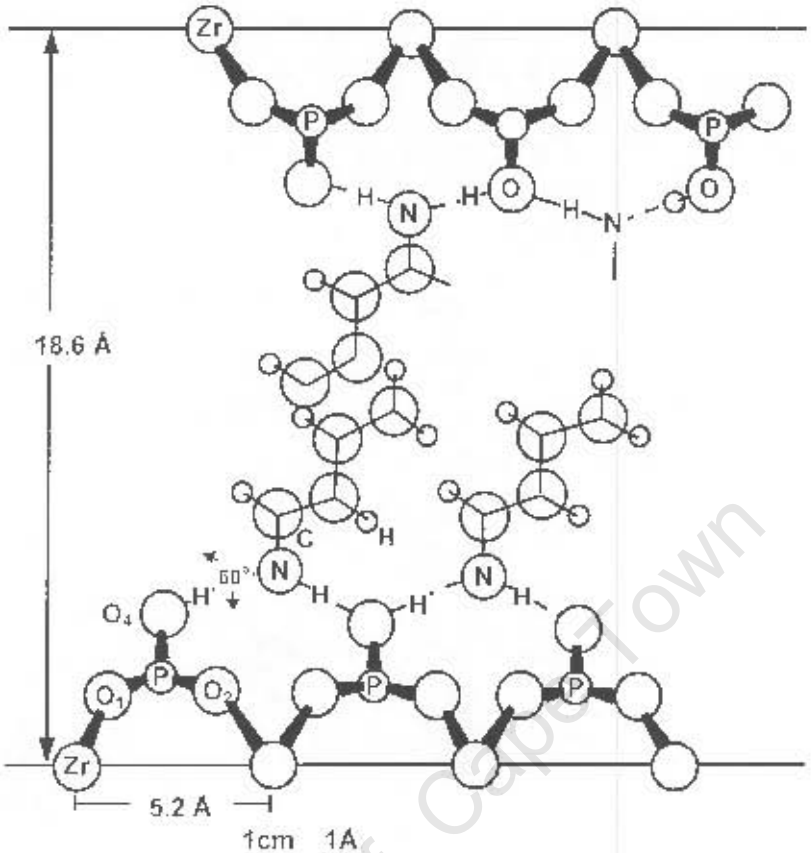


**Figure 2.26** Schematic depiction of n-alkyl-monoamine (e.g., butylamine) double layers being formed within $\alpha$-$Zr(HPO_4)_2 \cdot H_2O$ at maximum amine loading [Clearfield and Tindwa, 1977].



**(i) Intercalation of alcohols**

Very weak Brønsted bases such as alcohols, generally do not intercalate into crystalline $\alpha$-zirconium phosphate due to the electrostatic van der Waals forces holding the $\alpha$-zirconium phosphate layers together. Intercalation can only occur if the layer distance of $\alpha$-$Zr(HPO_4)_2 \cdot H_2O$ (7.55Å) is increased by forming polyhydrated zirconium phosphate salts $\alpha$-$NaH(PO_4)_2 \cdot 5H_2O$ (10.4Å) that are then treated with $HClO_4$ to remove the sodium ions [Costantino, 1979]. Another method is by exfoliation which involves regenerating alkyl amine intercalated $\alpha$-zirconium phosphate using HCl at pH~2 under vigorous stirring [Alberti *et al.*, 1985]. Also, more basic Brønsted bases such as pyridine [Yamanaka *et al.*, 1976] and imidazole and benzimidazole [Costantino *et al.*, 1986] encounter

difficulties in intercalating into the interlayer region. The intercalation ability of the latter molecules is reduced due to their bulky nature.

**(ii) Intercalation of amines**

Clearfield and Tindwa [1979] studied the intercalation of n-propylamine and n-butylamine into layered α-zirconium phosphate and showed that generally a maximum of one n-alkyl amine molecule is intercalated per acid site. A number of phase transitions of α-zirconium phosphate occur during the intercalation process (see Figure 2.27) of both components with the zirconium phosphate crystal becoming disordered during some phases, only to re-crystallise at higher loading. At maximum loading, a bilayer of the inclined n-alkyl amine is formed, in which the hydrophilic moieties are directed towards the inorganic layers, leaving the hydrophobic groups in their interlayer region. Total thermal removal of n-butylamine takes place between 280°C and 480°C [Dékány and Szirtes, 1995]

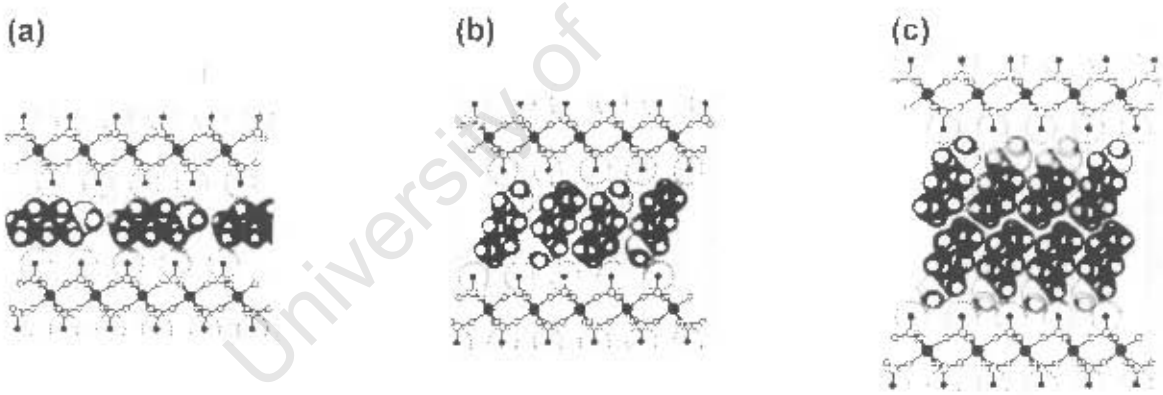


**Figure 2.27** Common orientations of n-alkyl-monoamines in the interlayer region of α-$Zr(HPO_4)_2 \cdot H_2O$: (a) alkyl chain axis parallel to the layer plane; (b) monolayer of extended molecules; (c) bilayer of extended molecules [Clearfield and Costantino, 1996].

Penetration of ethylenediamine into the α-zirconium phosphate structure occurs at an even lower pH than for n-alkyl amines. As expected, only half the number of moles of ethylenediamine could be intercalated since then the intercalated

ethylenediamine constitutes the same number of amine groups as the intercalated n-alkyl monoamines. At maximum loading, only a monolayer of extended alkyl-diamine molecules is thus expected [Clearfield and Costantino, 1996]. MacLachlan and Morgan [1990] have studied the maximum basal spacing for a range of compounds. Adsorption of ammonia from the liquid or gas phase into the interlayer region occurs in a simple step leading to the formation of α-$Zr(HPO_4)\cdot 2NH_3\cdot H_2O$ (d = 9.40Å) [Clearfield and Costantino, 1996]. Upon desorption of ammonia a partially-exchanged phase is obtained of composition $Zr(HPO_4)_2\cdot NH_3\cdot xH_2O$ with x being 0.5 or less [Clearfield and Hunter, 1976]. Aniline also adsorbs strongly with 2 moles of aniline intercalating into 1 mole of α-zirconium phosphate, forming a bilayer at maximum loading [Herzog-Cance *et al.*, 1992]. However, very large and bulky amine molecules such as crystal violet require some assistance, e.g., lower alcohols, to intercalate into α-zirconium phosphate [Hoppe *et al.*, 1997].

**(iii) Thermal desorption of guest molecules**

The 'moving boundary' model also applies to the desorption of guest molecules and hydrated water molecules upon thermal treatment. Since the removal of guest species start from the exterior parts of the intercalated α-zirconium phosphate crystal, during the desorption process the exterior layers assume a new basal spacing with a smaller interlayer distance. Thereby, the guest molecules situated towards the centre of α-zirconium phosphate lamella may become trapped [Alberti and Costantino, 1996] This is especially noticeable for larger crystals [Costantino *et al.*, 1997]. To ensure that the distance between the layers do not contract, it is often important to treat the intercalated α-zirconium phosphate first at a specific temperature for a few hours or days before heating it further. For the dehydration of water, La Ginestra *et al.* [1987] suggested keeping the solid at 180°C for 12hours before further ramping of the temperature.

### 2.3.2.2 INTERCALATION INTO $\gamma$-$Zr(PO_4)(H_2PO_4)\cdot H_2O$

The structural arrangement of the zirconium atoms in $\gamma$-$Zr(PO_4)(H_2PO_4)\cdot 2H_2O$ makes the lamella more rigid. Consequently, the 'moving boundary' concept is of far less importance for the $\gamma$-zirconium phosphate than the $\alpha$-type. Primarily only one interlayer distance is thus observed during each intercalation step. However exceptions do occur especially for larger molecules, e.g., the intercalation of 6-(2-aminopropylamino)-6-deoxy-β-cyclodextrin [Kijima, 1990]. The more widely separated lamella (12.20Å) and the more open interlayer arrangement of hydration water allows for easy access of guest molecules into the interlayer region (see Figure 2.23). The activation energies required for the individual phase transitions to occur during the intercalation process is therefore considerably less for the $\gamma$-zirconium phosphate than for the $\alpha$-zirconium phosphate. The adsorption of guest molecules principally occurs only on one of the Brønsted acid sites per $O_2P(OH)_2$ group. This would results in the formation of a monolayer adsorption of extended molecules where the steric hindrance is negligible. However, comparison of the free area (35.7Å$^2$) around each dihyodrogenphosphate with that required for accommodating two extended alkyl chains in a *trans-trans* conformation (2*18.6Å$^2$) results in the final intercalated phase forming a bimolecular film of extended molecules within the interlayer region [Clearfield and Costantino, 1996]. Szirtes and Raieh [1991] suggest from XRD and IR patterns that during the intercalation process some rearrangement from the $\gamma$-zirconium phosphate to $\alpha$-zirconium phosphate may take place. It seems however, that other authors did not verify the mentioned observation.



#### (i) Intercalation of alcohols

In $\gamma$-zirconium phosphate, alkanols [Costantino, 1981] and benzylalcohol and diethyleneglycol [Szirtes and Raieh, 1991] readily intercalate into the layered structure [Costantino, 1981]. Alcohol-intercalates, however, become unstable if the newly formed compounds are dried in air at ambient condition [Costantino,

1981]. Exfoliation of the γ-zirconium phosphate crystal is achieved in the presence of acetone in admixture with water at 55°C [Alberti *et al.*, 1997].

**(ii) Intercalation of amines**

Intercalated n-butylamine exists as a bilayer γ-zirconium phosphate complex, even at very low concentrations with only one mole n-butylamine adsorbing per mole γ-$Zr(PO_4)(H_2PO_4)\cdot 2H_2O$. Di-alkylamines intercalate as a monolayer with 0.5molecules of n-alkylamines adsorbing per one zirconium phosphate unit [Costantino, 1981]. A similar pattern is observed for aniline [Herzog-Cance *et al.*, 1992].

**(iii) Thermal desorption of guest molecules**

Even though the acid strength of the primary hydrogen on each dihydrogenphosphate group is greater than that of α-zirconium phosphate [Herzog-Cance, 1992], desorption of amine groups occur at a lower temperature [Dékány and Szirtes, 1995]. Desorption of the n-butylamine occurs between 250°C and 390°C [Dékány and Szirtes, 1995] due to lesser diffusional constrains offered by the more open arrangement within the interlamellar region. The discrepancies would have to be attributed to the higher diffusional constraints experience by the guest molecules during desorption in α-zirconium phosphate.



## 2.3.3 CHEMICAL AND THERMAL PROPERITES

The properties of zirconium phosphates vary according to preparation with their thermal and chemical properties being related to their crystallinity [Albertsson, 1966]. Due to the layered structures of zirconium phosphates, different types, i.e., phases, of α- and γ-layered zirconium phosphates are obtained as a consequence of thermal treatments and intercalation-deintercalation processes. i.e., adsorption-desorption methods. These phenomena can be attributed to the shifting of the layers relative to one another as well as the change in the

interlayer water content and thus the interlayer distance [Clearfield and Costantino, 1996]. Since the structure of the constituent layers does not change appreciably with the nature and amount of polar molecules present in the interlayer region, or with the nature of the organic components adsorbing onto the active sites, or with the manner in which the planar macromolecules are packed. the prefixes $\alpha$ and $\gamma$ are used to describe the type of macroanions. Their respective interlayer distances are given in parenthesis. Consequently, $\alpha$- and $\gamma$-zirconium phosphate will be written as $\alpha$-$Zr(HPO_4)_2{\cdot}H_2O$ (7.55Å) and $\gamma$-$Zr(PO_4)(H_2PO_4){\cdot}2H_2O$ (12.20Å), respectively.

### 2.3.3.1 CHEMICAL AND THERMAL PROPERTIES OF $\alpha$-$Zr(HPO_4)_2{\cdot}H_2O$

Clearfield and Stynes [1964] observed the very high stability of crystalline $\alpha$-$Zr(HPO_4)_2{\cdot}H_2O$ towards hydrolysis of phosphate groups into aqueous solutions. The hydrolysis of phosphate groups into solution is also dependent on the temperature and the solution pH, with the stability towards hydrolysis decreasing with increasing temperature and pH. According to Vesely *et al.* [1968], no change in the zirconium phosphate structure nor chemical property occurs if $\alpha$-$Zr(HPO_4)_2{\cdot}H_2O$ is treated at very high temperatures in slightly acidic (0.1mol/L HCl) solution. Titration studies of $\alpha$-zirconium phosphate against NaOH and CsOH show that the amount of phosphate released into solution is minimal below a pH of 8 [Albertsson, 1966]. However, it seems that the hydrolysis of phosphates into solution is also dependent on the activation energy required in increasing the interlayer distance, since the quantity of phosphates leaching into solution is far higher during proton-exchange with $Cs^+$ than with $Na^+$ that has a smaller ionic radius than $Cs^+$. A large activation energy implies that a large difference between the proton rich interlayer region and the more proton deficient concentration of the bulk solution has to exist before the incoming ion can diffuse into the interlayer region of the compound (see Section 2.3.2).

Interestingly, α-$Zr(HPO_4)_2 \cdot H_2O$ exhibits two different monohydrogen phosphate groups with different acid strengths ($+4.8>H_o>+3.3$ and $-3.0>H_o>-5.6$) as shown using Raman spectroscopy [Hattori *et al.*, 1977] and titration methods [Clearfield and Thakur, 1980]. A detailed study of the infrared and Raman spectra of crystalline α-zirconium phosphate is given by Horsley *et al.* [1974]. The ν(OH) stretch bands assigned to the Brønsted acidity of the POH groups is 3670 – 3660cm$^{-1}$ with the acid strength increasing slightly by calcination or bulk dehydration [La Ginestra and Patrono, 1987]. Thus, the Brønsted acidity on α-$Zr(HPO_4)_2 \cdot H_2O$ is less than the observed acidity for the aluminosilicates. Upon heating the crystalline zirconium compound to 400°C the ratio of strong to weak Brønsted acid sites increases while still maintaining the same number of acid sites [Clearfield *et al.* 1980]. Heating above 400°C leads to condensation of the hydroxyl groups to pyrophosphate or P-O-P bonds (970cm$^{-1}$), thus decreasing the number of acid sites [Hattori *et al.*, 1977]. The amount of acid sites decreases abruptly beyond 450°C and becomes negligible after a thermal treatment above 490°C. Hattori *et al.* [1977] showed by IR analysis of pyridine adsorbed onto the thermally treated α-type that the strong acid sites formed are of Brønsted type and concluded that α-zirconium phosphate exhibits acidity only when the POH groups remain.

The interlayer water situated within the cavity of α-$Zr(HPO_4)_2 \cdot H_2O$ is completely lost upon prolonged heating at 110°. At around the same temperature the α-zirconium phosphate undergoes a phase change to α-$Zr(HPO_4)_2$ (7.41Å) due to a re-arrangement of the layers relative to one another. It was proven that the endothermic loss of crystal water and the endothermic phase change of α-$Zr(HPO_4)_2 \cdot H_2O$ (7.56Å) to α-$Zr(HPO_4)_2$ (7.41Å) are kinetically and thermodynamically distinct processes [Clearfield and Pack, 1974]. Heating α-$Zr(HPO_4)_2$ (7.41Å) at 220°C leads to an endothermic, reversible phase transition to α-$Zr(HPO_4)_2$ (6.80Å) [La Ginestra *et al.*, 1987] that is stable up to temperatures of ca. 400°C – 450°C. Between 450°C and 600°C, the P-OH groups condense

irreversibly to form P-O-P bonds resulting in the above mentioned loss in acid sites and α-$Zr(HPO_4)_2$ (6.80Å) transforms itself to α-$ZrP_2O_7$ (6.10A) [Costantino and La Ginestra, 1982] or simply α-L-$ZrP_2O_7$ ('L' denoting that the new phase is a layered pyrophosphate) [Clearfield and Costantino, 1996]

### 2.3.3.2 CHEMICAL AND THERMAL PROPERTIES OF γ-$Zr(PO_4)(H_2PO_4)_2 \cdot 2H_2O$

Structural examination of γ-$Zr(PO_4)(H_2PO_4)\cdot 2H_2O$ suggests that γ-zirconium phosphate can be hydrolysed more easily than α-zirconium phosphate since the interlayer phosphate groups are bonded to the metal atoms with only two bonds. Nevertheless, γ-zirconium phosphate is very stable and reverts to α-zirconium phosphate only in the presence of zirconium complexing acids (HF) or in boiling $H_3PO_4$ [Alberti *et al.*, 1989].

Interestingly, the calorimetric studies of amine adsorption on α- and γ-titanium phosphate, which are iso-structures of α- and γ-zirconium phosphates, revealed that at low coverage the differential heats of adsorption for the γ-titanium phosphate are higher than on α-titanium phosphate. This proves that the $pK_a$ of the γ-compound ($H_2PO_4^-$ groups) is lower than that of the α-compound ($HPO_4^{2-}$ groups) [Espina *et al.*, 1998]. Vibrational spectroscopic studies performed on aniline intercalated α- and γ-zirconium phosphates led to the same conclusion by observing that the N–H···O hydrogen bonding is weaker for aniline adsorbed on γ-zirconium phosphate than on α-zirconium phosphate [Herzog-Cance *et al.*, 1992]. The Brønsted acidic surface $P(OH)_2$ groups are identified as having their ν(OH) stretch band at 3600$cm^{-1}$ [La Ginestra and Patrono, 1987], suggesting that the Brønsted acid strength is comparable to that of the aluminosilicates. However, the acid strength of the secondary proton on the $P(OH)_2$ groups must be weaker than the primary proton. The $pK_a$-value for ortho-phosphoric acid changes by 5units when comparing the acid strength of the primary to the

secondary proton. Therefore, a similar behaviour is expected for the zirconium phosphates. The large expected difference in the $pK_a$-values implies that organic compounds associate preferentially with the primary proton situated on each γ-$Zr(PO_4)(H_2PO_4)\cdot 2H_2O$ group. Adsorption onto the secondary proton requires basic solution that can result in the destabilisation of $P(OH)_2$ phosphate group [Herzog-Cance *et al.*, 1992]. This is explained on the basis that upon the adsorption of two components on the same phosphate group the whole grouping is destabilised since both negative sites are on the same phosphate group with the two adsorbed components themselves approaching each other very closely, thus causing steric problems [Clearfield, 1993]. Since the OH groups in γ-zirconium phosphate structure are closely placed and the free area associated with each OH group is 8.9Å$^2$, most guest molecules cannot occupy all acid centres due to steric hindrance [Clearfield and Costantino, 1996].

The hydration water (2 molecules per unit formula) that align the adjacent layers of γ-$Zr(PO_4)(H_2PO_4)\cdot 2H_2O$ via hydrogen bonding are completely lost between 50°C and 100°C [Clearfield *et al.*, 1968]. This loss in crystalline water is reversible with the anhydrous form, i.e., γ-$Zr(PO_4)(H_2PO_4)$ (9.4Å), being able to rehydrate fully at room temperature. The condensation of acid hydroxyl groups begins at about 230°C, loosing ca. 0.7 water molecules between 230°C and 500°C. The newly formed compound, i.e., γ-$ZrP_2O_7$ (8.26Å) or γ-L-$ZrP_2O_7$, is stable up to ca. 600°C, with usually 30% of the hydroxyl groups remaining [Alberti *et al.*, 1989].

# Chapter 3

## Experimental



The first rule of intelligent tinkering
is to save all the parts
(Paul Ehrlich)

# 3. EXPERIMENTAL

## 3.1 REAGENTS

Meta-phenylenediamine (MPDA, purity > 98%) is obtained from AECI (South Africa). Mineral acids used for the homogeneous acid catalysed hydrolysis of meta-phenylenediamine (MPDA) are $H_2SO_4$ (98 wt. %), $H_3PO_4$ (85 wt. %) and $(NH_4)H_2PO_4$ p.a. (all purchased from Saarchem). These materials are used without further purification.

Zeolites H-ZSM-5 (Südchemie AG, Si/Al = 13), H-ZSM-5 (Südchemie AG, Si/Al = 22), H-USY (Akzo Nobel, Si/Al = 5.6) and zeolite H-Beta (Südchemie AG, Si/Al = 14.4) are used. For comparison amorphous silica-alumina (Kalichemie AG, Si/Al = 6.9) and $\gamma$-$Al_2O_3$ (Kalichemie AG) are used. Before use in reactions, the aluminosilicates are calcined in a furnace in air at 180°C for 2hours followed by another 12hours at 450°C. After calcination, the solids are stored in a desiccator over a waterbed of de-ionised water for 24hours to allow for rehydration.

$\alpha$-$Zr(HPO_4)_2 \cdot H_2O$ ($\alpha$-ZrP) and $\gamma$-$Zr(H_2PO_4)(PO_4) \cdot 2H_2O$ ($\gamma$-ZrP) are donated by Daiichi Kigenso Kagaku Kogyo (Japan). The zirconium phosphates are either used as received or in calcined form. The calcination treatment includes heating the solids in a kiln in air for 12hours at 180°C and for another 12hours at 400°C. The step-wise ramping is employed to ensure the complete removal of crystalline water between the layers, since heating layered zirconium phosphates results in the contraction of their interlayer distances [La Ginestra *et al.*, 1987]. After calcination, the solids are slowly cooled from 400°C to ambient temperatures and stored in a desiccator over a waterbed for approximately 3days to allow for rehydration. $\alpha$-ZrP400 and $\gamma$-ZrP400 respectively denote the $\alpha$- and $\gamma$-zirconium phosphates calcined at 400°C.

## 3.2 SOLID CHARACTERISATION

The following sections detail the physicochemical characterisation techniques used. Since aluminosilicates and zirconium phosphates are quite different materials, different characterisation techniques are required. These are mentioned below. The aluminosilicates are, however, obtained from commercial vendors with their chemical compositions known. The same applies to crystalline zirconium phosphates.

### 3.2.1 ELEMENTAL ANALYSIS

Atomic Adsorption (AA) measurements (Varian SpectrAA-110) are used to check for both leached and extra-framework Al species after reaction. The final solution mixture is treated with HCl to pH 1. After 10 minutes, the solution is separated from the solids and analysed by AA for Al. The Ni, Fe and Cr content in the final reaction mixture is also analysed by AA to determine the state of leaching from the stainless steel reactor walls.

AA is also used to determine the Zr content in the reaction mixture after the reactions with zirconium phosphates. The phosphorous content in solution at the end of the reaction is measured by the method described by de Koning and Mol [1989]. One blank and a series of test-tubes containing solutions of known phosphorus concentrations are prepared and their volumes adjusted to 5.0ml with the pH adjusted to 0 using sulphuric acid. To each test-tube 0.2ml of 5% ammonium molybdate and 0.3ml of the *Fiske-Subbarow* reducing solution is added. After vigorous shaking and heating the solutions for 10minutes in boiling hot water, the content is cooled and diluted to 50ml in volumetric flasks. The adsorbance (Varian Superscan 3 spectrophotometer) of the blue molybdenum colour is read at 830nm against the blank and a graph of adsorbance versus µg/ml phosphorous is plotted. The solutions of unknown phosphorous

concentration are subjected to the same procedure as mentioned above and the obtained 830nm adsorbances are then compared with the previously obtained graph.

## 3.2.2 SOLID STRUCTURE AND MORPHOLOGY

### 3.2.2.1 X-RAY DIFFRACTION (XRD)

The crystallinity of the zeolites prior to and after reaction are examined using powder X-ray diffraction spectra by means of a Philips X-ray diffractometer (PW3710 mpd control) generating Cu-K$\alpha$ radiation ($\lambda$ = 1.542Å) in the 2-Theta region of 4 – 45° with a step size of 0.1° and operating at 40kV and 25mA.

A 2 Theta range of 3.5 38° is employed for the powder X-ray diffractograms performed on the zirconium phosphates. Due to the possible swelling properties of the zirconium phosphates, XRD's are taken after every calcination, rehydration and reaction step.



### 3.2.2.2 SCANNING ELECTRON MICROSCOPY (SEM)

Electron micrographs are obtained using a Leica S440 Scanning Electron Microscope (SEM). Samples are mounted on aluminium stubs using a mixture of carbon and water-soluble glue. Once dry, the mounted samples are coated with atomised Au/Pd. The following settings are employed with the pictorial settings used being predominantly a function of magnitude and sample conductivity: acceleration voltage (5 - 15keV), filament current (90 - 200pA), stage tilt (0°), working distance (9 - 15mm) and aperture size (30µm).

## 3.2.3 THERMAL STABILITY

Thermogravimetric (TGA) as well as differential thermal analysis (DTA) curves are obtained with a Stanton Redcroft STA-780 unit. A total of 25.0 ± 0.05mg of the from the manufacturer obtained zirconium phosphate or aluminosilicate sample is flushed with nitrogen (flow rate = 30ml(NTP)/min) at room temperature for 30minutes, prior to heating at 1°C/min to 550°C in nitrogen (flow rate = 30ml(NTP)/min). The standard or reference is reagent grade calcined $\alpha$-$Al_2O_3$.

## 3.2.4 ACIDITY OF SOLIDS

### 3.2.4.1 AMMONIA TEMPERATURE PROGRAMMED DESORPTION (TPD) METHOD

Ammonia TPD is carried out in a home-built equipment (see Figure 3.1 on Page 78) [Weber. 1998]. A total of ca. 0.25g of the solid is loaded into a quartz cell. After online calcination of the solid in air (60ml(NTP)/min), the temperature is stabilised at 150°C under a constant flow of He (60ml(NTP)/min). Subsequently, a 1% $NH_3$/He mixture (flow rate = 60ml(NTP)/min) is passed over the solid for precisely 1hour. The physisorbed ammonia is then flushed off the sample by flowing pure He (60ml(NTP)/min) over the sample at 150°C for 12hours. The temperature is subsequently raised at 10°C/min to the final temperature. The amount of ammonia desorbed as a function of the temperature is monitored using a thermal conductivity detector (TCD) with pure helium (flow rate = 60ml(NTP)/min) as a reference. Ammonia exiting is trapped in sulphuric acid of known concentration. The total amount of ammonia chemisorbed is determined by back-titration of the sulphuric acid with caustic soda.

**(i) Aluminosilicates**

A fresh aluminosilicate sample is loaded into the quartz cell and calcined in air (flow rate = 60ml(NTP)/min) at 450°C for 12hours. A very low ramping rate of 1°C/min is used to increase the calcination temperature from ambient temperature to 450°C to ensure that the online treated aluminosilicates roughly resemble the kiln treated aluminosilicates (see Section 3.1). The $NH_3$-TPD is carried out as described above. For every aluminosilicate, the TPD-procedure is repeated a further two times applying different ramping rates (2°C/min, 5°C/min). This allows for the strength of the ammonia adsorption on the aluminosilicates to be determined using the method outlined by Cvetanovic and Amenomiya {1967 and 1973} assuming a perfectly linear heating schedule.

**(ii) Zirconium phosphates**

Due to the contraction of the interlayer distances of α-ZrP and γ-ZrP with increasing temperature, the samples are calcined in air by slowly ramping (1°C/min) the temperature to 400°C. This allows the inter-crystalline water to be removed thermally. The $NH_3$-TPD is carried out under flow of helium as described above, except that the samples are ramped to 400°C instead of 450°C.

**(iii) Data evaluation**

Since the concentration inside the 1%$NH_3$/He bottle varies throughout its use, the ammonia concentration exiting the gas bottle is checked regularly by flowing the gaseous mixture (flow rate = 60ml(NTP)/min) for 1hour through a saturator containing aqueous sulphuric acid of known concentration. Thereby, the ammonia reacts with the acid while the remaining helium is vented. The resulting aqueous solution is then back-titrated with 0.1N NaOH to determine the total amount of ammonia absorbed by the sulphuric acid. From this information, the true ammonia concentration exiting the gas bottle is determined.

During each run, the calibration of the TCD occurs during the adsorption stage of ammonia onto the test sample. Adsorption of ammonia onto the sample is

considered to be complete after 60minutes. The difference in TCD counts between the baseline spectra and the average TCD counts measured towards the end of the adsorption stage is used for the calibration. The *Calibration Factor* is given by the difference in the TCD counts divided by the ammonia concentration exiting the 1% $NH_3$/He bottle.

The desorbing ammonia concentration, with the concentration being time- and temperature-dependent, is calculated by first subtracting the baseline spectra from the TPD spectra before dividing it by the *Calibration Factor*. The total area under the TPD concentration versus time curve divided by the flow rate and the sample mass yields the amount of acid sites available per gram of sample. The integrated value (in terms of mmol/g) is then compared to the number of moles of ammonia that reacts with the sulphuric acid solution inside the saturator.

The mathematical model of Cvetanovic and Amenomiya [1967] is used to determine the heat of desorption. This model is based on a material balance around the presorbed sample. Desorption and re-adsorption rate constants are taken as first order and by assuming a homogenous solid surface the rate constants are ***coverage independent***. Incorporating the Clausius-Clapeyron equation into the manipulated mass balance and determining the maximum concentration of the presorbed gas in the carrier gas with respect to temperature (dC/dT = 0), the heat of desorption is calculated using the following equation:

$$2 * \ln T_m - \ln \beta = \frac{\Delta H_{des}}{R * T_m} + \ln\left(\frac{(1-\theta_m)^2 * V_S * \Delta H_{des}}{F * \exp(\Delta S_{des}/R) * R}\right) \qquad 3.1$$

$T_m$ represents the temperature at which the ammonia concentration of the TPD curve is at its maximum, which is obtained at a certain linear heating rate $\beta$; $\Delta H_{des}$ and $\Delta S_{des}$ are the respective enthalpy and entropy change due to desorption; $\theta_m$ is the coverage at $T_m$, and $V_S$ is the volume of the solid phase in the catalyst bed; with $F$ equalling the flow rate of the carrier gas. Plotting (2 ln $T_m$ – ln $\beta$) versus

$1/T_m$ gives the slope of the straight line ($\Delta H_{des} / R$), thus allowing the determination of the heat of adsorption of a gas onto a solid.

### 3.2.4.2 TEMPERATURE PROGRAMMED DESORPTION (TPD) OF 4-METHYL-QUINOLINE

#### (i) TPD-MS of H-ZSM-5

The number of external acid sites on the H-ZSM-5 (Si/Al = 13) and H-ZSM-5 (Si/Al = 22) are determined by temperature programmed desorption of previously adsorbed 4-methyl-quinoline [Weber, 1998]. Weber proved that 4-methyl-quinoline ($d_{critical}$ ~ 7.3Å [Rollmann, 1991]) could not enter the pores of H-ZSM-5 (largest kinetic pore diameter of H-ZSM-5 = 5.4Å x 5.3Å [Haag and Chen, 1987]).

Calcination of the H-ZSM-5 is carried out in a kiln with the H-ZSM-5 being spread out evenly on a flat crucible. The zeolites are kept at 180°C for 2hours before being ramped to 450°C (9°C/min), where it is held for a further 12hours. After allowing the kiln to cool down to 120°C, the H-ZSM-5 crucible is immediately transferred into a desiccator present in an oven at 80°C. This is done to ensure minimal contact of the zeolite with the surrounding water vapours. A small flask containing the 4-methyl-quinoline is inserted into the desiccator before the desiccator is sealed and allowed to cool to ambient temperature. The desiccator is kept in a dark storage space for 3days to allow for the adsorption of the 4-methyl-quinoline. A total mass of 1g H-ZSM-5 presorbed with 4-methyl-quinoline is then inserted into a quartz cell that is heated to 150°C under flow of helium and kept there for 48hours to remove the phys sorbed 4-methyl-quinoline. The solid is kept in place by means of a plug of quartz-wool. The adsorbed samples are heated to 1100°C at 10°C/min in 100ml(NTP)/min He. Since 4-methyl-quinoline is found to decompose primarily into a benzene fraction on desorption from H-ZSM-5, the ion monitored is $m/e$ = 78 since it is the most abundant mass fraction obtained [Weber, 1998].

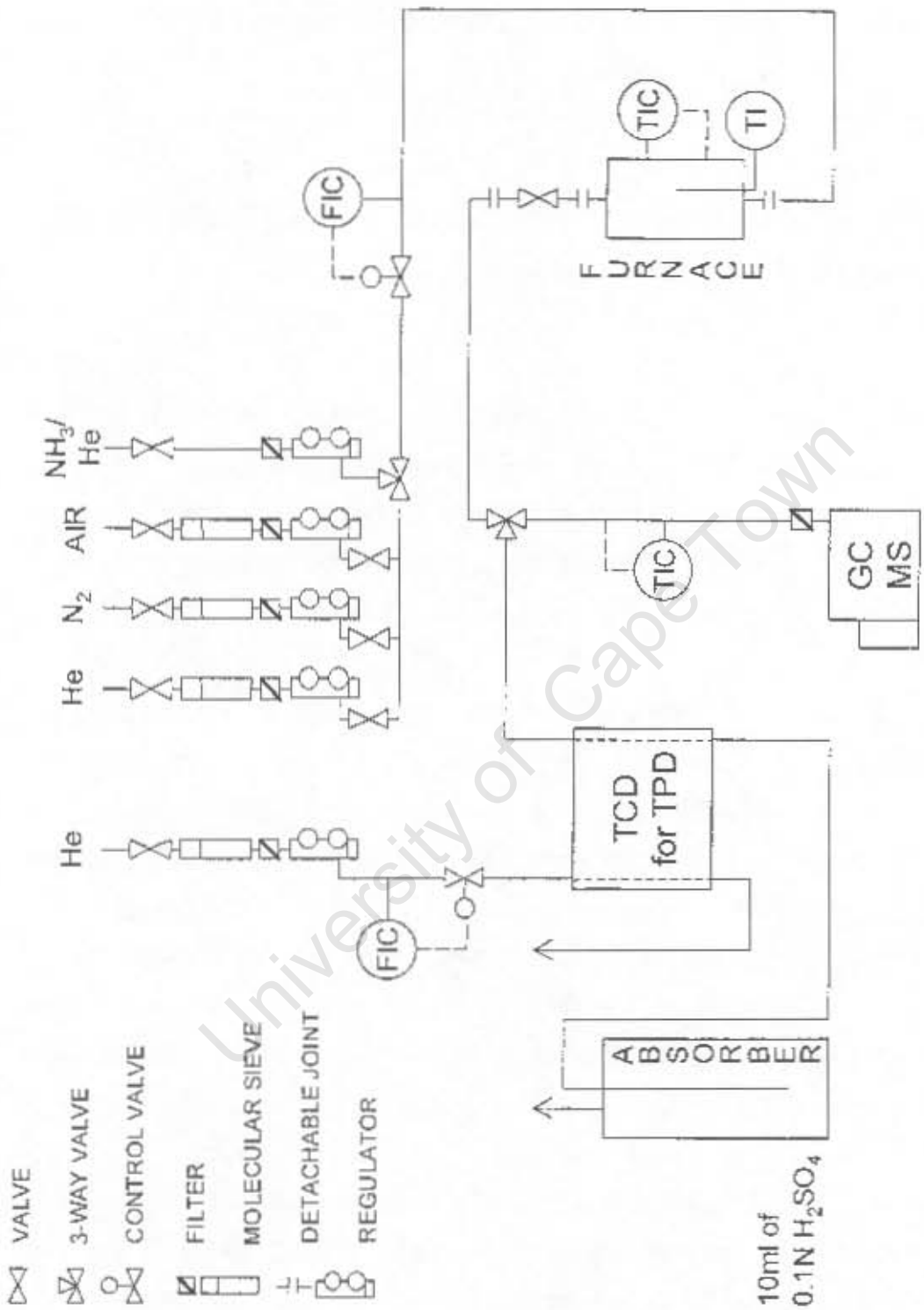




**Figure 3.1** Simplified schematic of the apparatus used for ammonia and 4-methyl-quinoline temperature programmed desorption studies.

The mass fractions are quantified using a Hewlett Packard 5971A Mass Selective Detector. A small fraction of the total flow (split ~ 1/250) enters a 15m long, 0.22mm I.D. polyimide coated deactivated fused silica capillary column. By adjusting the column head pressure the flow to the MS through the capillary column is regulated. A 1.5minutes lag time exists between the sample and the mass spectrometer primarily due to the capillary column. This is corrected by initiating the MS recording 1.5minutes after the ramping has commenced.

**(ii) Data evaluation**

Chemisorbed 4-methyl-quinoline decomposes upon desorption from the zeolite. The quantification of 4-methyl-quinoline by an ion-chromatography is quite inaccurate. This method is chosen to compare relatively the external acid sites of only the two H-ZSM-5 zeolite compounds. The $m/e$ = 78 area count obtained for the two H-ZSM-5 samples, i.e., Si/Al = 13 and Si/Al = 22, is presented as one relative ratio.



### 3.2.4.3 ADSORPTION STRENGTH OF WATER ON ALUMINOSILICATES

The adsorption strength of water onto the aluminosilicates is determined using TGA/DTA of the re-hydrated zeolite by means of the Stanton Redcroft STA-780 unit. A total of 25mg of the solid is placed into the apparatus, flushed with nitrogen (30ml(NTP)/min) for 4 – 5hours before being heated up to 450°C. The purpose of flushing the sample for an extended period is to ensure that essentially only the more strongly adsorbed (chemisorbed) water remains on the surface of the aluminosilicate sample. The temperature ramps (10°C/min, 5°C/min and 2°C/min) are varied to determine the average strength of adsorption by means of the method described by Cvetanovic and Amenomiya [1968] as shown in Section 3.2.4.1. The maximum peak temperature $T_m$ as illustrated in Section 3.2.4.1 corresponds to the point of inflexion obtained from the TGA curve.

### 3.2.4.4 FT-IR ACIDITY DETERMINATION

Attempts are also made to characterise the zirconium phosphates using IR analysis by noting shifts in the P-(OH) bands. The infrared spectra are run on a Nicolet 5ZDX FT-IR Spectrometer at a resolution of $4cm^{-1}$. Self-supporting wafers (13mm∅) are pressed (780MPa), which are then transferred into an IR cell equipped with heating element and thermocouple. This allows for online IR spectra being taken at ambient temperature, 180°C and 400°C. The samples are kept at a certain temperature for 1hour before taking a spectrum.

To obtain the full IR-spectrum from wavenumbers $4000cm^{-1}$ down to $400cm^{-1}$, the previously fitted $CaF_2$ windows have been removed. A large $N_2$-flowrate (ca. 200ml(NTP)/min) is applied to ensure the removal of any previously adsorbed compounds such as $H_2O$.

### 3.2.4.5 ADSORPTION STUDY

**(i) Experimental procedure**

The adsorption of meta-phenylenediamine (MPDA), meta-aminophenol (MAP), and resorcinol is investigated. Ca. 0.4g of the re-hydrated zeolite or zirconium phosphate is suspended in with 15ml aqueous solutions of meta-phenylenediamine (MPDA), meta-aminophenol (MAP), resorcinol, or ammonia. The concentration of these compounds in solution is varied. Before sealing the sample flask, the headspace is flushed with nitrogen to minimise the oxygen content inside the flask. The slurry is stirred using teflon-coated magnets and allowed to equilibrate for 6days in darkness. The temperature is kept constant between 30°C and 90°C in an oil bath controlled at −2°C. Syringe filters (0.2μm) are used to separate the liquid from the solid materials at the desired temperature. The concentration of the adsorbent in the liquid is determined using a HPLC. Phenol is used as the external standard that is added to a known

volume of the sample taken from the syringe. The HPLC is calibrated daily in order to keep the error as small as possible since the amount adsorbed is calculated over a mass balance. Ammonia concentrations are determined by titration against sulphuric acid.

**(ii) Data evaluation**

A negligible change in the liquid volume is assumed upon adsorption of a relevant compound onto a solid material. Consequently, the amount adsorbed per unit of solid material is given below:

$$\frac{\text{mmol of relevant compound}}{\text{unit of solid material}} = \frac{V_{liquid} * (C_{initial} - C_{final})}{\text{unit of solid material}} \qquad 3.2$$

$V_{liquid}$ is the volume of liquid added to the flask, whereas $C_{initial}$ and $C_{final}$ are respectively the initial and final concentration of the relevant compound per volume of water, given in mmol/ml. For zeolites the *unit of solid material* shown in Equation 3.2 represents the mass of the dehydrated zeolites (in grams). The dehydrated mass of the zeolite per sample flask is calculated by multiplying the weighed out mass (ca. 0.4g) with the ratio of the total zeolite mass taken out of the kiln at around 200°C over the total zeolite mass after re-hydration. The error in the adsorbed concentrations determined at low bulk solution concentration is greatest, unlike for high solute concentrations. For zirconium phosphates, however, the *unit of solid material* in Equation 3.2 is given in terms of the number of moles of zirconium atoms present in the solid sample.

The method used in deriving the HPLC response factors for each organic compound and subsequently calculating the concentration of the liquid solution given the area counts is detailed in APPENDIX-C. A worked example of evaluating the adsorbed amount of an organic compound on a solid is given in APPENDIX-D.

### 3.2.5 SURFACE AREA AND PORE VOLUME OF SOLIDS

$N_2$-BET surface areas and micropore volumes of the aluminosilicates and zirconium phosphates are determined using an ASAP 2000 apparatus. Prior to nitrogen adsorption, the samples are calcined at their respective temperatures. Samples are then degassed at 88K. The volumetric method is applied to determine the amount of $N_2$ adsorbed and desorbed at a certain pressure.

# 3.3 REACTOR CONFIGURATION AND EXPERIMENTAL PROCEDURE

## 3.3.1 REACTION STUDIES

Reactions are carried out batch-wise, in a 600ml Parr autoclave as shown in Figure 3.2. The impeller speed is kept constant at 1060 ± 10rpm for all reactions in order to minimise external mass transport limitations. At an impeller speed of 1060rpm, the liquid flow is turbulent since no vortex is visible, thereby ensuring that the power input is adequate. A sampling tube allowed for on-line sampling. The frit (0.2μm) at the end of the sampling tube prevented any solid material from entering the sampling tube, thus preventing pipe blockages. At recorded time intervals liquid (total volume ca. 10ml) is withdrawn from the reactor and weighed. In ensuring that the samples taken correspond to that of the reaction mixture, ca. 6ml liquid is drawn before the actual sample (pipe volume ca. 3ml). No gas phase probes are taken since it will essentially consist of water and nitrogen. Recording the total mass of liquid withdrawn from the reactor allows for the MPDA, MAP and resorcinol concentrations to be corrected since sampling affects the overall reactant concentration mixture inside the autoclave. Since sampling results in the lowering of the liquid level inside the reactor, additional water from the reaction mixture evaporates into the gas phase. Essentially pure water evaporates into the gas phase, since the boiling point of water is well below that of the organic compounds. By consulting steam tables, however, the effect of the removed liquid on the overall reaction system could be incorporated, as explained in Section 3.3.1.3. For the worst case scenario, e.g., sampling 100ml results in a 4.55% higher concentration as what would have been observed if there is no sampling involved.

Noting the mass removed from the reactor system upon sampling aids in checking whether water is lost during the reaction due to a possible leakage.

Therefore, an overall reactor mass balance (reactor weight before compared to reactor weight after reaction plus the sum over all the withdrawn sample weights) is done over every reaction to evaluate the amount of liquid lost to the surrounding. The mass of water lost is hardly evident.

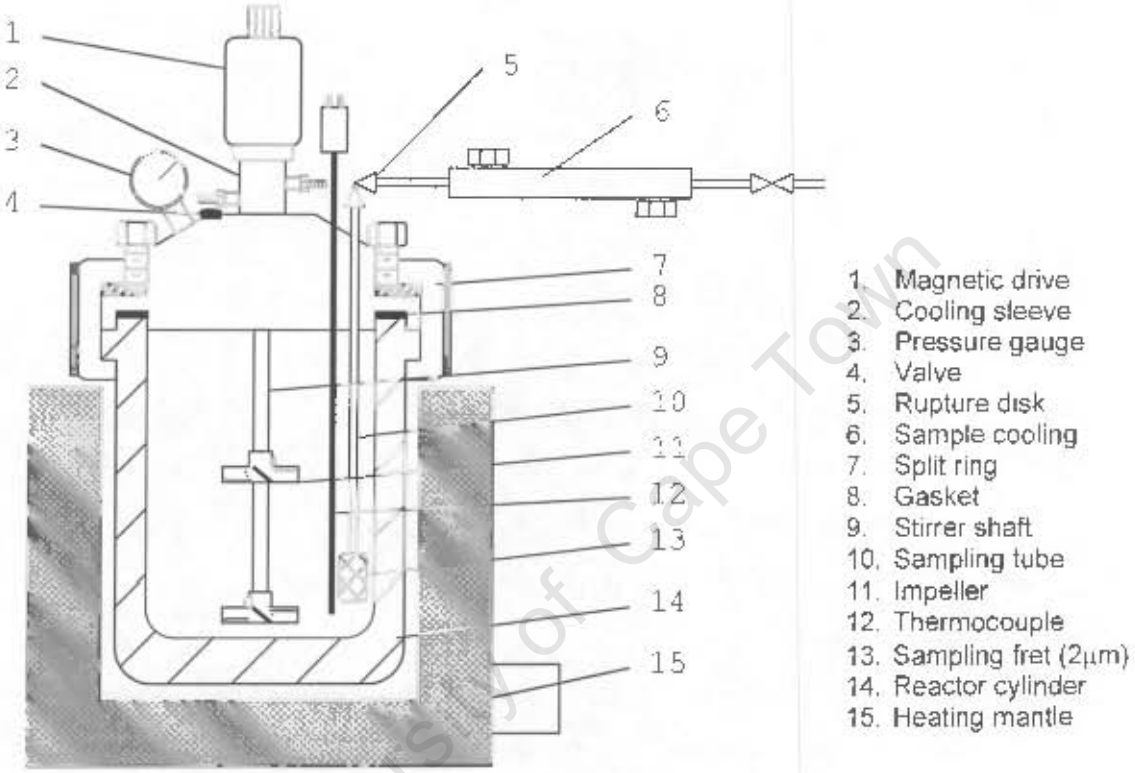


**Figure 3.2** Schematic of high-pressure batch reactor.



The autoclave walls as well as any other tubing inside the reactor (construction metal: Stainless Steel 316) was first poisoned by means of heating up 10g of MPDA in water and some phosphoric acid. This was done in order to try and minimise any polymer formation by the interaction of MPDA with the Cr, Ni and Fe commonly used in Stainless Steel (see Section 2.1.1.6). The autoclave was cleaned by means of ultrasound using water and acetone as solvent. No mechanical scrubbing has been applied.

### 3.3.1.1 HOMOGENEOUS REACTIONS

Into the reactor cylinder, 350ml of water and 1g of MPDA is added. Thereafter, the mineral acid ($H_2SO_4$, $H_3PO_4$) or salt ($NH_2H_2PO_4$) is weighed out and slowly added to the reactor vessel. The mass of the acid included in the reaction mixture is calculated by assigning an acid to meta-phenylenediamine (MPDA) mole ratio (3.4 or 6.8). Subsequently, the sealed reactor is flushed for 8minutes by injecting nitrogen (1MPa) through the sampling tube. The frit produces fine dispersion of nitrogen, displacing the dissolved oxygen. The nitrogen escapes the reactor via another valve (not shown in Figure 3.2). The sample tube valve is then closed before the other valve, thereby reducing the nitrogen pressure over the liquid to 0.1MPa. The reactor is heated to either 225°C or 275°C. Depending on the acid used, the sampling times are adjusted accordingly to allow for 5 to 6 samples being taken during the course of the reaction. The temperature, pressure and sample pH (taken at 25°C) is also recorded. After cooling the reactor to ambient temperatures, the reaction mixture is analysed.

### 3.3.1.2 HETEROGENEOUS REACTIONS

**(i) Aluminosilicates**

For every reaction, a total of 10 grams of the original aluminosilicate is added to the 1g MPDA in 350ml water. The mentioned 10 grams of aluminosilicates refers to the mass before any calcination at 450°C. The dehydrated mass is either noted or compared to the TG analyses because the concentrations of the relevant compounds are expressed in terms of the dehydrated solid mass. The sealed reactor is then flushed with nitrogen to displace all the oxygen present inside the reactor. Reactor temperatures chosen are 225°C, 275°C and 300°C. Samples are typically taken after 1, 5, 9 and 25 hours. The exact reaction time, temperature, pressure and pH (taken at 25°C) for every sample is noted. The aqueous solution of the quickly cooled reactor is also analysed. The spent solid is

recovered via centrifugation and transferred into 1L of hot, distilled water. The slurry is agitated to remove as many reaction-compounds as possible. After centrifuging a second time, the solid is dried at 50°C and then recalcined at the same temperature as used prior to the solid's first reaction.

**(ii) Zirconium phosphates**

The mass of solid added to the 1g MPDA in 350ml water is initially varied from 1g to 10g. Thereafter, all the reactions performed at the different temperatures are done using 10g of the original zirconium phosphate. The calcined zirconium phosphates also weigh 10g prior to their kiln calcination (see Section 3.1). For all reactions regarding zirconium phosphates, the mentioned mass corresponds to that before any calcination treatment. The sealed reactor is flushed with nitrogen to displace all the oxygen present inside the reactor. Temperatures selected when using zirconium phosphates are 225°C, 250°C and 275°C. Samples are generally taken after 1, 5, 9 and 25 hours. The exact reaction time, temperature, pressure and pH (taken at 25°C) for every sample is noted. The aqueous solution of the quickly cooled reactor is also analysed. The spent solid is recovered via centrifugation and transferred into 1L of hot, distilled water. The slurry is agitated to remove as many reaction-compounds as possible. After centrifuging a second time, the solid is dried at 50°C and then recalcined at the same temperature as used prior to the solids first reaction. The uncalcined zirconium phosphate is also washed in 1L of water and dried.

The zirconium phosphates are reused in a second reaction with the reaction temperature corresponding to the temperature used during the first reactions. The zirconium phosphate to MPDA mole ratio (mol Zr)/(mol MPDA) for the second set of reactions (regenerated samples) are roughly identical to those used during the first set of reactions. For the reactions conducted on the 400°C calcined zirconium phosphates, this is achieved by setting the mass ratio of the zirconium phosphate immediately after calcination (regenerated / original) equal to the MDPA mass ratio ($2^{rd}$ reaction / $1^{st}$ reaction). Similarly, the mass ratios of

zirconium phosphates without any calcination step (reused / original) are kept equal to the MPDA mole ratio ($2^{nd}$ reaction / $1^{st}$ reaction) by allowing the washed/dried (50°C) zirconium phosphates to stand in air (ambient temperature) for ca. 1day before recording its mass.

### 3.3.1.3 DATA EVALUATION

Conversion is reported as mole-% conversion of MPDA to MAP and resorcinol. Low quantities of by-products such as diphenylamines are also present in the reaction mixture. The conversion of MPDA is estimated based on the assumption that MPDA is converted to meta-aminophenol, resorcinol, 3,3'-diamino-diphenylamine and 3-hydroxy,3'-amino-diphenylamine. The formation of other side products is neglected. This is confirmed using a total mole balance.

Attempts have been made to find response factors relative to phenol for 3,3'-diamino-diphenylamine and 3-hydroxy,3'-amino-diphenylamine. The peaks or the retention time of the two diphenylamines are determined using HPLC-MS at AECI Ltd. Since these compounds cannot be bought, their response factors are determined using an array of data from homogeneous runs at higher MPDA and $H_3PO_4$ concentrations. Assuming a perfect mole balance existing between the mentioned compounds, the response factors are evaluated by least square methods. The heterogeneous reactions cannot be used in determining the response factors of the by-products since the amount adsorbed onto the solid material's surface is unknown. A detailed description of this method is given in APPENDIX-E.

The selectivity is generally given in terms of resorcinol with respect to MAP. It may also be given as the ratio of resorcinol to the sum of all the other products produced.

$$\% \text{ Conversion} = 100^{*}(M_{MAP}+M_{Res} + 2^{*}M_{Comp.A} + 2^{*}M_{Comp.B})/M_{MPDA,initial} \quad \textbf{3.3}$$

$$\text{Selectivity} = M_{Res}/(M_{MAP} + 2^{*}M_{Comp.A} + 2^{*}M_{Comp.B}) \quad \textbf{3.4}$$

$$\% \text{ Yield} = 100^{*}M_{Product}/(M_{MPDA,initial}) \quad \textbf{3.5}$$

where
- $M_{MPDA,initial}$ initial moles of MPDA
- $M_{MAP}$ number of moles of MAP
- $M_{Res}$ number of moles of Resorcinol
- $M_{Comp.A}$ moles of 3,3'-diamino-diphenylamine
- $M_{Comp.B}$ moles of 3-hydroxy,3'-amino-diphenylamine
- $M_{Product}$ either $M_{MAP}$, $M_{Res}$, $M_{Comp.A}$ or $M_{Comp.B}$

A correction in the concentration of the organic compounds may be necessary, depending on whether the removed samples are the true representative samples of the whole reaction system and not purely that of the liquid phase. Comparison of the boiling points of the different compounds reveals that the vapour phase consists of essentially water and produced ammonia. Since the liquid level decreases upon sampling, more water is able to evaporate into the gas phase, thus concentrating the organic compounds [Viljava and Krause, 1996]. Given the assumption that the gas phase consists entirely of water, the vapour and liquid specific volumes obtained from steam tables could be applied in correcting the observed sample concentration. This is illustrated in APPENDIX-F. It needs to be mentioned, though, that the procedure only applies if the concentration is based on water. For the case of mineral acids, the concentration may be based on the moles of 'hydrolytic hydrogen' available at the beginning of the reaction, where the term 'hydrolytic hydrogen' refers to the number hydrogen atoms able to form hydronium ions and thus participate in the reaction. When using solids, the concentration of the relevant compounds may also be written in terms of the solid's mass or the total number of acid sites available. The difference comes in with sampling since the mineral acid is removed with the reaction mixture

whereas the solid material remains with the reaction mixture. Correspondingly, each case needs to be treated slightly differently. A detailed calculation of mass balances and concentrations of the relevant compounds for homogeneous and heterogeneous reactions are shown in APPENDIX-F.

## 3.3.2 LIQUID SAMPLE ANALYSIS

### 3.3.2.1 HPLC SAMPLE PREPARATION

Phenol is chosen as the external standard. 1ml of a reactor sample is combined with 1ml of a known phenol solution (ca. 3g/L) and subsequently diluted.

### 3.3.2.2 HPLC ANALYSIS

The reaction compounds are separated using a HPLC (column: Spherisorb 80-3 ODS-2, l=250mm, ID=4.6mm) employing a mobile phase gradient. The initial mobile phase used during the first 4minutes of the analysis consists of 0.05vol% $H_3PO_4$ and 0.1vol% triethylamine in de-ionised water. This mobile phase is then gradually changed over a period of 2minutes to a mobile phase consisting of 80% deionised water (0.1vol% $H_3PO_4$, 0.1vol% triethylamine) and 20% acetonitrile (0.1vol% triethylamine). After a further 10minutes, the mobile phase is reversed back to the original mobile phase linearly over a period of 1minute. A liquid flow rate of 1.0ml/min is used. The total run time for one sample analysis lasts 20minutes. The compounds are analysed with an UV detector operating at 280nm.

The method used to derive the response factors and consequently calculating the concentration of the liquid solution given the area counts is detailed in APPENDIX-C.

## 3.4 ERROR ANALYSIS

Some of the error analyses ($NH_3$-TPD take 2-3days) are based solely on a few reproducibility experiments and thus true statistical analysis is not possible. The HPLC response factors varied over the experimental period, so the response factors are calculated prior sample analysis. Where possible the accuracy of measurements is given according to the manufacturer's claims.

**Table 3.1 Error analysis**

| Measurement | Units | Technique | Error |
|---|---|---|---|
| Water Content | wt% | TGA-DTA | 5% |
| Crystallinity | %-ratio | XRD | 5% |
| $NH_3$-TPD peak temp | °C | TPD | 3°C |
| $NH_3$-TPD total acidity | mmol/g | TPD | 9% |
| Lepidine-TPD total acidity | mmol/g | MS-TPD | 20% |
| IR | $cm^{-1}$ | FTIR | $4cm^{-1}$ |
| Surface Area | $m^2/g$ | $N_2$-BET | 10% |
| Concentration | mmol/g | HPLC | 5% |

**Table 3.2 Error analysis of reaction work**

| Measurement | Units | Error |
|---|---|---|
| Pressure | bar | 5% |
| Temperature | °C | 1°C |
| Reaction time | min | <1min |
| HPLC | mol/L | 3% |

# Chapter 4

## Results and Discussion



The great tragedy of Science - the slaying of a beautiful hypothesis by an ugly fact
(Thomas Henry)

# 4. RESULTS AND DISCUSSION

## 4.1 REACTOR RAMPING / HEATING PROFILES

The period required in bringing the charged reactor from ambient to reaction temperature forms part of the reaction time illustrated in all reaction result figures unless stated otherwise. The heating profiles to various final reaction temperatures, i.e., 225°C, 250°C, 275°C and 300°C, are shown in Figure 4.1. For each heating profile shown in Figure 4.1, the reactor is charged with 350ml water and 10g solids.

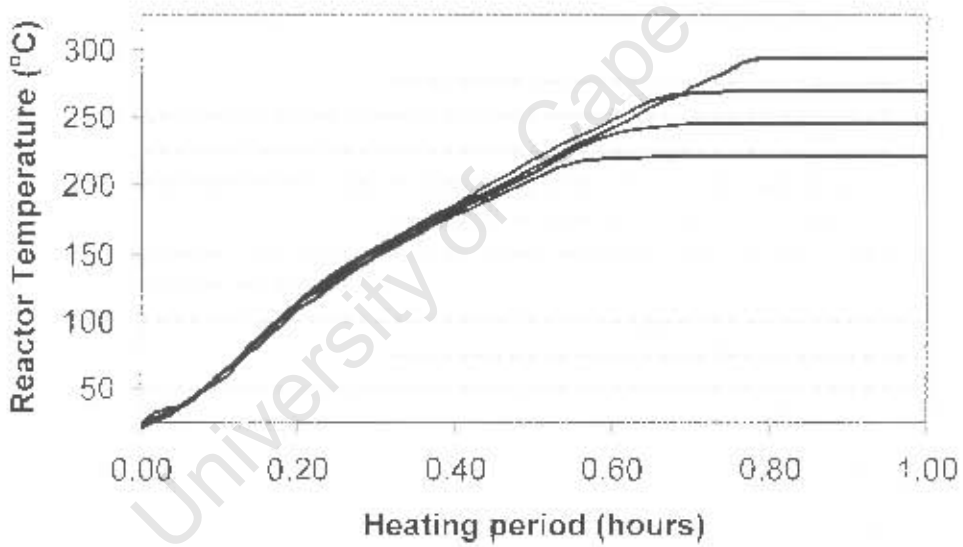


**Figure 4.1** 225°C, 250°C, 275°C and 300°C heating profiles of the Parr autoclave charged with 350ml water and 10g solid acid.

A simplistic mathematical linear reaction profile is obtained by assuming a linear ramping rate (383 ± 10.5 °C/hour) from ambient temperature to ca. 15°C below the final reaction temperature. After reaching a temperature of ca. 15°C below the intended reaction temperature, the ramping rate decreases. As illustrated in Figure 4.1, the reaction mixture approaches the intended reaction temperature

only very slowly, often requiring a further 1hour to heat the reaction mixture by 3°C to 5°C before attaining the final temperature.

## 4.2 REACTIONS IN ABSENCE OF ACIDS

It is worth mentioning again that the autoclave walls as well as any other tubing inside the reactor are poisoned by means of previous reactions with MPDA (see Section 3.3.1) prior to the start of the true analytical work. Charging the 600ml Parr autoclave with 350ml of deoxygenated water and 1g of MPDA results in no detectable formation of resorcinol, even after 49hours (reaction temperature = 275°C). Hardly any observable change in the concentration of MPDA occurs during the course of the reaction. Minor quantities of 3,3'-diamino-diphenylamine and 3-hydroxy,3'-amino-diphenylamine (yields << 1mole-%) are detected.

This is in stark contrast to the thermodynamically predicted resorcinol yield at 275°C (see Figure 2.8) where the resorcinol yield is predicted as being ca. 57% for an initial water to MPDA mole ratio of 2100:1. A 2100:1 water to MPDA mole ratio essentially corresponds to 1g MPDA in 350ml water, the conditions used for the blank run. Considering these observations, it can be deduced that the reaction rate in the absence of an acid is very small. The assumptions taken by setting the activity coefficients equal to 1 during the thermodynamic analysis would not lead to such a large deviation.

## 4.3 REACTIONS USING MINERAL ACIDS

Mineral acids of different acid strengths, i.e., $H_2SO_4$ ($pK_a$ = -2), $H_3PO_4$ ($pK_a$ = 2.12) and $(NH_4)H_2PO_4$, ($pK_a$ = 7.4), are chosen to verify the conclusions of Greco [1969 - 1972] that polymeric ethers are formed in the presence of sulphuric acid for all reaction conditions, resorcinol of high yields and purity is obtained in the presence of phosphoric acid, $(NH_4)H_2PO_4$ inhibits the formation of polymers, and no conversion of MPDA occurs in the presence of $(NH_4)H_2PO_4$. The use of mineral acids also allows for establishing the influence of the acid strength on the product distribution, establishing the reaction order and kinetic model in the absence of diffusion and adsorption / desorption constraints, and providing a basis for comparison with heterogeneous acids. A detailed reaction pathway for the hydrolysis reaction can then be proposed.

### 4.3.1 REACTIONS WITH SULPHURIC ACID

Figure 4.2 shows the MPDA, MAP and resorcinol concentration as a function of time when MPDA is treated with $H_2SO_4$ at various temperatures. The concentrations of the relevant compounds are expressed as mole-%, obtained by dividing the measured concentrations with the initial MPDA concentration, i.e., 26.4mmol/L. The pH of the reaction solution (pH reading taken at ambient temperatures) remains constant throughout the reactions carried out at 225°C measuring 1.35 ± 0.06 in the presence of 3.39 mole $H_2SO_4$ per mole MPDA and 1.17 ± 0.04 in the presence of a 6.77 $H_2SO_4$ to MPDA mole ratio.

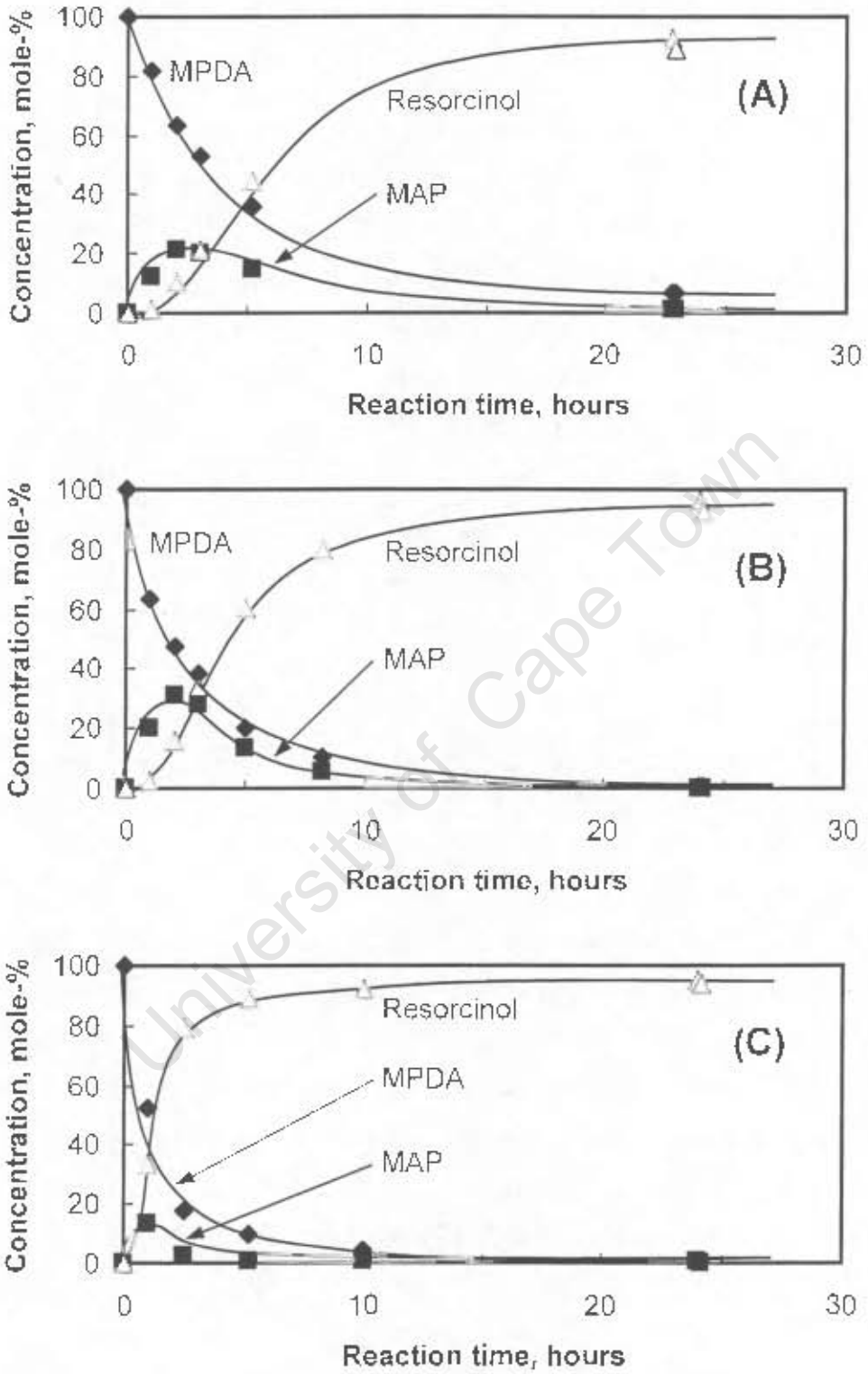




**Figure 4.2** Concentration versus time (init. MPDA conc. = 26.4mmol/L) at (A) 225°C (init. $H_2SO_4$:MPDA mole ratio = 3.39); (B) 225°C (init. $H_2SO_4$:MPDA = 6.77): and (C) 275°C (init. $H_2SO_4$:MPDA = 3.38).

The reaction pathway for the conversion of MPDA in the presence of sulphuric acid (see Figure 4.2) follows that of a typical consecutive reaction. MPDA reacts to form MAP that is subsequently converted to resorcinol. The MAP concentration profile goes through a maximum and the resorcinol concentration profile follows that of an S-shaped curve with the initial slope of the time-concentration curve equalling zero. The time-concentration profiles in Figure 4.2 further suggest that the reactions MPDA → MAP as well as MAP → resorcinol are essentially irreversible since the MPDA concentration and MAP concentration approach zero after prolonged reaction periods. The resorcinol yields measured after 24 hours of reaction time (heating period included) when using a $H_2SO_4$ to MPDA mole ratio of 3.39 (T = 225°C) is 93mole-% and in the presence of a 6.77 $H_2SO_4$ to MPDA mole ratio (T = 225°C) the resorcinol yield is 96mole-%. Increasing the reaction temperature to 275°C while maintaining a constant $H_2SO_4$ to MPDA molar ratio of 3.38 leads to a resorcinol yield of 95mole-% (Figure 4.2C) after 24hours.

The maximum observed yield of MAP (21mole-% after 2 hours) when using a $H_2SO_4$:MPDA molar ratio of 3.39 (at 225°C) is less than that at a higher initial $H_2SO_4$ to MPDA molar ratio (31mole-% after 2 hours). This suggests that the reaction rate is dependent on the initial acid concentration.

Also, the rate of formation of resorcinol increases with an increase in the $H_2SO_4$:MPDA ratio. An increase in the reaction temperature to 275°C (Figure 4.2C) from 225°C (Figure 4.2A) has a marked effect on the observed reaction rate further suggesting that the reaction is virtually irreversible.

Mole balances (see APPENDIX-G) conducted over all sample points reveal that between 95% and 100% of the initial MPDA can be accounted for (only one sample point returns a 86% accountability, which is quite likely due to analytical errors since this phenomenon is not repeated). The erratic variations in the mole balances between 95% and 100% suggests that these are due to experimental

errors and not to the formation of insoluble phenyl-ethers since the formation of phenyl-ethers is typically regarded as being irreversible (see Section 2.1).

Figure 4.3 shows the yield-time profiles of minor intermediates 3,3'-diamino-diphenylamine and 3-hydroxy,3'-amino-diphenylamine. The yield profiles of 3-hydroxy,3'-amino-diphenylamine traverse through a maximum of between 0.7 and 1.2mole-% (corresponding to ca. 1.5% - 2.3% of initial MPDA) and approach zero after prolonged reaction periods. The initial rate of formation of 3-hydroxy,3'-amino-diphenylamine tends towards zero, suggesting a consecutive reaction that is likely to originate from 2 MAP molecules, or from 1 MPDA and 1 MAP molecule. Rather for the monomer-dimer reaction to be reversible as illustrated in Figure 2.10 in Chapter 2, the low 3-hydroxy,3'-amino-diphenylamine concentration after prolonged reaction time points towards the direct conversion of the dimer to resorcinol and MAP by acid hydrolysis rather than the reversibility of the reaction leading to its formation from MPDA. The formation of 3,3'-amino-diphenylamine is clearly a minor reaction pathway

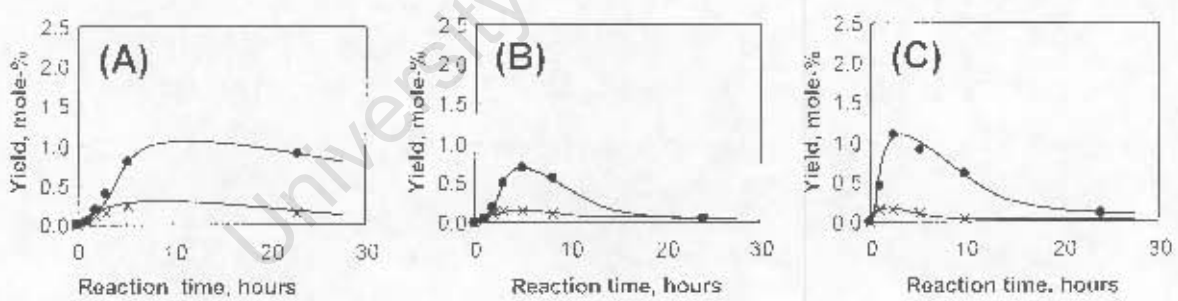


**Figure 4.3** Yield versus time (init. MPDA conc. = 26.4mmol/L) profiles for 3,3'-diamino-diphenylamine (x) and 3-hydroxy,3'-amino-diphenylamine (●) for reactions at (A) 225°C (init. $H_2SO_4$:MPDA molar ratio = 3.39); (B) 225°C (init. $H_2SO_4$:MPDA = 6.77); and (C) 275°C (init. $H_2SO_4$:MPDA = 3.38).

## 4.3.2 REACTIONS WITH PHOSPHORIC ACID

Figure 4.4 shows the MPDA, MAP and resorcinol concentration as a function of time in the presence of phosphoric acid. Mole balances conducted over all sample points reveal that all the initial MPDA (within experimental errors) can be accounted for throughout the reactions (see APPENDIX-G). At 225°C the mole balance averages 98.9 ± 2.4%. At 275°C the mole balance amounts to 99.4 ± 0.9%. The pH for the reaction at 225°C (pH taken at ambient temperature)

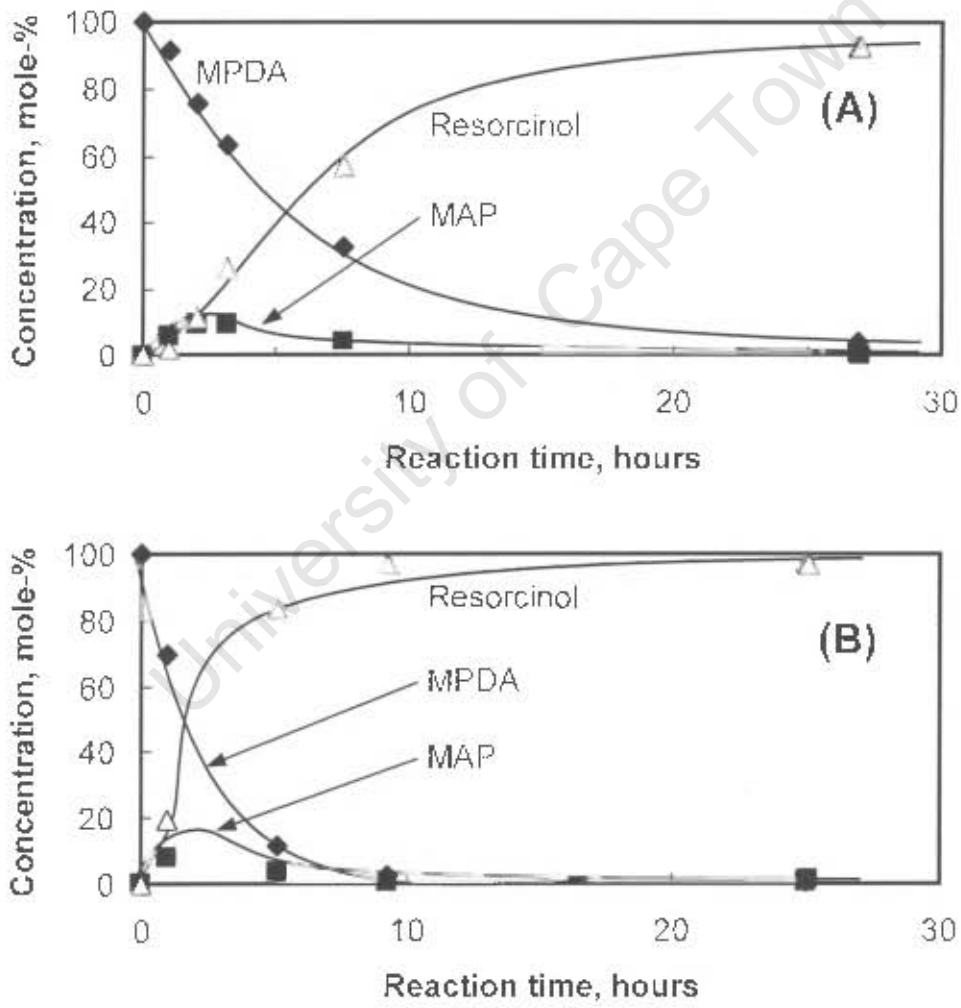




**Figure 4.4** Concentration versus time (init. MPDA conc. = 26.4mmol/L) with an initial $H_3PO_4$ to MPDA mole ratio of 6.77 and reaction temperature set at (A) 225°C and (B) 275°C respectively.

remained constant at 1.72 ± 0.02, whereas the pH measured during the reaction at 275°C (pH taken at ambient temperature) remained at 2.06 ± 0.06.

The yield versus time curves of 3,3'-diamino-diphenylamine and 3-hydroxy,3'-amino-diphenylamine are shown in Figure 4.5. The yield-profiles of both dimers traverse through a maximum and approach zero concentration after prolonged reaction periods (after 25hours). The low concentrations measured for 3,3'-diamino-diphenylamine makes it difficult to interpret the initial slope. A slope greater than zero is, however, expected for a primary product. The slope of the initial concentration-time curve of 3-hydroxy,3'-amino-diphenylamine equals zero (see Section 4.3.1). For the reaction at 225°C and 6.77 $H_3PO_4$:MPDA mole ratio (Figure 4.3A), 3,3'-diamino-diphenylamine reaches a maximum after ca. 7.5 hours (yield = 0.4mole-%), while the maximum for 3-hydroxy,3'-amino-diphenylamine occurs after ca. 7.5 hours (yield = 1.7mole-%). During the reaction at 275°C and a $H_3PO_4$:MPDA mole ratio of 6.77, 3,3'-diamino-diphenylamine and 3-hydroxy,3'-amino-diphenylamine go through a maximum between reaction times 1.0 hour and 5.1 hours, however, due to the absence of sampling points within this time frame, more accurate maxima for these dimers cannot be established. As already mentioned in Section 4.3.1, the shape of the dimer curves in Figure 4.3 tend to suggest that all reactions pathways to resorcinol are consecutive and all reactions can be regarded as irreversible.



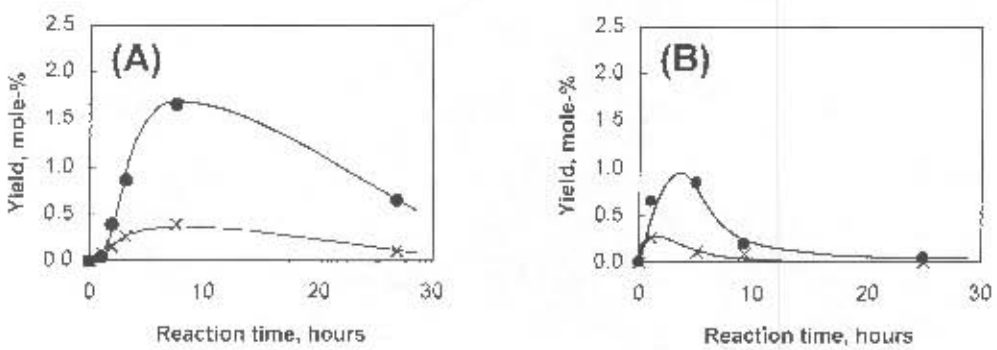


**Figure 4.5** Yield versus time plots (init. MPDA conc. = 26.4mmol/L) for 3,3'-diamino-diphenylamine (x) and 3-hydroxy,3'-amino-diphenylamine (●) for reactions with an initial $H_3PO_4$ to MPDA molar ratio of 6.77 and temperatures: (A) 225°C and (B) 275°C.

### 4.3.3 REACTIONS WITH AMMONIUM-DIHYDROGEN PHOSPHATE

Figure 4.6 shows the MPDA, MAP and resorcinol concentration-time profiles in the presence of ammonium dihydrogen phosphate, i.e., $(NH_4)H_2PO_4$, which is a considerably weaker mineral acid than phosphoric acid. The initial $(NH_4)H_2PO_4$ to MPDA molar ratios are chosen in conformity with the molar ratios used for the reactions in the presence of sulphuric acid and phosphoric acid.

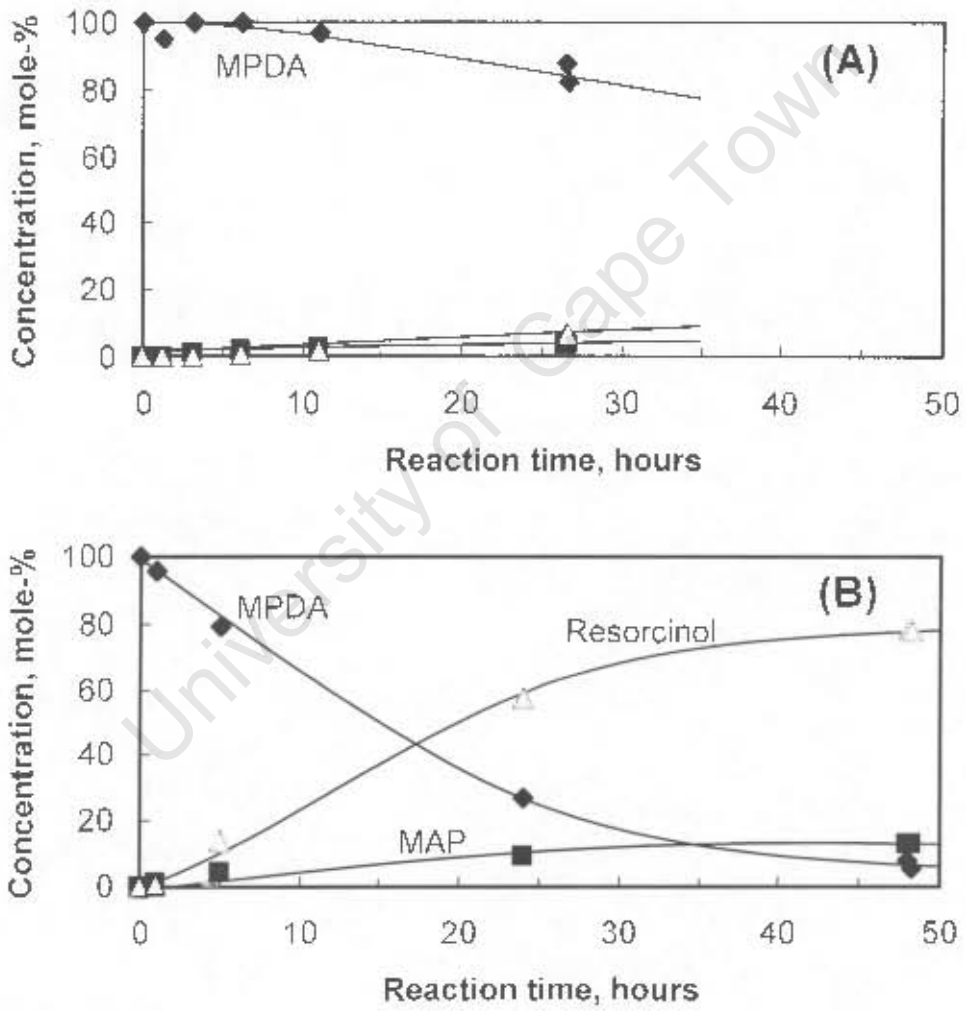


**Figure 4.6** Concentration-time plots (initial MPDA conc. = 26.4mmol/L) for reaction temperatures (A) 225°C (init. $(NH_4)H_2PO_4$:MPDA mole ratio = 6.76) and (B) 275°C (init. $(NH_4)H_2PO_4$:MPDA = 6.63); (◆), (■) and (Δ) respectively denote the species MPDA, MAP and resorcinol.

Mole balances conducted over all the sample points again show that most of the initial MPDA can be accounted for in terms of reactant MPDA and products MAP, resorcinol, 3,3'-diamino-diphenylamine and 3-hydroxy,3'-amino-diphenylamine. For the reaction carried out at 225°C the mole balances averaged over all 6 sample points is 99.3% ± 4.0%. The average mole balance for the reaction at 275°C is 98.6% ± 1.2%. The pH for the reaction at 225°C (pH taken at ambient temperature) remains constant at 5.26 ± 0.05, which is considerably higher than the pH measured for reactions with phosphoric or sulphuric acid. At 275°C, a reasonable conversion of MPDA to resorcinol is observed, and the pH changes from 5.81 to ca. 6.42 (pH reading taken at ambient temperature) during the course of the 48 hours of reaction. During this time the resorcinol yield increases from 0.5% (after 1 hour) to 78% (after 48 hours).

The concentration-time profiles in Figure 4.6 are similar to those in the presence of sulphuric and phosphoric acid, albeit at a considerably lower reaction rates. After 24 hours of reaction time, the resorcinol yield at 225°C is ca. 6% while at 275°C the resorcinol yield is ca. 57%. The maximum MAP concentration at 225°C occurs beyond the measured 24 hours reaction period, while at 275°C the maximum MAP-concentration is likely to occur between the reaction periods of 24 hours and 48 hours. The zero slope resorcinol concentration profile during the first hour of reaction is clearly identifiable with the resorcinol concentration being very close to zero after 1 hour of reaction time. At that stage, the reaction temperature is within 5°C of the final temperature.

The yield-time profiles of 3,3'-diamino-diphenylamine and 3-hydroxy-3'-amino-diphenylamine are illustrated in Figure 4.7. The very low yields measured for 3,3'-diamino-diphenylamine coupled with the associated errors in analysis result in irregularities and make it very difficult to interpret the overall yield-time curve for this compound. The maximum concentration of 3-hydroxy-3'-amino-diphenylamine at a reaction temperature of 225°C cannot be established since its maximum is likely to occur far beyond the sampled 26.5 hours reaction period.

However, at 275°C a clear-cut maximum yield for 3-hydroxy-3'-amino-diphenylamine (yield = 2.0mole-%) is observed after ca. 24 hours; the total reaction time equalled 48hours. After 48 hours the yield of 3-hydroxy-3'-amino-diphenylamine is 0.8mole-% (see APPENDIX-G).

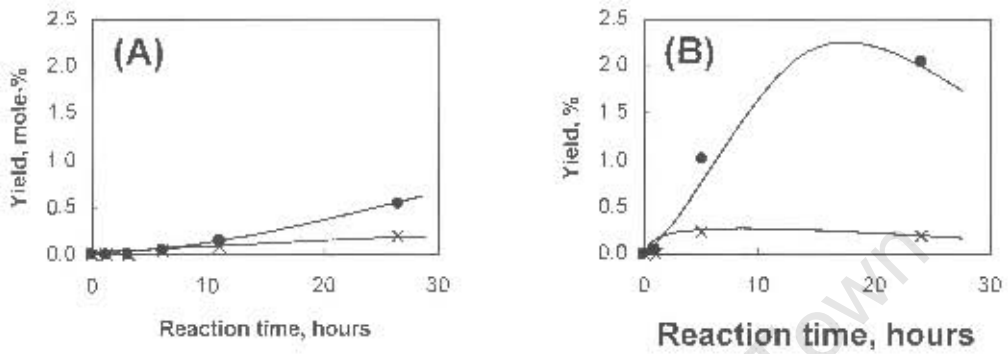


**Figure 4.7** Yield-time plots (init. MPDA conc. = 26.4mmol/L) for 3,3'-diamino-diphenylamine (x) and 3-hydroxy,3'-amino-diphenylamine (●) for reactions at (A) 225°C (init. $H_2SO_4$:MPDA molar ratio = 3.39); (B) 225°C (init. $H_2SO_4$:MPDA = 6.77); and (C) 275°C (init. $H_2SO_4$:MPDA = 3.38).

## 4.3.4 OBSERVATIONS REGARDING USE OF MINERAL ACIDS

Under the dilute reaction conditions (initial MPDA concentration equals 26.4mmol/L and mineral acid concentrations < 200mmol/L), resorcinol is obtainable in high yields (resorcinol yield >95% for $H_2SO_4$ and $H_3PO_4$) at reaction temperatures between 225°C and 275°C. Mole-balances over all sample points reveal that, essentially, no polymer ethers are formed. From these results and those of Greco [1969 - 1972], it can be concluded that the acid strength and the acid concentration affect the production of polymeric ethers. Furthermore, contrary to the reports of Greco [1969 - 1972], as shown in Figure 4.6, resorcinol can be produced in the presence of $(NH_4)H_2PO_4$, albeit at a considerably lower

reaction rate. Therefore, the reaction rate at a particular temperature is strongly dependent on the acid strength of the mineral acid.

The conversion of MPDA to resorcinol in the presence of mineral acids is a consecutive reaction with the intermediate product being MAP. The reaction MPDA → MAP → resorcinol can be regarded as being irreversible. The initial zero slope observed for the concentration-time curve of 3-hydroxy-3'-amino-dipheneylenediamine reveals that it is produced consecutively, either from 2 MAP molecule or from 1 MAP and 1 MPDA molecule. After prolonged reaction periods the concentration of 3-hydroxy-3'-amino-diphenylenediamine tends to zero. The cleavage of the dimer is likely to occur via an acid hydrolysis of the diphenylamine leading to the formation of resorcinol and MAP. Alternatively, it is also feasible that the formed 3-hydroxy-3'-amino-diphenylenediamine first breaks up into its individual components. i.e., assuming a reversible monomer-dimer reaction. after which the monomers are further hydrolysed towards resorcinol as depicted in Figure 2.10 in Chapter 2.

# 4.4 REACTIONS WITH ALUMINOSILICATES

## 4.4.1 CHARACTERISATION OF UNCALCINED ALUMINO-SILICATES

Typically, 10grams of an aluminosilicate is first calcined at 450°C and then rehydrated before being used for reaction studies. All results are based on the calcined, dehydrated form. Consequently, the weight lost during the calcination of an aluminosilicates (H-USY (Si/Al = 5.6), H-Beta (Si/Al = 14.4), H-ZSM-5 (Si/Al = 13.0), silica-alumina (Si/Al = 6.9) and H-ZSM-5 (Si/Al = 22)) needs to be determined. Two methods are applied, viz. TGA in $N_2$ and weight loss determination upon shallow bed calcination in air at 400°C. It is observed using TGA that during the initial 30minutes of $N_2$-flushing at 20°C, zeolite H-ZSM-5 (Si/Al = 13) experiences a considerable weight loss which is unusual for ZSM-5 zeolites. The initial weight loss is likely due to the evaporation of some volatile compounds. Consequently, high standard deviations are measured for H-ZSM-5 (Si/Al = 13) in Table 4.1. Only slight weight losses are observed for the remaining aluminosilicate during the initial flushing period. Table 4.1 compares the TGA results with the aluminosilicate weight losses experienced during calcination, where the samples are weighed out before calcination and then immediately afterwards.

Weight losses during shallow bed calcination in air for silica-alumina, H-USY and H-ZSM-5 (Si/Al = 13) differ from the TGA results. The weight loss upon shallow bed calcination shows a greater weight loss than by TG analysis. The discrepancies between the two methods can vary considerably, e.g., the weight loss of the kiln treated silica-alumina is ca. 9.4%w/w while the weight loss determined by TG analysis is only 6.2%w/w. A similar trend is observed for H-USY (20.4%w/w vs. 17.6%w/w) and H-ZSM-5 (Si/Al = 13) (18.3%w/w vs. 16.5%w/w). The different calcination atmospheres can explain this phenomenon.

In the presence of air, the organic materials adsorbed on aluminosilicates will be removed by oxidation.

**Table 4.1 Observed weight loss at 450°C of relevant aluminosilicates**

| Aluminosilicate | Percent Weight Loss | |
|---|---|---|
| | TGA[1] | Kiln[2] (no. of measurements) |
| silica-alumina | 6.2 | 9.4 ± 1.4 (5) |
| H-USY | 17.6 | 20.4 ± 0.7 (7) |
| H-Beta | 7.0 | 6.5 ± 0.6 (9) |
| H-ZSM-5 (Si/Al = 13) | 16.5 | 18.3 ± 3.3 (6) |
| H-ZSM-5 (Si/Al = 22) | 5.6 | 5.7 ± 0.3 (2) |

[1] $N_2$-flowrate: 30ml(NTP)/min
[2] calcined in air; shallow zeolite bed

Reasons for the percent weight loss of H-Beta being slightly larger for the TG analysis (7.0%w/w) than for the kiln treated H-Beta (6.5%w/w) can be ascribed to handling errors. The standard deviation calculated for the kiln treated H-Beta (0.6%w/w) would, however, still cover the 7.0%w/w weight loss measured during the TG analysis. Both methods used for determining the percent weight loss for H-ZSM-5 (Si/Al = 22) are essentially identical at 5.6%w/w. This indicates the absence of adsorbed organic species on this material.



## 4.4.2 CHARACTERISATION OF CALCINED ALUMINOSILICATES

### 4.4.2.1 STRUCTURE AND MORPHOLOGY

**(i) X-ray diffraction**

Powder X-ray diffraction patterns of calcined H-USY, H-Beta, H-ZSM-5 (Si/Al = 13) and H-ZSM-5 (Si/Al = 22) are shown in Figure 4.8. Generally, the powder patterns compare well with those found in literature. However, the samples

show diffraction patterns with broader lines than the simulated patterns due to disorder and small crystallite size. Also, the relatively large step size of 0.1° limits the peak details.

The powder patterns of H-USY compare well with the simulated powder patterns of the Faujasite family [Treacy *et al.*, 1996; pg. 643]. Significant FAU/EMT intergrowths are not detected although a 10% intergrowth of the EMT-structure into the FAU-structure could be feasible. The powder pattern of H-Beta shows significant overlapping of closely spaced reflections in the 2-Theta regions of 5° and 10° as well as 20° to 25°. The very broad peaks noticed for H-Beta implies that the H-Beta sample is likely to consist of very small crystallites. However, the broad peaks could also imply that the H-Beta crystallites consist of polymorph-A and polymorph-B stacking faults. The simulated X-ray powder pattern of 50% stacking fault probability [Treacy *et al.*, 1996; pg. 641] compares well with the spectra given in Figure 4.8. The powder patterns of ZSM-5 show similarities to the simulated patterns with some overlapping of closely spaced reflections.



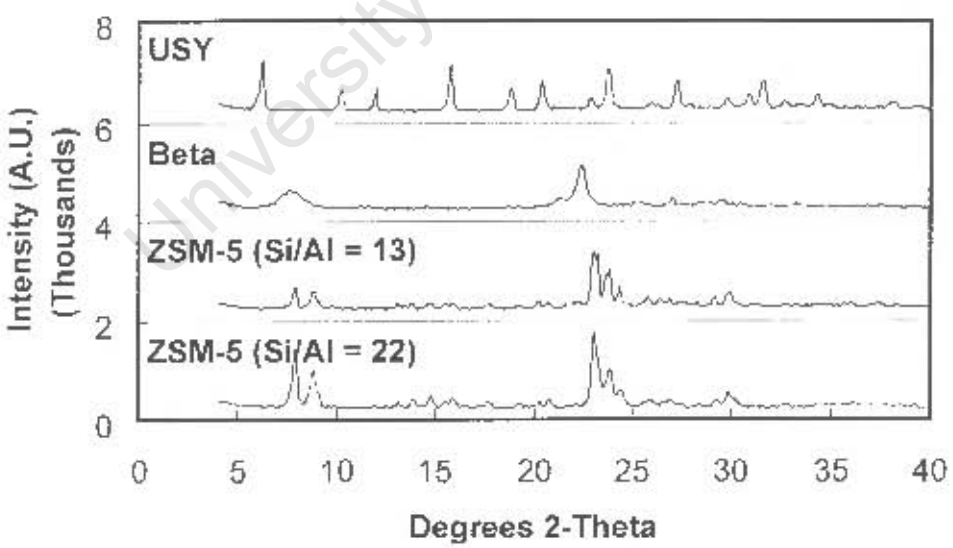


**Figure 4.8** XRD patterns of USY, H-Beta, ZSM-5 (Si/Al = 13) and ZSM-5 (Si/Al = 22) using Cu-K$\alpha$ radiation and step size = 0.1°.

**(ii) Crystallite particle size, particle size distribution and morphology**

The crystallite particle sizes of the zeolites are determined from electron micrographs. The crystallite particle size of USY ranges from 0.4μm to 0.6μm. Figure 4.9 shows no deposit of amorphous materials, only some agglomeration of crystallites. The shape of the crystallites is of a cubic nature.

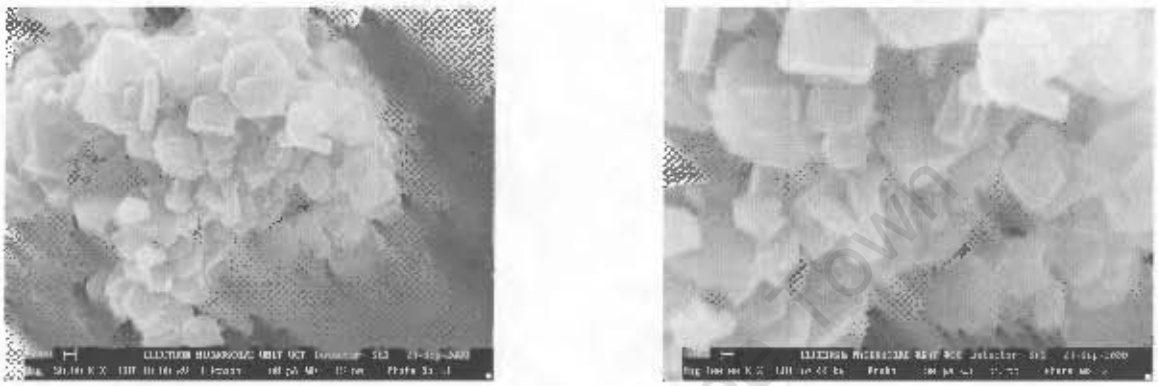

**Figure 4.9** Electron micrographs of USY.

The crystallite particle sizes for Beta are generally smaller than 0.3μm (Figure 4.10). No accurate estimation of the average crystallite particle size could be made because of strong agglomeration of the crystallites. No distinct shape can be observed for the crystallites of H-Beta.

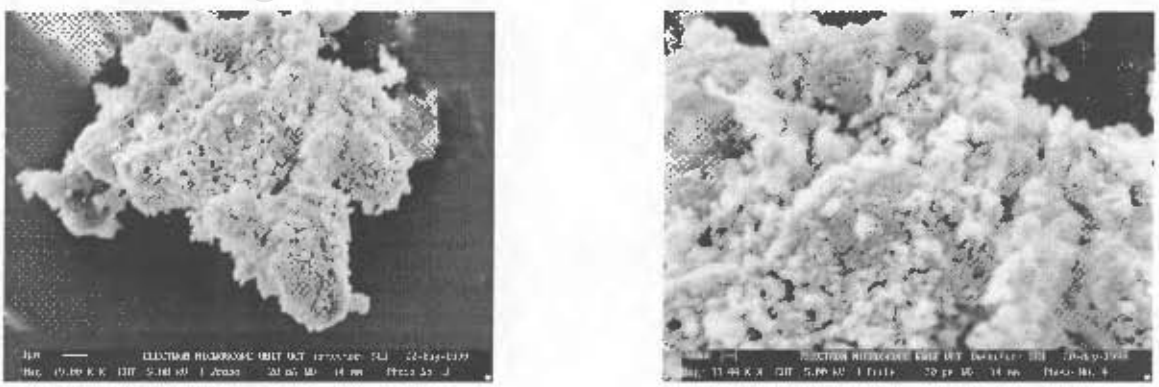

**Figure 4.10** Electron micrographs of Beta.

Illustrated in Figure 4.11 are the crystallites of ZSM-5 (Si/Al = 13). The shape of the crystallites can be described as being long and rectangular (coffin-like; $d_{crystal}$ = 1-5μm) with some crystallites having pointed (tetrahedral) ends, showing monoclinic symmetries. The crystallites agglomerate into particles.

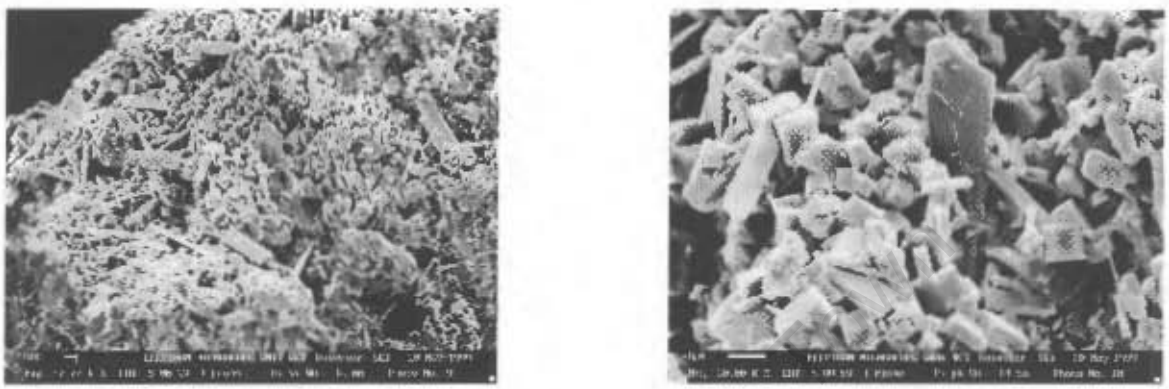

**Figure 4.11** Electron micrographs of ZSM-5 (Si/Al = 13)

The average crystallite particle sizes for ZSM-5 (Si/Al =22) is ca. 0.5μm (Figure 4.12). The shape of the ZSM-5 (Si/Al = 22) crystallites is similar to that of ZSM-5 (Si/Al = 13). The ZSM-5 (Si/Al = 22) crystallites do agglomerate into particles.

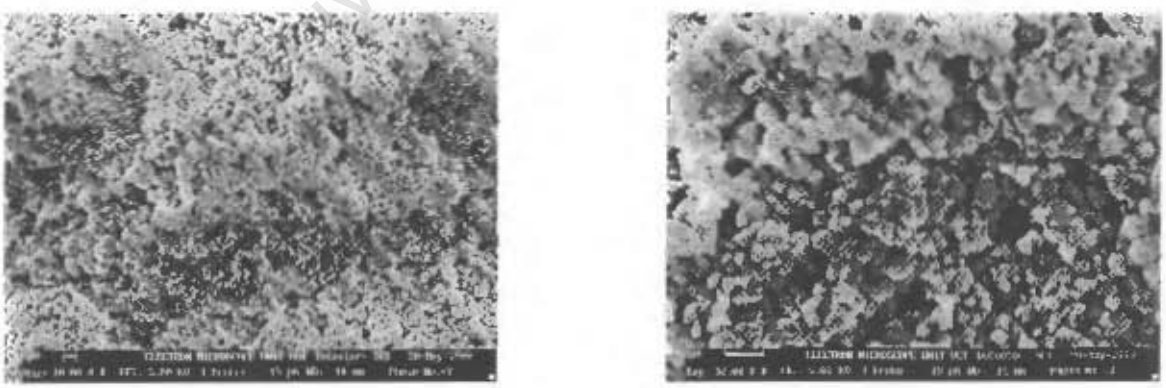

**Figure 4.12** Electron micrographs of ZSM-5 (Si/Al = 22).

### 4.4.2.2 ADSORPTION STRENGTH OF WATER ON REHYDRATED ALUMINO-SILICATES

Since MPDA and water react on the aluminosilicates, the interaction of water with the surface is of importance. The affinities of the respective alumino-silicates for water are determined using DTA-TGA of the rehydrated solids. The heat of adsorption is determined using the method developed by Cventanovic and Amenomiya [1967 and 1973]. The heat of adsorption is assumed to be independent of coverage. The maximum peak temperature $T_m$ required for the application of the Cventanovic and Amenomiya method corresponds to the point

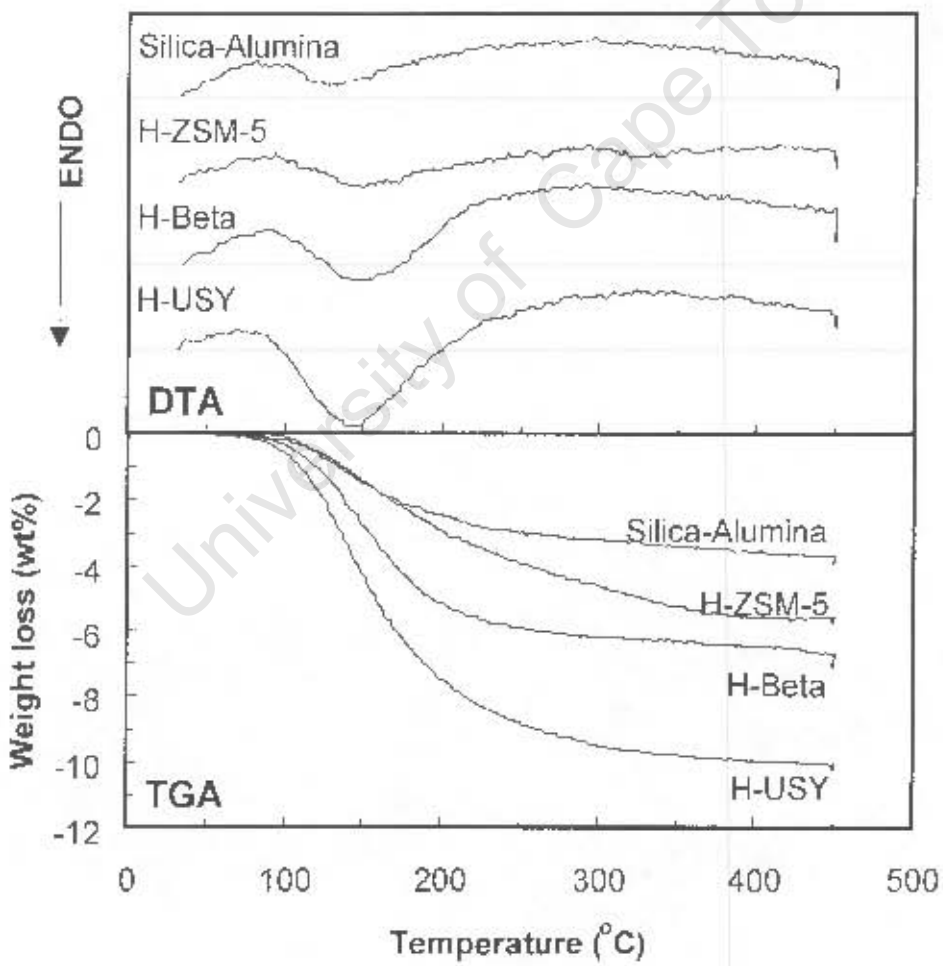


**Figure 4.13** TGA and DTA curves of relevant aluminosilicates with ramping rate set at 10°C/min ($N_2$-flowrate equals 30ml(NTP)/min).

of inflection obtained from the TG-curve. Figure 4.13 illustrates aluminosilicate TGA-DTA results with ramping rate = 10°C/min. The water uptake decreases in the order H-USY > H-Beta > H-ZSM-5, showing the expected decrease in the hydrophilic properties of the zeolites with increasing Si/Al ratio.

The DTA curves show a minimum between 100°C and 150°C which corresponds only to a certain extent with the point of inflection on the TGA curves. This is especially true for the lower ramping rates, i.e., 5°C/min and 2°C/min. Table 4.2 gives the heat of desorption of water onto the aluminosilicates.

**Table 4.2 Heat of desorption of water onto the aluminosilicates by the method of Cventanovic and Amenomiya**

| Aluminosilicate | $H_2O$ remaining adsorbed after 4-5h $N_2$-flushing (mmol $H_2O$ / g) | $\Delta H_{des}$ of water (kJ / mol) | $(R^2)^{(a)}$ |
|---|---|---|---|
| silica-alumina | ca. 2.24 | 46 | 0.885 |
| H-USY | ca. 6.32 | 45 | 0.972 |
| H-Beta | ca. 4.27 | 37[b] | 0.944 |
| H-ZSM-5 (Si/Al = 13) | ca. 3.35 | 27 | 0.932 |
| H-ZSM-5 (Si/Al = 22) | – | – | – |

(a) Square of the Pearson Product Moment Correlation of a straight line fitted through $1/T_m$ versus $2*\ln(T_m)$ - ln(ramping rate) according to equation 3.1
(b) Includes a ramping rate at 20°C/min in addition to 2, 5 and 10°C/min



It is of interest to compare the heat of vaporisation, $\Delta H_{vap}$, of water with that of the heat of desorption, $\Delta H_{des}$, –values determined for the 4 different aluminosilicates. Between temperatures 100°C and 150°C, the heat of vaporisation of water lies between 40.6kJ/mol (at 100°C) and 38.1kJ/mol (at 150°C) [Sandler, 1989]. The temperature range is chosen since it includes most of the data points (points of inflection) used to calculate the $\Delta H_{des}$-values. The $\Delta H_{des}$-values of water adsorbed on silica-alumina and H-USY is clearly greater than the $\Delta H_{vap}$-values, whereas for H-Beta $\Delta H_{des}$ is comparable to $\Delta H_{vap}$ of water, while $\Delta H_{des}$ of water for H-ZSM-5

(Si/Al = 13) is considerably less than $\Delta H_{vap}$ of water. It can thus be concluded that a favourable interaction exists between water and silica-alumina or between water and H-USY, possibly due to the strong ionic framework charges existing within these aluminosilicates. The strength of interaction of water onto the walls of H-Beta is less than that of H-USY or silica-alumina, however, since the difference between $\Delta H_{ads}$ and $\Delta H_{vap}$ is relatively small the overall interaction may be regarded as being ideal. Although H-ZSM-5 (Si/Al = 13) has a very low Si/Al ratio, strong repulsion forces are likely to exist between the water molecules and H-ZSM-5 (Si/Al = 13) resulting in a low $\Delta H_{ads}$.

### 4.4.2.3 STRENGTH OF ADSORPTION OF $NH_3$ ON ALUMINOSILICATES

The heat of adsorption / desorption of gaseous $NH_3$ is determined by means of temperature programmed desorption (TPD) using the method described by Cventanovic and Amenomiya [1967 and 1973]. A strong interaction of the product $NH_3$ with the Brønsted acid site is required to drive the reaction MPDA to resorcinol forward (see Section 2.1.2.1). The $NH_3$–TPD spectra (see Figure 4.14) shows the rate of $NH_3$ desorption versus temperature and time for silica-alumina (Si/Al = 6.9), H-USY (Si/Al = 5.6), H-Beta (Si/Al = 14.4) and H-ZSM-5 (Si/Al = 13). Although the temperature ramping rate chosen in Figure 4.14 is 10°C/min, the $NH_3$-TPD for every one of the aluminosilicates is repeated applying ramping rates of 5°C/min and 2°C/min, with all other conditions remaining constant, i.e., mass solid = 0.25g and $He_2$-flow rate = 63ml(NTP)/min.

Only a single high temperature desorption (HTD) peak is observed for $NH_3$ desorption from H-USY, H-Beta and H-ZSM-5 (Si/Al =13) under the experimental conditions used. The absence of low temperature desorption (LTD) peaks would indicate that the zeolite samples shown in Figure 4.14 contain no physisorbed ammonia. The $NH_3$ desorption spectrum from the silica-alumina sample has a shoulder at a temperature above that of the peak maximum temperature ($T_{max}$) at

309°C. Blank run TPD spectra show no $H_2O$ loss due to dehydroxylation of previously calcined silica-alumina (at 450°C) while ramping from 150°C to 450°C. Thus, the high temperature shoulder cannot be attributed to dehydroxylation.

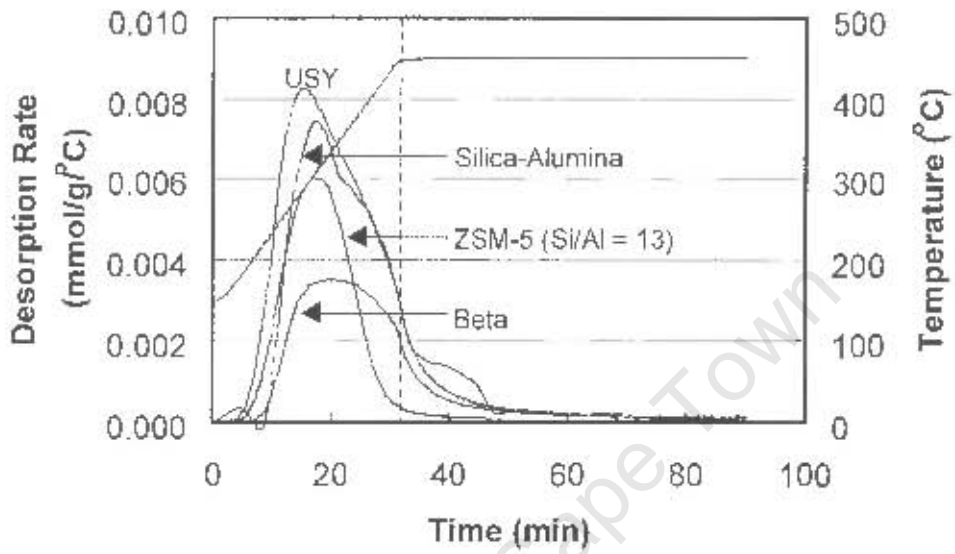


**Figure 4.14** $NH_3$-TPD spectra of silica-alumina, ZSM-5 (Si/Al = 13), Beta and USY (ca. 0.25g (hydrated), 63ml(NTP)/min helium, 10°C/min).

The dashed line in Figure 4.14 indicates the time period after which the temperature remains constant at 450°C. At that time (dashed line) the $NH_3$ desorption rate from silica-alumina, H-Beta and H-USY show a distinct bend due to the change in the temperature ramping rate. When using a ramping rate of 10°C/min, the peak maximum temperature, $T_m$, of H-USY (289°C) is lowest, followed by silica-alumina (309°C), H-ZSM-5 (Si/Al = 13) (312°C) and H-Beta (338°C). It is, however, interesting that $T_m$ observed for H-ZSM-5 (Si/Al = 13) (312°C) is below that of H-Beta (338°C) since typically the acid site strength, the pore diffusional constraints as well as the ammonium desorption / re-adsorption effects in the channels are usually greater for ZSM-5 (crystallite sizes 1μm -5μm) than for Beta zeolites (crystallite sizes < 0.3μm). Similar to the discrepancies observed for the maximum peak temperature of H-ZSM-5 (Si/Al = 13) the shape of the $NH_3$-TPD desorption curve from H-ZSM-5 (Si/Al = 13) should consist of a

more leading edge, especially since the H-ZSM-5 (Si/Al = 13) sample consists of large crystallites ranging between 1μm and 5μm [Gorte, 1982; Jones and Griffin, 1983; Rieck and Bell, 1984]. In addition to the pore diffusion, desorption / readsorption effect and particle size, both the position and shape of the spectra are also sensitive functions of the catalyst bed depth, the carrier flow rate and the temperature ramping rate [Jones and Griffin, 1983; Rieck and Bell, 1984].

**Table 4.3 The heat of desorption of $NH_3$ onto the alumino-silicates by the method of Cventanovic and Amenomiya [1967 and 1973]**

| Aluminosilicates | Al content (mmol / g) | No. of acid sites (mmol / g)[(b)] | $\Delta H_{ads}$ of $NH_3$ (kJ / mol) | $(R^2)^{(a)}$ |
|---|---|---|---|---|
| silica-alumina | 2.11 | 1.70 ± 0.14 | 62 | 0.974 |
| H-USY | 2.52 | 2.16 ± 0.07 | 44 | 0.965 |
| H-Beta | 1.08 | 0.83 ± 0.09 | 75 | 0.998 |
| H-ZSM-5 (Si/Al = 13) | 1.19 | 1.04 ± 0.13 | 89 | 0.999 |
| H-ZSM-5 (Si/Al = 22) | 0.72 | – | – | – |

(a) Square of the Pearson Product Moment Correlation of a straight lines fitted through $1/T_m$ versus $2*\ln(T_m)$ - ln(ramping rate) according to equation 3.1
(b) Based relative to the respective dehydrated aluminosilicate mass.

Table 4.3 presents the heat of adsorption of $NH_3$ calculated by fitting a straight line through $1/T_m$ versus $2*\ln(T_m)$ - $\ln(ramping\ rate)$. The slope equals $\Delta H / R$ as described by the method Cventanovic and Amenomiya [1967 and 1973]. The square of Pearson Product Moment are all greater than 0.95 implying a good straight line fit through all points. The $NH_3$ heat of desorption is calculated as being greatest for H-ZSM-5 (Si/Al = 13) (89kJ/mol), followed by H-Beta (75kJ/mol), silica-alumina (62kJ/mol) and H-USY (44kJ/mol).

The number of acid sites obtained by $NH_3$-TPD of the silica-alumina, H-USY, H-Beta and H-ZSM-5 (Si/Al = 13) samples, which are repeated 3 times at different ramping rates (10°C/min, 5°C/min and 2°C/min), are 1.70 ± 0.14, 2.16 ± 0.07, 0.83 ± 0.09 and 1.04 ± 0.13, respectively. The number of acid sites predicted

from the Si/Al ratio of the aluminosilicates (assuming only framework Al-species) are, however, greater than the equivalent experimentally determined number of acid sites. Nevertheless, Figure 4.14 shows that the $NH_3$-TPD spectrum of all aluminosilicate samples do return to the baseline before reaching 450°C. The underestimation of the experimentally determined number of acid sites on the aluminosilicates can be explained on the basis that not all the $NH_3$ was able to desorb during the given time period of 60 minutes whilst keeping the temperature at 450°C. Another possible explanation includes the removal of chemisorbed $NH_3$ while flushing the freshly adsorbed $NH_3$ at 150°C (instead of 100°C used by Hidalgo *et al.*, 1984) for 12 hours before commencing with the TPD spectrum.

#### 4.4.2.4 QUANTIFICATION OF EXTERNAL ACID SITES OF ZSM-5 SAMPLES

The number of external acid sites on H-ZSM-5 (Si/Al = 13, $d_{crystal}$ = 1-5μm) and H-ZSM-5 (Si/Al = 22, $d_{crystal}$ = ca. 0.5μm) are determined by means of temperature programmed desorption (TPD) of 4-methyl-quinoline to check whether the reaction rate of MPDA to resorcinol depends on the crystal diameter. Weber [1998] showed that 4-methyl-quinoline adsorbs only on the external surface of H-ZSM-5.

Since the thermal removal of 4-methyl-quinoline on H-ZSM-5 causes the 4-methyl-quinole to react upon desorption, the mass fractions obtained via TPD are not the same as those obtained by direct injection of 4-methyl-quinoline into the injector port of the detector [Weber, 1998]. Consequently, the determination of the external acid sites on the H-ZSM-5 zeolites is only relative. The most abundant ion in the spectrum of 4-methyl-quinoline-TPD is $m/e$ = 78, which is ascribed to benzene being formed from the decomposition of the quinoline ($m/e$ = 128) radical [Weber, 1998]. The 4-methyl-quinoline TPD spectra (based on the response signal of the most abundant fraction, viz. benzene is $m/e$ = 78) for H-ZSM-5 (Si/Al = 13) and H-ZSM-5 (Si/Al = 22) are presented in Figure 4.15.

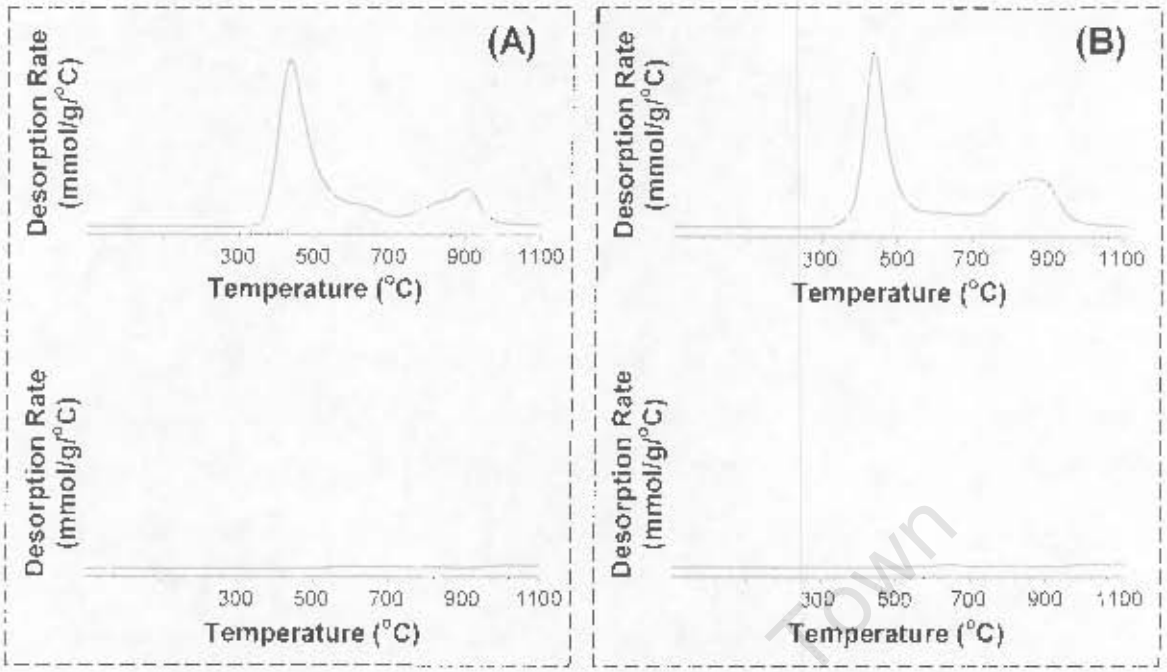


**Figure 4.15** 4-Methyl-quinoline TPD spectra of ZSM-5 (Si/Al = 22) (top curves) and ZSM-5 (Si/Al = 13) (bottom curves), (1.0g, 100ml(NTP)/min He, 10°C/min, *m/e* = 78). The experiment is repeated to check its reproducibility; compare dashed boxes (A) and (B).

The 4-methyl-quinoline TPD for both H-ZSM-5 zeolites are repeated to check for their reproducibility. All 4-methyl-quinoline TPD spectra tend to show two peaks, i.e., one low temperature desorption peak (LTD peak) and one high temperature desorption peak (HTD peak), respectively. For zeolite H-ZSM-5 (Si/Al = 22), both TPD-spectra reveal distinct LTD peaks and HTD peaks. The LTD peak maximum temperatures of the two spectra are 434°C and 440°C, and the respective HTD peak maximum temperatures are 903°C and 867°C. The HTD peaks are comparable to those obtained by Weber [1998], viz. 803 - 820°C.

The LTD peak of the H-ZSM-5 (Si/Al = 13) zeolite of the two spectra occur at 610°C and 655°C. Due to the low amount of 4-methyl-quinoline desorbing from H-ZSM-5 (Si/Al = 13), the high temperature desorption peak tends to be non-reproducible.

The areas under both the LTD peak and HTD peak for H-ZSM-5 (Si/Al = 22), however, are considerably larger than the equivalent areas for H-ZSM-5 (Si/Al = 13). From the areas given by the HTD peaks in Figure 4.15A and Figure 4.15B, the ratio of the number of external acid sites on H-ZSM-5 (Si/Al = 22) (HTD peak from 700°C - 1100°C) relative to H-ZSM-5 (Si/Al = 13) is determined. The area under the HTP peak for H-ZSM-5 (Si/Al = 13) is also arbitrarily taken from 700°C -1100°C to remain consistent with the HTP peak for H-ZSM-5 (Si/Al = 22). Subsequently, the relative number of external acid sites (H-ZSM-5 (Si/Al = 22) / H-ZSM-5 (Si/Al = 13)) calculated for Figure 4.15A and Figure 4.15B equals 16.4 and 15.2, respectively. Although determining the relative external acid sites via 4-methyl-quinoline does not prove itself as being very reproducible, the measurements do show very large differences in the number of external acid sites for the two ZSM-5 zeolites.



#### 4.4.2.5 PORE VOLUME ANALYSIS

The pore volume of silica-alumina, H-USY, H-Beta, H-ZSM-5 (Si/Al = 13) and H-ZSM-5 (Si/Al = 22) are analysed using nitrogen adsorption ($N_2$-BET) as described in Section 3.2.5. Microporous and mesoporous surface areas are also obtained (Table 4.4). Because $N_2$-BET cannot measure pore sizes below ± 17A, the micropore surface areas and pore volumes are taken as being obtained from pores less than 17A, and the mesopore surface areas and pore volumes as being obtained from pores larger than 17Å. The mesopore volumes given in Table 4.4 are further subdivided into 17Å < $d_{pore}$ < ± 115Å and $d_{pore}$ > 115Å. The combined mesopore surface area ($d_{pore}$ > 17Å) gives an indication of the external surface area of the sample. The nitrogen adsorption (coupled with desorption) isotherms for samples silica-alumina, H-USY, H-Beta, H-ZSM-5 (Si/Al = 13) and H-ZSM-5 (Si/Al = 22) show a hysteresis for all five samples. This is especially true for silica-alumina and H-Beta, indicating that mesopores are present.

H-USY is found to have the largest total surface area (607$m^2$/g) and H-ZSM-5 (Si/Al=13) the smallest (303$m^2$/g) (Table 4.4). Apart for the amorphous silica-alumina, the mesopore surface area for H-Beta is found to be by far the largest (199$m^2$/g) of all the zeolites analysed. The smallest mesopore surface areas are that of ZSM-5(Si/Al=13) (26$m^2$/g) and ZSM-5(Si/Al=22) (28$m^2$/g).

**Table 4.4 Surface area and pore volume data for Silica-Alumina, H-USY, H-Beta, H-ZSM-5 (Si/Al=13), H-ZSM-5 (Si/Al=22)**

| | | silica-alumina | H-USY | H-Beta | H-ZSM-5 Si/Al = 13 | H-ZSM-5 Si/Al = 22 |
|---|---|---|---|---|---|---|
| BET surface area | ($m^2$/g) | 367 ± 17 | 607 ± 5 | 559 ± 16 | 303 ± 2 | 312 ± 5 |
| Micropore surface area | ($m^2$/g) | – | 559 | 359 | 278 | 284 |
| Mesopore surface area | ($m^2$/g) | 390 | 48 | 199 | 26 | 28 |
| Pore volume ($d_{pore}$ < 17Å) | (cc/g) | – | 0.260 | 0.166 | 0.129 | 0.132 |
| Pore volume (17Å < $d_{pore}$ < = 115Å) | (cc/g) | 0.464 | 0.030 | 0.190 | 0.018 | 0.017 |
| Pore volume ($d_{pore}$ > 115Å) | (cc/g) | 0.018 | 0.054 | 0.242 | 0.009 | 0.013 |



Reasons for subdividing the mesopore volume into 17Å < $d_{pore}$ < ± 115Å and $d_{pore}$ > 115Å can be explained on the basis of Figure 4.16, which illustrates the pore size distributions for all the considered aluminosilicates. H-Beta shows a wide pore size distribution. In contrast, the ZSM-5 zeolites show hardly a distribution in the mesopore range. Although few data points are taken in the mesopore region, reproducibility of $N_2$-adsorption on H-Beta and H-ZSM-5 (Si/Al = 13) is consistent with the manufacturers error (<10%) specifications (cumulative surface area). A distinct peak in the incremental pore volume versus pore diameter can be made out for silica-alumina and H-Beta, with the peak starting at 17Å and ending at 115Å. For $d_{pore}$ > 115Å, the incremental pore volume remains constant with respect to the pore diameter. Similar trends are observed for H-USY, H-ZSM-5 (Si/Al = 13) and H-ZSM-5 (Si/Al = 22) where the downward sloping curve (17Å <

$d_{pore}$ < 115Å) tends to be a carry-over from the micropore volumes before levelling out to a constant incremental pore volume for $d_{pore}$ > 115Å. Only the spectrum obtained for H-USY shows a second peak between $d_{pore}$ = 115Å and $d_{pore}$ = 398Å before levelling out. H-Beta is the only aluminosilicate that shows large (ca. 0.02cc/g) incremental pore volumes for $d_{pore}$ > 115Å.

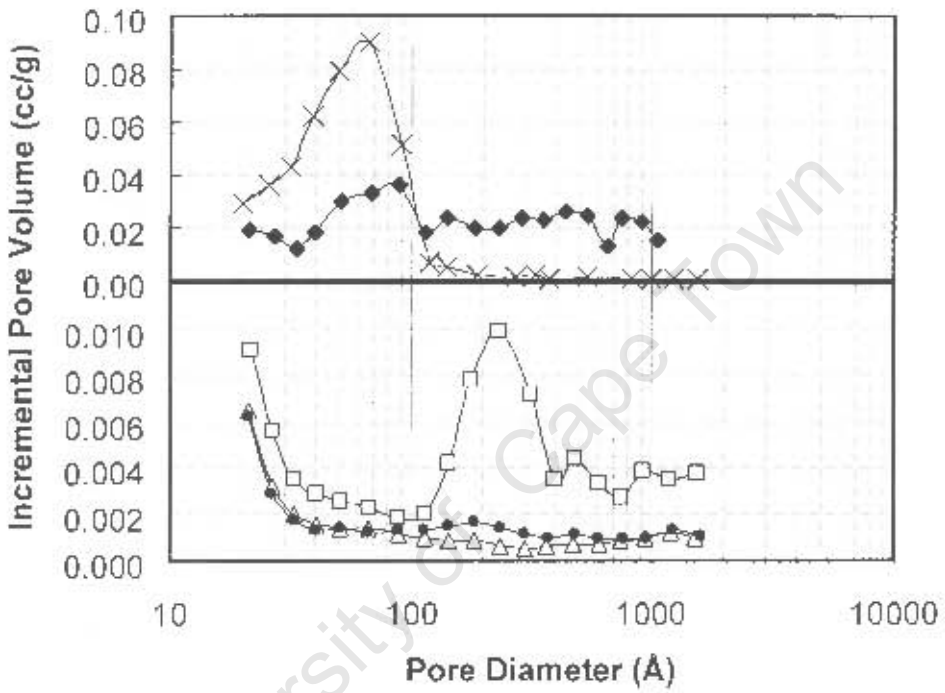


**Figure 4.16** Pore size distribution of silica-alumina (×), H-USY ( ), H-Beta (♦), H-ZSM-5(Si/Al=13) (∧) and ZSM-5(Si/Al=22) (•).



### 4.4.2.6 ADSORPTION STUDIES OF SOLUTES ON ZEOLITES

Figures 4.17 through to 4.22 show the adsorption of dissolved MPDA, MAP, resorcinol and ammonia onto the zeolites H-USY, H-Beta and H-ZSM-5 (Si/Al = 13). The adsorbed amount is plotted against the mole fraction of the solute in solution at various adsorption temperatures. The method used for predicting the adsorption isotherms at reaction temperature is by means of batch adsorption

experiments at low temperatures. As outlined in Section 3.2.4.5, the amount of zeolites (ca. 0.4g) used per 15ml of aqueous solution corresponds roughly to the amount of zeolite used during the reaction (10g zeolites per 350ml of solution). The numerical adsorption data are given in APPENDIX-H.

**(i) Adsorption of MPDA on zeolites**

Figure 4.17 illustrates the adsorption data of MPDA on zeolites H-USY, H-Beta and H-ZSM-5 (Si/Al = 13) at temperatures 30°C, 50°C, 70°C and 90°C. The adsorbed amount is plotted against the mole fraction of the solute in solution.

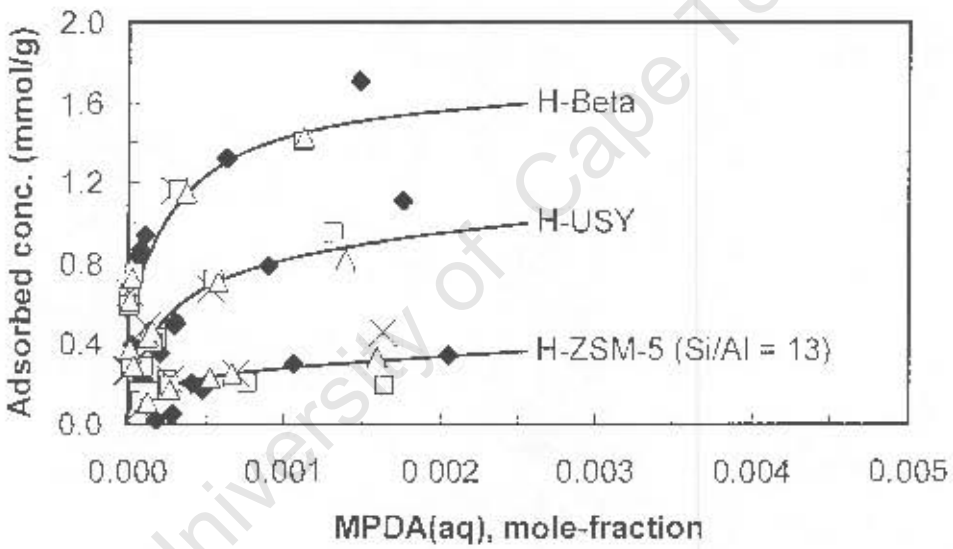


**Figure 4.17** Adsorption-equilibrium data for aqueous MPDA on USY, Beta and ZSM-5 (Si/Al = 13) at 30°C (♦), 50°C (_), 70° (^) and 90°C (×).

Irrespective of the adsorption temperature, the amount of MPDA adsorbed (see Figure 4.17) is larger for H-Beta than for H-USY which in turn is larger than for H-ZSM-5 (Si/Al = 13). In fact, for each zeolite considered, the MPDA adsorption isotherms at temperatures 30°C, 50°C, 70°C and 90°C tend to overlap and thus the adsorption is seemingly temperature independent. From the initial slope of the adsorption curves and taking into consideration the differences in the total

MPDA uptake, it can be deduced that the strength of adsorption follows the order H-Beta > H-USY > H-ZSM-5. The difference in the MPDA adsorption strength between H-Beta and H-USY can be expected based on the $NH_3$-TPD results (Section 4.4.2.3). The heat of desorption of ammonia is higher for H-Beta (75kJ/mol) than for H-USY (44kJ/mol). The observed adsorption strength of MPDA on H-ZSM-5 (Si/Al = 13) contradicts the $NH_3$-TPD study since a strong interaction between the base MPDA and H-ZSM-5 (Si/Al = 13) would have been expected given that $\Delta H_{des}(NH_3)$ on H-ZSM-5 (Si/Al = 13) equals 89kJ/mol. The solution pH measured during the adsorption of MPDA onto the zeolites is ca. 6.0 for H-Beta, 7.0 for H-USY and 8.5 for H-ZSM-5 (Si/Al = 13) with the pH increasing only slightly with increasing MPDA bulk concentrations. Extracting any direct correlation between the different adsorption systems may not be entirely correct since the pH of the bulk solution affects the equilibrium $H_2O + C_6H_4(NH_2)_2 = [C_6H_4(NH_2)(NH_3)]^+ + OH^-$ ($pK_a$ of $MPDA^+$ = 8.89 [Adrien and Serjeant, 1983]) in the bulk solution.

**Table 4.5 Comparison of MPDA adsorption capacity observed during liquid phase adsorption with the number of acid sites and BET pore volume**

| Zeolite | MPDA ads. capacity (mmol/g) | Al content (mmol/g) | Cumulative BET pore Volume[a] (equiv. mmol MPDA per gram zeolite) | | |
|---|---|---|---|---|---|
| | | | $d_{pore}$ < 17Å | $d_{pore}$ < 115Å | $d_{pore}$ < 3000Å |
| H-USY | 1.0 | 2.52 | 2.6 | 2.9 | 3.5 |
| H-Beta | 1.5 | 1.08 | 1.7 | 3.6 | 6.1 |
| H-ZSM-5 (Si/Al = 13) | 0.3 | 1.19 | 1.3 | 1.5 | 1.5 |

(a) Cumulative pore volume (as determined by BET analysis) multiplied by the density of liquid MPDA at 70°C = 10.17mmol/ml

In Table 4.5 a comparison is made between the experimentally observed adsorption capacity during liquid phase adsorption and the number of Brønstec acid sites found within each type of zeolite. The number of Brønsted acid sites is taken as being directly related to the aluminium content since the $NH_3$-TPD study

showed a good relationship between the number of Brønsted acid sites and the zeolitic aluminium content. The BET-study allows for a crude estimation of the maximum amount of MPDA able to fit into the zeolite pores. Three different boundary conditions are chosen for establishing the volume that the MPDA molecules occupy, i.e., $d_{pore} < 17Å$, $d_{pore} < 115Å$ and $d_{pore} < 3000Å$. The density chosen for MPDA is that at 70°C (10.17mmol/ml [Daubert and Danner, 1989]).

The average maximum observed amount of MPDA adsorbed during the liquid phase adsorption study onto H-USY for isotherms 30°C, 50°C, 70°C and 90°C is ca. 0.95mmol MPDA per gram dehydrated H-USY zeolite. This is considerably less than the total amount of Brønsted acid sites (2.52mmol/g) available on H-USY or the predicted amount of MPDA able to reside within the $d_{pore} < 17Å$ region (2.6mmol MPDA/g), assuming that a strong interaction is likely to exist between the basic MPDA molecules and the Brønsted acid sites. It can, however, be argued that the hydrophilic nature of H-USY allows for a strong water-faujasite interaction (as shown in Section 4.4.2.2) and the relatively weak Brønsted acid strength relative to the other zeolites (see Section 4.4.2.3) could lead to a water-MPDA phase within the zeolite structure.

Unlike for H-USY, the maximum adsorption capacity of MPDA on H-Beta (ca. 1.50mmol/g) is considerably larger than the number of Brønsted acid sites (1.08mmol/g) available for H-Beta and approximately identical to the theoretical amount MPDA able to reside within the $d_{pore} < 17Å$ region (1.7mmol MPDA/g). Easy penetration of MPDA molecules into the three dimensional channel system of H-Beta is expected since H-Beta is a large pore zeolite (aperture = 7.6Å x 6.4Å) consisting of very small crystallites (<0.3μm). Nevertheless, an MPDA adsorption capacity greater than the number of acid sites available on H-Beta implies that the H-Beta must act as some form of concentrating vessel with the MPDA-water concentration in the region ($17Å < d_{pore} < 115Å$) being greater than the concentration in the region ($115Å < d_{pore} < 3000Å$) which in turn is greater than the bulk solution concentration. It is improbable that physisorbed MPDA

molecules reside directly on top of the chemisorbed MPDA monolayer given that steric hindrance does exist within the micropore region. Thus, the notion that the MPDA concentration in the capillary region (17Å < $d_{pore}$ < 3000Å) is greater than in the bulk solution must be correct. The TGA and the $NH_3$-TPD study complement the observed phenomena since the water-Beta interaction is weaker than that between water and H-USY, while the interaction of base $NH_3$ on H-Beta is considerably stronger than on H-USY, and thus a greater attraction is observed for MPDA onto zeolite H-Beta than onto H-USY.

Comparison of the observed MPDA adsorption capacity on H-ZSM-5 (Si/Al = 13) (ca. 0.30mmol MPDA/g) with the number of Brønsted acid sites (1.19mmol/g) and/or the theoretical amount of MPDA able to fill in the micropore region (1.3mmol MPDA/g), it seems that MPDA molecules do not enter the pore structure as readily as originally thought. The hydrophobic characteristics of the H-ZSM-5 (Si/Al = 13) zeolite as shown by TGA (see Section 4.4.2.2) and the very strong adsorption of $NH_3$ onto H-ZSM-5 (Si/Al = 13) (see Section 4.4.2.3) would further suggest that the MPDA adsorption capacity should be larger than 0.30mmol MPDA/g if the aqueous MPDA molecules are able to penetrate the ZSM-5 pore structure (aperture = 5.3Å x 5.6Å). Although gaseous MPDA (6.6Å x 4.8Å) can enter the pore structure of ZSM-5, the hydrated MPDA (at least at 30°C due to little lattice vibration) is restricted with the difference between the usually stronger acid sites located between the channel intersections and the acid strength of the previously MPDA adsorbed external surface acid sites being too small to strip the MPDA of its hydration water. Alternatively, the initial strong driving force existing between the MPDA molecules and H-ZSM-5 leads to the external surface acid sites interacting very strongly with the MPDA, which results in pore mouth narrowing / blocking [Parton *et al.*, 1989] with only a limited amount of MPDA being able to diffuse into the pore channels. Considering the relatively small external surface area observed for H-ZSM-5 (Si/Al = 13) by 4-methyl-quinoline adsorption (Section 4.4.2.4) and the large H-ZSM-5 crystallite sizes (1μm - 5μm) shown Figure 4.10, some of the MPDA must, however,

penetrate the pore channels of H-ZSM-5 (Si/Al = 13) since the mesopore volume (17Å < $d_{pore}$ < 3000Å) for H-ZSM-5 (Si/Al = 13) can only take on a maximum of 0.2mmol MPDA/g (see Table 4.5). Since the activity coefficient of water in MPDA is close to unity it is however unlikely that pure MPDA will surround the H-ZSM-5 (Si/Al = 13) and therefore, approximately half of the observed MPDA molecules adsorbed onto H-ZSM-5 (Si/Al = 13) must reside within the zeolite pore structure.

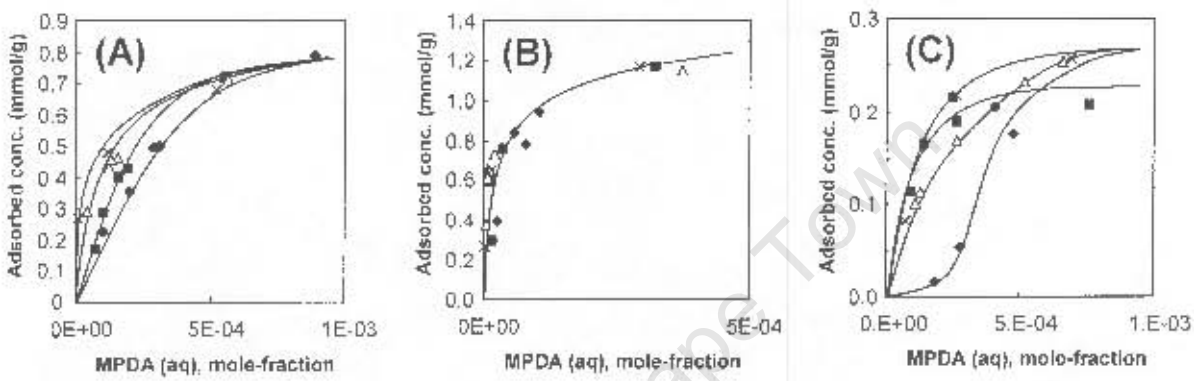


**Figure 4.18** Adsorption-equilibrium data with the focus primarily on the initial slopes of the adsorption isotherms of aqueous MPDA on (A) H-USY, (B) H-Beta and (C) H-ZSM-5 (Si/Al = 13) at 30°C (♦), 50°C (■), 70° (Δ) and 90°C (×).



Unlike in Figure 4.17 where the focus was more on the adsorption capacity, the emphasis in Figure 4.18 is on the initial slopes of the adsorption isotherms. The overall trend is for the initial slopes of the adsorption isotherms to increase with temperature, i.e., to be endothermic. This is especially true for MPDA adsorbed onto H-USY (Figure 4.18A). However, since MPDA is more basic than water and the zeolite surfaces consist of Brønsted acids, it would be reasonable to assume that the exchange of the previously water adsorbed zeolite with MPDA would result in a decrease in the surface free energy, $\Delta G_a$. The extent that certain degrees of freedom are either lost or gained after the confinement of the MPDA molecules to an aluminosilicate surface layer is debatable, since one MPDA molecule would result in the displacement of several water molecules and

therefore the entropy term, $\Delta S_a$, could be either positive or negative. Making use of Equation 4.1 then shows that the heat of competitive adsorption, $\Delta h_{ad}$, could be exothermic as is usually the case for gas phase adsorption or endothermic as is the case for aqueous MPDA onto H-USY (Figure 4.18A).

$$\Delta G_a = \Delta h_{ad} - T\Delta S_a \qquad \textbf{4.1}$$

Considering the favourable interaction of water with H-USY and its the relatively weak acid strength, $\Delta G_a$ will be less negative for H-USY after the water-MPDA exchange process than for example H-Beta. The acid strength of the latter zeolite is considerably greater and the surface-water interaction is less favourable. Consequently, assuming $\Delta S_a$ to be of the same magnitude for both zeolites presently considered, $\Delta h_{ad}$ for H-USY will be greater than for H-Beta. This corresponds exactly to the observations in Figure 4.18A and Figure 4.18B, where $\Delta h_{ad}$ for MPDA on H-USY is > 0kJ/mol, while $\Delta h_{ad}$ of H-Beta tends to ⊥0kJ/mol.

Extending the above-mentioned thought to the case of H-ZSM-5 (Si/Al = 13), an exothermic $\Delta h_{ad}$ is expected since the associated very strong Brønsted acid sites and the water repelling characteristic of H-ZSM-5 (Si/Al = 13) should return the lowest $\Delta G_a$-value relative to all zeolites considered. However, the conclusion of a negative $\Delta h_{ad}$ only holds for the 50°C to the 70°C isotherm if the 30°C and 90°C isotherms are excluded. This would imply that other factors must be responsible for the great variations in the adsorption isotherms with changing temperatures. Contrary to the Langmuir-type shape of the 50°C, 70°C and 90°C isotherms, the 30°C isotherm (Figure 4.18C) follows an S-shaped curve. Considering the strong interaction forces that exist between the basic MPDA molecules and that the relatively water repelling H-ZSM-5 (Si/Al = 13) surface, the S-shaped isotherm at 30°C can only be explained on the basis that MPDA ($d_{molecule}$ equals ca. 6.6Å x 4.8Å) cannot enter the pore channel system of the medium pore zeolite ($d_{aperture}$ = 5.3Å x 5.6Å). This is in contradiction to the observations made by Dessau [1980] stating that only molecules having a minimum elliptical cross-section greater than

6.4Å x 6.9Å would be excluded from the interior of the ZSM-5 zeolites. Since MPDA is in solution, the kinetic diameter should be greater than 6.6Å x 4.8Å. The formation of the S-shaped curve is thus justified by noting that H-ZSM-5 (Si/Al = 13) must act as a concentrating agent and the low solubility of MPDA in water at 30°C leads to an increase in the MPDA concentration around the zeolite. The MPDA-water solubility at 30°C (solubility at 25°C = 0.055 mole fraction [Perry, 1989]) may to a certain degree have an influence on the adsorption isotherm. At 50°C, however, it seems that lattice vibration is large enough to accommodate the solvated MPDA molecule. Contrary to the adsorption isotherms at 70°C and 90°C, the 50°C isotherm reaches a plateau at low $x_{MPDA}$. The varying shapes in adsorption isotherms as well as the existence of a negative $\Delta h_{a,l}$ between the 50°C and 70°C isotherms and a positive $\Delta h_{a,l}$ between isotherms 70°C to 90°C must be due to a number of factors. The anomalous temperature dependence can be attributed to chemical transformations that the adsorbed MPDA species undergo on the zeolite surface. This finding is expected to be more prevalent on the surface of H-ZSM-5 (Si/Al = 13) due to its the hydrophobic nature and its strong Brønsted acid sites. It remains unknown whether the chemical transformation is due to the presence of dissolved oxygen that may lead to endothermic polymerisation reactions via oxidation or whether the concentration of MPDA molecules around the zeolite may lead to the formation of poly-phenyleneamines. No experimental proof is, however, available for the hypothesis. The reason is simply that in order to examine whether side reactions did occur on the heterogeneous acid, the adsorbents need to be desorbed into water to make comments on the reversibility of the adsorption-desorption process. Since amine compounds interact strongly with the surface acid sites, a substantial amount of water is required to desorb most of the previously adsorbed amine compounds. The concentration of the original adsorbent and the possibly transformed compounds required for their roughly complete desorption would be too low to be accurately detected by an HPLC.

**(ii) Adsorption of MAP on zeolites**

The amount of MAP adsorbed as a function of the mole fraction of MAP in the bulk aqueous phase is shown in Figure 4.19. The chosen adsorption temperatures are 30°C and 70°C.

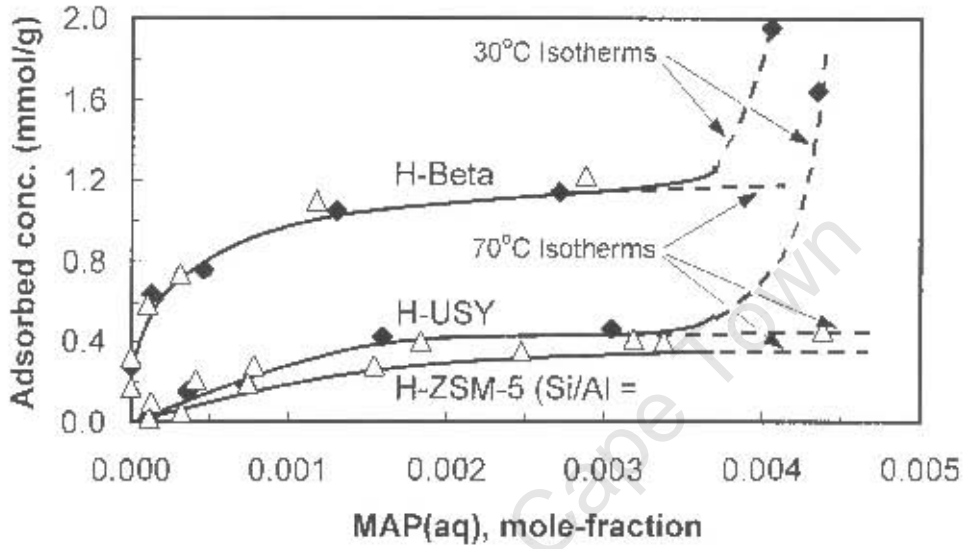


**Figure 4.19** Adsorption-equilibrium data for aqueous MAP on USY, Beta and ZSM-5 (Si/Al = 13) at 30°C (♦) and 70° (Δ).

The adsorption isotherms at the two different temperatures are grouped together for the sake of presenting an overall adsorption picture. As observed in Figure 4.19, the initial slopes of the 30°C and 70°C adsorption isotherm tend to overlap, again giving the perception of temperature independent isotherms. However, the adsorption isotherm obtained at 30°C show a marked increase in the adsorption concentration after reaching a bulk MAP mole-fraction of ca. 0.0035. Beyond an equilibrium bulk solution mole fraction of ca. 0.0036 there tends to be a preferential adsorption only for MAP, and water which is co-adsorbed is ejected out thereby increasing the adsorption of MAP. This sudden increase in uptake of MAP suggests a phase change in the pores of adsorbed MAP from MAP in water solution to water in MAP solution. According to Sidgwick and Callow [1924], the solubility of MAP in water at 32.6°C is 3.69wt%, which converts to a mole fraction

of 0.006285. Since the melting point of MAP is between 122°C and 123°C, MAP within the pores may exist as a solid. Consequently, only the data below the equilibrium bulk solution mole-fraction of 0.0035 is relevant for the adsorption study.

From the initial slopes of the MAP adsorption isotherms, the strength of adsorption of MAP on H-Beta is greatest followed by H-USY and H-ZSM-5 (Si/Al = 13). Also the adsorption capacity (plateau) follows the same trend. Thus, the overall trend regarding the adsorption of MAP on zeolites is identical to that of MPDA on zeolites, although the adsorption strength of MAP on zeolites is weaker. This can be attributed to the difference in basicity of the two components ($pK_a$ of $MAP^+$ = 9.63 versus $pK_a$ of $MPDA^+$ = 8.89 [Adrien and Serjeant, 1983]). The lower average solution pH of ca. 6.0 for MAP on H-Beta, 6.7 for MAP on H-USY and 7.5 for MAP on H-ZSM-5 (Si/Al = 13) relative to the pH's measured during the adsorption of MPDA is another confirmation of the MAP-zeolite interaction being weaker than that of MPDA.

**Table 4.6 Comparison of the adsorption capacity during liquid phase adsorption of MAP and MPDA on relevant zeolites**

| Zeolite | Al Content (mmol/g) | Adsorption Capacity (mmol/g) | | Ratio MAP:MPDA Ads. Capacity |
|---|---|---|---|---|
| | | MAP | MPDA | |
| H-USY | 2.52 | 0.45 | 0.95 | 0.5 |
| H-Beta | 1.08 | 1.10 | 1.50 | 0.7 |
| H-ZSM-5 (Si/Al = 13) | 1.19 | 0.30 | 0.30 | 1.0 |

Since the dimensions of the MPDA and MAP molecule are identical with MAP being theoretically the slightly smaller of the two, the adsorption capacity of the molecules is thought to be at least equal. However, this is not the case since the amount of MAP on H-USY is ca. 0.45mmol MAP/g, H-Beta ca. 1.10mmol MAP/g and H-ZSM-5 (Si/Al = 13) ca. 0.30mmol MAP/g compared to 0.95mmol MPDA/g, 1.50mmol MPDA/g and 0.30mmol MPDA/g for the respective zeolites. The

comparison is tabulated in Table 4.6. The biggest difference between the adsorption capacity of MAP and MPDA on a particular zeolite is that of H-USY with twice the amount of MPDA adsorbing per gram of zeolite than MAP. On H-Beta, the amount of MAP adsorbing is ca. 70% of that of MPDA on H-Beta, while the adsorption capacity of MAP on H-ZSM-5 (Si/Al = 13) is equal to that observed for MPDA. These trends can again be explained on the basis of the competitive behaviour between MAP and water molecules interacting with the zeolite walls. Since MAP is less basic than MPDA, the MAP molecules chemisorb less strongly onto the surface of the zeolites than MPDA molecules. Thus, the decrease in the surface free energy, $\Delta G_s$, after replacing the previously sorbed water with MAP is less pronounced than is case with MPDA. The lower bulk solution pH measured for the MAP-water-zeolite system combined with a lesser change in $\Delta G_s$ allows for greater adsorption of water. Consequently, the ratio of the adsorption capacity of MAP relative to that of MPDA on the individual zeolites must show the lowest fraction for zeolites possessing the strongest interactions with water. This is precisely what is observed with the adsorption capacity ratio of MAP:MPDA being 0.5 on H-USY ($\Delta H_{des}$ of $H_2O$ = 45kJ/mol), 0.7 on H-Beta ($\Delta H_{des}$ of $H_2O$ = 38kJ/mol) and 1.0 on H-ZSM-5 (Si/Al = 13) ($\Delta H_{des}$ of $H_2O$ = 27kJ/mol) (see Section 4.4.2.2). A very strong hydrophilic interaction exist between water and H-USY followed by an almost ideal (actvity coefficient ~ 1) water-surface interaction on H-Beta. The interaction of water with H-ZSM-5 (Si/Al = 13) is hydrophobic. As a result, the change in the adsorption capacity of MAP and MPDA on H-ZSM-5 (Si/Al = 13) is similar. This could have two implications. Either the weaker MAP-zeolite surface interaction allows for easier penetration of the MAP molecules into the zeolite pore structure (see Table 4.5 for roughly estimated amount of MPDA molecules able to reside in the micropores of H-ZSM-5) due to easier adsorption-desorption of MAP while migrating toward the intersecting channels. The other implication is that if the same amount of MAP enters the pore structure of MPDA the amount of water present in the nearest proximity of H-ZSM-5 (Si/Al = 13) for both adsorption systems is minimal. For the case of MAP adsorbing on H-Beta, it is interesting that the adsorption capacity of MAP on H-Beta (Table 4.6) equals

the amount of aluminium atoms per gram of solid. Although this would point towards one MAP molecule being bonded to one Brønsted acid site (assuming all aluminium being framework aluminium), this may not necessarily be the case even though theoretically all molecules (if ideally packed) should be able to reside in the micropore region (see Table 4.5). The molecules within the rigid channel system are, however, exerted to steric constraints and in admixture with water molecules it may be unlikely that each Brønsted acid is occupied by the amine functional group of one MAP molecule. It must be remembered, that adsorption of the non-ionic MAP can also occur by the adsorption of the hydroxy-group onto the hydrophobic oxygen anions of the zeolite surface [Narita *et al.*, 1985; Niwa *et al.*, 1997]. As already discussed during the adsorption study of MPDA, endothermic coupling reactions may also occur with MAP molecules being linked via the oxygen or nitrogen atom.

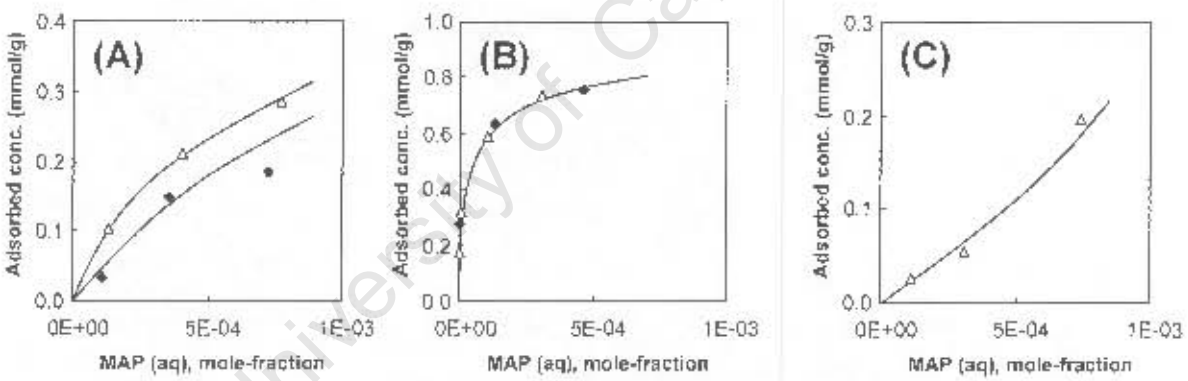


**Figure 4.20** Adsorption-equilibrium data with the focus primarily on the initial slopes of the adsorption isotherms of aqueous MAP on (A) H-USY, (B) H-Beta and (C) H-ZSM-5 (Si/Al = 13) at 30°C (●) and 70° (Δ).

Figure 4.20 focuses on the initial slopes of the MAP adsorption isotherms. The MAP adsorption isotherms show identically the same temperature dependence for H-USY and H-Beta as discussed previously during the MPDA adsorption study. The favourable interaction of water with the H-USY surface in combination with its relatively weak Brønsted acid site strength gives rise to a positive $\Delta h_{ad}$.

Since the Brønsted acid site strength of H-Beta is greater than that for H-USY and surface-water interaction on H-Beta is less strongly influenced, $\Delta h_{ad}$ for MAP on H-Beta should return a less positive value than for the case of MAP adsorbing onto H-USY. This is observed in Figures 4.20A and 4.20B. Since MAP is less basic than MPDA, $\Delta h_{ad}$ for MAP adsorbing on a particular zeolite should theoretically be greater than that for MPDA adsorbing. Stated differently, the adsorption of MPDA onto a zeolite is more exothermic than the respective adsorption of MAP. Although, the qualitative analysis of the adsorption isomers prevents any value being ascribed to the relevant $\Delta h_{ad}$-terms, it is of interest to note that as was the case for MPDA adsorbing on H-Beta, the $\Delta h_{ad}$ for MAP on H-Beta is ±0kJ/mol (similar to that obtained for MPDA adsorption). Therefore, the adsorption of a weaker base onto H-Beta has a lesser impact on the $\Delta h_{ad}$-value than initially estimated. Having similar $\Delta h_{ad}$-value for the adsorption of MPDA and MAP would imply that the MAP-surface adsorption strength is affected less strongly by the weaker base and thus the MAP molecules must primarily adsorb onto Brønsted acid sites via the $-NH_2$ functional group. The change in the adsorbent from MPDA to MAP seems to affect the adsorption capacity more strongly than the surface-acid base interaction. This implies that although the rate of adsorption of MPDA (initial slope) is greater than that of MAP, the adsorption strength between the amine functional group and the Brønsted acid site remains essentially the same.

The adsorption isotherm of MAP on H-ZSM-5 (Si/Al = 13) is illustrated in Figure 4.20C. Although the isotherms of MAP on H-USY and H-Beta is that of a Langmuir isotherm, the adsorption isotherm for MAP on H-ZSM-5 (Si/Al = 13) has a tendency to be slightly S-shaped. Since not enough data points are available for the true identification of the shape of the MAP on H-ZSM-5 (Si/Al = 13), the interpretation is only speculative. The initial slope of the adsorption isotherm at 70°C of MAP on H-ZSM-5 (Si/Al = 13) is considerably flatter than that of MPDA on H-ZSM-5 (Si/Al = 13). Consequently, the strength of adsorption of MAP is less than that of MPDA.

**(iii) Adsorption of resorcinol on zeolites**

The adsorption data of resorcinol onto H-USY, H-Beta and H-ZSM-5 (Si/Al = 13) at 70°C is shown in Figure 4.21. The absence of functional amine groups on the benzene ring and the larger solubility of resorcinol in water causes resorcinol to have a much lower adsorption affinity then MPDA or MAP. The overall pattern of H-Beta adsorbing more solutes than H-USY and H-ZSM-5 (Si/Al = 13) is also observed for the adsorption of resorcinol. The solution pH of the bulk solution is ca. 5.0 for H-Beta, 6.2 for H-USY and 7.0 for H-ZSM-5 (Si/Al = 13).

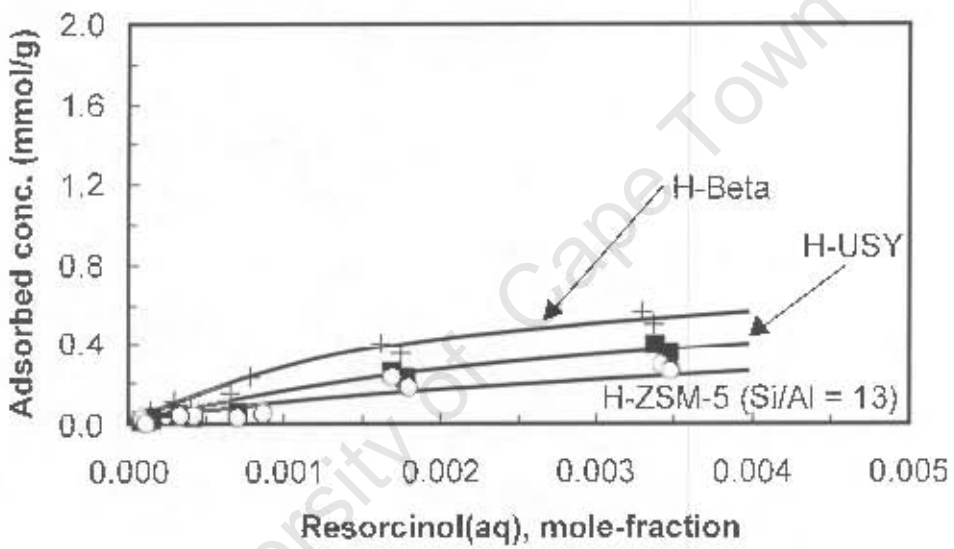


**Figure 4.21** Adsorption-equilibrium data for aqueous resorcinol on USY (■), Beta (+) and ZSM-5 (Si/Al = 13) (O) at 70°.

The flatter slopes of the resorcinol adsorption isotherms point towards considerably weaker adsorption strength of resorcinol if compared to those of MAP and MPDA. This indicates that the adsorption driving force created by the resorcinol zeolite-surface interaction strength is less. Since resorcinol is a weak acid ($pK_a$ = 9.32 [Adrien and Serjeant, 1981]) with only -OH functional groups being bonded to its benzene ring, the adsorption strength is significantly reduced. This would further imply that the $\Delta h_{ad}$-terms return much more positive

(endothermic) values than those obtained during the adsorption of MPDA and MAP.

**(iv) Adsorption of aqueous $NH_3$ on zeolites**

Figure 4.22 presents the adsorption isotherms of ammonia onto H-USY, H-Beta and H-ZSM-5 (Si/Al) at 70°C. The error in those measurements is expected to be greater for the volatile ammonia due to ammonia escaping from solution. The amount of ammonia lost in the headspace of the sampling flask is estimated by use of a phase equilibrium program [Sandler. 1989].

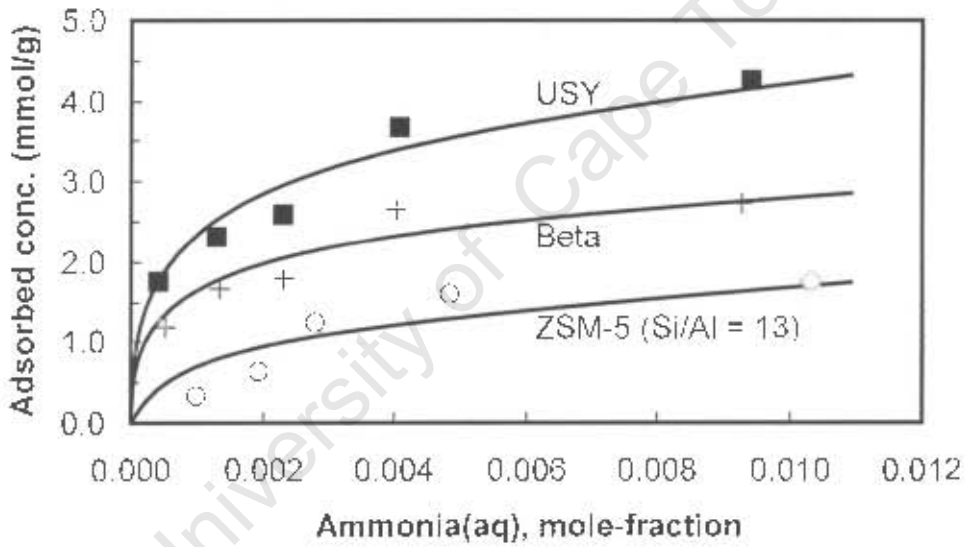


**Figure 4.22** Adsorption-equilibrium data for aqueous ammonia on USY (■), Beta (+) and ZSM-5 (Si/Al = 13) (O) at 70°.

Contrary to previous adsorption studies where H-Beta is shown to have the greatest uptake of MPDA, MAP and resorcinol, the amount of ammonia adsorbed is greatest for H-USY followed by H-Beta and H-ZSM-5 (Si/Al = 13). The latter trend is more in line with the obtained $NH_3$-TPD results with regards to the amount of Brønsted acid sites available.

**Table 4.7 Comparison of the adsorption capacity during liquid phase adsorption of MAP and MPDA on relevant zeolites**

| Zeolite | $\Delta H_{ads}$ (kJ/mol) $NH_3$-TPD | Al Content (mmol/g) | Vol. ($d_{pore}$<17Å) (ml/g) | Max. $NH_{3(aq)}$ Adsorbed in Figure 4.22 (mmol/g) |
|---|---|---|---|---|
| H-USY | 44 | 2.52 | 0.26 | 4.3 |
| H-Beta | 75 | 1.08 | 0.17 | 2.8 |
| H-ZSM-5 (Si/Al = 13) | 89 | 1.19 | 0.13 | 1.7 |

Comparison of the amount of $NH_{3(aq)}$ adsorbed on the zeolites with the zeolites' respective aluminium content (assuming framework Al) shows that considerably more $NH_3$ is adsorbed than predicted by the aluminium content of these substances. H-USY adsorbs 1.8mmol/g more $NH_{3(aq)}$ than that predicted by its aluminium content, followed by H-Beta (1.7mmol/g) and H-ZSM-5 (Si/Al = 13) with 0.5mmol/g. Comparison of the excess amounts of aqueous $NH_3$ adsorbed with the $N_2$-BET determined pore volumes ($d_{pore}$ < 17Å) suggests a linear trend. The greater the zeolite surface area the more ammonia tends to adsorb. This would imply that $NH_{3(aq)}$ must adsorb onto other weaker acid sites that are, to a large extent, a function of the zeolite surface area. The acid sites of considerably weaker Brønsted acid site strength can be ascribed to silanol (Si-OH) groups that generally correspond to an I.R. band at 3720-3740 $cm^{-1}$ [Topsoe *et al.*, 1981]. Adsorption of ammonia on the silanol groups is favoured over water because of the basic nature of ammonia and its molecular diameter being of similar dimensions to that of water. Since the interaction of ammonia with water is quite favourable, a large presence of physisorbed ammonia on the walls of the zeolite is less likely to occur.

## 4.4.3 HETEROGENEOUS REACTIONS USING ALUMINO-SILICATES

The results for the reaction studies performed on the aluminosilicates including an alumina sample are presented in Figures 4.23 through 4.27. These findings are illustrated by means of concentration-time reaction profiles with the concentration given in terms of mole-%, derived by dividing the *corrected mole concentration* by the initial number of moles of MPDA used (see APPENDIX-F). In addition, each figure (Figures 4.23 to 4.27) includes a mole balance versus reaction time (dashed line) that displays the total number of moles in the bulk solution relative to the initial amount of MPDA, as analysed by HPLC. Reaction results for H-USY, H-Beta and H-ZSM-5 (Si/Al = 13) are reported at reaction temperatures 225°C, 275°C and 300°C, whereas reactions with H-ZSM-5 (Si/Al = 22) and silica-alumina are conducted solely at 300°C. A test reaction with alumina is performed at 225°C. As explained in Section 4.1, the 1-hour heating period required to bring the reaction temperature from ambient to reaction temperature forms part of the reaction time.

The numerical concentration-time data is given in APPENDIX-H with the *corrected mole concentration* of the bulk solution being expressed in terms of the number of moles of a component in solution per unit volume, i.e., in terms of mmol/L. In addition to the reported bulk liquid phase concentrations of MPDA MAP and resorcinol, the concentration of 3,3'-diamino-diphenylamine and 3-hydroxy-3'-amino-diphenylamine as well as the sample pH and mole-balance are also included in the appendix.

### 4.4.3.1 REACTIONS WITH H-USY

The concentration-time profiles for reactions with zeolite H-USY, which prior to calcination amounts to 10g of zeolites, are shown in Figure 4.23. According to

Table 4.1, 10g of uncalcined H-USY converts to 7.96g after calcination. Since 1g of the dehydrated H-USY contains 2.52mmol of Brønsted acid sites (Table 4.3), this means that a total of 20.1mmols of fixed Brønsted acid sites centres are added to the reaction mixture. The concentrations of the relevant compounds MPDA, MAP and resorcinol are expressed as mole-%, obtained by dividing the measured concentrations by the initial MPDA concentration, i.e., 26.4mmol/L. Consequently, at the start of every reaction, the ratio of Brønsted acid sites relative to the initial amount of MPDA is ca. 2.2. The amount of acid site centre available outweighs the amount required for the complete conversion of MPDA (2moles acid sites per mole of MPDA) if the zeolite is solely used as a regenerable reagent.

The concentration-time profiles for reactions with zeolite H-USY at 225°C, 275°C and 300°C are shown in Figure 4.23. Because the amount of Brønsted acid sites situated on the H-USY surface are in excess, the overall reaction mechanism should follow a similar trend to that obtained for the mineral acids in Section 4.3, even if the reaction mechanism is strongly influenced by adsorption / desorption limitations. All three reactions show a strong initial decrease in the concentration of MPDA, but thereafter (after 9hours at 225°C, 5hours at 275°C, 1hour at 300°C) remain relatively constant at ca. 60mole-%.

The MAP concentration profiles move through a maximum, which is not well defined. Once reaching the maximum, the MAP concentration only decreases slowly. According to Figure 4.23A, the maximum MAP concentration is ca. 25mole-%. The maximum in the MAP concentration is more distinct at higher reaction temperatures. At a reaction temperature of 275°C, the maximum of the MAP reaction-time profile occurs after ca. 3.5hours with the MAP concentration equalling ca. 23mole-%. The MAP concentration (at 275°C) reduces to ca. 15mol-% after a reaction time of 49hours (not shown in Figure 4.23B). At 300°C (Figure 4.23C), the maximum MAP concentration (25mole-%) occurs between reaction times 1hour and 5hours. Observing the MAP

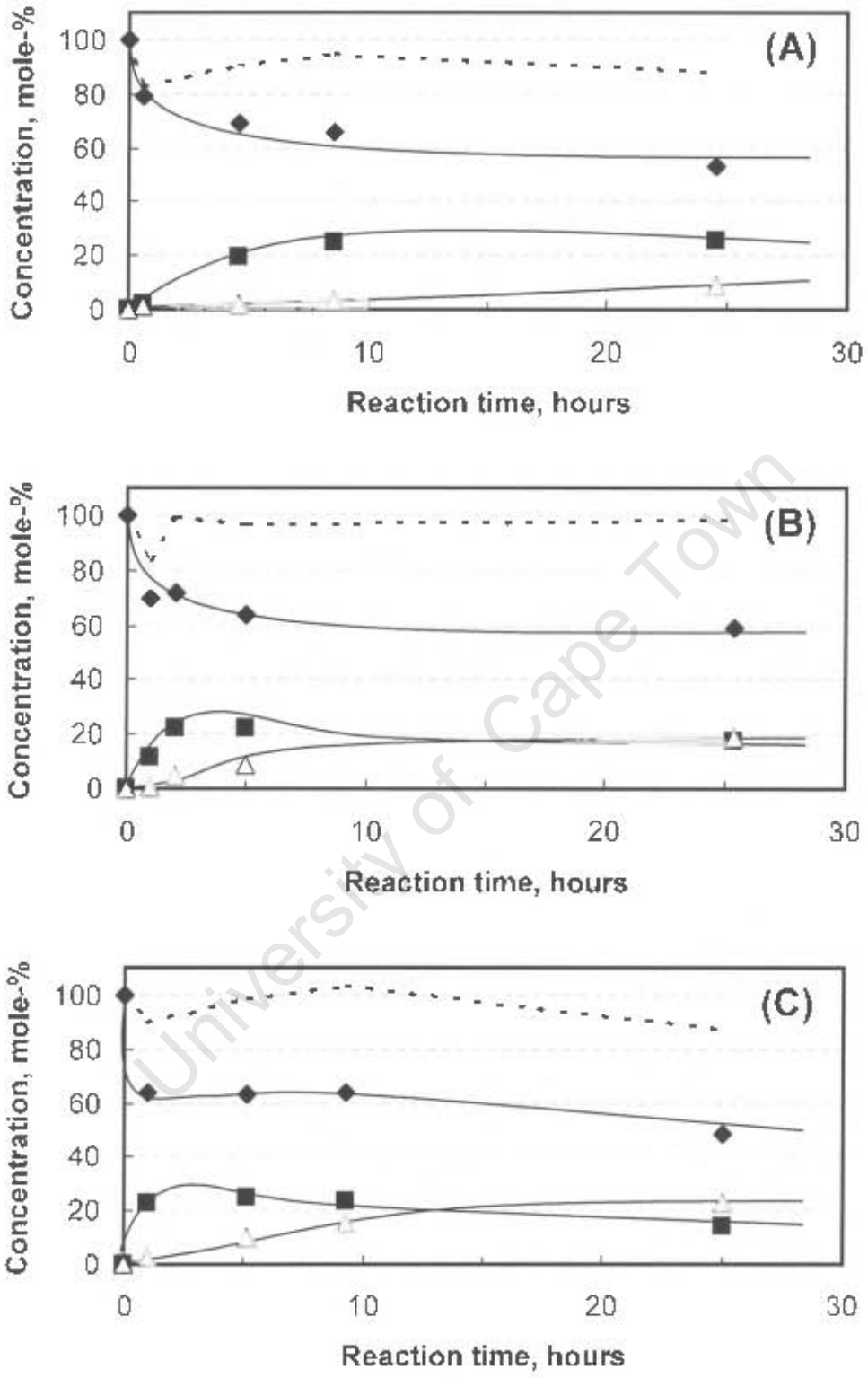




**Figure 4.23** Concentration profiles of MPDA (◆), MAP (■) and resorcinol (△) (given as mole percent of organic compounds relative to the initial moles of MPDA) versus reaction time over zeolite USY at temperatures (A) 225°C, (B) 275°C and (C) 300°C.

concentration profiles at reaction temperatures 225°C, 275°C and 300°C, there is a tendency for the maximum to shift to shorter reaction times with increasing temperatures, even though the maximum detected MAP concentration is around 25mol-% at all measured temperatures.

Similarly to the reaction with mineral acid, the resorcinol concentration-time profile is that of an S-shaped curve. This indicates that resorcinol is formed by means of a consecutive reaction with MAP being the intermediate product. The yield of resorcinol after 25hours increases with increasing temperature.

The mole balances (dashed lines in Figure 4.23) move through a definite minimum after 1hour (82mole-%, 84mole-% and 90mole-% for reactions carried out at 225°C, 275°C and 300°C, respectively). Towards the end of the reaction, the mole-balances for H-USY at 275°C tends to stabilise at 98mole-%. Mole balances for reaction at 225°C and 300°C decline towards the end of the reaction to 88mole-% and 89mole-%, respectively. Judging from the mole balance, most of the organic components can be accounted for. The initial modest decrease in the mole-balance-time curves can be attributed to MPDA adsorbing onto the H-USY surface resulting in a decrease in the bulk solution. During the course of the reaction, the amount of organic compounds adsorbed seems to be greatest for the reaction at 225°C, followed by 275°C. At 300°C, acceptable mole-balances are observed between reaction times 5hours and 9hours (> 98mole-%), although a poor mole-balance is returned after 25hours (87mole-%). The formation of polyethers may account for this.

Judging from the reaction profiles of MPDA, MAP and resorcinol a number of possible reaction pathways is feasible. Firstly, for the case of a consecutive conversion of MPDA to MAP to resorcinol the reaction must be considered as being reversible since the concentration of the relevant components tend to equilibrate without the reaction going to completion (see Figure 4.23). Assuming a simple first order reaction and in the absence of diffusional constraints, the final

concentration of the different reactants tend to suggest that the equilibrium constants, i.e., for the conversion of MPDA to MAP and of MAP to resorcinol, are quite close to unity. The equilibrium constant of MPDA to MAP is, however, less than unity (max. one order of magnitude) since the final concentration of MPDA is greater than that of MAP. The equilibrium constant of MAP to resorcinol should be greater than unity (max. one order of magnitude) since the resorcinol concentration after reaction is greater than that of MAP. Regardless, the observed equilibrium constants deviate considerably from the large equilibrium constants obtained during the thermodynamic analysis when assuming that ammonia reacts with the mineral acid. Therefore, this would imply that some of the ammonia is likely to desorb from H-USY into solution, which is plausible since the solution pH changes from 6.3 to 7.6 (at 225°C), 8.8 (at 275°C) and 8.6 (at 300°C) during the course of the reaction. No aqueous alumina could be detected by means of AA measurements, even after the addition of concentrated HCl (see Section 3.2.1.2).

A second possible reason for explaining the observed MPDA, MAP and resorcinol concentration in Figure 4.23, while still maintaining the reaction irreversibility aspect as characterised during the reactions with mineral acids, is that the rate constants of the consecutive reactions are seemingly time dependent, i.e., the catalyst deactivates. The fact that the initial MPDA concentration at all three reaction temperatures decreases quite rapidly and then remains constant at 40% conversion suggests that the reaction rate constant for MPDA –› MAP decreases with reaction time. The same must be true for the reaction rate constant for MAP → resorcinol. The MAP concentration hardly decreases after attaining its maximum. The fact that the reaction rate constants change with reaction time then implies that other factors are involved. Since for a irreversible reaction, the product ammonia must be chemisorbed permanently on the H-USY surface (see Section 2.1.2.1), a low MPDA conversion points towards a reduction in the number of Brønsted acid sites, i.e., the amount of $NH_3$ produced relative to the initial number of Brønsted acid sites is quite low.

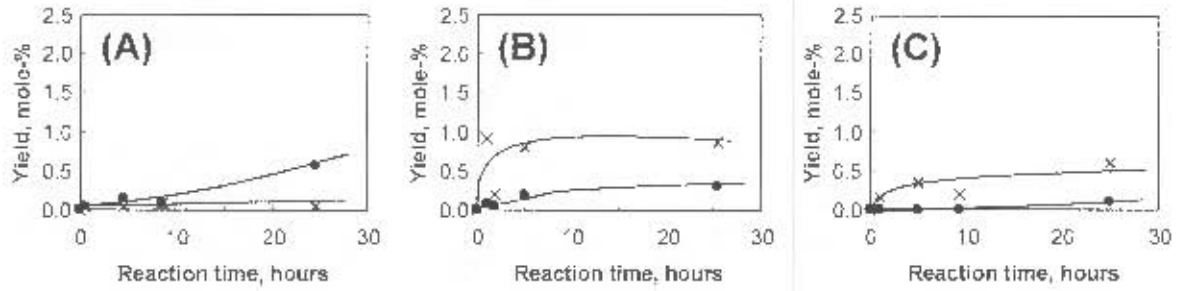


**Figure 4.24** Yield profiles of 3,3'-diamino-diphenylamine (x) and 3-hydroxy,3'-amino-diphenylamine (●) versus reaction time over zeolite H-USY at temperatures (A) 225°C, (B) 275°C and (C) 300°C.

During the conversion of MPDA to resorcinol, minor amounts of 3,3'diamino-diphenylamine and 3-hydroxy-3'amino-diphenylamine are produced. Although the measured amounts of diphenylamines are minor, an interesting phenomenon is observed. At 225°C, more of 3-hydroxy-3'-amino-diphenylamine than 3,3'-diamino-diphenylamine is produced with the maximum observed concentration being 0.15mmol/L and 0.02mmol/L, respectively (see Figure 4.24). However, at higher temperatures the concentration of 3,3'-diamino-diphenylamine is greater than that of 3-hydroxy-3'amino-diphenylamine, which was not observed for reactions involving mineral acids. For reactions with H-USY, the maximum 3,3'-diamino-diphenylamine concentration at 275°C equals 0.23mmol/L, while the maximum concentration at 300°C is 0.16mmol/L. The respective maxima observed for 3-hydroxy-3'-amino-diphenylamine are only 0.08mmol/L and 0.03mmol/L. Thus, it seems that at higher reaction temperatures the formation of 3,3'-diamino-diphenylamine is preferred over the formation of 3-hydroxy-3'amino-diphenylamine, which is not the case in the presence of mineral acids. Although the mole-balance for the last reaction point at 300°C is relatively low (Figure 4.23C) and the di- or poly-phenylamine concetrations could be higher, the maximum amount of HPLC detectable diphenylamines at any given time during the reaction makes up less than 1.2% of the initial amount of MPDA molecules. The concentration-time profiles, however, do not seem to follow the same smooth

trend as described for the mineral acids. This observation can possibly be ascribed to diffusional effects in the H-USY pore structure. Nevertheless, the maximum amount of MPDA being converted to diphenylamines in the presence of H-USY (< 1.2%) is considerably less than that observed when using mineral acids (< 4.5%). This would imply enhanced shaped selectivity occurring in the presence of H-USY relative to the mineral acids. The interaction of MPDA with the 'inert' wall of the stainless steel reactor combined with the presence of only fixed acid sites on H-USY could also influence the findings.

### 4.4.3.2 REACTIONS WITH H-BETA

The concentration-time profiles for the conversion of 1g MPDA to resorcinol in the presence of zeolite H-Beta (mass H-Beta equals 10g prior to calcination) and 350ml water are illustrated in Figure 4.25. According to Table 4.1, 10g of uncalcined H-Beta amounts to 9.35g immediately after calcination. Since the number of Brønsted acid sites on the H-Beta sample is 1.08mmol/g (Table 4.3), the amount of fixed Brønsted acid sites added to the autoclave totals 10.1mmols. In contrast to the reactions with H-USY, at the start of every reaction with H-Beta the ratio of Brønsted acid site centres relative to the initial number of moles of MPDA is ca. 1.1. Since each MPDA molecule contains two amine functional groups that need to be replaced by hydroxyl groups, the total number of Brønsted acid sites is slightly more than half that required for the full conversion of MPDA to resorcinol if H-Beta is to act purely as a regenerable reagent. Thus, it is expected that hydroxyl groups replace only half the number of amine functional groups.

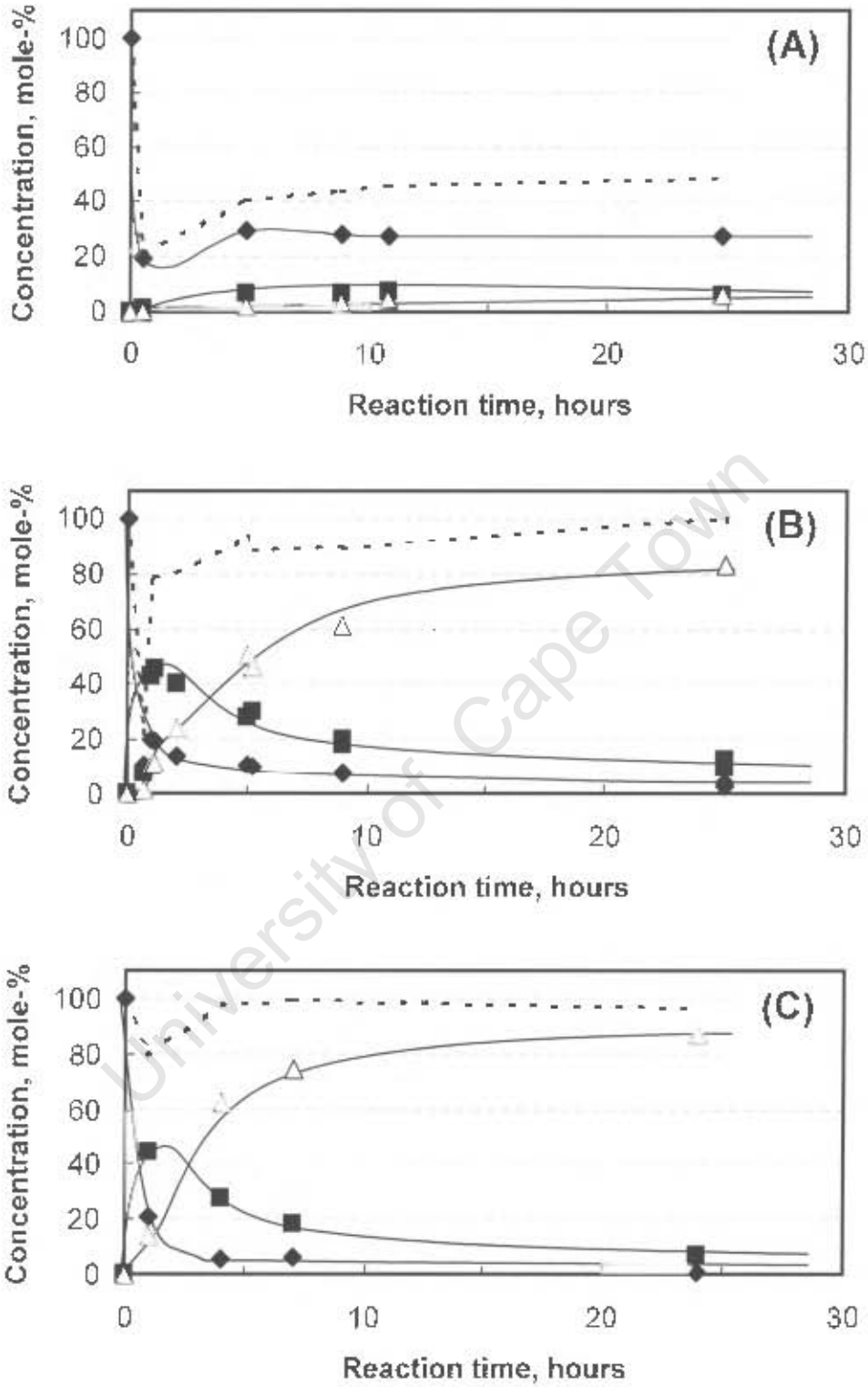


**Figure 4.25** Concentration profiles of MPDA (◆), MAP (■) and resorcinol (△) (given as mole percent of organic compounds relative to the initial moles of MPDA) versus reaction time over zeolite H-Beta at temperatures (A) 225°C, (B) 275°C and (C) 300°C.

The concentration-time profiles for reactions with zeolite H-Beta at 225°C, 275°C and 300°C are shown in Figures 4.25. At lower reaction temperatures (i.e., 225°C), the most striking difference between the reaction profiles for the conversion of MPDA to resorcinol in the presence of H-Beta relative to that of H-USY is given by the mole-balance and the MPDA concentration-time profiles. For the reaction carried out at 225°C, a strong initial decrease in the MPDA concentration combined with poor mole-balances shows that an initial strong uptake of MPDA by H-Beta must occur during the 1-hour ramping period. The largest amount of MPDA is adsorbed during the initial reaction period, which after 0.5hours (according to Figure 4.1, temperature = 150°C) accounts for only 21% of the initial amount of MPDA. However, even after a reaction period of 4.8hours and reaching the final temperature of 225°C, the mole-balance still indicates that only 40.3% of the initial amount of MPDA can be accounted for. Towards the end of the reaction (225°C), the mole-balance shows a value of 48.3%. At reaction temperatures of 275°C and 300°C, the mole-balance versus the reaction time curves also show a strong initial decrease in the number of accountable organic compounds relative to the original quantity of MPDA. After a reaction time of 1hour, the mole-balances for reactions at 275°C and 300°C are 77mole-% and 90mole-%, respectively. However, in contrast to the reaction at 225°C, the percentage of organic components relative to the initial quantity of MPDA used for reactions at 275°C and 300°C after 25hours reaction periods are both 97mole-%.

Taking into consideration the excessively low mole-balance calculated during the 225°C reaction, a further sample is taken during the 275°C reaction during the ramping period (after 0.7hours) with the corresponding autoclave temperature equalling 200°C for which the mole-balance reveals a value of only 22-mole%. This implies that the strong adsorption of MPDA on H-Beta around 200°C is likely to be responsible for the undershoot in the MPDA concentration observed at 225°C. The explanation is also in agreement with the strong adsorption of MPDA on H-Beta observed during the adsorption studies given in Section 4.4.2.6.

All three reactions carried out at different temperatures show a very strong initial decrease in the concentration of MPDA in the bulk solution. The reason is principally due to the strong uptake of MPDA by H-Beta, which further suggests that adsorption-equilibrium is attained quite quickly. This in effect distorts the MPDA concentration-time profile. Consequently, Figure 4.25A shows a decrease in the MPDA bulk concentration from the initial 100mole-% to 20mole-% after 0.5hours. The MPDA concentration in the bulk solution stabilises at 28mole-% after a reaction period of 9hours. Although strong adsorption during the ramping period also occurs at reaction temperatures 275°C and 300°C, the MPDA concentration-time profile is comparable to the usual exponential decrease observed for reactant concentration-time curves. After 25hours the concentration of MPDA in solution is 3mole-% and 1mole-% for reactions at 275°C and 300°C, respectively.

The maximum MAP concentration at 225°C is ca. 7mole-% and is attained after 5hours. However, within the 25hours reaction time span, there is no evidence for the MAP concentration decreasing after reaching a concentration of 7mole-%. A completely different MAP concentration profile is obtained for reactions at 275°C and 300°C. The MAP concentration-time curves follow those of a consecutive reaction with MAP being the intermediate compound. The excessively large maximum MAP concentration of ca. 45mole-% occurring immediately after the 1-hour ramping period is unexpected. The very high concentration of MAP in the bulk solution during the start of the reactions at 275°C and 300°C suggests that after the initial strong adsorption during the ramping period (T < 200°C), MPDA desorbs immediately from the zeolite as MAP. Consequently the first hydrolysis step of MPDA and desorption of MAP over H-Beta occurs at temperatures slightly above 225°C since small amounts of MAP and resorcinol are formed at that temperature (Figure 4.25A). Below 200°C, MPDA on H-Beta can be regarded as being solely adsorbed without any reactions taking place. The large amount of MAP desorbing is in line with the suggestion in Section 4.4.2.6 that

typically only one amine group of the two amine functional groups on each MPDA molecule chemisorbs with a Brønsted acid site on H-Beta.

The resorcinol concentration-time profile follows that of an S-shaped curve. A small amount of resorcinol is produced at 225°C with the concentration of resorcinol in the bulk solution towards the end of the reaction (25hours) being ca. 6mole-%. It is of interest to note that during the reaction at 225°C the number of moles of components that can be accounted for improves in proportion to the amount of resorcinol produced. Therefore, at 225°C the overall reaction does seems to proceed towards the formation of resorcinol, albeit at a slow rate. Increasing the reaction temperature to 275°C and 300°C leads to a pronounced increase in the resorcinol yield. The resorcinol yield measured at the end of the reaction (25hours) is 83% at 275°C and 87% at 300°C. The initial part of the S-shaped resorcinol-time curves for reactions at 275°C and especially at 300°C does not have a zero slope. Considering that 1 hour is required for heating the autoclave to reaction temperature, a possible explanation regarding the reaction pattern in Figures 4.25B and 4.25C is that some of the MPDA is likely to react twice while residing in the pore structure of H-Beta only to emerge into the bulk solution as resorcinol. Stated differently, some MPDA is hydrolysed to MAP which remains in the pores to be hydrolysed further to resorcinol, which then emerges into the bulk solution.

According to Section 4.4.2.6, the MPDA on H-Beta adsorption study would have rather predicted that the MPDA molecules chemisorbs only via one amine functional group. Considering the findings of the adsorption study, a second explanation for the rather sharp initial increase in the resorcinol concentration is that because the MAP concentration is so large at the start of the reaction (ca. 45mole-%), some MPDA molecules inside the pore of H-Beta can react further to form resorcinol before diffusing into the bulk solution. Thus, the MPDA molecule adsorbs via one amine group, converts to MAP and desorbs from the surface, then readsorbs onto another Brønsted acid site via the second amine group until

resorcinol is formed, which desorbs into the bulk solution. Therefore, while the resorcinol concentration profile alone suggests some direct conversion of MPDA to resorcinol, consideration of the other product profiles suggests a consecutive reaction pathway to resorcinol. As suggested by the adsorption study (Section 4.4.2.6), the $\Delta h_{ad}$ upon adsorption of MPDA or MAP via its amine group is essentially the same. Thus the chance for the two components adsorbing once in the pore structure is dictated mainly by their respective concentrations inside the pore structure and their respective orientations with the probability of MPDA adsorbing being greater than that of MAP since it possesses two amine functional groups compared to only one for MAP.

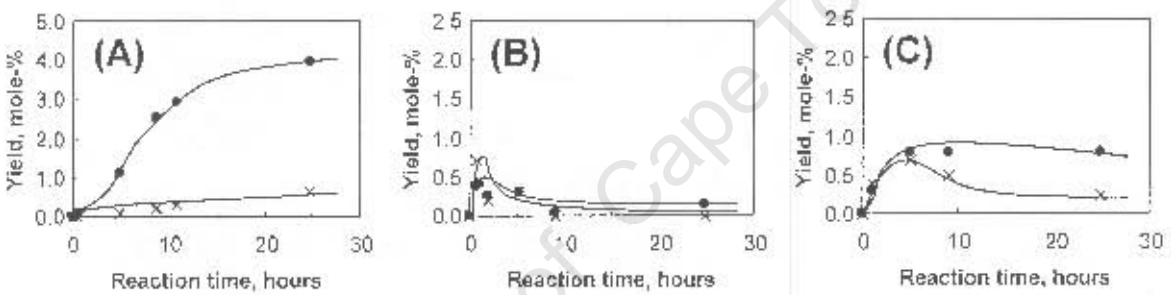


**Figure 4.26** Yield profiles of 3,3'-diamino-diphenylamine (x) and 3-hydroxy,3'-amino-diphenylamine (●) versus reaction time over zeolite H-Beta at temperatures (A) 225°C, (B) 275°C and (C) 300°C.

The conversion of MPDA over zeolite H-Beta leads to the additional formation of 3,3'-diamino-diphenylamine and 3-hydroxy-3'-amino-diphenyl-amine. Unlike the reaction of MPDA over H-USY, the amount of 3-hydroxy-3'-amino-diphenyl-amine produced in the presence of H-Beta at the temperatures studied is always greater than that of 3,3'-diamino-diphenylamine. At the low reaction temperature of 225°C, where a considerable amount of MPDA tends to be permanently adsorbed to the surface of H-Beta, a relatively large amount of 3-hydroxy-3'-amino-diphenylamine (1.05mmol/L) is produced with only 0.17mmol/L of 3,3'-diamino-diphenylamine being formed over a reaction period of 25hours. Thus 8% of the original 1g of MPDA is converted to 3-hydroxy-3'-amino-diphenyl-amine.

while ca. 1% is converted to 3,3'-diamino-diphenylamine during the duration of the reaction at 225°C. The shapes of the diphenylamine (3,3'-diamino-diphenylamine and 3-hydroxy-3'-amino-diphenyl-amine) concentration-time curves follow that of an S-shaped curve, signifying that these compounds are produced via a consecutive reaction. As discussed in Section 4.3 regarding the conversion of MPDA in the presence of mineral acids, 3-hydroxy-3'-amino-diphenyl-amine is likely to be produced from MPDA and MAP, with MAP being produced first. However, the formation of 3,3'-diamino-diphenylamine, as observed in the presence of mineral acids (Section 4.3), is not a consecutive reaction. Since the amount of 3-hydroxy-3'-amino-diphenyl-amine is considerably greater than that of 3,3'-diamino-diphenylamine, it is likely that the large concentration of MPDA in the pore structure, which is not necessarily chemisorbed to the H-Beta surface (see Table 4.5), leads to the formation of diphenylamines. At reaction temperatures 275°C and 300°C the diphenylamine concentration-time curves of 3,3'-diamino-diphenylamine are fluctuating with the maximum concentration at 275°C and 300°C being 0.19mmol/L and 0.21mmol/L, respectively. The concentration-time profiles of 3-hydroxy-3'-amino-diphenyl-amine clearly proceed through a maximum, 0.21mmol/L at 275°C (between 5hours and 25hours) and 0.27mmol/L (after 4hours) at 300°C. The maximum conversion of MPDA to diphenylamines during the course of the reactions carried out at 275°C and 300°C is ca. 3%.

During the course of the reaction at 225°C, the solution pH changes from 7.7 (measured after 0.5hours) to 9.0 at the end of the reaction. Likewise for the reaction at 275°C, the sample pH changes from 7.3 (after 1hour) to 9.8 (after 25hours). For the reaction at 300°C, only one sample pH reading (9.7 after 24hours) is taken. The distinct smell of ammonia could not be detected. However, considering that a total of only 10.1mmols of Brønsted acid sites are present in the reaction mixture at any given time (see above) and that the amount of acid sites required for the observed yields in MAP, 3-amino-3'-hydroxy-diphenylamine and resorcinol require 2.0mmol (at 225°C), 16.5mmol (at 275°C)

and 16.8mmol (at 300°C), clearly shows that more hydrolysis type reactions take place than is allowed by the total number of Brønsted acid sites if H-Beta is to act solely as a regenerable reagent. Therefore, some form of 'catalysis' does seem to take place since some of the ammonia formed on the Brønsted acid sites need to give way to allow for the chemisorption of another molecule consisting of an amine functional group. The fact that the solution pH increases during the reaction must, by rule of deduction, be due to the formation of ammonia. Alternatively, some of the formed ammonia can also be sorbed onto the silanol groups. However, the sorption of ammonia onto silanol groups cannot explain the high pH measured in the sample solutions.

#### 4.4.3.3 REACTIONS WITH H-ZSM-5 (Si/Al = 13)

Reactions of 1g MPDA (9.25mmol) and 350ml water in the presence of H-ZSM-5 (Si/Al = 13), which amounts to 10g of zeolite prior to calcination, have been carried out at temperatures 225°C, 275°C and 300°C (Figure 4.27). A total of 10g of uncalcined H-ZSM-5 (Si/Al = 13) on average leads to 8.17g after calcination (see Table 4.1). The number of localised Brønsted acid sites added to the autoclave amounts to 9.25mmol (see Table 4.3). Thus, the ratio of MPDA versus the number of Brønsted acid sites added to the autoclave equals 1, although for an irreversible reaction the ratio should equal 2. Although all three reactions at different temperatures reveal very good mass balances with more than 90% of the original MPDA being accounted for throughout the reactions, conversion of MPDA remains poor, increasing slightly with increasing temperature.

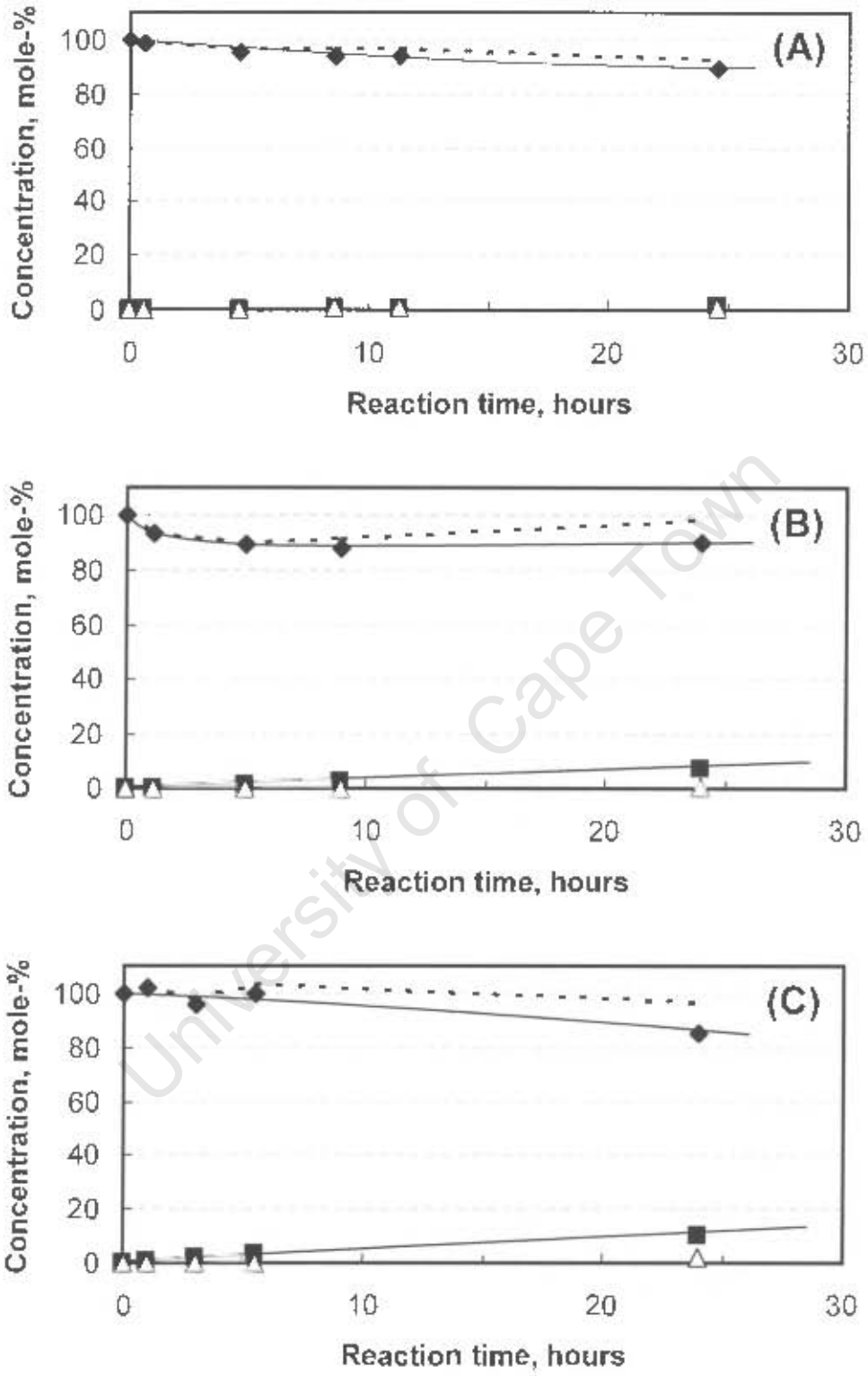


**Figure 4.27** Concentration profiles of MPDA (◆), MAP (■) and resorcinol (Δ) versus reaction time over ZSM-5 (Si/Al = 13) at (A) 225°C, (B) 275°C and (C) 300°C.

The resorcinol yields after 25hours are very low (1% at 225°C, 1% at 275°C, and 2% at 300°C). The difference between the observed MPDA conversion and the MPDA being converted to MAP and resorcinol (8mole% at 225°C; 3mole-% at 275°C; 3mole-% at 300°C) is likely to be purely due to adsorption phenomena since at 225°C only minor traces of 3-hydroxy,3'-amino-diphenylamine (yield < 0.5mole-%) is observed. At higher temperatures of 275°C and 300°C, no dimer formation is observed.

The absence of an initial dip in the shape of the mole-balance and MPDA concentration-time curves during the 1-hour heating period suggest that diffusional constraints due to the medium pores channels (5.3Å x 5.6Å) lowers the rate at which equilibrium is reached. However, the adsorption study predicts that at low temperatures a total of ca. 1.5mmol (16%) of the initial MPDA added to the reactor adsorbs on H-ZSM-5 (Si/Al = 13). Since, after 0.6hours the observed MPDA uptake on H-ZSM-5 is low, it can be concluded that MPDA does not enter the pore structure very quickly.

During the course of the reaction at 225°C, the pH changes from 7.5 (after 0.6hours) to 7.9 (after 25hours). Likewise at 275°C and 300°C, the pH changes from 8.6 (after 1.1hours) to 8.7 (after 24hours) and 8.5 (after 1hour) to 8.9 (after 24hours), respectively. As shown by the pH readings, the pH does not change by as much as observed in the presence of H-Beta. This is most likely to be due to the fact that less ammonia is formed. It is, however, interesting to note that the initial pH for reactions in the presence of H-ZSM-5 (Si/Al = 13) is generally ca. 1unit greater than that measured when using other aluminosilicates. A similar observation was made during the adsorption study (Section 4.4.6.2).

#### 4.4.3.4 REACTIONS WITH H-ZSM-5 (Si/Al = 22)

To confirm that the poor reaction performance observed during the conversion of MPDA to resorcinol in the presence of zeolite H-ZSM-5 (Si/Al = 13) is endemic to the whole ZSM-5 group, a reaction is conducted over zeolite H-ZSM-5 (Si/Al = 22) at 300°C. The characterisation on H-ZSM-5 (Si/Al = 22) is not as in-depth as the characterisation of H-ZSM-5 (Si/Al = 13). Assuming that the zeolite H-ZSM-5 (Si/Al = 22) consists entirely of framework aluminium species and taking Table 4.1 into consideration, a total of ca. 6.8mmol Brønsted acid sites (10g zeolite before calcination) are added to the autoclave prior to reaction. The amount of MPDA (9.25mmol) and water (350ml) added to the reactor remain identical to that of previous reactions with aluminosilicates.

According to Figure 4.28, a vast difference in the reaction performance is noticed when the reaction at 300°C is carried out in the presence of H-ZSM-5 (Si/Al = 22), a zeolite consisting of a lower aluminium content than the previously used H-ZSM-5 (Si/Al = 13). The mole-balance as a function of time shows, as expected, an initial decrease (after 1hour) towards 80% before recovering slightly to 85% (after 9hours). Interestingly, towards the end of the reaction, the mole-balance decreases to only 71%, implying that after a reaction period of 25hours only 71% of the original MPDA can be accounted for in the bulk solution. However, since the formed resorcinol is a weak acid and is more weakly sorbed to a zeolite surface than the base MPDA, an increase in the mole-balance was expected towards the end of the reaction. No 3,3'-diamino-diphenylamine is observed in the bulk solution phase. However, the concentration of 3-hydroxy-3'-amino-diphenylamine increases towards the end of the reaction (constituting 2% of the original MPDA) while being still virtually undetected after a reaction period of 9hours. The increase in the production of 3-hydroxy-3'-amino-diphenylamine together with the decreasing mole-balance towards the end of the reaction points to a possible formation of polyethers after a prolonged reaction period.

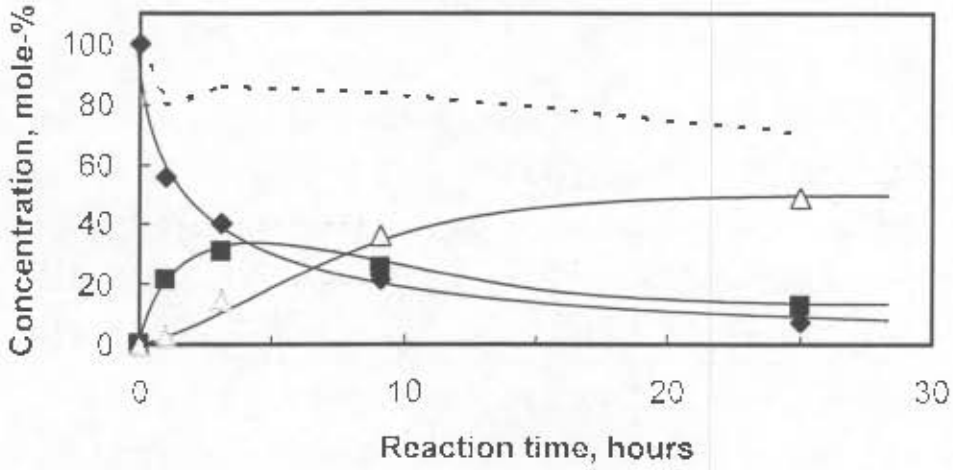


**Figure 4.28** Concentration profiles of MPDA (◆), MAP (■) and resorcinol (Δ) versus reaction time over H-ZSM-5 (Si/Al = 22) at 300°C.

The MPDA, MAP and resorcinol concentration-time curves follow that of a consecutive reaction with MAP being the intermediate and resorcinol the final product. As already discussed previously with H-USY (Section 4.4.3.1), the shape of the concentration-time curves of MPDA, MAP and resorcinol tend to suggest that either the zeolite deactivates or the reactions are reversible since the concentration of MPDA and MAP do not approach zero after a prolonged reaction period. Likewise, the concentration of resorcinol does not approach 100%. Instead, the resorcinol concentration tends to a constant 49mole-%. The maximum MAP concentration occurs after ca. 3hours (31mole-%) and the final concentration is ca. 13mole-%. The concentration of MPDA in the bulk solution towards the end of the reaction (after 25hours) is ca. 7mole-%. The amount of Brønsted acid sites that is required for attaining the observed MAP and resorcinol yields is 10.2mmol when assuming that the reaction is irreversible. This amount is considerably more than the 6.8mmol present on 10g of zeolite H-ZSM-5 (Si/Al = 22). It may be safely concluded that the tendency towards an incomplete conversion of MPDA to resorcinol is due to a lack of available Brønsted acid sites, since the reaction MPDA › MAP › resorcinol returns very low resorcinol yields in the absence of mineral or solid acid co-reagents. A certain amount of the produced ammonia needs to desorb into aqueous solution to allow for the

conversion of other amino-benzene until an equilibrium is attained between the ammonia-adsorbed-on-zeolite system is in equilibrium with the ammonia-in aqueous-solution system. Once the ammonia concentration in the bulk solution reached a concentration of 3.4mmol (10.2 minus 6.8mmol) per 350ml, the rate of ammonia desorption becomes very low and the reaction comes to a standstill. The product spectrum of the reaction MPDA to resorcinol in the presence of H-ZSM-5 (Si/Al = 22) suggests that all the Brønsted acid sites of a ZSM-5 zeolite are utilised and accessible, at least at 300°C, to aqueous molecule having the dimensions of a meta-substituted benzene molecule. This is unlike the conclusion arrived at in the presence of H-ZSM-5 (Si/Al = 13).

During the course of the reaction the solution pH steadily changes from 7.7 to 8.9 after 25hours. As in reactions over H-Beta, this points towards the presence of ammonia in the aqueous phase. As is the case for the reactions over H-Beta, there is no other compound formed during the reaction that leads to an increase in the solution pH. This is consistent with the thermodynamic investigation in Section 2.1.2.1 (Figure 2.9) predicting an equilibrium resorcinol yield of ca. 60% (mole ratio of water to MPDA = 2100) in the absence of a mineral or solid co-reagent (assumption of all activity coefficients = 1), and the consequent presence of ammonia in the aqueous phase. Considering that in the absence of a chemical promoter no MAP or resorcinol is formed at 275°C after a reaction period of 25hours (Section 4.2), it can further be concluded that zeolites act as a catalyst, even though its catalytic function is very limited.

#### 4.4.3.5 REACTIONS WITH SILICA-ALUMINA

The absence of micropores in the amorphous hydrogen exchanged silica-alumina enhances the accessibility of reactant MPDA and the intermediate MAP onto the Brønsted acid sites of the aluminosilicate. Taking Table 4.1 and 4.3 into account, the total amount of acid sites present on 10g of previously uncalcined silica-alumina amounts to 19.7mmol. Interestingly, however, the mole-balance versus time curve during the reaction at 300°C reveals that most of the relevant components in the aqueous phase can be accounted for throughout the reaction (>90%). This is despite the fact that the presence of 19.7mmol of Brønsted acid sites would lead to a large uptake of MPDA on the mesoporous silica alumina during the ramping period. Hardly any MPDA is adsorbed onto the surface of silica-alumina during the 1-hour ramping period.

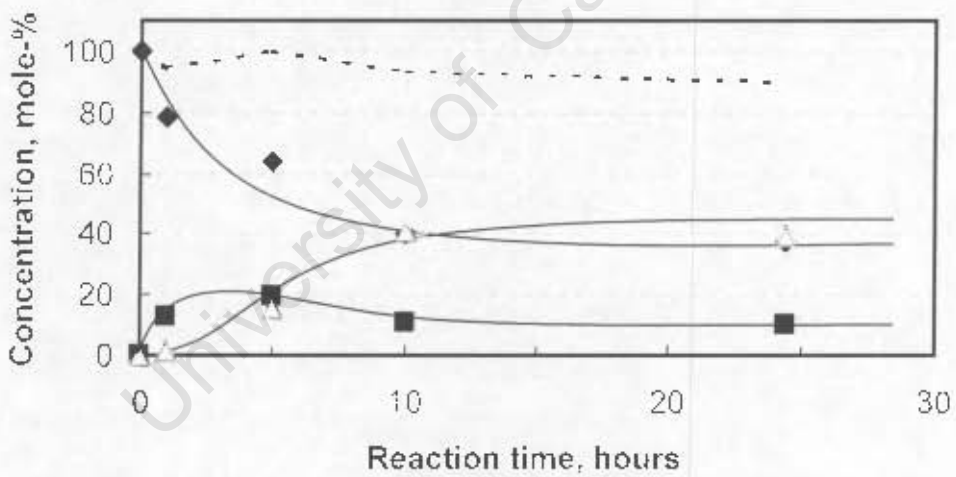


**Figure 4.29** Concentration-time profiles of MPDA (◆), MAP (■) and resorcinol (▲) versus reaction time over H-exchanged silica-alumina at 300°C.

According to Figure 4.29, MPDA at a reaction temperature of 300°C is converted relatively quickly during the initial reaction period. However, after ca. 4hours the rate of MPDA conversion slows down considerably. Between 9 and 25hours reaction time, an additional 2% of the original MPDA is converted, thus signalling the end of the reaction. The concentration-time profiles of MAP and resorcinol

flatten towards the end of the reaction. After a reaction period of 9hours, the concentration of MPDA, MAP and resorcinol seem to stabilise at 38mole-%, 10mole-% and 40mole-%, respectively with the maximum MAP concentration amounting to ca. 23mole-% (after 3hours). After a reaction period of 25hours, the concentration of 3,3'-diamino-diphenylamine equals 0.11mmol/L and that of 3-hydroxy-3'-amino-diphenyl amine is 0.27mmol/L. The identified dimer products are made up of ca. 3% of the original amount of MPDA.

The most striking observation made with the reaction in the presence of silica-alumina is that only 8.43mmol Brønsted acid sites are required for the product spectrum obtained in Figure 4.28 after a 25hour reaction period at 300°C. The total amount of fixed Brønsted acid sites added to the autoclave is 19.7mmol. Consequently, a near complete conversion of MPDA to resorcinol would have been expected, especially since silica-alumina consists solely of mesopores ($d_{pore}$ > 17Å) that would eliminate any significant diffusional restrictions.



#### 4.4.3.6 REACTIONS WITH γ-ALUMINA

The reaction with γ-alumina at 225°C (see APPENDIX-H) shows that no MAP (< 0.2mole-%) nor resorcinol (< 0.3mole-%) is produced in the presence of 10g of γ-alumina. The formation of dimers could not be detected (<0.02mole-%). The concentration of MPDA in the bulk solution is only 98mole-%, which implies that some MPDA (<2%) is adsorbed onto the alumina. The solution pH during the course of the reaction changes from 8.2 (after 0.7hours) to 9.0 (after 25hours), thus implying that the presence of alumina tends to lower the solution pH since the change in the sample pH cannot be due to the formation of $NH_3$. The zero yields in MAP and resorcinol during the reaction at 225°C suggest that the reaction MPDA › MAP › resorcinol over an aluminosilicate can only proceed in the presence of very strong Brønsted acid sites.

## 4.4.4 CHARACTERISATION OF SPENT ALUMINOSILICATES

The observations regarding the varying activities of the different aluminosilicates used in Section 4.2.3 cannot be solely explained on the basis of the reaction results. If the aluminosilicates are regarded as being solely heterogeneous reagents with the meta-substituted benzene ring able to access all the pores equal to or greater than those of a ZSM-5 zeolite (5.3Å x 5.6Å) at 300°C as illustrated by H-ZSM-5 (Si/Al = 22) (Section 4.4.3.4), further questions still arise regarding the poor utilisation of the total number of Brønsted acid sites on H-USY (Section 4.4.3.1), H-ZSM-5 (Si/Al = 13) (Section 4.4.3.3) and silica-alumina (Section 4.4.3.5). One simplistic method of characterisation of the spent aluminosilicates is to compare their respective colours. After reaction, the aluminosilicates H-USY, H-Beta and hydrogen-exchanged silica-alumina are dark auburn in colour whereas zeolite H-ZSM-5 (Si/Al = 22) has a light auburn colour and H-ZSM-5 (Si/Al = 13) is even paler. This suggests that ZSM-5 is less poisoned by organic components than the other aluminosilicates. Interestingly, the colour of γ-alumina after reaction is grey and not brown as for the aluminosilicates.

The aluminosilicates recovered from reactions at 300°C are calcined under the same conditions used for the calcination of the aluminosilicates prior to the reactions. They are subsequently characterised by X-ray diffraction, SEM and BET. The number of Brønsted acid sites present on the aluminosilicates after reaction could not be quantified using $NH_3$-TPD.



### 4.4.4.1 STRUCTURE AND MORPHOLOGY

**(i) X-ray diffraction**

The X-ray diffraction patterns of spent (reaction temperature = 300°C), recalcined USY, Beta, ZSM-5 (Si/Al = 13) and ZSM-5 (Si/Al = 22) are shown in Figure 4.30.

Comparison with the X-ray diffraction patterns prior to reaction given in Figure 4.8 (Section 4.4.2.1) provides evidence that previously crystalline USY becomes totally amorphous during the course of the reaction at 300°C. The crystallinity of Beta also decreases appreciably during the course of the reaction, although some of the characteristic Beta diffraction peaks are still visible, which indicates only a partial collapse of the framework. The ZSM-5 (both, for Si/Al = 13 and Si/Al = 22) zeolites retain their characteristic X-ray fingerprint (peak position and intensity) after the reaction.

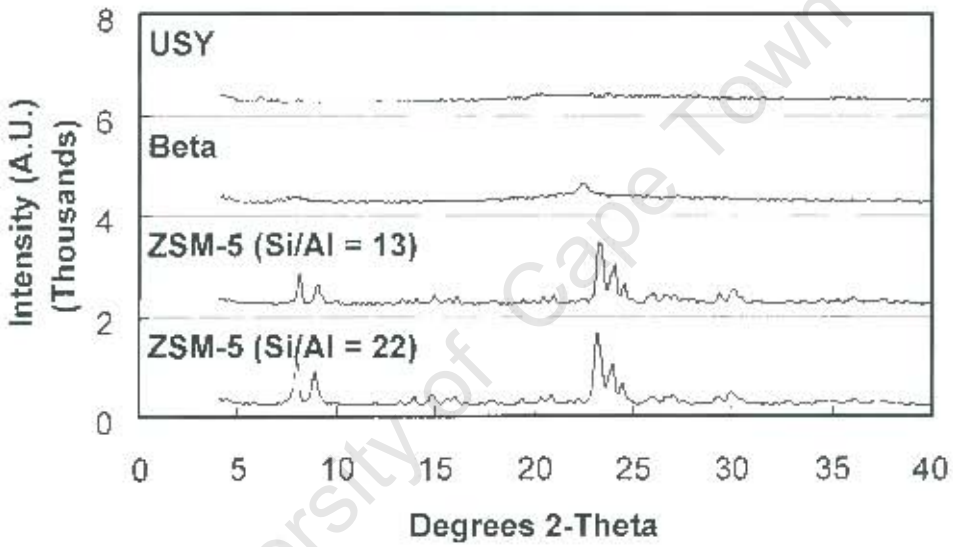


**Figure 4.30** XRD patterns of spent and recalcined USY, Beta, ZSM-5 (Si/Al = 13) and ZSM-5 (Si/Al = 22) applying Cu-K$\alpha$ radiation with step size equal to 0.1°.

Zeolite crystallinities after the reactions at 300°C relative to that before the reaction are determined by the ratio of the integrated peak areas after the reaction relative to the respective peak areas before the reaction. The peak in the range 21-24° is chosen for Beta [(2-Theta = 22.4°) Camblor and Pérez-Pariente, 1991], and the three largest peaks in the range 22-25° are selected for ZSM-5 [Hardenberg *et al.*, 1992]. After reactions at 300°C, the XRD spectrum of spent USY shows no peaks. Table 4.8 confirms the above interpretation with total loss

in the crystallinity of USY, ca. 60% loss in crystallinity for Beta and virtually no loss in the crystal structure of ZSM-5.

**Table 4.8 XRD determined change in crystallinity after reaction at 300°C relative to that before reaction.**

| | % zeolite crystallinity after reaction |
|---|---|
| USY | 0 |
| Beta | 37 - 44 |
| ZSM-5 (Si/Al = 13) | 95 - 100 |
| ZSM-5 (Si/Al = 22) | 95 - 100 |

**(ii) Crystallite morphology**

The electron micrograph of the spent zeolite USY visually confirms its total loss in crystallinity after the reaction at 300°C. The shape of the cubic crystallites (particle sizes between 0.4μm and 0.6μm) observed for USY prior to reaction (Figure 4.9 in Section 4.4.2.1) is totally absent upon examination of the spent USY, Figure 4.31 (left). The compound shown on the left-hand side of Figure 4.31 is amorphous.



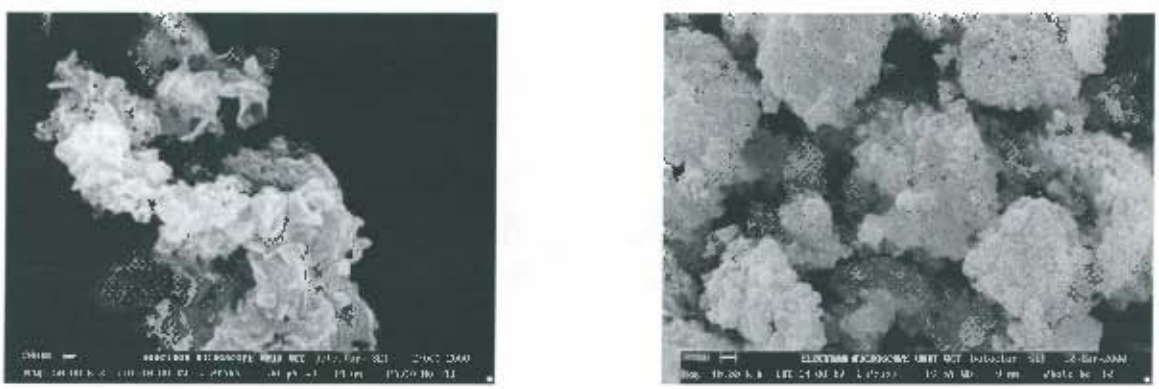

**Figure 4.31** Electron micrographs of USY (left) and Beta (right) after reactions at 300°C.

A change in the morphology of Beta after the reaction at 300°C (see Figure 4.31) from that before the reaction (see Figure 4.10) is not clear. The particle agglomerates tend to be more spherical after reaction. The ZSM-5 samples after the reaction at 300°C (Figure 4.32) are identical to the respective scanning electron micrographs in Figure 4.8 (ZSM-5 (Si/Al = 13)) and Figure 4.12 (ZSM-5 (Si/Al = 22)).

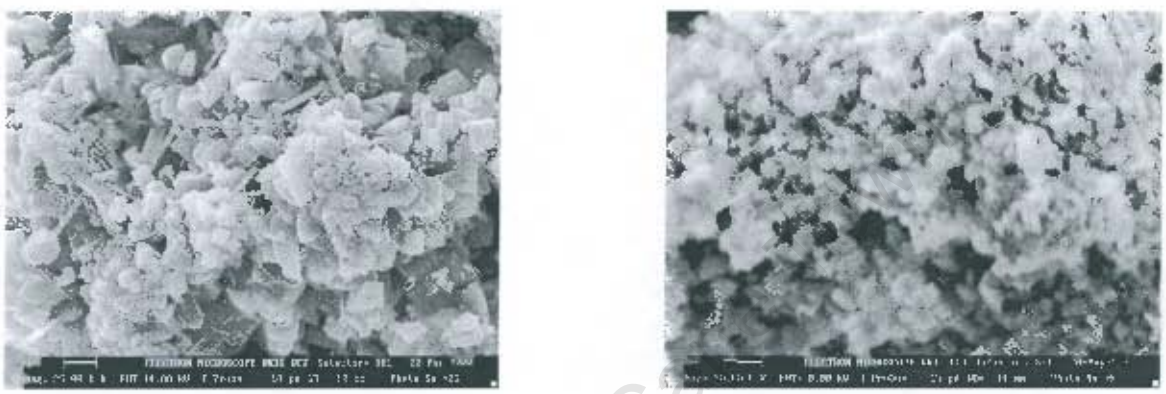

**Figure 4.32** Electron micrographs of ZSM-5 (Si/Al = 13) (left) and ZSM-5 (Si/Al = 22) (right) after reaction at 300°C.



### 4.4.4.2 PORE VOLUME ANALYSIS

The pore volume analysis of the spent silica-alumina, USY, Beta, ZSM-5 (Si/Al = 13) and ZSM-5 (Si/Al = 22) after reactions at 300°C are analysed using nitrogen adsorption ($N_2$-BET). Table 4.9 tabulates the $S_{BET}$ as well as the microporous and mesoporous surface areas. Because $N_2$-BET cannot measure pore sizes below ± 17Å, the micropore surface areas and pore volumes are taken as being obtained from pores less than 17Å, and the mesopore surface areas and pore volumes as being obtained from pores larger than 17Å. The mesopore pore volumes given are further subdivided into 17Å < $d_{pore}$ < 115Å and $d_{pore}$ > 115Å. The combined mesopore surface area ($d_{pore}$ > 17Å) gives an indication of the external surface area of the sample.

**Table 4.9 Surface area and pore volume data for spent silica-alumina, USY, Beta, ZSM-5 (Si/Al=13) and ZSM-5 (Si/Al=22)**

| | | Silica-Alumina | H-USY | H-Beta | H-ZSM-5 Si/Al = 13 | H-ZSM-5 Si/Al = 22 |
|---|---|---|---|---|---|---|
| BET surface area | ($m^2$/g) | 33 ± 2 | 61 ± 7 | 151 ± 10 | 285 ± 11 | 298 ± 7 |
| Micropore surface area | ($m^2$/g) | 2 | 22 | 110 | 249 | 268 |
| Mesopore surface area | ($m^2$/g) | 31 | 39 | 41 | 36 | 30 |
| Pore volume ($d_{pore}$ < 17Å) | (cc/g) | 0.001 | 0.010 | 0.051 | 0.110 | 0.121 |
| Pore volume (17Å < $d_{pore}$ < ± 115Å) | (cc/g) | 0.020 | 0.036 | 0.025 | 0.020 | 0.020 |
| Pore volume ($d_{pore}$ > 115Å) | (cc/g) | 0.154 | 0.114 | 0.054 | 0.032 | 0.025 |

Of the spent heterogeneous acids, the aluminosilicates with the largest total BET surface area are H-ZSM-5 (Si/Al = 13) (285$m^2$/g) and H-ZSM-5 (Si/Al = 22) (298$m^2$/g). The smallest BET surface area is that of spent silica-alumina (33$m^2$/g), followed by H-USY (61$m^2$/g) and H-Beta (151$m^2$/g). The micropore surface area of the spent H-USY (22$m^2$/g) is very small in comparison to that of the spent zeolite with the largest micropore surface area, i.e., H-ZSM-5 (Si/Al = 22) (268$m^2$/g). The mesopore surface area of all the spent aluminosilicates range between 30 and 42$m^2$/g. According to Table 4.9, the spent silica-alumina and H-USY contain hardly any pores having a pore diameter less than 115Å. Only above $d_{pore}$ = 115Å, do the spent aluminosilicates show a pore volume of 0.15cc/g and 0.11cc/g, respectively. The spent H-Beta, however, contains some micropores (pore volume = 0.05cc/g), while the mesopore volume ($d_{pore}$ > 17Å) only amounts to a total of 0.08cc/g. Nevertheless, it is unusual for zeolites such as H-USY and H-Beta to have a micropore volume less than the mesopore volume. Only the spent ZSM-5 zeolites consist of a micropore volume (ca. 0.12cc/g) greater than the mesopore volume (ca. 0.05cc/g). A pore size distribution of the spent aluminosilcates is presented in Figure 4.33.

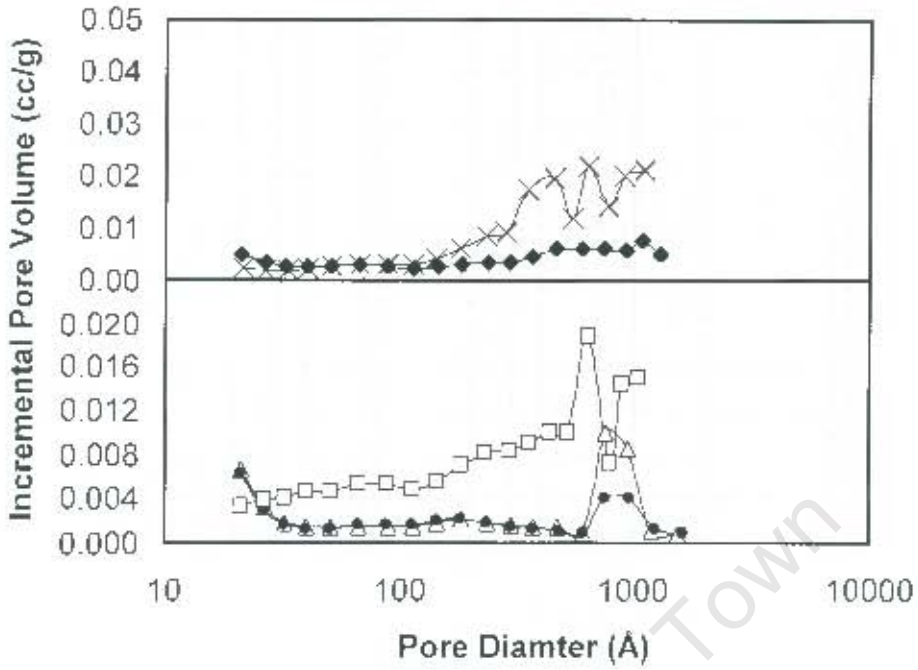


**Figure 4.33** Pore size distribution of spent USY (□), Beta (♦), ZSM-5 (Si/Al=13) (△), silica-alumina (×) and ZSM-5 (Si/Al=22) (•).



Comparisons of the $N_2$-BET analyses of the respective aluminosilicates before the reaction at 300°C (Table 4.4 in Section 4.4.2.5) with those after the reaction (Table 4.9) clearly shows that all the aluminosilicates used experience a decrease in the BET surface areas as well as a decrease in the micropore volumes during the course of the reaction. Table 4.10 allows for a more detailed interpretation regarding the change in the framework structure of the aluminosilicates during the course of the reaction by calculating ratios of the BET surface area ($S_{BET}$), microporous and mesoporous volumes of the respective aluminosilicates after the reaction relative to that before the 300°C reaction. As mentioned above, the mesoporous volume is subdivided into a 17Å < $d_{pore}$ < 115Å and a $d_{pore}$ > 115Å region.

**Table 4.10 Comparison of $S_{BET}$ surface area, and selective pore volume data of spent silica-alumina, USY, Beta, ZSM-5 (Si/Al = 13) and ZSM-5 (Si/Al = 22)**

| Zeolite | Ratio of aluminosilicates after reaction relative to before reaction at 300°C | | | |
|---|---|---|---|---|
| | $S_{BET}$ | $d_{pore} < 17Å$ | $17Å < d_{pore} < 115Å$ | $d_{pore} > 115Å$ |
| Silica-Alumina | 0.09 | - | 0.04 | 8.56[a] |
| USY | 0.10 | 0.04 | 1.20[a] | 2.11 |
| Beta | 0.27 | 0.31 | 0.13 | 0.22 |
| ZSM-5 (Si/Al = 13) | 0.94 | 0.85 | 1.11[a] | 3.56[a] |
| ZSM-5 (Si/Al = 22) | 0.96 | 0.92 | 1.18[a] | 1.92[a] |

[a] The pore volume of the *original* aluminosilicate between the given ranges ($d_{pore}$) is less than 0.03cc/g.

Silica-alumina, H-USY and H-Beta endure considerable structural changes during the course of the reaction with the $S_{BET}$ surface area for the respective spent aluminosilicate being only 9%, 10% and 27% of their original surface area. Only the ZSM-5's retain their surface area. The destruction of the micropore pore volume ($d_{pore} < 17Å$) follows a similar pattern to that in Table 4.8, which shows the XRD determined change in the zeolite crystallinity after reaction at 300°C relative to that before reaction. This is to be expected since the crystallinity can be correlated with the micropore volume. Therefore, the zeolite USY, Beta, ZSM-5 (Si/Al = 13) and ZSM-5 (Si/Al = 22) respectively are only 4%, 31%, 85% and 92% as crystalline as prior to the reaction at 300°C. Conversely, the micropores of USY experience a near total collapse, followed by Beta, ZSM-5 (Si/Al = 13) and ZSM-5 (Si/Al = 22). Similarly, the mesopore region $17Å < d_{pore} < 115Å$ which is predominantly present in the original silica-alumina disappears fully, resulting in mesopores of diameters greater than 115Å. Interestingly, H-USY shows hardly any change in the pore volume between diameters 17Å and 115Å and above 115Å the pore volume changes only by a factor of 2 which if compared to the amount of micropore volume lost during the 300°C reaction points towards a total disintegration of the zeolite pore structure. The $17Å < d_{pore} < 115Å$ and $d_{pore} > 115Å$ regions of H-Beta both tend to decrease by a factor of 8 and 5 respectively.

thus also suggesting a disintegration of some of the zeolite pore structure. Since, however, a large amount of micropores are still available it tends to suggest that the disintegration is likely to start from the outside and works itself to the centre of the H-Beta crystallite. The least affected by the reaction at 300°C are the ZSM-5 zeolites with only the 115Å < $d_{pore}$ tending to increase by factor of ca. 3, thereby confirming the hypothesis made previously for H-Beta.

## 4.5 REACTIONS WITH ZIRCONIUM PHOSPHATES

The use of layered compounds such as α-zirconium phosphate (α-ZrP) and γ-zirconium phosphate (γ-ZrP) as heterogeneous regenerable reagents for the acid hydrolysis of MPDA can enhance the accessibility of reactant MPDA to surface acid sites. The great advantage of using layered compounds as opposed to the rigid 3 dimensional aluminosilicates is the fact that the interlayer distances of the zirconium phosphates increase to accommodate larger molecules, thereby ensuring greater access of the reactant MPDA onto active P-(OH) sites. Furthermore, the macromolecular zirconium phosphate planes consist of *fixed* ionogenic phosphate groups similar to mineral ortho-phosphoric acid. Therefore, it is likely that, as with phosphoric acid, a high yield of resorcinol can be produced in the presence of zirconium phosphates. The stability of crystalline α-zirconium phosphate towards the hydrolysis of phosphate groups into aqueous solutions [Clearfield and Stynes, 1964] further supports the investigation into their use for the synthesis of resorcinol from MPDA.

### 4.5.1 CHARACTERISATION OF ZIRCONIUM PHOSPHATES

Typically, 10grams of the obtained α-zirconium phosphate (α-ZrP) or γ-zirconium phosphate (γ-ZrP) was used for each reaction. The use of the 400°C pre-calcined zirconium phosphates also amount to 10grams prior to their respective calcination, and allowed for monitoring the stability of the thermally treated α-ZrP and γ-ZrP and their reuse in subsequent reactions. Calcined forms of the original α-ZrP and γ-ZrP are termed α-ZrP400 and γ-ZrP400 respectively to denote their calcination at 400°C. Since zirconium phosphates consist of ionogenic phosphate groups and resemble the regular structure of an inorganic salt quite closely, certain properties of the zirconium phosphates, e.g., number of Brønsted acid sites, are known prior to characterisation (see Section 2.3).

### 4.5.1.1 THERMOGRAVIMETRIC DIFFERENTIAL ANALYSIS

Thermogravimetric (TG) and differential temperature analysis (DTA) curves of α-$Zr(HPO_4)_2 \cdot H_2O$ (7.55Å) and γ-$Zr(PO_4)(H_2PO_4) \cdot 2H_2O$ (12.20Å) are illustrated in Figure 4.34. A low ramping rate (1°C/min) is chosen for the TG-DTA curves to allow for a reasonable comparison being made between the weight loss of the zirconium phosphates during the TG-DTA and the 400°C kiln calcined zirconium phosphate equivalents.

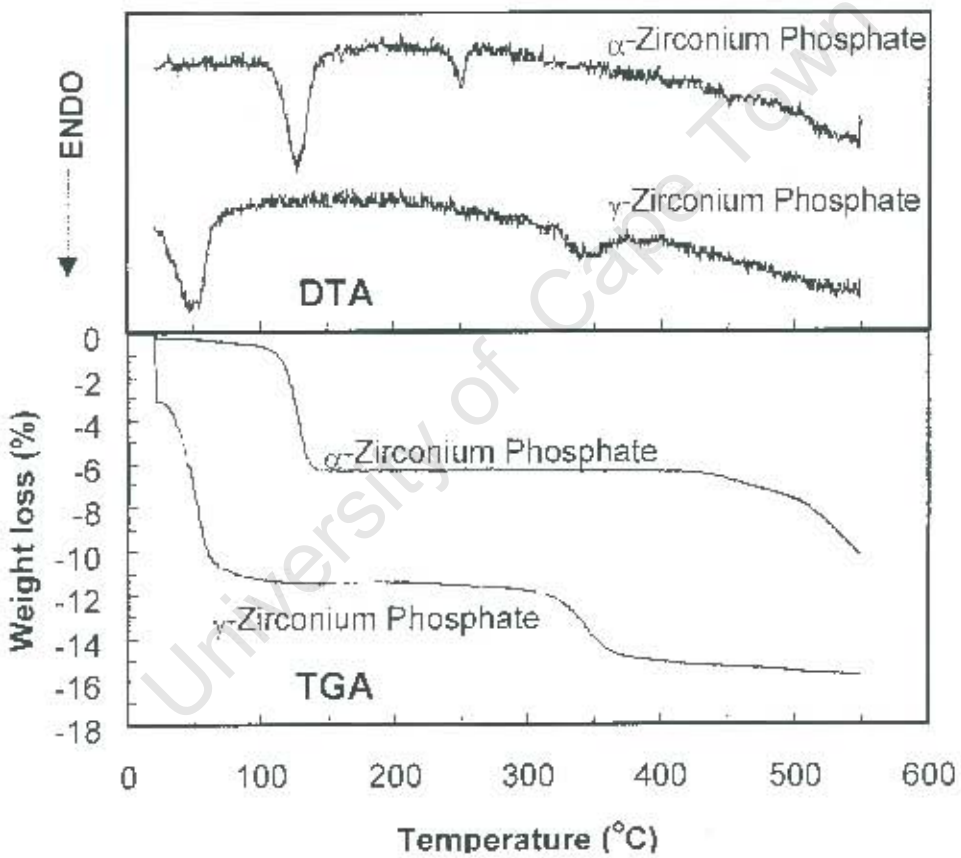


**Figure 4.34** TGA and DTA curves of relevant zirconium phosphates with ramping rate set at 1°C/min ($N_2$-flowrate = 30ml(NTP)/min).

As observed in Figure 4.34, α-ZrP experiences a weight loss of 0.2% whilst flushing the sample for 30minutes at constant temperature under flow of nitrogen (Section 3.2.3). The TG curve of γ-ZrP shows a strong initial weight loss of 3.1%

after flushing the sample for ca. 1hour under the flow of nitrogen. The prolonged flushing period for γ-ZrP prior to the temperature ramping is due to the continued loss of weight throughout the flushing period with seemingly no pseudo-equilibrium state of constant weight being attainable.

After the flushing period, the TG curve of α-ZrP shows a minor weight loss between ambient temperature and 100°C (0.4%). This is followed by a large weight loss (5.7%) between temperatures 100°C and 150°C. Between 150°C and ca. 430°C, the TG curve for α-ZrP remains virtually flat with the weight loss equalling less than 0.1%. Beyond 430°C, α-ZrP experiences a second substantial weight loss that lasts beyond the temperature of 550°C. The DTA curve of α-ZrP shows a large endothermic peak at 129°C that coincides with the TG weight loss. A second endothermic peak for α-ZrP is observed at 252°C, which does not coincide with a weight loss. The TG-DTA curves on α-ZrP are, however, thoroughly researched with the most recent detailed study being given by Costantino *et al.* [1997]. The endothermic peak at 129°C is only partly due to the loss of 1mole of crystal water per mole of α-$Zr(HPO_4)_2 \cdot H_2O$ (7.55Å), which in theory (molecular weight) accounts for a weight loss of 6.0%. This is in good agreement with the total weight loss (6.3%) between ambient temperature and 150°C, implying that 0.3% of the sample weight loss remains unaccountable. According to Costantino *et al.* [1997], at around the same temperature (129°C), α-$Zr(HPO_4)_2 \cdot H_2O$ (7.55Å) undergoes a phase change to α-$Zr(HPO_4)_2$ (7.41Å) in which the interlayer distance of α-ZrP becomes altered (see Section 2.3.3.1). It is proven that the loss of crystal water and the phase change to α-$Zr(HPO_4)_2$ (7.41Å) are kinetically and thermodynamically distinct process [Clearfield and Pack, 1975]. The second endothermic peak (252°C) is due to another reversible phase transition to α-$Zr(HPO_4)_2$ (6.8Å). The weight loss experienced by α-ZrP upon further heating beyond 430°C is due to the slow formation of a layered zirconium pyrophosphate α-$ZrP_2O_7$ (6.1Å) with the loss of an additional mole of water per mole of α-ZrP [Costantino and La Ginestra, 1982].

The TG curve for γ-ZrP shows a total weight loss of 11.3% even before the thermoanalytical study has reached a temperature of 100°C. Between the temperatures 100°C and 300°C, the weight loss is minimal (0.6%). An additional weight loss of 3.2% occurs between 300°C and 400°C, followed by a gradual decrease in the TG curve beyond 400°C. The initial decrease of 11.3% observed for γ-$Zr(PO_4)(H_2PO_4)\cdot 2H_2O$ (12.20Å) is due to the loss of two moles of crystal water per formula weight to form γ-$Zr(PO_4)(H_2PO_4)$ (9.4Å). This is supported by the presence of an endothermic peak at 55°C (DTA curve). The endothermic peak at 351°C is due to the condensation of P-(OH) hydroxyl groups [Alberti *et al.*, 1989]. A layered γ-$ZrP_2O_7$ (8.26Å) (or γ-L-$ZrP_2O_7$) structure should result that is stable till ca. 600°C [Costantino and La Ginestra, 1982; Alberti *et al.*, 1989].

**Table 4.11 Observed weight loss at 180°C and 400°C of α- and γ-zirconium phosphates**

| Zirconium Phosphate | Percent Weight Loss | |
|---|---|---|
| | TGA[1] | Kiln[2] (no. of measurements) |
| α-ZrP at 180°C | 6.3 | 6.2 ± 0.3 (3) |
| γ-ZrP at 180°C | 11.4 | 11.5 ± 0.4 (5) |
| α-ZrP at 400°C | 6.4 | 7.2 ± 0.5 (5) |
| γ-ZrP at 400°C | 15.0 | 15.6 ± 0.5 (4) |

[1] $N_2$-flowrate: 30ml(NTP)/min

[2] calcination at 180°C last for 12hours; calcination at 400°C involves 12hours at 180°C followed by 12hours at 400°C; calcination in air and shallow ZrP bed.

Table 4.11 compares the thermoanalytical results with the zirconium phosphate weight losses experienced during calcination, where the samples are weighed out before calcination and then immediately afterwards. As shown in Table 4.11, the observed weight loss for the 12hour kiln treated zirconium phosphates at 180°C compare quite well with the TGA data. This implies that the weight losses incurred by α-ZrP (6.3%) and γ-ZrP (11.4%) after prolonged heating at 180°C are in reasonable alignment with those determined by TG analysis. The weight

losses are in agreement with the theoretically predicted weight losses of α-ZrP (6.0%) and γ-ZrP (11.3%) upon removal of the hydration water.

Weight losses determined manually by means of a kiln at 400°C for α-ZrP and γ-ZrP differ from the TGA results with the kiln treated zirconium phosphates showing greater percent weight losses than by TG analyses. The discrepancies are due to the condensation of the P-(OH) hydroxyl groups and the formation of P-O-P bonds. This also tends to be a common observation for α-ZrP if kept at 400°C for a prolonged period of time [Clearfield and Thakur, 1980], thus resulting in the partial transformation of α-$Zr(HPO_4)_2$ (6.80Å) to α-$ZrP_2O_7$ (6.10Å). Consequently, only the 400°C kiln treated α-ZrP shows a loss of 0.16 moles of water per mole of α-ZrP as a result of P-(OH) hydroxyl condensation. For γ-ZrP, the prolonged heating at 400°C results in 4.4% of the weight lost being due to the partial transformation of γ-$Zr(PO_4)(H_2PO_4)$ (9.4Å) to γ-$ZrP_2O_7$ (8.26Å) as opposed to the 3.6% observed during the TG analysis. Considering the TGA results, the amount of water lost as a result of the condensation of P-(OH) hydroxyl groups are 0.63 moles per mole of γ-ZrP whereas the kiln treated γ-ZrP shows a loss of 0.71 moles of water per mole of γ-ZrP.

From examination of the 400°C kiln treated zirconium phosphates, it is calculated that α-$Zr(HPO_4)_2{\cdot}H_2O$ and γ-$Zr(PO_4)(H_2PO_4){\cdot}2H_2O$ lose ca. 0.32moles and 1.42moles of Brønsted acid sites per mole of zirconium phosphate, respectively. Consequently, the amount of Brønsted acid sites on α-ZrP400 and γ-ZrP400 is 1.68moles and 0.58moles per mole Zr. Since the unit mass of zirconium phosphate changes consistently with temperature as water is lost, any concentration term regarding the involvement of zirconium phosphates is expressed relative to the number of moles of zirconium atoms.

### 4.5.1.2 STRUCTURE AND MORPHOLOGY

#### (i) X-ray diffraction

The *d*-spacing of α-ZrP and γ-ZrP, as well as the rehydrated α-ZrP400 and γ-ZrP400 as determined from XRD are summarised in Table 4.12. The *d*-spacing and relative intensities of α-ZrP and γ-ZrP are in agreement with those found in literature [Clearfield and Pack, 1975; Alberti *et al.*, 1989]. Furthermore, the very high peak intensities observed during the XRD-powder patterns of α-ZrP and γ-ZrP (Figure 4.35) reveal that these compounds are highly crystalline. The extent of broadening of the peak width due to the XRD-apparatus was not determined.

**Table 4.12 *d*-Spacing and relative intensities of the X-ray powder patterns of α-ZrP and γ-ZrP as well as the 400°C calcined equivalents α-ZrP400 and γ-ZrP400**

| α-ZrP | | γ-ZrP | | α-ZrP400 | | γ-ZrP400 | |
|---|---|---|---|---|---|---|---|
| *d* (Å) | $I/I_o$ | *d* (Å) | $I/I_o$ | *d* (Å) | $I/I_o$ | *d* (Å) | $I/I_o$ |
| 7.55 | 77 | 12.21 | 100 | 7.45 | 100 | 8.28 | 40 |
| 4.49 | 27 | 5.81 | 23 | 4.56 | 21 | 5.18 | 61 |
| 4.43 | 17 | 4.63 | 7 | 4.43 | 18 | 3.86 | 100 |
| 3.56 | 100 | 4.47 | 3 | 3.68 | 22 | 3.31 | 59 |
| 3.52 | 54 | 4.34 | 10 | 2.64 | 13 | 2.69 | 11 |
| 3.30 | 3 | 3.74 | 15 | | | 2.58 | 15 |
| 3.21 | 6 | 3.50 | 14 | | | 2.50 | 14 |
| 3.08 | 3 | 3.31 | 13 | | | | |
| 2.64 | 18 | 3.20 | 5 | | | | |
| 2.62 | 22 | 3.10 | 4 | | | | |
| 2.40 | 10 | 3.07 | 3 | | | | |
| | | 2.69 | 17 | | | | |

The α-ZrP400 has a similar XRD powder pattern to that of α-$Zr(HPO_4)_2$ (7.41Å) [Clearfield and Pack, 1975]. Comparison of the *d*-spacing and relative intensities of α-ZrP400 with those of α-$Zr(HPO_4)_2$ (7.41Å) reported in the literature [Clearfield and Pack, 1975] suggests that the layers of α-ZrP400 are slightly distorted. This phenomenon may be due to the fact that not all of the α-$Zr(HPO_4)_2$ (6.80Å) has been transformed back to α-$Zr(HPO_4)_2$ (7.41Å) within the given 3day rehydration period. Although the thermoanalytical investigation predicts some

P-O-P bond formation, the XRD-spectrum of α-ZrP400 shows no traces of the pyrophosphate phase, i.e., α-$ZrP_2O_7$ (6.1Å). The lower peak intensities of α-ZrP400 when compared to α-ZrP (Figure 4.35) suggest a slightly more disordered unit cell arrangement within the α-ZrP400 crystallite.

The structure of γ-ZrP400 perfectly matches that of layered γ-$ZrP_2O_7$ (8.26Å) [Costantino and La Ginestra, 1982]. This is despite the fact that not all the P-(OH) hydroxyl groups on γ-ZrP400 condense to P-O-P bonds during the 400°C kiln treatment (Section 4.5.1.1). The retention of some stable hydroxyl groups (0.58mol / (mol Zr)) has also been observed by other authors [Costantino and La Ginestra, 1982; Alberti *et al.*, 1989]. At higher diffraction angles the peaks are generally broader than those of the original γ-ZrP. This implies that during the calcination the crystallites of γ-ZrP in the direction normal to the diffracting plane break up into smaller crystals [Reynolds Jr., 1989]. The lower peak intensities further suggests that γ-ZrP400 is less crystalline than the original γ-ZrP.

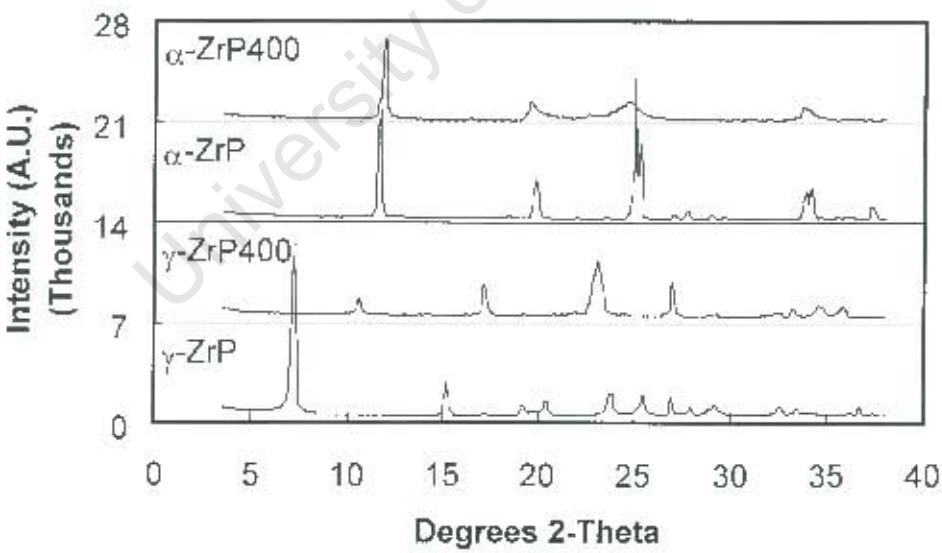


**Figure 4.35** XRD-spectra of α-ZrP400, α-ZrP, γ-ZrP400 and γ-ZrP using Cu-Kα radiation and step size = 0.1°.

**(ii) FT-IR analysis**

FT-IR of $\alpha$-ZrP recorded at 25°C, 180°C and 400°C are similar to those reported by Horsley *et al.* [1974] Due to the method used in obtaining the FT-IR spectra, the band at ca. 2300cm$^{-1}$ is attributed to varying concentration of $CO_2$ present in the air and is not part of the $\gamma$-ZrP FT-IR spectra. The peaks at 3590cm$^{-1}$, 3510cm$^{-1}$, 3150cm$^{-1}$ and 1618cm$^{-1}$ are attributed to the lattice water molecule (see $\alpha$-ZrP at 25°C) and disappear upon dehydration (see $\alpha$-ZrP at 180°C and 400°C). The band at 3280cm$^{-1}$ is attributed to a (P)-O-H streching mode that disappears during the formation of pyrophosphate groups at >400°C. Since the absorbance at 3280cm$^{-1}$ for $\alpha$-ZrP at 400°C does not diminish, it can be concluded that no P-O-P bonds are produced while keeping $\alpha$-ZrP at 400°C for 1hour. This is further confirmed by the absence of any band at 970cm$^{-1}$, which is characteristic of pyrophosphate groups. Associated with the bands at 3280cm$^{-1}$

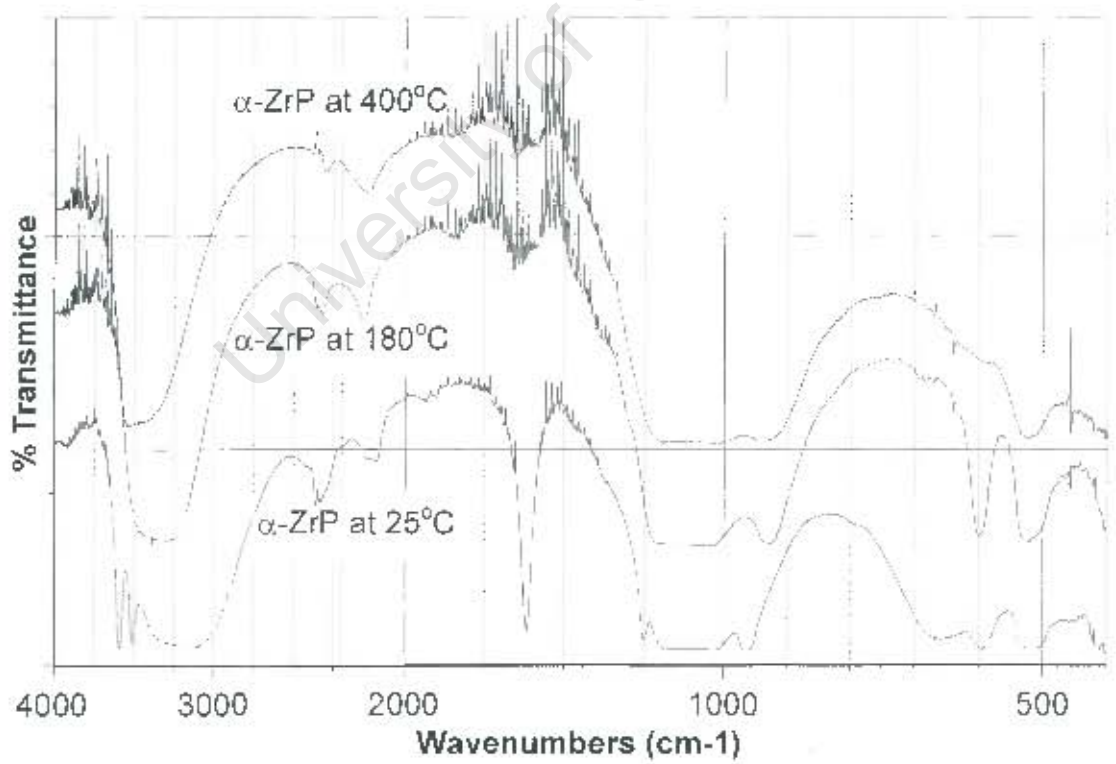


**Figure 4.36** FT-IR spectra of the original $\alpha$-zirconium phosphate recorded at ambient temperature, 180°C and 400°C

are the weak bands at 2300cm$^{-1}$ (atmospheric $CO_2$ interference with this band) and 2100cm$^{-1}$, which correspond to weak (P)-O-H streching vibrations. Not to be confused with the 970cm$^{-1}$ band (pyrophosphate) are the bands at 980cm$^{-1}$ (attributed to vibrations of the orthophosphate group) and 935cm$^{-1}$ (observed for $\alpha$-ZrP in the absence of crystalline water, i.e. $\alpha$-$Zr(HPO_4)_2$ (7.44Å)). The $\nu$(OH) stretch bands assigned to the Brønsted acidity of the POH groups (3670 – 3660cm$^{-1}$) with the acid strength increasing slightly by calcination [La Ginestra and Patrono, 1987] can only be made out with difficulty.

FT-IR of $\gamma$-ZrP are also recorded at 25°C, 180°C and 400°C. No FT-IR spectra on $\gamma$-ZrP could be found in literature and thus the spectra given in Figure 4.37 cannot be compared. Therefore, the interpretation of the peaks are solely based on the band identifications given by Horsley *et al.* [1974] on $\alpha$-ZrP. Similar to

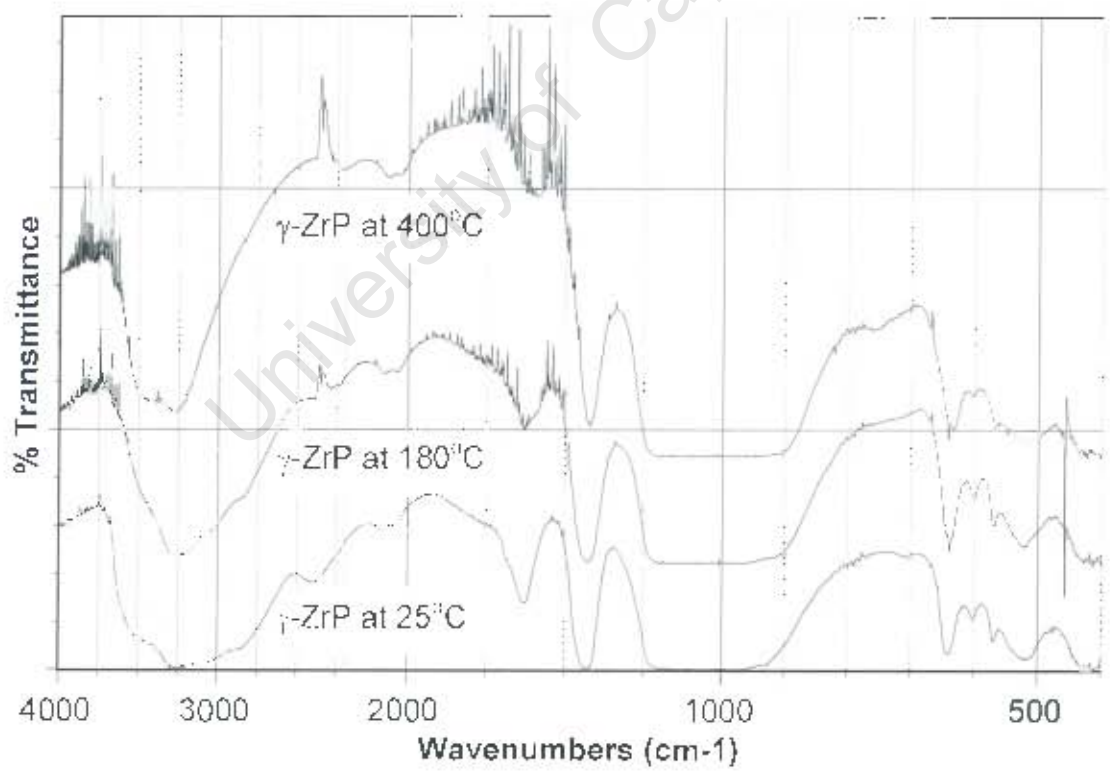


**Figure 4.37** FT-IR spectra of the original $\gamma$-zirconium phosphate recorded at ambient temperature, 180°C and 400°C

α-ZrP, the band at ca. 2300cm$^{-1}$ is attributed to $CO_2$ present in the air and could interfere with an absorption band originating from γ-ZrP. The band at 1630cm$^{-1}$ observed for α-ZrP at 25°C may be ascribed to lattice water molecules since no significant condensation of $P(OH)_2$ would occur at 180°C. The narrowing of bands between 3600cm$^{-1}$ and 2800cm$^{-1}$ could also partially be ascribed to lattice water molecules. In conformity to the FT-IR of α-ZrP, the bands between 3500cm$^{-1}$ and 3250cm$^{-1}$ may be attributed to (P)-O-H stretching modes. The ν(OH) stretch bands assigned to the Brønsted acidity of the P-$(OH)_2$ groups (3600cm$^{-1}$) [La Ginestra and Patrono, 1987] are not observed. Since the band at 1400cm$^{-1}$ does not change when heating γ-ZrP from ambient temperature through to 400°C, the associated absorption band could be due to the vibrations of the $PO_4$ groups. The strong bands between 1250cm$^{-1}$ and 950cm$^{-1}$ are possibly due to the phosphate ($PO_4$ and $O_2P(OH)_2$) groups present on γ-ZrP. For γ-ZrP recorded at 400°C, the characteristic band (asymmetric) attributed to the formation of pyrophosphates (970cm$^{-1}$) cannot be found. The likely reason is that the pressed γ-ZrP wafer is too thick; thinner wafers proved difficult to handle. Nevertheless, the γ-ZrP spectrum at 400°C shows a band at 760cm$^{-1}$, which is ascribed to the symmetric vibration of the P-O-P bridge [Ramis *et al.*, 1988].

**(iii) $N_2$-BET surface area**

The BET surface area of α-ZrP and γ-ZrP is 7.7±0.1m$^2$/g (repeated once) and ca. 16.7m$^2$/g, respectively. The large ratio obtained when dividing the theoretically predicted (exfoliated) surface areas (Equation 2.31) of α-ZrP (960m$^2$/g) and γ-ZrP (674m$^2$/g) by the respective BET surface area indicates that the zirconium phosphates are reasonably crystalline. For example, for α-ZrP a BET surface area of 2.4m$^2$/g is due to a highly crystalline compound whereas the surface area of a low crystalline α-ZrP is >72m$^2$/g (Section 2.3.1). The surface area of the 400°C calcined equivalents α-ZrP400 (ca. 8.8m$^2$/g) and γ-ZrP400 (17.0m$^2$/g) is greater than the original zirconium phosphates, probably due to an increase in

the number of disordered zirconium phosphate layers after calcination. The true change in the BET surface area from the original to the 400°C zirconium phosphates would be slightly greater than the ones given in this section since the molecular weight of the original α-ZrP (301g/mol) and γ-ZrP (319g/mol) is larger than the respective molecular weights of α-ZrP400 (280g/mol) and γ-ZrP400 (270g/mol). The change in the molecular weight is due to the absence of crystalline water in the latter compounds. The new molecular weights are estimated by means of Table 4.11.

**(iv) Crystallite particle size and morphology**

The crystallite particle sizes of the zirconium phosphates are determined from scanning electron micrographs. The crystallites of α-ZrP (Figure 4.38 left) are flat platelets that are ca. 0.1μm in thickness. The platelets are oval in shape with an average dimension of ca. 0.7 x 0.5μm. According to the manufacturer specification the particle agglomerates (grain size) are less than or equal to 200mesh. This would correspond to α-ZrP agglomerates smaller than 74μm. After calcination of α-ZrP at 400°C (α-ZrP400), the crystallite dimensions remain unaffected (Figure 4.38 right).

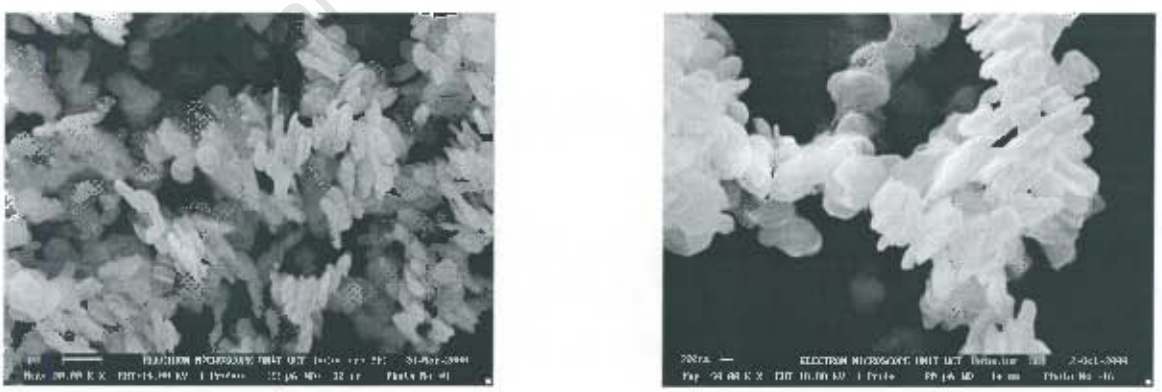

**Figure 4.38** Scanning electron micrographs of α-ZrP (left) and α-ZrP400 (right).

The γ-ZrP agglomerates consist of slate-like crystallites of different dimensions. According to the manufacturer specification, the agglomerates are also smaller than 74μm (200mesh). The 400°C kiln-calcined γ-ZrP (γ-ZrP400) is similar in appearance to the original γ-ZrP. Nevertheless, the slates of γ-ZrP400 may on average be smaller than those of γ-ZrP

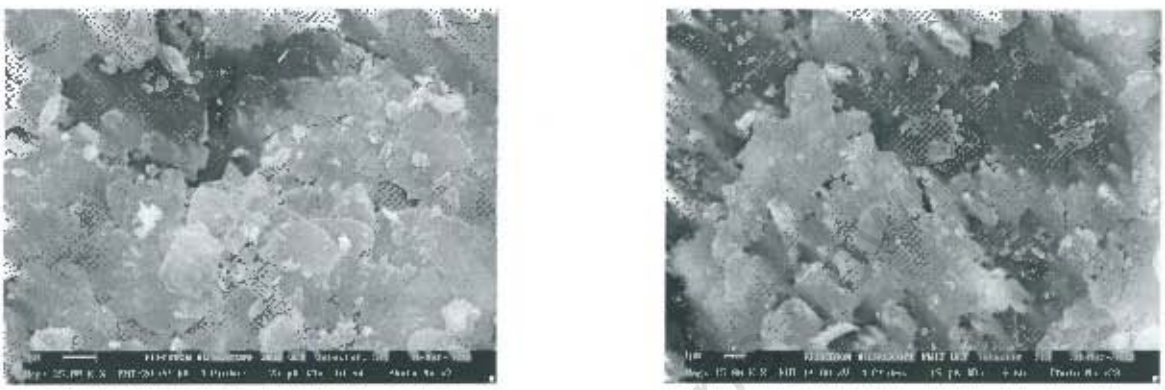

**Figure 4.39** Scanning electron micrographs of γ-ZrP (left) and γ-ZrP400 (right).



### 4.5.1.3 ADSORPTION OF SOLUTES ON ZIRCONIUM PHOSPHATES

Figures 4.40 through to 4.43 show the adsorption of dissolved MPDA, MAP and resorcinol onto the zirconium phosphates at 70°C as a function of the respective mole fractions of the organic compounds in solution. This gives an indication of the accessibility of the acid sites. The adsorption isotherms are determined by means of batch adsorption experiments. As outlined in Section 3.2.4.5, the amount of zirconium phosphates (ca. 0.4g) used per 15ml of aqueous solution roughly corresponds to the amount of zirconium phosphate used during the reaction (10g zirconium phosphate per 350ml of solution). Due to loss of water of crystallisation and loss of water through condensation of P-(OH) groups in α-ZrP400 and γ-ZrP400, the adsorbed concentration is expressed as per mole zirconium instead of per unit mass.

**(i) Adsorption of MPDA on zirconium phosphates**

While the adsorption isotherms at 30°C and 70°C tend to overlap, the adsorption isotherms at 50°C are generally below the isotherms at 30°C and 70°C. This phenomenon is observed quite often during the adsorption of organic compounds from aqueous solutions on activated carbon [Chiou and Manes, 1974]. In the presence of activated carbon, the usually expected consistent decrease with increasing temperature is disrupted at temperatures in close proximity to the solute melting point (MPDA melting point occurs at 61°C [Daubert and Danner, 1989]). This phenomenon has been explained in terms of the relatively more efficient packing of organic molecules in carbon pores when present in liquid state at temperatures above the melting point [Chiou and Manes, 1974]. However, the explanation given by Chiou and Manes [1974] is disputed by Ravi *et al.* [1998] by proving that these adsorption effects are noticed during the adsorption of only some organic compounds from aqueous solution.

Only the adsorption data of MPDA on $\alpha$-ZrP, $\alpha$-ZrP400, $\gamma$-ZrP and $\gamma$-ZrP400 at 70°C will be presented in this chapter. The raw adsorption data for the remaining isotherms (mole-fraction of the solute MPDA in aqueous solution) are given in APPENDIX-J.

The amount of MPDA adsorbed from aqueous solution onto the zirconium phosphates is largest for $\alpha$-ZrP, which is followed by $\alpha$-ZrP400 and $\gamma$-ZrP. The uptake of MPDA on $\alpha$-ZrP400 and $\gamma$-ZrP is in turn larger than that observed for $\gamma$-ZrP400. From the initial slope of the curves (see Figure 4.40), it can be deduced that MPDA has a high affinity for adsorption onto $\alpha$-ZrP, $\alpha$-ZrP400 and $\gamma$-ZrP. The maximum initial uptake of MPDA onto $\alpha$-ZrP (0.60 - 0.69 mol/mol(Zr)) is greater than that of $\alpha$-ZrP400 (0.42 - 0.48 mol/(mol Zr)) and $\gamma$-ZrP (ca. 0.48 mol/(mol Zr)). For $\alpha$-ZrP and $\alpha$-ZrP400, a plateau is reached relatively quickly after the initial strong uptake of MPDA. $\gamma$-ZrP shows a rapid initial uptake of 0.48 mol MPDA per mole zirconium phosphate, followed by a much slower continuing adsorption, which is indicative of another $\gamma$-ZrP mode of adsorption. In contrast to the

adsorption isotherms of the aforementioned, γ-ZrP400 possesses a low tendency to adsorb MPDA.

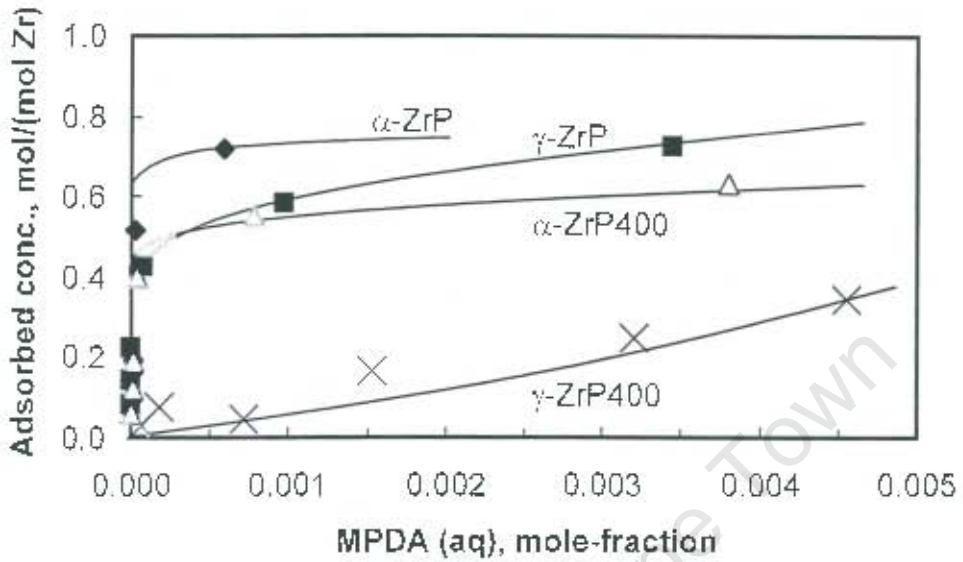


**Figure 4.40** Adsorption-equilibrium data for aqueous MPDA on α-ZrP (◆), α-ZrP400 (Δ), γ-ZrP (■) and γ-ZrP400 (x) at 70°C.

Both amine groups present on MPDA are capable of interacting with an acid site present on the zirconium phosphates, as shown previously by Clearfield *et al.* [1979] during the adsorption of ethylenediamine. The MPDA molecule should not destabilise upon adsorption / co-ordination of both amine groups, considering that the resonance theory predicts no destabilisation of the second amine group (in meta-position) by an attack onto the first ortho-, para-directing $NH_2$–group. Consequently, the maximum amount of MPDA able to adsorb is equivalent to half the number of available sites on α-ZrP, γ-ZrP, α-ZrP400 and γ-ZrP400 if the acid sites are close enough. The five units difference in the $pK_a$–values of the two protons on the dihydrogenphosphate [Clearfield, 1993] present in γ-ZrP implies that the maximum amount of MPDA adsorbed onto γ-ZrP is essentially halved once more. Accordingly, the maximum of MPDA expected to intercalate onto α-ZrP is 1.0 mol/(mol Zr) and onto γ-ZrP is 0.5 mol/(mol Zr). The condensation of Brønsted acid sites upon prolonged heating of α-ZrP at 400°C, results in a 16%

reduction of acid sites on α-ZrP400 relative to α-ZrP. Thus, the amount of MPDA adsorbing onto the layers of α-ZrP400 is roughly 0.84 mol/(mol Zr). Likewise for γ-ZrP400, it is calculated that a total of 71% of Brønsted acid sites are lost per mole of γ-ZrP due to condensation of the hydroxyl groups at 400°C. Thus γ-ZrP400 has 2*(1-0.71) = 0.58 mol/(mol Zr) acid sites. Based on the assumption that all the first hydroxyl groups are lost per dihydrogenphosphate group before the removal of the second set of hydroxyl groups, it can be determined that 0.29 moles of MPDA interacts with 1 mole of γ-ZrP400.

The area covered by one $PO_3(OH)$ group in α-ZrP is ca. 24Å$^2$ with the closest acid to acid distance on a particular layer being 5.3Å [Alberti and Costantino, 1974 and 1984]. Therefore, considering the dimensions of MPDA and assuming flat penetration of MPDA molecules into the layers of α-ZrP, a possible reason for observing ca. 0.66 mole of MPDA adsorbing instead of the theoretical 1.0 mole MPDA per mole of zirconium phosphate could be that steric hindrance is created by the already adsorbed MPDA. Calcining α-ZrP at 400°C results in an increase in the ratio of strong to weak acid sites [Hattori *et al.*, 1977; Clearfield and Thakur, 1980]. Therefore, it is expected that the amount of MPDA adsorbing onto α-ZrP400 is equal to 0.84 mole MPDA per mole of Zr. The initial MPDA uptake on α-ZrP400 is only 0.45 mol/(mol Zr). This observation could be ascribed to the added steric hindrances created by the presence of P-O-P bonds in α-ZrP400. The initial uptake of MPDA by γ-ZrP is essentially the same as predicted in theory, with the number of MPDA molecule adsorbed being equal to 0.5 mol/(mol Zr). This suggests that steric hinderance is not significant for case of γ-ZrP. A slight positive inclination in the slope of the adsorption isotherm after the initial uptake is noticed. This is possibly due to some interaction with the second much weaker acid sites after all the strong sites are occupied. In contrast, γ-ZrP400 hardly shows any uptake of MPDA. The very low adsorption of MPDA onto γ-ZrP400 confirms that the formation of P-O-P bonds hinders the MPDA molecules from gaining access to the Brønsted acid sites.

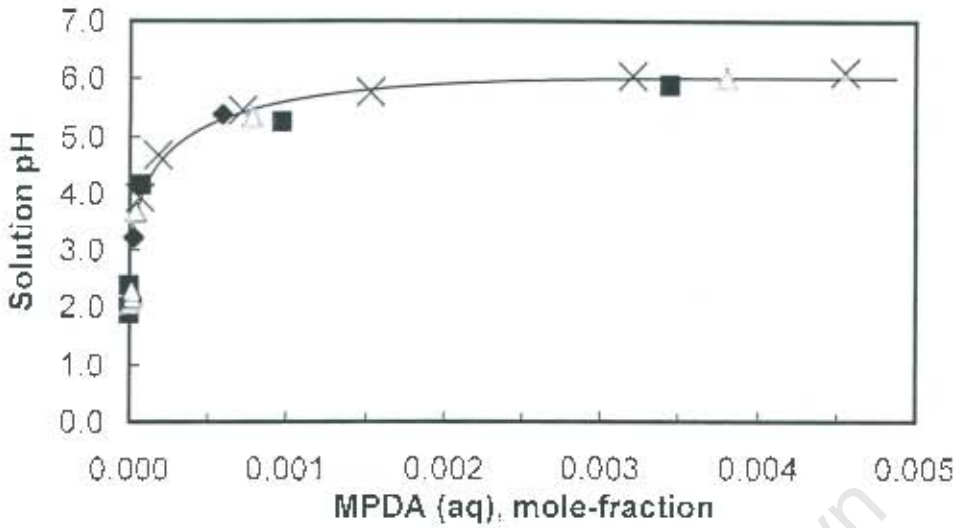


**Figure 4.41** Correlation of the measured solution pH versus the MPDA concentration (T = 70°C) after removal of adsorbents α-ZrP (◆), α-ZrP400 (Δ), γ-ZrP (■) and γ-ZrP400 (x) from the bulk solution.

Compared to the solution pH measured for the liquid phase after the adsorption of MPDA on the aluminosilicates (see Section 4.4.2.6), the pH obtained for the adsorption of MPDA onto the zirconium phosphates vary considerably. After adsorption of MPDA on the zirconium phosphates there is an identical correlation between the solution pH and the MPDA concentration for each zirconium phosphate sample. This correlation holds true for all the zirconium phosphate phases that have been considered. At very low MPDA concentration the sample pH is ca. 2 and at high concentrations (MPDA mole-fraction of 0.005) the pH is ca. 6.0. Since the solution pH measured for very low MPDA concentrations clearly lies within the acid region, phosphate-ions in the form of $H_3PO_4$ ($pK_a$ = 2.12 [Shriver *et al.*, 1994]) must go into solution. The low pH cannot be ascribed to leaching and subsequent dissociation of $H_2PO_4^-$ ($pK_a$ = 7.4 [Shriver *et al.*, 1994]) from the γ-zirconium phosphates nor to the leaching of $HPO_4^{2-}$ ($pK_a$ = 12.2 [Shriver *et al.*, 1994]) from the α-zirconium phosphates.

In a separate experiment, suspension of 0.42g of pure γ-ZrP in 15ml of water at 30°C for 6days resulted in ca. 0.13mg/ml of phosphate ions detectable in

solution. Atomic Adsorption measurements confirmed the absence of any zirconium ions in solution (<0.06ppm). This suggests that 0.05mmol of extra-framework phosphate ions are present per 1g of γ-ZrP. Since the measured pH of the final solution is below 2, it is likely that the extra-framework phosphate ions are simply present as $H_3PO_4$.

**(ii) Adsorption of MAP on zirconium phosphates**

The slopes of the MAP adsorption isotherms are less steep than those observed for MPDA. Apart for γ-ZrP, none of the other zirconium phosphate phases follow the Langmuir isotherm. α-ZrP, α-ZrP400 and γ-ZrP400 initially show a concave-up adsorption isotherm, assuming a Langmuir type isotherm only after reaching a certain aqueous MAP mole fraction. The monolayer adsorption equilibrium concentration is greatest for γ-ZrP (0.83 mol/(mol Zr)) and α-ZrP400 (0.72 - 0.81 mol/(mol Zr)) followed by α-ZrP (0.60 mol/(mol Zr)) and γ-ZrP (>0.13 mol/(mol Zr)). Similarly to the adsorption of MPDA on the zirconium phosphates, the pH measured for the liquid phase after removal of the adsorbent is ca. 2 at low MAP concentrations. At higher concentrations of MAP (mole-fraction of MAP = 0.005) the pH measures ca. 4 instead of ca. 6 for the case of MPDA. This is explained on the basis of MAP being a weaker base ($pK_a$ of $MAP^+$ = 4.37 [Adrien and Serjeant, 1981]) than MPDA ($pK_a$ of $MPDA^+$ = 5.11 [Adrien and Serjeant, 1981]).

The monolayer adsorption of MPDA on the zirconium phosphates (α-ZrP > γ-ZrP ≈ α-ZrP400 > γ-ZrP400) differs from the observations made with MAP (γ-ZrP ≈ α-ZrP400 > α-ZrP > γ-ZrP400). Nevertheless, justifiable explanations are available when considering a combination of influences such as the acid site availability, steric hindrance and the activation energy required in separating the zirconium phosphate layers.

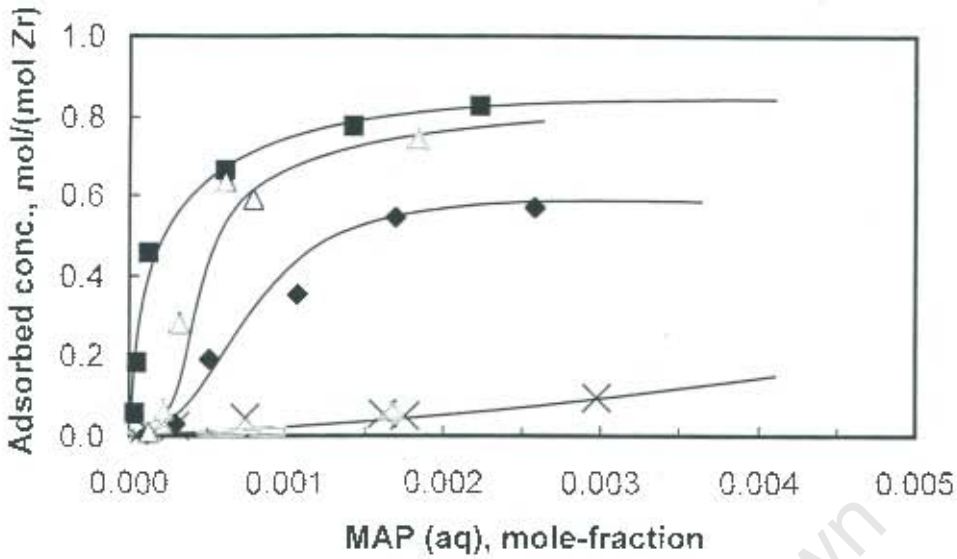


**Figure 4.42** Adsorption-equilibrium data for aqueous MAP on α-ZrP (◆), α-ZrP400 (△), γ-ZrP (■) and γ-ZrP400 (x) at 70°C.

Following the same logic of reasoning as for the uptake of MPDA on the zirconium phosphates, the maximum uptake of MAP is expected to be α-ZrP = 2.0 mol/(mol Zr), α-ZrP400 = 1.68 mol/(mol Zr), γ-ZrP = 1.0 mol/(mol Zr) and γ-ZrP400 = 0.58 mol/(mol Zr). The notion that only the amine group interacts with the Brønsted acid is given by the greater basicity of the amine group, which generally always displaces a phenolic hydroxyl group attached to an acid site.

Since the initial slope of the adsorption isotherm of MAP on α-ZrP follows an S-shaped curve, the driving force for MAP to split the interlayer distance of α-ZrP is lower than that for MPDA. Nevertheless, at higher MAP concentrations the monolayer adsorption attained for MAP is ca. 0.6 mol/(mol Zr), which is in good agreement with the ***initial*** (see Figure 4.40) amount of MPDA strongly adsorbed on α-ZrP. In contrast to the observations made with MPDA, the monolayer adsorption of MAP on α-ZrP400 is greater than that of MAP on α-ZrP. This could partly be ascribed to the fact that calcining α-ZrP at 400°C results in an increase in the ratio of strong to weak acid sites since the initial slope of the MAP on α-

ZrP400 adsorption isotherm is steeper than for the uncalcined α-ZrP. Due to the greater chemical potential difference between the stronger acid sites of α-ZrP400 [Clearfield and Thakur, 1980], MAP is adsorbed more strongly from solution. MAP has only one amine group available for adsorption, and a monolayer adsorption of 0.75 mole MAP per mole α-ZrP400 is acceptable since it occupies fewer acid sites than MPDA.

Examining the initial slopes of the MAP on γ-ZrP adsorption isotherms may lead to the false conclusion that the acid strength present on γ-ZrP is greater than that found for the other zirconium phosphates. The 12.20Å interlayer distance of γ-ZrP, which are hydrogen bonded via water molecules connecting the $PO_2(OH)_2$ groups of the adjacent layers [Clearfield and Troup, 1977], suggests that the potential energy difference for the relevant compounds to access the acid sites is reduced considerably. The monolayer adsorption of MAP on γ-ZrP ca. 0.85 mol/((mol Zr). This is less than the predicted maximum amount of MAP chemisorbed on γ-ZrP, i.e., 1.0 mol/(mol Zr). This is likely to be due to steric hindrance existing between the flat-adsorbed MAP molecules. In contrast, γ-ZrP400 hardly shows any uptake of MAP.



**(iii) Adsorption of resorcinol on zirconium phosphates**

The uptake of resorcinol on α-ZrP and γ-ZrP is very low (see Figure 4.43). Interestingly, γ-ZrP adsorbs more resorcinol than α-ZrP. No resorcinol uptake is observed on the 400°C calcined zirconium phosphates, i.e., α-ZrP400 and γ-ZrP400. The pH of the liquid phase remains between ca. 2 and 3 for all sample concentrations considered.

The adsorption isotherms of resorcinol confirm the fact that only weak interactions exist between the phenolic hydroxyl groups and the zirconium phosphate Brønsted acid sites. The potential difference existing between the

phenolic hydroxyl groups and the proton rich interlayer regions tends to be too weak to spread the layer of α-ZrP400 and γ-ZrP400.

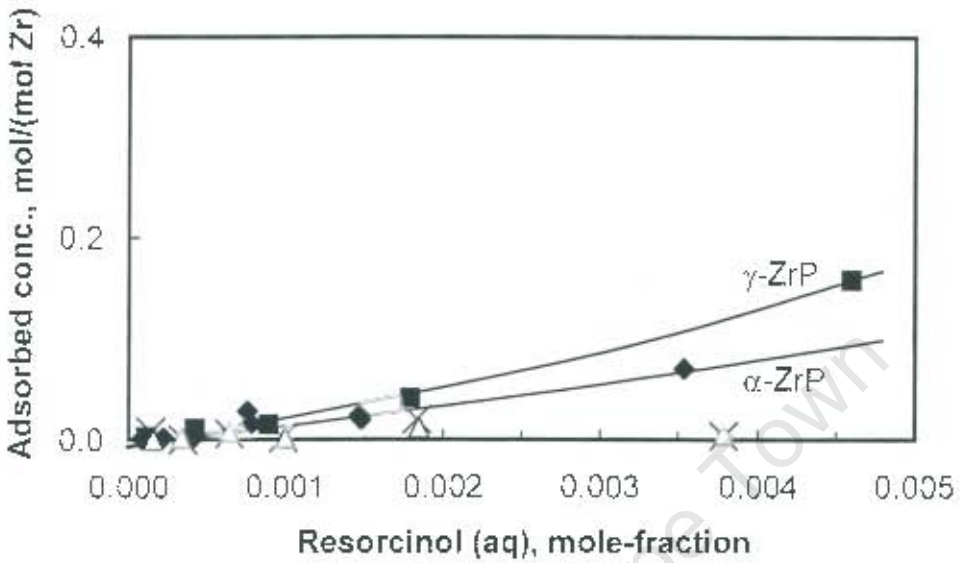


**Figure 4.43** Adsorption-equilibrium data for aqueous resorcinol on α-ZrP (◆), α-ZrP400 (Δ), γ-ZrP (■) and γ-ZrP400 (x) at 70°C.

## 4.5.2 HETEROGENEOUS REACTIONS USING ZIRCONIUM PHOSPHATES

The results for the reaction studies performed on the zirconium phosphates are presented in Figures 4.44 through 4.47. These findings are illustrated by means of concentration-time reaction profiles with the concentration given in terms of mole-%, derived by dividing the *corrected mole concentration* by the initial number of moles of MPDA used (see APPENDIX-F). In addition, each figure (Figures 4.44) includes a plot of the mole balance versus the reaction time (dashed) that displays the total number of moles in the bulk solution relative to the initial amount of MPDA as analysed by HPLC. Reaction results for α-ZrP, α-ZrP400, γ-ZrP and γ-ZrP400 are reported solely for reaction temperatures at

225°C. The respective spent zirconium phosphates after the first set of reactions at 225°C are recovered by centrifugation and regenerated using the same procedure as prior to their first use (see Section 3.3.1.2). Briefly, the previously calcined zirconium phosphates are recalcined at 400°C while the formerly uncalcined zirconium phosphates are simply washed in warm water and dried. The information (concentration data given in terms of mmol/L) regarding reactions conducted at 225°C and 275°C are given in APPENDIX-K. As explained in Section 4.1, the 1-hour heating period required in bringing the reaction temperature from ambient to reaction temperature forms part of the reaction time.

#### 4.5.2.1 REACTIONS WITH PREVIOUSLY UNUSED ZIRCONIUM PHOSPHATES

At the start of each reaction, the ratios of Brønsted acid sites to the initial amount of MPDA using α-ZrP, α-ZrP400, γ-ZrP and γ-ZrP400 are 7.2, 6.0, 3.4 (taking only the primary Brønsted acid site per $P(OH)_2$–group) and 2.0, respectively. As a result, the available Brønsted acid sites during all four reactions is greater than or equal to (for γ-ZrP400) the amount required for the complete conversion of MPDA (i.e., 2moles acid sites per mole of MPDA) if the zirconium phosphate is purely used as a regenerable reagent.

Figure 4.44 illustrates the MPDA, MAP and resorcinol concentrations as a function of reaction time for the reactions performed at 225°C. Included in each diagram is an overall mole balance versus the reaction time, which is depicted by the dashed lines. The mole balances of α-ZrP400 (B), γ-ZrP (C) and γ-ZrP400 (D) go through a definite minimum of 92mole-% (after 1hour), 72mole-% (after 1hour) and 87mole-% (after 5hours), respectively. Towards the end of the reaction, the mole balances for the reactions with α-ZrP, α-ZrP400, γ-ZrP and γ-ZrP400 tend to stabilise at 86mole-%, 99mole-%, 90mole% and 95mole-%, respectively. The

apparent losses can be ascribed to the adsorption of the relevant compounds on the zirconium phosphate layers.

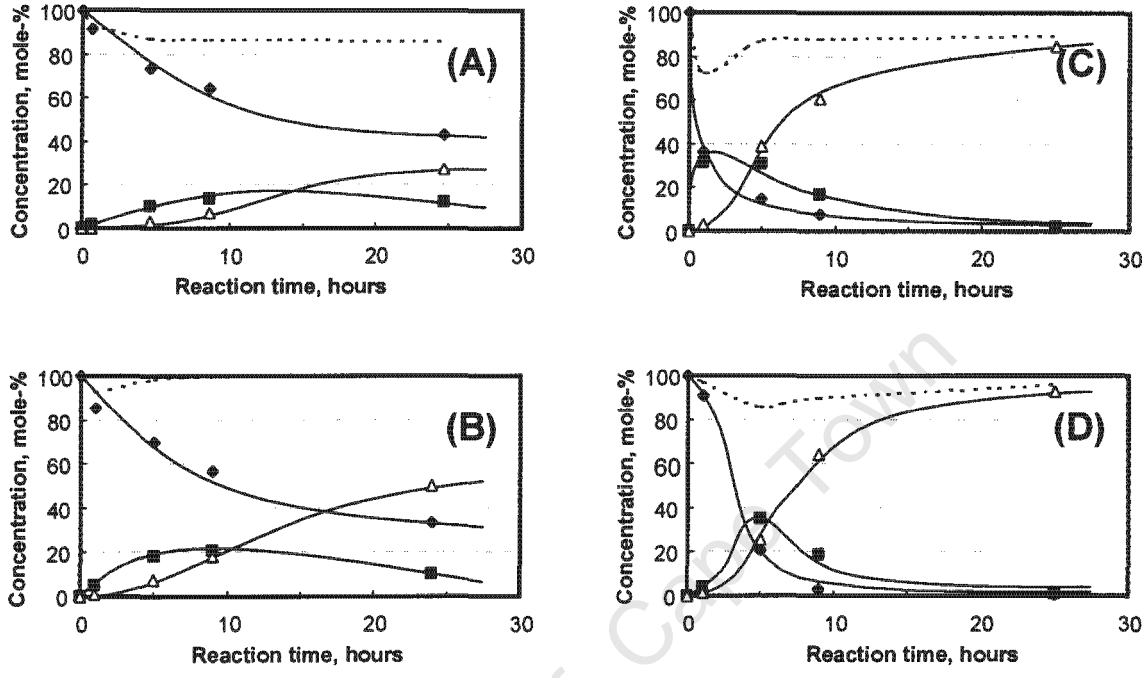


**Figure 4.44** Concentration profiles of MPDA (◆), MAP (■) and resorcinol (Δ) versus reaction time with (A) α-ZrP, (B) α-ZrP400, (C) γ-ZrP and (D) γ-ZrP400; (- - -): mole balance of the organic compounds found in solution. (Reaction temperature = 225°C)



The initial rate of MPDA conversion seems to differ for all four samples of zirconium phosphates. The strong adsorption of MPDA on α-ZrP and α-ZrP400 (see Figure 4.40) is reflected in Figures 4.44A and 4.44B where a strong decrease in the MPDA concentration and mole balance (dashed line) during the temperature ramping period is observed. The first hour of the reaction time is required to bring the reactor from ambient temperature to the final reaction temperature (see Figure 4.1). γ-ZrP (Figure 4.44C) is the most reactive, adsorbing a considerable amount of MPDA in the process. The strong decline in the overall mole-balance when using γ-ZrP can be explained on the basis of easy penetration of MPDA in the γ-ZrP layers and the subsequent adsorption onto the

surface acid sites. Comparison of the MPDA adsorption curves (see Figure 4.40) with the overall mole-balance curves in Figure 4.44 suggests that the rate of adsorption of MPDA on γ-ZrP is greatest. γ-ZrP400 (Figure 4.44D) is relatively inactive during the first two hours, although the reaction rate increases appreciably thereafter. Hardly any MPDA adsorption takes place on γ-ZrP400 in the first hour as already predicted by the adsorption study (see Figure 4.40). However, after ca. 5 hours, the MPDA does adsorb on γ-ZrP400 as indicated by the mole-balance. This change in the adsorption property of the zirconium phosphate can only be explained on the basis that additional splitting of the γ-L-$ZrP_2O_7$ layers does occur. This will then give the MPDA molecules easier access to adsorb on the remaining γ-ZrP400 Brønsted acid sites. It is likely that splitting the layers of γ-ZrP400 requires the cleavage of interlayer P-O-P bonds, which seems to occur at elevated temperatures in water, resulting in possible leaching of phosphate groups.

Regarding the reaction in the presence of α-ZrP and α-ZrP400, the levelling-out of the MPDA concentration-time curves after 25hours suggests that complete conversions of MPDA under the given reaction conditions are not achieved. The resorcinol yields after 25hours are 29mole-% (α-ZrP) and 51mole-% (α-ZrP400), respectively. The shape of the resorcinol-yield curves for both α-ZrP and α-ZrP400 also suggest that the reaction does not go to completion even though enough acid sites is available for complete conversion. In contrast, the resorcinol yield after 25hours when using γ-ZrP (83mole-%) or γ-ZrP400 (94mole-%) is high with the shape of the curves suggesting complete conversion of MPDA towards resorcinol.

The reaction pathway follows that of a consecutive reaction where MPDA reacts to form MAP, which is subsequently converted to resorcinol (see also Sections 4.3 and 4.4.3). The MAP concentration-time profile goes through a maximum, whereas the resorcinol concentration-time profile follows an S-shaped curve. This

phenomenon is observed for all types of zirconium phosphates. The maximum observed yield of MAP when using γ-ZrP (ca. 36mole-% after 2.0 hours) and γ-ZrP400 (ca. 35% after 5.0 hours) is larger than for α-ZrP (ca. 15% after 13.5 hours) and α-ZrP400 (ca. 22% after 8.7 hours).

The difference in the maximum MAP concentration peaks between α-ZrP (after 13.5 hours) and α-ZrP400 (8.7 hours) indicates that the overall rate of MPDA conversion is greater for α-ZrP400 than for α-ZrP. It appears that it is more difficult for the MPDA molecules to penetrate the layers of α-ZrP. This arises from the fact that for α-ZrP and α-ZrP400 swelling of the layers does not occur when suspended in water [Clearfield, 1993]. The difference in the chemical potential generated between the proton-rich acid sites and the more basic bulk solution enables the penetration of reactants. Due to the stronger acid sites of α-ZrP400, more compounds seem to penetrate since the final resorcinol yield is higher when using α-ZrP400 (51mole-%) than with α-ZrP (29mole-%). An increase in the solution temperature does not encourage the spreading of the zirconium phosphate layers, since it is solely the crystallite perfection that brings about the strong binding of the layers in α-ZrP [Clearfield and Troup, 1977].

The MAP concentration when using γ-ZrP reaches a higher maximum at a greater rate (ca. 36mole-% after 2.0hours) than in the presence of α-ZrP or α-ZrP400. This is despite the fact that γ-ZrP has fewer strong Brønsted acid sites than the α-zirconium phosphates. The more widely separated γ-ZrP lamellae (12.20Å) and the more open interlayer arrangement due to hydrogen bonded water, provide for easy access of MPDA molecules into the interlayer region. The activation energy required between the proton-rich acid sites and the more basic bulk solution is thereby considerably reduced. Consequently, the reaction in the presence of γ-ZrP is less diffusion controlled than is generally the case when using α-ZrP or α-ZrP400. Further, in the presence of γ-ZrP the formation of resorcinol is observed after a very short reaction time (see Figure 4.44C). Since

the adsorption study shows that both amine groups on MPDA may adsorb / co-ordinate concurrently, an apparent direct formation of resorcinol is mechanistically feasible.

Although the difference in the maximum MAP concentration observed for γ-ZrP (ca. 36mole-%) and γ-ZrP400 (ca. 35mole-%) is relatively small, the corresponding reaction times differ considerably. The reaction-profile in the presence of γ-ZrP400 suggests that during the initial ca. 2 hours hardly any reaction takes place. After the induction period the reaction rate increases considerably and after a reaction time of 25 hours the resorcinol yield in the presence of γ-ZrP400 (93mole-%) is greater than for γ-ZrP (83mole-%).

Illustrated in Figure 4.45 is the yield-time profile for 3,3'-diamino-phenylenediamine and 3-hydroxy-3'-amino-diphenylamine. The general yield-profiles 3,3'-diamino-diphenylamine and 3-hydroxy-3'-amino-diphenylamine follow similar curves as described previously (see Sections 4.3 and 4.4.3). The initial rate of formation of 3-hydroxy-3'-amino-diphenylamine is close to zero, suggesting a consecutive reaction that is likely to originate from 2 MAP-molecules or from 1 MPDA- and 1 MAP-molecule. The positive initial slope observed for the yield-curve of 3,3'-diamino-diphenylamine is consistent with the compound being produced directly from 2 MPDA-molecule. The amount of 3,3'-diamino-diphenylamine and 3-hydroxy-3'-amino-diphenylamine produced in the presence of the different zirconium phosphates differ considerably. In the presence of α-ZrP, the yield of 3-hydroxy-amino-diphenylamine is distinctly larger than the amount of 3,3'-diamino-diphenylamine. However, upon calcination of α-ZrP at 400°C, the yield of 3,3'-diamino-diphenylamine increases substantially. This could be ascribed to a change in the surface property of α-ZrP after calcination, possibly due to the formation of some Lewis acid sites. The combined presence of Brønsted and Lewis acid sites favours the formation of diphenylamine [Warawdekar and Rajadyaksha, 1996].

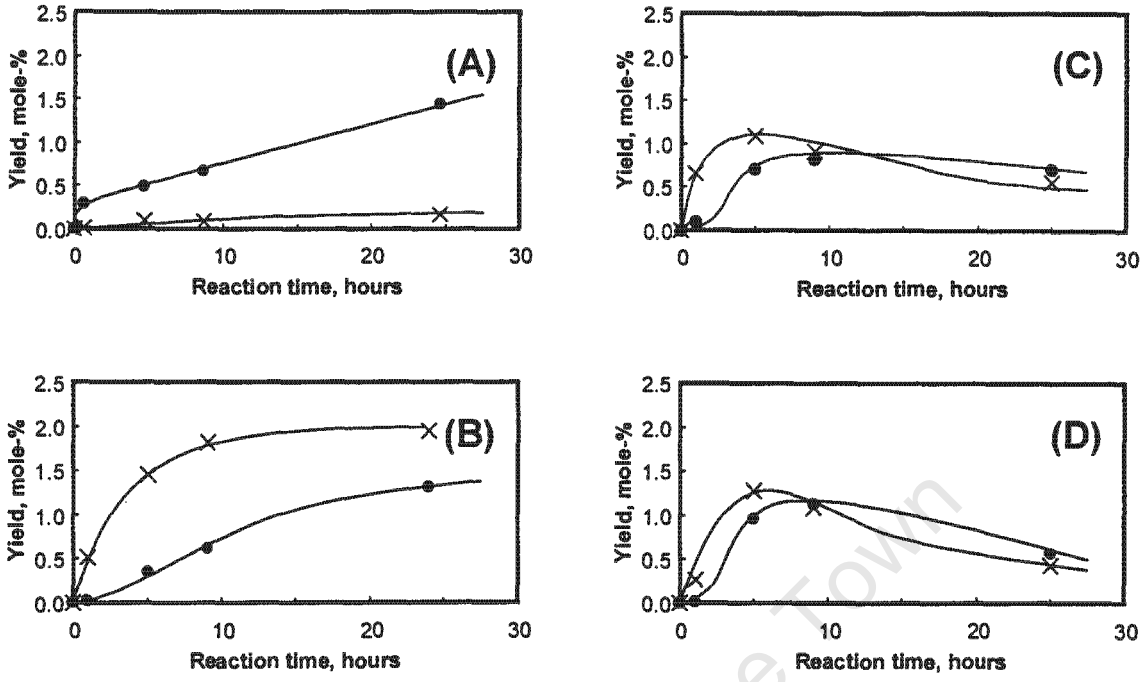


**Figure 4.45** Yield profiles of 3,3'-diamino-diphenylamine (x) and 3-hydroxy-3'-amino-diphenylamine (●) versus reaction time with (A) α-ZrP, (B) α-ZrP400, (C) γ-ZrP and (D) γ-ZrP400 (Reaction temp. = 225°C)

The pH of the removed sample as a function of reaction time is shown in Figure 4.46. During the course of the reactions at 225°C, the sample pH of the reactions in the presence of α-ZrP and α-ZrP400 decrease slightly from 6.0 to 5.3 and stabilises thereafter. When using γ-ZrP, the sample pH decreases gradually from 4.9 (after 1hour) to 3.9 (after 25hours). The sample pH of γ-ZrP400 initially remains stable at pH = 6.0 (measured after 1.1hours), but decreases strongly towards pH = 2.8 after 25hours. The pH does to a certain degree correlate with the yields of resorcinol. However, a pH of below 3 cannot be attributed solely to resorcinol since it is only a weak acid. Thus, other factors such as leaching of phosphates into solution are involved. This is confirmed by the detection of phosphates in the aqueous reaction mixtures of α-ZrP, α-ZrP400, γ-ZrP and γ-ZrP400, to the extent of 0.045, 0.050, 0.169 and 0.189 moles phosphates per mole zirconium phosphate, respectively. The absence of Zr in solution

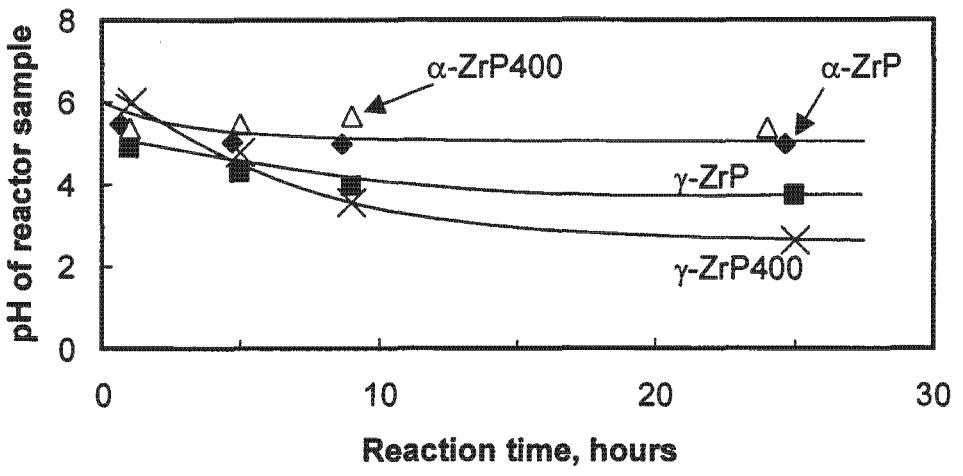


**Figure 4.46** pH of solution (without solid) as a function of reaction time for α-ZrP (◆), α-ZrP400 (Δ), γ-ZrP (■) and γ-ZrP400 (x). The reaction temperature is 225°C.

(Zr < 0.2ppm; Atomic Adsorption), suggests that the drop in the pH is not due to the formation of zirconyl phosphate salts. However, as shown in Section 4.5.1.3, the obtained γ-ZrP is likely to contain ca. 0.015 moles $H_3PO_4$ per mole of γ-ZrP.

On repeating the reaction at 225°C in the presence of γ-ZrP (batch no.: G05-7) after first washing a γ-ZrP (batch no.: E0906) in warm water (T = 30°C), an increase in the pH during the course of the reaction to ca. 8 was observed. This reproducible result (see Figure 4.47) is unlike the phenomenon observed for γ-ZrP (batch no.: G05-7). Thus, it can be deduced that the solution pH is not the determining factor when conducting reactions in the presence of zirconium phosphate, i.e. although phosphates leach into solution, the conversion of MPDA takes place on the zirconium phosphate surfaces. This is probably due to the fact that the amount of $H_3PO_4$ initially present on γ-ZrP (batch no.: G05-7) is too little to have a significant impact on the reaction results even though the pH remains relatively low. The leaching and subsequent dissociation of $H_2PO_4^-$ ($pK_a$ = 7.4 [Shriver *et al.*, 1994]) from the γ-zirconium phosphates hardly affects the

resorcinol yield as shown in Section 4.3.3, where at 225°C hardly any resorcinol is produced in the presence of $(NH_4)H_2PO_4$.

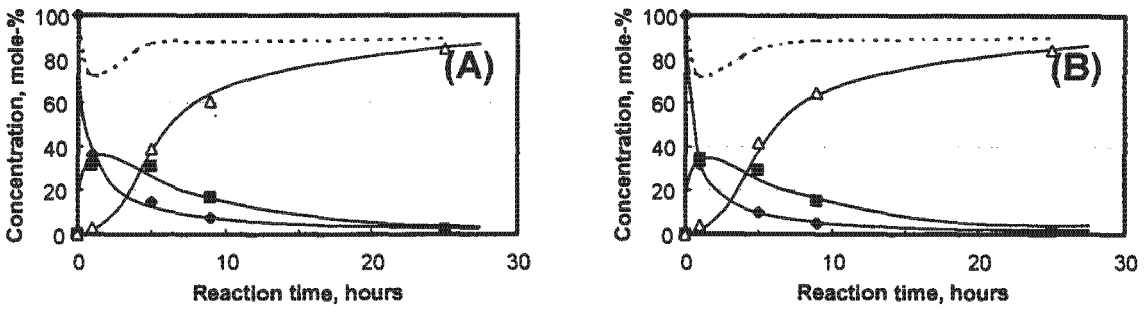


**Figure 4.47** Concentration profiles of MPDA (◆), MAP (■) and resorcinol (Δ) versus reaction time with (A) γ-ZrP(batch no. E0906) and (B) γ-ZrP(batch no. G05-7); (- - -): mole balance of the organic compounds found in solution. (Reaction temperature = 225°C)



### 4.5.2.2 REACTIONS WITH REGENERATED ZIRCONIUM PHOSPHATES

Table 4.13 shows the effect of regeneration on the activity of zirconium phosphates by comparing the resorcinol yields and solution pH's after 25h reaction time. The performance of the regenerated α-ZrP400 is similar to that of the freshly prepared α-ZrP400 since the resorcinol yield after 25hours remains essentially unchanged, i.e., 50mole-%. The pH of the final solution after the second reaction (4.7) is less than that measured after the first reaction (5.4). This would point towards the formation of some acidic MPDA-phosphate salt, since the drop in the pH during the second reaction cannot be ascribed to phosphoric acid being present on the regenerated α-ZrP400. In contrast, the yield of resorcinol when using γ-ZrP decreases significantly from 83mole-% (after 25hours) in the first reaction to 17mole-% in the second reaction, while the pH increases substantially from 3.9 to 7.6. A possible cause for the γ-ZrP deactivation is the irreversible poisoning by the formed product ammonia. The

relatively high pH recorded when using γ-ZrP for a second time further proves that the low pH measured during the first set of reactions is due to phosphoric acid residing on the obtained γ-ZrP. The resorcinol yield measured at the end of the first and second reactions for γ-ZrP400 again remains virtually unchanged at 92mole-%. The solution pH when using γ-ZrP400 increases from 2.6 to 4.2, which indicates that some leaching of phosphates in the form of $H_2PO_4^-$ ($pK_a$ of $H_2PO_4^-$ = 7.4 [Shriver *et al.*, 1994]) does occur. A simple calculation reveals that a 0.1molar $H_2PO_4^-$ solution could, depending on the counter-ion, lead to a solution pH of ca. 4.2.

**Table 4.13 Comparison of resorcinol yields (reaction temperature = 225°C) and solution pH's measured after 25h reaction time during the first set of reactions with those measured during the second set of reactions where the regenerated zirconium phosphate is used.**

| | Resorcinol Yield (mole-%) | | Solution pH | |
|---|---|---|---|---|
| | 1st Reaction | 2nd Reaction | 1st Reaction | 2nd Reaction |
| α-ZrP | 27 | n.a. | 4.96 | n.a. |
| α-ZrP400 | 50 | 50 | 5.38 | 4.68 |
| γ-ZrP | 83 | 17 | 3.85 | 7.62 |
| γ-ZrP400 | 93 | 92 | 2.64 | 4.20 |

## 4.5.3 CHARACTERISATION OF ZIRCONIUM PHOSPHATES AFTER REACTION

The XRD and FT-IR spectra of the spent α-ZrP, α-ZrP400 γ-ZrP and γ-ZrP400 are compared to the respective spectra recorded prior to reaction in order to establish the extent of degradation of the solids during reaction.

### 4.5.3.1 STRUCTURE AND MORPHOLOGY

**(i) X-ray diffraction**

The XRD spectra of (A) α-ZrP and (B) α-ZrP400, (C) γ-ZrP and (D) γ-ZrP400 before reaction and the corresponding spectra after the first and second reaction at 225°C are shown in Figure 4.48. α-ZrP hardly undergoes any detectable structural changes during the course of the reaction, whereas α-ZrP400 does not maintain its structure during the two reactions. The appearance of additional peaks at 2-Theta = 27.9°, 30.2° and the gradual decrease in the intensity of the peaks at 2-Theta = 11.9° suggest the formation of a new structure. From XRD fingerprint analysis, the formation of a new three dimensional structure of the form $(NH_4)Zr_2(PO_4)_2$ or $(H_3O)Zr_2(PO_4)_3$ is suggested.

The XRD peaks of the γ-zirconium phosphates generally tend to be less well defined after the reactions at 225°C. The first peak of γ-ZrP signifies the interlayer distance of the layered compound and changes from 12.21Å (2-Theta = 7.2°) before the reaction to 10.92Å (2-Theta = 8.1°) after the reaction. It could be argued that the shift in the first peak is due to the formation of ammonium intercalated γ-ZrP, which has a smaller interlayer distance (11.25Å [Alberti *et al.*, 1989]). The remaining XRD peaks of the spent γ-ZrP show little resemblance to the original γ-ZrP used. This could be either due to the formation of a new zirconium phosphate structure or the occurrence of stresses within the γ-ZrP

structure. The latter seems to take place in γ-ZrP400 since all peaks appear at precisely the same diffraction angles, but are broader and have lower intensities.

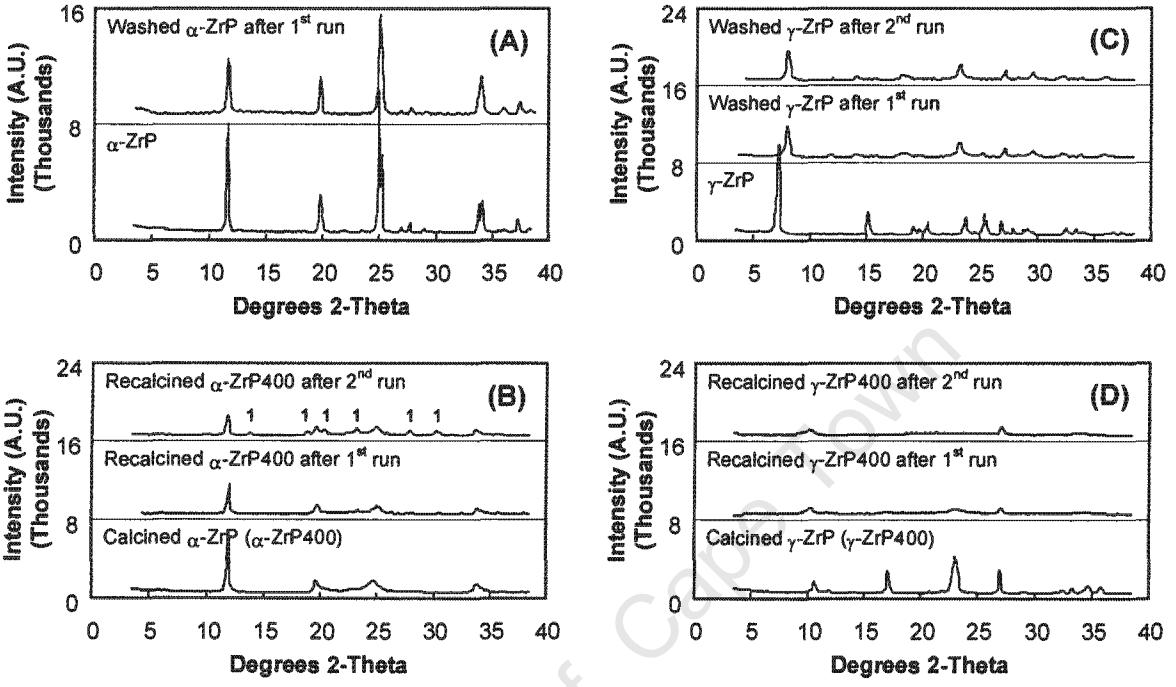


**Figure 4.48** XRD-spectra of (A) α-ZrP, (B) α-ZrP400, (C) γ-ZrP and (D) γ-ZrP400 before the first reaction, after the first reaction at 225°C and after the second reaction at 225°C. Symbol '1' illustrates the appearance of a new phase $(NH_4)Zr_2(PO_4)_3$ or $(H_3O)Zr_2(PO_4)_3$.

The formation of the new zirconium phosphate structure is confirmed by repeating reactions at 275°C using α-ZrP, α-ZrP400 and γ-ZrP (see Figure 4.49) upon which a sharp decrease in the solution pH is measured and the distinct formation of $(NH_4)Zr_2(PO_4)_3$ is observed (see APPENDIX-K). The rate of transformation at 275°C seems to be greatest for α-ZrP400 (see Figure 4.48), followed by α-ZrP and γ.ZrP. The γ-ZrP is transformed more slowly than α-ZrP since its structure towards the end of the first reaction at 275°C can still be identified. Interestingly, γ-ZrP400 does not seem to adopt the structure of the new compound. A likely explanation is that the large amount of pyrophosphate bonds present in γ-ZrP400 makes the compound more stable and less likely to be

transformed. The newly formed $(NH_4)Zr_2(PO_4)_2$ or $(H_3O)Zr_2(PO_4)_3$ compound seems to be stable under the reaction conditions since the structure is maintained when repeating the reaction.

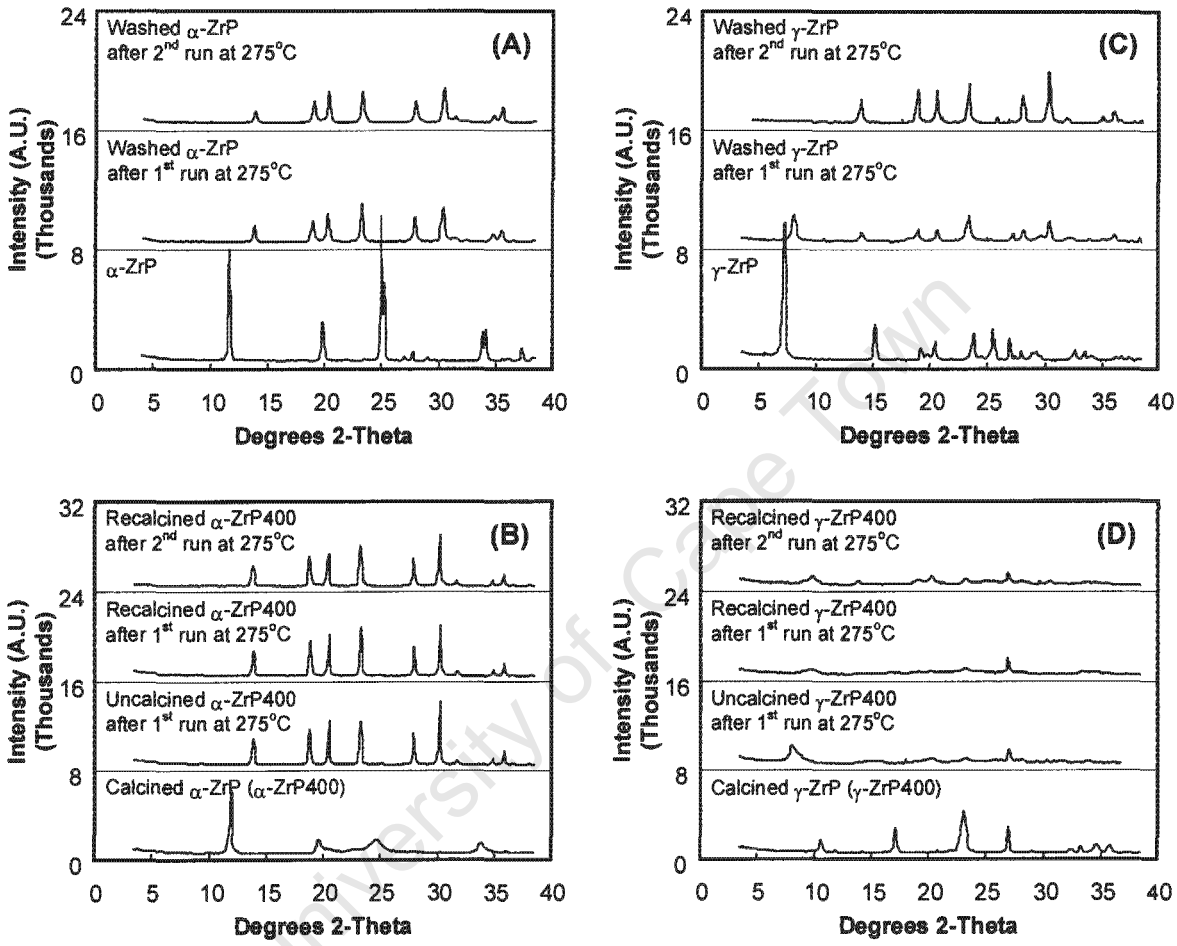


**Figure 4.49** XRD-spectra of (A) α-ZrP, (B) α-ZrP400, (C) γ-ZrP and (D) γ-ZrP400 after the first reaction at 275°C and after the second reaction at 275°C, clearly illustrating the formation of the new phase $(NH_4)Zr_2(PO_4)_3$ or $(H_3O)Zr_2(PO_4)_3$.

Clearfield *et al.* [1984] documented the hydrothermal structural transformation of a methylamine-intercalated $\alpha$-$Zr(HPO_4)_2 \cdot H_2O$ towards $(NH_4)Zr_2(PO_4)_3$ in the presence of water at 300°C. According to Clearfield *et al.* [1984], the reaction is a general one and depends upon the ease with which the amine is decomposed.

The crystallinity of the zirconium phosphate does not influence the conversion of zirconium phosphate to a great extent.

The structure of the newly formed, highly stable compound, $(NH_4)Zr_2(PO_4)_3$, exhibits a robust negatively charged, three-dimensional lattice with 4 cavities per formula [Clearfield *et al.*, 1984]. The NASICON-type framework consists of a network of corner-sharing $PO_4$ tetrahedra and $ZrO_6$ octahedra, with each $ZrO_6$ octahedra being connected to six $PO_4$ tetrahedra [Hong, 1976]. The interstitial voids generated within the network are of two types: Type I and Type II. It is interesting to note that at 300°C both $NH_4^+$ and $Na^+$ are too large to move through the channels / bottlenecks, connecting Type I cavities with Type II cavities. Similar to $Na^+$, $NH_4^+$ ions occupy Type I cavities. Calcining the ammonium exchanged compound at 450°C yields $HZr_2(PO_4)_3$ and refluxing $HZr_2(PO_4)_3$ in water leads to $(H_3O)Zr_2(PO_4)_3$ [Subramanian *et al.*, 1984]. Although the hydrogen exchanged form $HZr_2(PO_4)_3$ is likely to act as a heterogeneous acid reagent much the same as a zeolite, the MPDA molecule will be too bulky to fit in the NASICON channel system. Consequently, whilst $HZr_2(PO_4)_3$ presents itself as a very stable and regenerable acid reagent, it cannot be used for the reaction under investigation in this study.

For the case of MPDA, the following reaction is likely to occur when assuming that only one $-NH_2$ functional group on each MPDA molecule is adsorbed at any given time:

$$2\ Zr(HPO_4)_2{\cdot}2(MPDA) + H_2O \longrightarrow (NH_4)Zr_2(PO_4)_3 + MAP + [(MPDA^+)_3PO_4] \qquad \textbf{4.2}$$

The reaction predicts the simultaneous conversion of an amine compound to the corresponding hydroxyl compound while the layered α-zirconium phosphates structure assumes that of $(NH_4)Zr_2(PO_4)_3$. Since it is well documented that γ-ZrP tends to transform into the α-phase in boiling $H_3PO_4$ at concentrations higher

than 1 molar [Alberti *et al.*, 1989], the transformation of the more meta-stable γ-ZrP to $(NH_4)Zr_2(PO_4)_3$ is explained. Given that the final solution is found to be acidic, Clearfield *et al.* [1984] postulated that the following reaction also takes place: Since

$$(MPDA^+)_3PO_4 + 3H_2O \longrightarrow 3\ MAP + (NH_4)H_2PO_4 + 2\ NH_3 \qquad \textbf{4.3}$$

During the conversion of the α-zirconium phosphates to $(NH_4)Zr_2(PO_4)_3$ (see Reactions 4.2 and 4.3), 1mole of aqueous phosphoric acid is produced per 2moles of converted α-zirconium phosphates. For the reaction of α-ZrP at 225°C, the presence of 4.25mmol/L phosphates ((0.045mole phosphates)/mole Zr)) in aqueous solution at the end of the first reaction suggests that a maximum of 8.9% of the original α-ZrP is converted to the new compound. The maximum percent conversion calculated for α-ZrP400 is 9.5%. Both calculations neglect the fact that the obtained α-ZrP may contain small quantities of phosphoric acid. The same logic cannot be applied to the reactions with γ-zirconium phosphates. The γ-zirconium phosphates adopt the new structure more slowly than the α-zirconium phosphates (see Figures 4.48 and 4.49) although the amounts of phosphates in solution at 225°C is between 0.169 and 0.189 mole phosphates per mole zirconium. Due to the leaching of hydrogen-phosphates into solution, it is likely that the γ-zirconium phosphates can never be fully transformed.



**(ii) FT-IR spectra**

The FT-IR spectra of the zirconium phosphates before reaction and the corresponding spectra after the second reaction at 275°C are shown in Figure 4.50 (assignments of adsorption bands according to Horsley *et al.* [1974], Ramis *et. al.* [1988] and Clearfield et al. [1984]). Due to the method used in obtaining the FT-IR spectra, the band at 2300cm$^{-1}$ is attributed to varying concentrations of $CO_2$ present in the air and is not part of the zirconium phosphate FT-IR spectra. The zirconium phosphates used for the reactions at 275°C instead at 225°C are

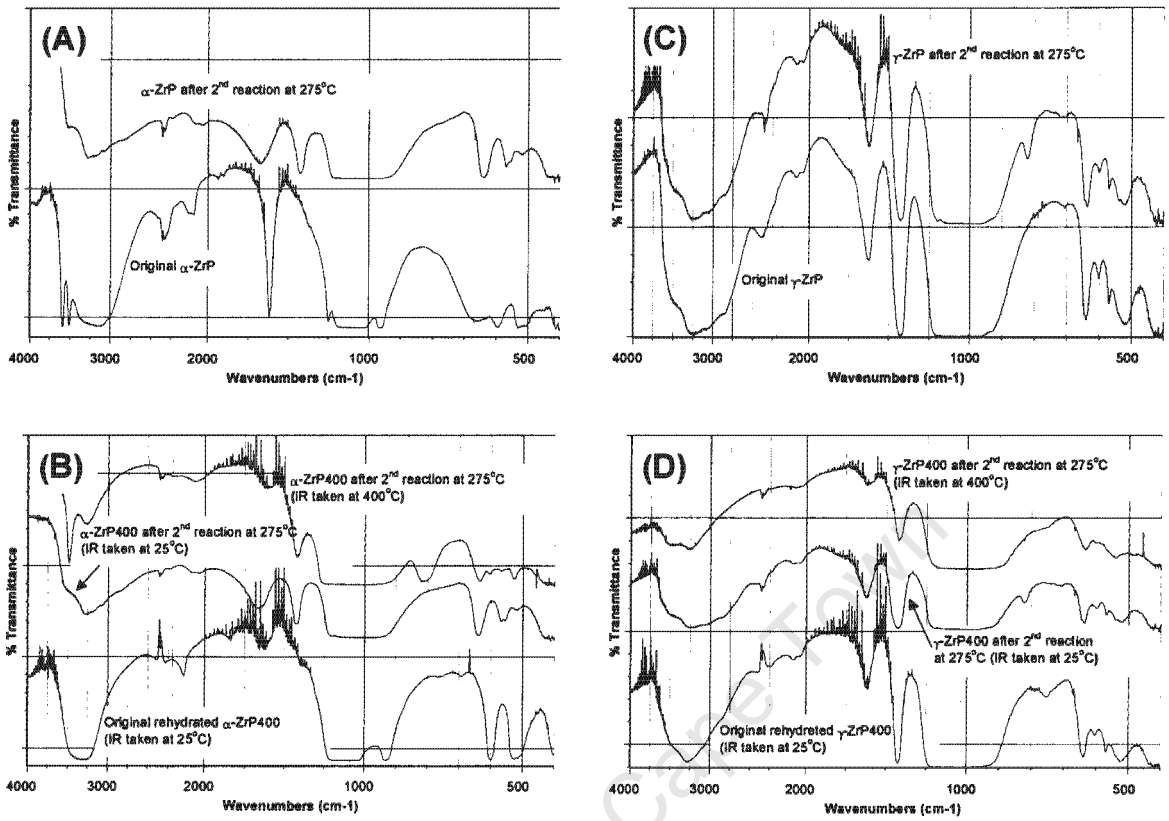


**Figure 4.50** FT-IR spectra of (A) α-ZrP, (B) α-ZrP400, (C) γ-ZrP and γ-ZrP400 before the first reaction and after the second reaction at 275°C.

chosen to establish the end-case scenario if the zirconium phosphates used at 225°C are reused several times. The FT-IR spectra of the uncalcined α-ZrP and α-ZrP400 after the second reaction at 275°C clearly differ from the original α-ZrP and α-ZrP400. The infrared spectra of both spent α-zirconium phosphates are identical and show a broad OH stretch band at 3500cm$^{-1}$ due to water and three bands in the N-H stretch region between 3100cm$^{-1}$ and 3300cm$^{-1}$. All four bands are overlapping and give the impression of one broad band that ranges over several-hundred wavenumbers. Another intense band at 1460cm$^{-1}$ is characteristic of $NH_4^+$. In fact, the FT-IR spectra of the spent α-zirconium phosphates (4000cm$^{-1}$ < wavenumber < 400cm$^{-1}$) closely match the spectrum of $(NH_4)Zr_2(PO_4)_3$ given by Clearfield *et al.* [1984]. Thereby it is confirmed that ammonia is present on the newly formed NASICON structure and the amount of organic material adsorbed is minimal. Heating the FT-IR cell containing a wafer

of the spent α-ZrP400 slowly to 400°C and maintaining the temperature for 1hour leads to the removal of water and some removal of ammonia since the broad band at 3500cm$^{-1}$ disappears and the peak intensities between 3100cm$^{-1}$ and 3300cm$^{-1}$ are reduced. The peak at wavenumber 1460cm$^{-1}$ is hardly affected, implying that only minor amounts of the strongly adsorbed ammonia is removed. However, the new very sharp peak that appears at 3500cm$^{-1}$ is due to the P-OH type indicating some conversion towards $HZr_2(PO_4)_3$ [Clearfield *et al.*, 1984].

The infrared spectra of the spent γ-zirconium phosphates do not clearly resemble the $(NH_4)Zr_2(PO_4)_3$ spectrum. Although the bands between 3500cm$^{-1}$ and 3100cm$^{-1}$ as well as the band at 1460cm$^{-1}$ are clearly visible on the FT-IR spectra of the spent γ-zirconium phosphate, these bands are also present on the original γ-ZrP. Therefore, it can neither be proved nor disproved whether the new compound is formed. Nevertheless, the fingerprint region between wavenumbers 610cm$^{-1}$ and 400cm$^{-1}$ of the spent γ-ZrP and γ-ZrP400 remain identical to the corresponding unused γ-zirconium phosphates, but show no resemblance to the spectrum of the new compound. Although bands at 635cm$^{-1}$ and 600cm$^{-1}$ of the spent γ-ZrP and γ-ZrP400 do compare to those of $(NH_4)Zr_2(PO_4)_3$, these bands are also characteristic of the unused γ-ZrP. The spent γ-ZrP and γ-ZrP400 show a band at 820cm$^{-1}$ that is neither observed for the infrared spectra of γ-ZrP nor of $(NH_4)Zr_2(PO_4)_3$. Upon the online calcination of the spent γ-ZrP400 at 400°C, the ensuing infrared spectrum resembles the spectrum of the original γ-ZrP400 more closely than the spectrum of $HZr_2(PO_4)_3$. It can thus be deduced that the γ-zirconium phosphates are less likely to transform into the NASICON structure than the α-zirconium phosphates. Also the structure of the usually more meta-stable γ-zirconium phosphates seems to be retained, although some transformation towards the new NASICON does occur as shown by the XRD study. A possible reason for the high resistance towards transformation may be ascribed to the fact that the leaching and loss of dihydrogen-phosphates into solution partially prevents its full transformation towards the NASICON structure.

**(iii) Crystallite morphology**

The electron micrograph of the spent α-ZrP and α-ZrP400 visually confirms their respective transformation towards a new crystalline compound. The new (NASICON) crystal structure is rhombohedrally shaped with the average crystal size measuring ca. 0.2μm. The most common space group that the NASICON crystal adopts is rhombohedral [Hong, 1976].

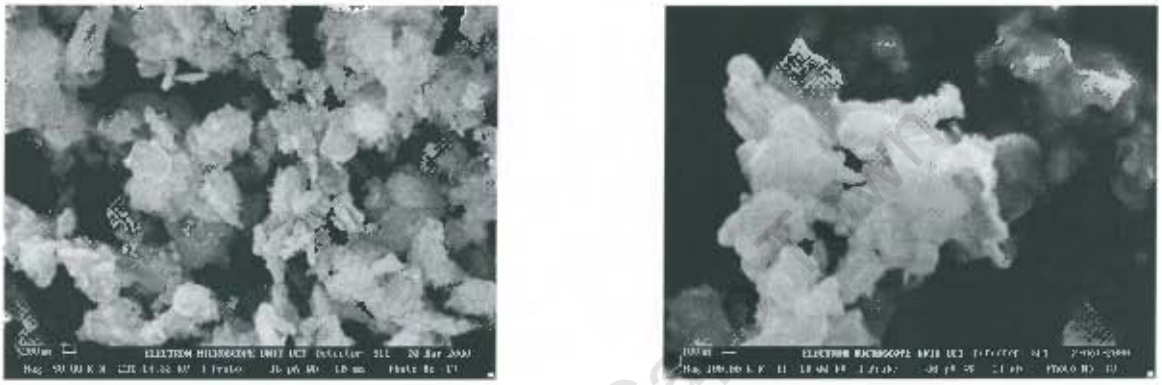

**Figure 4.51** Electron micrographs of spent α-ZrP (left) and α-ZrP400 (right) after second reaction at 275°C.

In contrast to the SEM images observed for the spent α-zirconium phosphate, those of the γ-zirconium phosphates show retention of most of the layered structure. Thus, visual proof is provided that neither γ-ZrP nor γ-ZrP400 readily adopt the NASICON structure under the given reaction conditions.

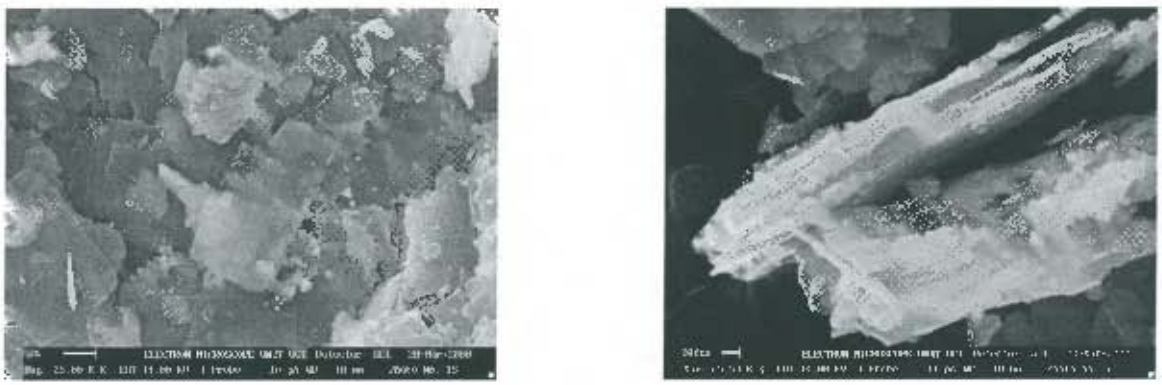

**Figure 4.52** Electron micrographs of spent γ-ZrP (left) and γ-ZrP400 (right) after second reaction at 275°C.

# 4.6 COMPARISON OF MINERAL ACID AND SOLID REAGENTS / CATALYSTS

## 4.6.1 REACTION MECHANISM AND MODEL DEVELOPMENT

The role of the mineral acids and solid reagents / catalysts in this reaction are compared by means of the experimentally determined reaction rates of major compounds, i.e., MPDA, MAP and resorcinol. The concentrations of the dimers are low and have thus been ignored in the modelling of the reaction MPDA → MAP → resorcinol.

### 4.6.1.1 PROPOSED REACTION MECHANISM FOR HOMOGENEOUS ACIDS

Since the conversion of MPDA to resorcinol occurs in the presence of a mineral acid, the first step would involve protonation of the basic amine functional group present on the benzene ring to give $-NH_3$ (the conjugate acid). This leads to a deactivation of the aromatic nucleus. The removal of $NH_3$ in the form of an ammonium salt and its replacement by a hydroxyl group (in the form of water) leads to MAP. The same sequence, i.e. the amine protonation, the attack of water and the elimination of $NH_3$ leads to the final product, resorcinol (see Figure 4.53).

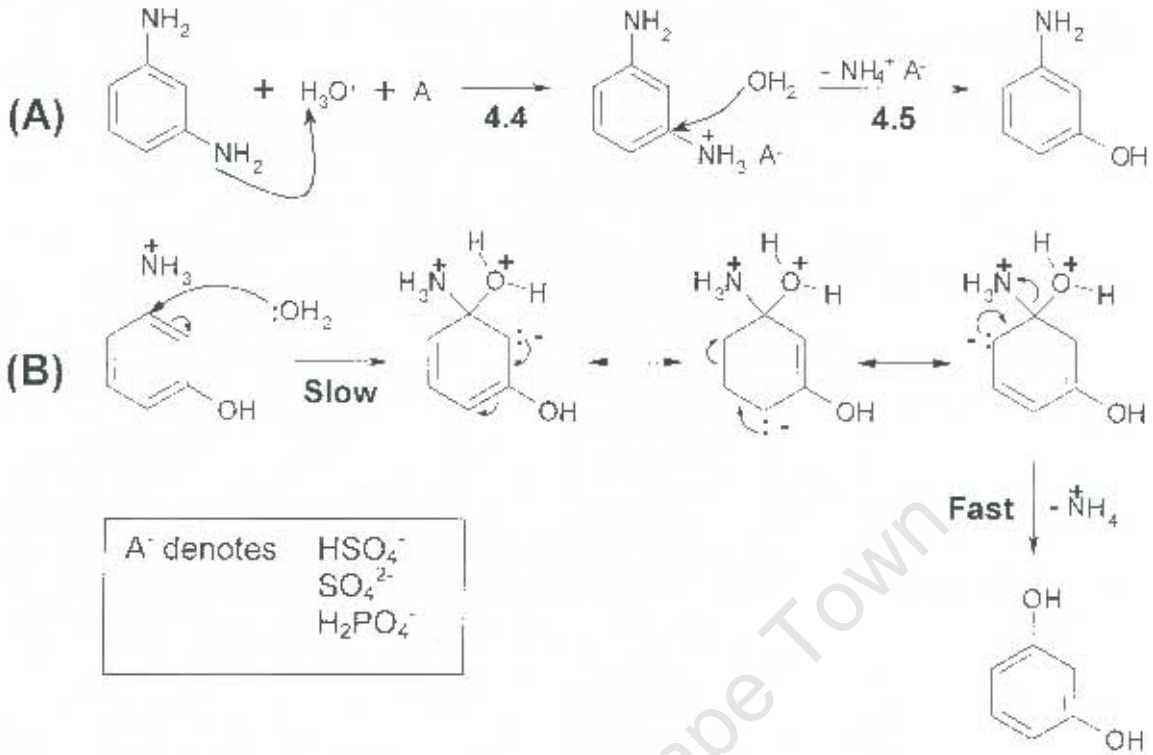


**Figure 4.53** Proposed mechanism for the formation of MAP from MPDA (A) and for the formation of resorcinol from MAP (B) in the presence of mineral acids.



### 4.6.1.2 PROPOSED MECHANSIM FOR HETEROGENEOUS ACIDS

In conformity with the mechanism proposed for the homogeneous acids in Figure 4.53, a similar mechanism can be proposed for the reaction occurring on a heterogeneous solid (see Figure 4.54). The chemisorption of MPDA and MAP onto the Brønsted acid sites via the $-NH_2$ functional groups occur relatively quickly. This is shown by the large uptake of MPDA after sampling the autoclave after 1hour of reaction time. The rate determining step is thus likely to be the reaction between the adsorbed molecule and water leading to the release of the electron withdrawing $-NH_3^+$ group from the benzene ring and its simultaneous replacement with an –OH function group. The ammonia thus released neutralises

the Brønsted acid sites and drives the thermodynamically unfavourable reaction towards the formation of resorcinol.

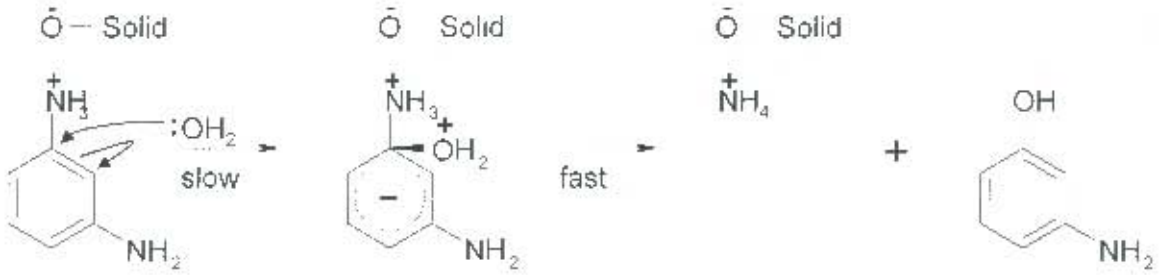


**Figure 4.54** Proposed mechanism for the conversion of MPDA to MAP over a heterogeneous acid reagent / catalyst. The electron donating effect of the second amine group on the intermediate aromatic nucleus has been ignored.



### 4.6.1.3 DEVELOPMENT OF REACTION MODEL

The absence of any ortho- and para-isomers suggests an addition-elimination reaction or an aromatic nucleophilic substitution *ipso* attack [Sykes, 1992]. Since the hydronium ion attack on the basic $-NH_2$ functional group on MPDA (Reaction 4.4) occurs quite readily, the addition of water during the second step (Reaction 4.5) is likely to be the rate-determining step. Figure 4.53B depicts a detailed version of the rate-determining step during the conversion of MAP to resorcinol. Similar arguments hold for the heterogeneous solids, i.e., the rate of adsorption of the amine-containing compound relative to the overall substitution reaction is fast. Considering the conversion of MPDA to MAP, the reaction rate can then be expressed as:

$$\frac{d}{dt}\left[MPDA^{ipso}\right] = -k_1\left[MPDA^{ipso}\right] \times \left[H_2O\right] \qquad 4.6$$

, where $[MPDA^{prot}]$ is the concentration of the protonated MPDA. In aqueous solution $[MPDA^{prot}]$ refers to the concentration of ionised MPDA in solution, while for heterogeneous systems $[MPDA^{prot}]$ refers to the concentration of MPDA (mmol/L) adsorbed. $[H_2O]$ refers to the concentration of water and $k_1$ depicts the reaction rate constant for the conversion of the protonated MPDA to MAP.

The protonated MPDA concentration is a function of the number of acid sites available. The acid-base reaction between the basic MPDA and the homogeneous or heterogeneous acid sites can be assumed to be in equilibrium, since in relation to the substitution of $-NH_3^-$ with an –OH functional group the formation of the $-NH_3^+$ occurs very quickly.

$$K_{MPDA} \quad \frac{[MPDA^{prot}]}{[MPDA]\times[AS]} \qquad 4.7$$

, where $[MPDA]$ is the aqueous bulk MPDA concentration and $[AS]$ the concentration of acid sites; and $K_{MPDA}$ the equilibrium constant. For homogeneous reactions $K_{MPDA}$ refers to the constant of MPDA hydrolysis with $[AS]$ corresponding to the hydronium ion concentration. For heterogeneous systems $K_{MPDA}$ is the equilibrium MPDA adsorption constant, while $[AS]$ refers to the number of Brønsted acid sites relative to the volume of the **bulk liquid phase at ambient temperature**. Substitution of Equation 4.7 for $[MPDA^{prot}]$ in Equation 4.6 leads to the expression:

$$\frac{d}{dt}[MPDA^{prot}] = -k_1 K_{MPDA}[MPDA]\times[H_2O]\times[AS] \qquad 4.8$$

Applying the same method as used for the derivation of the rate equation for MPDA, expressions for MAP and resorcinol can be obtained:

$$\frac{d}{dt}[MAP] \quad k_1 K_{MPDA}[MPDA]\times[H_2O]\times[AS] - k_2 K_{MAP}[MAP]\times[H_2O]\times[AS] \qquad 4.9$$

$$\frac{d}{dt}[RES] = k_2 K_{MAP}[MAP] \times [H_2O] \times [AS] \qquad 4.10$$

### 4.6.1.4 INCLUSION OF REACTOR RAMPING / HEATING PROFILES INTO THE RATE EQUATION

Generally, only a limited amount of data points are available per reaction (ca. 5 samples per run) with reactions over any particular reagent being typically performed at 2 different temperatures, i.e. 225°C and 275°C. Therefore, connecting the equilibrium constants $K_{MPDA}$ and $K_{MAP}$ in the above equations by means of van't Hoff Equations would not lead to a reduction in the number of degrees of freedom. The same is true for the rate constants when applying the Arrhenius Equation.

The actual time at which the reaction starts is difficult to determine, since the reactor is charged, sealed and only then heated up from ambient temperature to the desired reaction temperature. To account for the effect of the ramping period on the reaction rate, the reaction time, i.e., time zero, has to be altered. Arbitrarily, assuming an activation energy, $E_a$, of 100kJ/mol, the difference in temperature required to double the reaction time can be calculated by means of the Arrhenius Equation:

$$\frac{r_1}{r_2} = \frac{1}{2} = \frac{A \times e^{-E_a / RT_1}}{A \times e^{-E_a / RT_2}} \qquad 4.11$$

Since the ramping rate decreases when approaching the final reaction temperature, the time zero used equals the time at which the reactor temperature equal $(T_1 + T_2)/2$ (see Table 4.14).

**Table 4.14 Determination of the time period to be subtracted from the observed reaction time to account for the ramping period**

| Temperature (°C)[1] | | | Time (h)[2] |
|---|---|---|---|
| $T_2$ | Corresponding $T_1$ | $(T_1 + T_2)/2$ | $(T_1 + T_2)/2$ |
| 225 | 211 | 218 | 0.56 |
| 250 | 235 | 242 | 0.66 |
| 275 | 258 | 267 | 0.72 |
| 300 | 282 | 291 | 0.77 |

[1] $T_1$ refers to the temperature having ½ the reaction rate than temperature $T_2$, assuming an activation energy of 100kJ/mol

[2] Time to reach $(T_1 + T_2)/2$ after starting to heat from ambient temperature



## 4.6.2 MODELLING OF HOMOGENEOUS REACTIONS

According to Section 4.3 (see also APPENDIX-G), the measured sample pH (pH reading taken at ambient temperature) remains constant throughout the reactions carried out at 225°C and 275°C. This observation is also applicable to reactions with weak acids, i.e., $(NH_4)HSO_4$, where the measured pH increases by only half an order of magnitude during the course of the reactions. Therefore, the hydronium ion concentration, i.e., $[AS]$ in Equations 4.8 through 4.10, can be assumed to remain constant throughout the reactions. The pH, however, is still dependent on the concentration and acid strength of the mineral acid.

Although the pH is expected to increase with reaction time due to the fact that the formed ammonia is a stronger base than the initially used MPDA, the excess mineral acid keeps the pH constant. At the reaction temperatures, however, the dissociation constant of the mineral acids and the autoprotolysis constant of water (see APPENDIX-B) differ considerably from those at ambient temperature. Conducting a hydronium ion charge balance, whilst ignoring the presence of hydrolysed MPDA, MAP, resorcinol and ammonia, gives:

$$[AS] = \frac{C_{HA}}{1 + [AS]/K_{HA}} + \frac{K_w}{[AS]} \qquad \textbf{4.12}$$

, where $[AS]$ is the hydronium ion concentration, $C_{HA}$ the acid concentration during the reaction, $K_{HA}$ the dissociation constant of the mineral acid and $K_w$ the autoprotolysis constant of water. For the homogeneous reactions, the produced ammonia reacts with the mineral acid to from a weaker mineral salt. This effectively results in a reduction in the total number of acid sites available. It can therefore be assumed that the mineral acid concentration is reduced linearly with the amount of ammonia formed, i.e., Equation 4.12 can be rewritten as:

$$[AS] = \frac{C_{HA,i} - [MAP] - 2[RES]}{1 + [AS]/K_{HA}} + \frac{K_w}{[AS]} \qquad \textbf{4.13}$$

, with $C_{HA,i}$ corresponding to the initial mineral acid concentration.

**Table 4.15 Water autoprotolysis constants and first and second dissociation constants of phosphoric and sulphuric acid at relevant temperatures**

| Ionisation Reaction | Ionisation Constant ($pK_{HA}$ or $pK_w$) at 25°C | 225°C | 275°C | Reference |
|---|---|---|---|---|
| $H_2O = OH^- + H^+$ | 14 | 11.24 | 11.30 | [Weast *et al.*, 1986] |
| $H_3PO_4 = H_2PO_4^- + H^+$ | 2.15 | 3.59 | 4.17 | [Mesmer and Baes, 1973] |
| $H_2PO_4^- = HPO_4^- + H^+$ | 7.20 | 8.14 | 8.71 | [Mesmer and Baes, 1973] |
| $H_2SO_4^- = HSO_4^- + H^+$ | -2 | 0.02 | 0.30 | [Quist, *et al.*, 1965][(1)] |
| $HSO_4^- = SO_4^- + H^+$ | 1.99 | 4.58 | 5.34 | [Marshall and Jones, 1966] |
| $H_2SO_4 = SO_4^{2-} + 2H^+$ | 0.01 | 4.60 | 5.64 | $pK_{H2SO4} + pK_{(HSO4)-}$ |

(1) Rough estimation by means of extrapolating (van't Hoff Equation) the first ionisation constants of $H_2SO_4$ measured at 400°C, 450°C and 500°C (density = 0.8g/cm ~ density of water at 225°C and 275°C) and forcing linear curve through the $K_{HA}$–value of $H_2SO_4$ at 25°C.

Since the initial amount of mineral acid added to the reaction is known, the hydronium ion concentration can be calculated by means of Equation 4.13. Different yields in ammonia can be assumed, i.e., 0, 1 or 2 times the initial

concentration of MPDA (0.0264mol/L). Since the first ionisation constant of $H_3PO_4$ and $H_2SO_4$ is considerably larger than their respective second ionisation constant, only the $pK_{HA}$–values for the first ionisation is considered. A similar reasoning is applied to the dissociation of $H_2PO_4^-$, thereby ignoring the third ionisation constant of phosphoric acid. Relative to the base ammonia ($pK_a$ of $NH_4^+$ at 20°C = 9.40; Weast *et al.*, 1986), $H_2PO_4^-$ ($pK_a$ $H_2PO_4^-$ at 25°C = 7.20; Mesmer and Baes, 1973) is a relatively weak acid, and thus the hydronium ion concentration given in Table 4.16 may be less than the shown values. However, since ammonia is very volatile at reaction temperature and the interaction of $HPO_4^-$ and $NH_4^+$ is very weak, a large amount of ammonia might accumulate in the headspace of the autoclave and reduce the ammonia concentration in the bulk solution.

**Table 4.16 Prediction of the hydronium ion concentration [$AS$] at different temperatures and ammonia concentrations relevant to the modelling of the homogeneous reactions**

| Run No. | Mineral Acid | Temp. (°C) | Acid Conc. (mol/L) | Estimated [$AS$] (mol/L) at different Ammonia Conc. | | |
|---|---|---|---|---|---|---|
| | | | | $[NH_3]=0$ | $[NH_3] = 0.0264$ | $[NH_3] = 0.0528$ |
| 1 | $H_2SO_4$ (1) | 225 | 0.090 | 8.2E-2 | 5.9E-2 | 3.5E-2 |
| 2 | $H_2SO_4$ (1) | 225 | 0.179 | 1.5E-1 | 1.3E-1 | 1.1E-1 |
| 3 | $H_2SO_4$ (1) | 275 | 0.179 | 7.8E-2 | 5.7E-2 | 3.4E-2 |
| 4 | $H_3PO_4$ (1) | 225 | 0.179 | 6.7E-3 | 6.1E-3 | 5.6E-3 |
| 5 | $H_3PO_4$ (1) | 275 | 0.179 | 3.4E-3 | 3.2E-3 | 2.9E-3 |
| 6 | $H_2PO_4^-$ (2) | 225 | 0.179 | 3.6E-5 | 3.3E-5 | 3.0E-5 |
| 7 | $H_2PO_4^-$ (2) | 275 | 0.175 | 1.9E-5 | 1.7E-5 | 1.6E-5 |

(1) Only the dissociation of the primary hydrogen, e.g. $H_2SO_4 = HSO_4^- + H^+$
(2) Since ammonia is a relatively strong base if compared to the acid strength of $H_2PO_4^-$, the hydronium ion concentration may be less than the shown values. Due to the weaker $HPO^-$ and $NH_4^+$ interaction, a small amount of ammonia can also be present in the gas phase.

For homogeneous reactions, Equations 4.8 through 4.10 can be used to model the MPDA, MAP and resorcinol concentration profiles given in APPENDIX-G. Assuming $[H_2O]$ in Equations 4.8 through 4.10 to remain constant during the course of the reaction, the rate constants for the homogeneous reactions are

then defined as, $k_1^* = k_1 K_{MPDA}[H_2O]$ and $k_2^* = k_2 K_{MAP}[H_2O]$. Since the protonation in relation to the substitution reaction occurs relatively fast ($K_{MPDA}$ at 25°C = $10^{+5.11}$ and $K_{MAP}$ at 25°C = $10^{+4.37}$; Daubert and Danner, 1989), the rate of change of the protonated MPDA and MAP concentration can be assumed to be equal to the rate of change in the bulk solution. $K_{MPDA}$ and $K_{MAP}$ are defined according to Equation 4.7. The hydronium ion concentration can be assumed constant throughout the reaction (see Table 4.16). $[AS]$ is assumed to equal the hydronium ion concentration when [$NH_3$] in Table 4.16 equals 0.0264mol/L.

The $k_1^* = k_1 K_{MPDA}[H_2O]$ and $k_2^* = k_2 K_{MAP}[H_2O]$ values obtained for the homogeneous ($H_2SO_4$, $H_3PO_4$ and $(NH_4)H_2PO_4$) reactions at the specified reaction conditions are obtained by means of minimising the sum-squared errors of $((y_i - \hat{y}_i)/\hat{y}_i)^2$ ($\hat{y}_i$ represents the data points and $y_i$ the curve fitted values) (see Table 4.17). Error analyses are not provided.



**Table 4.17 Rough evaluation of rate constants for the conversion of MPDA to resorcinol in the presence of mineral acids $H_2SO_4$, $H_3PO_4$ and $(NH_4)H_2PO_4$**

| Run No. | Mineral Acid | Temp. (°C) | $[AS]$ [1] (mol/L) | $k_1^*$ [2] (L/mol/h) | $k_2^*$ [2] (L/mol/h) | No. Data Points | Range (hours) |
|---|---|---|---|---|---|---|---|
| 1 | $H_2SO_4$ | 225 | 5.9E-2 | 4.0E+0 | 1.0E+1 | 6 | 0 - 23 |
| 2 | $H_2SO_4$ | 225 | 1.3E-1 | 3.1E+0 | 4.6E+0 | 7 | 0 - 24 |
| 3 | $H_2SO_4$ | 275 | 5.7E-2 | 3.1E+1 | 1.6E+2 | 6 | 0 - 24 |
| 4 | $H_3PO_4$ | 225 | 6.1E-3 | 2.6E+1 | 1.9E+2 | 6 | 0 - 27 |
| 5 | $H_3PO_4$ | 275 | 3.2E-3 | 3.5E+2 | 3.5E+3 | 5 | 0 - 25 |
| 6 | $(NH_4)H_2PO_4$ | 225 | 3.3E-5 | 1.3E+2 | 3.0E+3 | 6 | 0 - 27 |
| 7 | $(NH_4)H_2PO_4$ | 275 | 1.7E-5 | 3.1E+3 | 1.1E+4 | 5 | 0 - 48 |

[1] $[AS]$ is assumed to remain constant and equal the hydronium ion concentration when $[NH_3]$ in Table 4.16 is equal to 0.0264mol/L.
[2] The given values for $k_1^* = k_1 K_{MPDA}[H_2O]$ and $k_2^* = k_2 K_{MAP}[H_2O]$ only represent a rough evaluation thus an error analysis is excluded.

A change in the hydronium ion concentration whilst maintaining the reaction temperature constant should lead to the same rate constants for $k_1^*$ =

$k_1K_{MPDA}[H_2O]$ and $k_2^* = k_2K_{MAP}[H_2O]$ regardless of the type of mineral acid used. At any particular temperature, the equilibrium constants $K_{MPDA}$ and $K_{MAP}$ remain constant. Due to the large excess of water and relatively low hydronium ion concentration, the water concentration can also be regarded as being constant. Comparison of the rate constants in Table 4.17 at a given temperature show that the rate constants $k_1^*$ and $k_2^*$ depending on the mineral acid used, varies by 2 orders of magnitude. The rate constants obtained for reactions in the presence of $H_2SO_4$ are generally quite low ($k_1^*{}_{225℃}$ = ca. 3.6E+0, $k_2^*{}_{225℃}$ = ca. 7.3E+0; and ($k_1^*{}_{275℃}$ = ca. 3.1E+1, $k_2^*{}_{275℃}$ = ca. 1.6E+2), while the rate constants for reactions with $(NH_4)H_2PO_4$ are quite large ($k_1^*{}_{225℃}$ = ca. 1.3E+2, $k_2^*{}_{225℃}$ = ca. 3.0E+3; and ($k_1^*{}_{275℃}$ = ca. 3.1E+3, $k_2^*{}_{275℃}$ = ca. 1.1E+4).

The respective rate constants for $H_3PO_4$ are ca. 1 order of magnitude larger than the those of $H_2SO_4$, and 1 order of magnitude less than those of $(NH_4)H_2PO_4$. It is likely that the rate constants obtained for $H_3PO_4$ are the most accurate since its ionisation constant (unlike for $H_2SO_4$) at reaction temperature is known. Due to the rough prediction of the ionisation constants for $H_2SO_4$, the ionisation constants could quite easily be one order of magnitude less than those predicted in Table 4.15. In fact, using the equilibrium constants obtained for $H_2SO_4 = SO_4^{2-} + 2H^+$ (with appropriate adjustments made to Equation 4.13) would lead to a value quite close to those for $H_3PO_4$. Regarding the use of $(NH_4)H_2PO_4$, small deviations may influence the solution pH because $H_2PO_4^-$ is a very weak acid. Since the reactant used is $(NH_4)H_2PO_4$, the system may equilibriate resulting in the formation of some $NH_3$ (gas phase) and $H_3PO_4$ (liquid phase). This would result in a more acidic solution.

Comparison of the rate constants $k_1^*$ and $k_2^*$ (see Table 4.17) reveals that the observed $k_2^*$ is between 2 and 10 times larger than $k_1^*$. This is quite interesting because a larger value is expected for $k_1^*$ rather than $k_2^*$, since $K_{MPDA}$ at 25°C = $10^{+5.11}$ is greater than $K_{MAP}$ at 25°C = $10^{+4.37}$ [Daubert and Danner, 1989] by a factor of 5.5. It is reasonable to assume that $K_{MPDA}$ / $K_{MAP}$ = 5.5 irrespective of

temperature despite the fact that a decrease in the dielectric constant (78.4 at 25°C, 30.4 at 225°C and 23.0 at 275°C; Akerlof and Oshry, 1950) would result in a decrease in $K_{MPDA}$ and $K_{MAP}$ at reaction temperature by several orders of magnitude. The most likely reason for $k_2^*$ being greater than $k_1^*$ is that the time zero chosen to correct for the ramping period should be taken at a temperature even closer to the final temperature than the one chosen in Section 4.6.1.4.

**Table 4.18 Comparison of activation energies of $H_2SO_4$, $H_3PO_4$ and $(NH_4)H_2PO_4$**

| Mineral Acid or Aluminosilicate | Activation Energy, $E_{a,1}$ [(1)] (kJ / mol) | Activation Energy, $E_{a,2}$ [(1)] (kJ / mol) |
|---|---|---|
| $H_2SO_4$ | 99 | 144 |
| $H_3PO_4$ | 118 | 132 |
| $(NH_4)H_2PO_4$ | 144 | 59 |

(1) $E_{a,1}$ and $E_{a,2}$ respectively refer to the activation energies obtained for $k_1^*$ and $k_2^*$ for the mineral acids; and $k_1^{**}$ and $k_2^{**}$ for the heterogeneous aluminosilicates.

The activation energies obtained for the reactions with $H_2SO_4$, $H_3PO_4$ and $(NH_4)H_2PO_4$ do not follow any particular trend regarding the acid strength of the mineral acids. The grouping together of constants to $k_1^* = k_1 K_{MPDA}[H_2O]$ and $k_2^* = k_2 K_{MAP}[H_2O]$ may hardly affect relative changes in the activation energies since large changes in the hydronium ion concentration between 225°C and 275°C is unlikely. The observed differences in the activation energies of the reactions in the presence of homogeneous acids might be ascribed to the differences in the ionic strengths of the solutions.

Mole-balances larger than 95% confirm that only minute amounts of resorcinol ethers are produced. This is even true when using $H_2SO_4$ at 275°C, where additional products may be formed since $H_2SO_4$ at 275°C becomes an oxidising agent [Taylor and Battersby, 1967]. The resorcinol ether formation is controlled if the mineral acid is diluted to such an extent so as it not being able to exert an strong hydrophilic force that encourages the formation of ethers. The formation of

ether is controlled by either using a weaker acid that still allows for an appreciable hydronium ion concentration, or diluting the strong acid to such an extent that its quest in search of additional water to allow for its hydrolysis is reduced. The disadvantage of very strong acids is, however, that upon strong dilution, its concentration does not correspond to the stoichiomentric amount required for the complete conversion.

### 4.6.3 HOMOGENEOUS ACIDS VERSUS ALUMINOSILICATES

Equations 4.9 and 4.10 derived to model the concentration-profile of MAP and resorcinol are also applicable to heterogeneous reactions, i.e. reactions in the presence of aluminosilicates. As for the case of the mineral acids, the rate of change of MAP adsorbed can be assumed to be equal to the rate of change in the bulk solution. Equation 4.8 cannot be fitted to the concentration data of MPDA due to its strong adsorption during the initial ramping period. Consequently, the reaction rate data have to be modelled according to Equations 4.9 and 4.10. During optimisation, the pseudo MPDA concentration is obtained by means of a simple mass balance, i.e., $[MPDA]$ = $[MPDA_{init}]$ - $[MAP]$ - $[RES]$, with only the concentration curves of MAP and resorcinol being optimised.



It can be assumed, as with the homogeneous reactions, that the produced ammonia poisons the Brønsted acid sites on the heterogeneous solids. An overall mass balance gives an expression for the number of acid sites available during the course of the reaction:

$$[AS] = [AS_i] - [MAP] - 2[RES] - [MPDA^{prot}] - [MAP^{prot}] \qquad \textbf{4.14}$$

, where $[AS_i]$ refers to the initial number of acid sites; $[MAP]$ and $[RES]$ to the equivalent bulk concentrations of MAP and resorcinol; and the superscript '*prot*' refers to the compounds chemisorbed to the Brønsted acid sites via the $-NH_2$

functional group. Developing a similar expression for $[MAP^{prot}]$ as for $[MPDA^{prot}]$ in Equation 4.7, Equation 4.14 can be rearranged to give:

$$[AS] = \frac{[AS_i] - [MAP] - 2[RES]}{1 + K_{MPDA}[MPDA] + K_{MAP}[MAP]} \qquad \textbf{4.15}$$

Substitution of Equation 4.15 for $[AS]$ in Equations 4.9 and 4.10, leads to the expressions:

$$\frac{d}{dt}[MAP^{prot}] = k_1 K_{MPDA}[MPDA] \times [H_2O] \frac{[AS_i] - [MAP] - 2[RES]}{1 + K_{MPDA}[MPDA] + K_{MAP}[MAP]} - k_2 K_{MAP}[MAP] \times [H_2O] \frac{[AS_i] - [MAP] - 2[RES]}{1 + K_{MPDA}[MPDA] + K_{MAP}[MAP]} \qquad \textbf{4.16}$$

$$\frac{d}{dt}[RES] = k_2 K_{MAP}[MAP] \times [H_2O] \frac{[AS_i] - [MAP] - 2[RES]}{1 + K_{MPDA}[MPDA] + K_{MAP}[MAP]} \qquad \textbf{4.17}$$

The adsorption study in Section 4.4.2.6, however, shows that the amount of MPDA and MAP physisorbed on the zeolites is much larger than the amount chemisorbed. The equilibria between the compounds in the bulk of the solution and the physisorbed compounds have to be taken into consideration.

$$K_{MPDA}^{phys} = \frac{[MPDA]}{[MPDA^{phys}]} \quad \text{and} \quad K_{MAP}^{phys} = \frac{[MAP]}{[MAP^{phys}]} \qquad \textbf{4.18}$$

The constant $K_{MPDA}$ as given by Equation 4.7 is still valid, however, the equilibrium constant now refers to an equilibrium existing between $[MPDA^{phys}]$ and $[MPDA^{prot}]$. The same is true for $K_{MAP}$. Due to the large assimilation of organic species around the heterogeneous solids, the concentration of physisorbed water inside the pore structure ($[H_2O^{phys}]$ can differ considerably from the concentration of water in the bulk solution. Similarly to Equation 4.18, another equilibrium constant term, i.e., $K_{Water}^{phys}$, is required to account for the change in bulk to physisorbed water concentration. Equations 4.16 and 4.17 are rewritten as:

$$\frac{d}{dt}[MAP] = k_1 K_{MPDA}^{phys} K_{MPDA}[MPDA] \times K_{Water}^{phys}[H_2O] \frac{[AS_i] - [MAP] - 2[RES]}{1 + K_{MPDA}^{phys} K_{MPDA}[MPDA] + K_{MAP}^{phys} K_{MAP}[MAP]} - k_2 K_{MAP}^{phys} K_{MAP}[MAP] \times K_{Water}^{phys}[H_2O] \frac{[AS_i] - [MAP] - 2[RES]}{1 + K_{MPDA}^{phys} K_{MPDA}[MPDA] + K_{MAP}^{phys} K_{MAP}[MAP]} \quad \textbf{4.19}$$

$$\frac{d}{dt}[RES] = k_2 K_{MAP}^{phys} K_{MAP}[MAP] \times K_{Water}^{phys}[H_2O] \frac{[AS_i] - [MAP] - 2[RES]}{1 + K_{MPDA}^{phys} K_{MPDA}[MPDA] + K_{MAP}^{phys} K_{MAP}[MAP]} \quad \textbf{4.20}$$

The number of parameters given in Equations 4.19 and 4.20 need to be reduced. Since the amount of MPDA adsorbed on the aluminosilicates (see Section 4.4.2.6) is relatively large, the equilibrium constants may not automatically be assumed as being small. Equations 4.19 and 4.20 can be simplified by means of the following ratio $R$:

$$R = \frac{K_{MPDA}^{phys} K_{MPDA}}{K_{MAP}^{phys} K_{MAP}} \quad \textbf{4.21}$$

The $R$-term is expected to be greater than 1 since the adsorption of MPDA relative to MAP onto the heterogeneous solids is preferred. Substitution of $R$ into Equations 4.19 and 4.20 gives:

$$\frac{d}{dt}[MAP] = \left(k_1 R[MPDA] \times K_{Water}^{phys}[H_2O] - k_2[MAP] \times K_{Water}^{phys}[H_2O]\right) \frac{[AS_i] - [MAP] - 2[RES]}{\frac{1}{K_{MAP}^{phyd} K_{MAP}} + R[MPDA] + [MAP]} \quad \textbf{4.22}$$

$$\frac{d}{dt}[RES] = k_2[MAP] \times K_{Water}^{phys}[H_2O] \frac{[AS_i] - [MAP] - 2[RES]}{\frac{1}{K_{MAP}^{phys} K_{MAP}} + R[MPDA] + [MAP]} \quad \textbf{4.23}$$

The denominator in Equations 4.22 and 4.23 can then be simply rewritten as '$R[MPDA]$' by assuming that the term $R[MPDA]$ is considerably larger than '$1/(K_{MAP}{}^{phys} K_{MAP})$ + [MAP]'. This assumption is, however, only valid for the first few sampling points of a given reaction, i.e., when the concentration of MPDA in the bulk solution is larger than the MAP concentration. The term '$1/(K_{MAP}{}^{phys} K_{MAP})$' is

expected to be small since the adsorption of MAP onto the heterogeneous solids is quite large (see Section 4.4.2.6 for aluminosilicates and Section 4.5.1.3 for zirconium phosphates).

$$\frac{d}{dt}[MAP] = \left( k_1 \times K_{Water}^{phys}[H_2O] - k_2 \times K_{Water}^{phys}[H_2O]\frac{[MAP]}{R[MPDA]} \right)([AS_i] - [MAP] - 2[RES]) \qquad \textbf{4.24}$$

$$\frac{d}{dt}[RES] = k_2 \times K_{Water}^{phys}[H_2O]\frac{[MAP]}{R[MPDA]}([AS_i] - [MAP] - 2[RES]) \qquad \textbf{4.25}$$

Equations 4.24 and 4.25 can now be expressed in terms of 2 parameters by assuming that $R$ and $[H_2O]$ remain constant throughout the reaction. According to Equations 4.24 and 4.25, the rate constants for the heterogeneous reactions are then defined as, $k_1^{**} = k_1 K_{Water}^{phys}[H_2O]$ and $k_2^{**} = k_2 K_{Water}^{phys}[H_2O]/R$.

**Table 4.19 Evaluation of rate constants for the conversion of MPDA to resorcinol in the presence aluminosilicates H-USY, H-BETA, H-ZSM-5 (Si/Al = 13), H-ZSM-5 (Si/Al = 22) and silica-alumina**

| Run No. | Alumino silicate[1] | Temp. °C | $[AS_i]$ mol/L | $k_1^{**}$[2] L/mol/h | $k_2^{**}$[2] L/mol/h | No. Pts. | Range hours | Remarks |
|---|---|---|---|---|---|---|---|---|
| 8 | USY | 225 | 5.7E-2 | 2.6E-2 | 1.8E-2 | 3 | 0 - 5 | framework destruction |
| 9 | USY | 275 | 5.7E-2 | 1.1E-1 | 1.2E-1 | 3 | 0 - 2 | framework destruction |
| 10 | USY | 300 | 5.7E-2 | 5.5E-1 | 3.6E-1 | 2 | 0 - 1 | framework destruction |
| 11 | Beta | 225 | 2.9E-2 | 1.2E-2 | 9.3E-2 | 5 | 0 - 11 | low activity |
| 12 | Beta | 275 | 2.9E-2 | 2.1E+0 | 1.0E+0 | 2 | 0 - 1 | partially catalytic |
| 13 | Beta | 275 | 2.9E-2 | 2.6E+0 | 1.4E+0 | 2 | 0 - 1 | partially catalytic |
| 14 | Beta | 300 | 2.9E-2 | 3.6E+0 | 2.1E+0 | 2 | 0 - 1 | partially catalytic |
| 15 | ZM(13) | 225 | 2.6E-2 | 8.3E-4 | 3.5E-3 | 7 | 0 - 36 | low activity |
| 16 | ZM(13) | 275 | 2.6E-2 | 3.7E-3 | 1.1E-2 | 5 | 0 - 24 | low activity |
| 17 | ZM(13) | 300 | 2.6E-2 | 5.5E-3 | 1.5E-2 | 5 | 0 - 24 | low activity |
| 18 | ZM(22) | 300 | 1.9E-2 | 1.7E+0 | 1.4E+0 | 2 | 0 - 1 | partially catalytic |
| 19 | Si-Al | 300 | 5.6E-2 | 3.1E-1 | 4.3E-1 | 2 | 0 - 1 | dealumination |

[1] ZM(Si/Al=13) and ZM(Si/Al=22) respectively refer to ZSM-5 (Si/Al = 13) and ZSM-5 (Si/Al = 22)
[2] For heterogeneous systems, $k_1^{**} = k_1 K_{Water}^{phys}[H_2O]$ and $k_2^{**} = k_2 K_{Water}^{phys}[H_2O]/R$.

Apart for the aluminosilicates showing low activities (see Table 4.19), only the first 2 to 3 data points can be used for the optimisation since other effects

(dealumination and some catalytic activity) occur during the course of the reactions that have not been considered during the derivation of the original equations. Also Equations 4.24 and 4.25 are only valid for low conversions of MPDA due to the assumptions made during their respective derivation. The number of data points as well as the reaction-time period used for the calculation of $k_1^{**}$ and $k_2^{**}$ are included in Table 4.19. For each reaction, the main reason for the chosen data range is also included.

The framework structure of H-USY during the reaction is destabilised very quickly, even at the relatively low reaction temperatures of 225°C. The framework collapse coupled with the ensuing dealumination and destruction of Brønsted acid results in the reaction not being able to go to completion. This is despite the fact that the initial number of acid sites on H-USY added to the reactor exceeds the number of acid sites required. Considering Equation 2.30 in Chapter 2 derived by Wang *et al.* [1991] on the dealumination of USY at given temperatures and pressures, the half-life of H-USY in saturated water at 225°C, 275°C and 300°C is respectively calculated to occur after 493, 45 and 16hours. The relatively rapid serious destruction of H-USY after a reaction time of only 5hours at 225°C and 1hour above 275°C can therefore be due to the presence of aqueous MPDA in the reaction mixture. The presence of amine containing MPDA molecules in aqueous solution is likely to aid the dealumination process and thereby enhance the rate of destruction of the H-USY framework.

Although H-Beta also undergoes some framework destruction during the course of the reaction (see Section 4.4.4), the reason for including only the first few data points during the kinetic analysis is due to the reaction being partially catalytic, viz. the number of Brønsted acid sites on H-Beta added to the reactor is less than the amount required to obtain the observed resorcinol yields. Consequently, at reaction temperature an equilibrium is likely to exist between ammonia adsorbed on H-Beta and the ammonia in solution and ammonia in the reactor head space.

H-ZSM-5 (Si/Al = 13) and H-ZSM-5 (Si/Al = 22) do not show framework destruction during the course of the reaction. However, the activities of the two zeolites are remarkably different. Whereas the activity of H-ZSM-5 (Si/Al = 13) is very poor, H-ZSM-5 (Si/Al = 22) is much more active. Similarly to H-Beta, reaction in the presence of H-ZSM-5 (Si/Al = 22) also tends to be partially catalytic and thus only the first 2 data points can be used for predicting the rate constants for reactions in the presence of H-ZSM-5 (Si/Al = 22).

Similarly to H-USY, the BET-surface area is reduced considerably during the course of the reaction using silica-alumina at 300°C (see Section 4.4.4). The dealumination of silica-alumina leads to the loss of Brønsted acid sites, which is also reflected in the concentration profile. Therefore, only the first 2 data points collected during the reaction with silica-alumina can be used for the kinetic analysis.

Comparison of the rate constants of zeolites H-USY, H-Beta, H-ZSM-5 (Si/Al = 13) and H-ZSM-5 (Si/Al = 22) with their respective crystallite sizes (see Table 4.18) suggests that some sort of relationship does exist between these two parameters. A decrease in the crystallite size leads to an increase in activity. Assuming a constant aluminium gradient existing within the zeolite crystal, the fraction of external [$AS_{ext}$] relative to the total number of acid sites [$AS_t$] can be calculated. This fraction depends on the average crystal diameter and the framework density of USY (13.3T-atoms per 1000Å$^3$), Beta (15.3T-atoms per 1000Å$^3$) and ZSM-5 (18.4T-atoms per 1000Å$^3$) [Meier *et al.*, 1996]. Assuming that the crystals are spherical, the external area relative to the total area can be calculated. This ratio can then be assumed proportional to [$AS_{ext}$] / [$AS_t$].

Division of the rate constant, $k_1^{**}$, obtained for each zeolite at 300°C by [$AS_{ext}$] leads to a value of 5.5E+2 for USY, 2.6E+3 for Beta, 5.5E+1 for ZSM-5 (Si/Al = 13) and 3.4E+3 for ZSM-5 (Si/Al = 22). The $k_1^{**}$/[$AS_{ext}$] values calculated for Beta and ZSM-5 (Si/Al = 22) become identical, while the $k_1^{**}$/[$AS_{ext}$] value for ZSM-5

**Table 4.20 Comparison of runs in presence of zeolites at 300°C with their respective crystallite sizes and external acid concentrations**

| Run No. | Aluminosilicate | $k_1^{**(1)}$ L/mol/h | $k_2^{**(1)}$ L/mol/h | Crystal diameter (diameter mean) (μm) | density (g/ml) | $[AS_{ext}]$ mol/L |
|---|---|---|---|---|---|---|
| 10 | USY | 5.5E-1 | 3.6E-1 | 0.4 - 0.5 (0.45) | 1.33 | 1.0E-3 |
| 14 | Beta | 3.6E+0 | 2.1E+0 | < 0.3 (0.15) | 1.53 | 1.4E-3 |
| 17 | ZSM-5 (Si/Al=13) | 5.5E-3 | 1.5E-2 | 1.0 - 5.0 (3.0) | 1.84 | 1E-4[(2)] |
| 18 | ZSM-5 (Si/Al=22) | 1.7E+0 | 1.4E+0 | 0.5 (0.5) | 1.84 | 3E-4[(2)] |

[(1)] For heterogeneous systems, $k_1^{**} = k_1 K_{Water}^{phys}[H_2O]$ and $k_2^{**} = k_2 K_{Water}^{phys}[H_2O]/R$.
[(2)] The adsorption of 4-methyl-quinoline predicts the external area of ZSM-5 (Si/Al = 22) being 16 times the area of ZSM-5(Si/Al = 13)

(Si/Al = 13) deviates the most. However, the adsorption of 4-methyl-quinoline does predict that the external area of ZSM-5 (Si/Al = 22) is 16 times the area of ZSM-5 (Si/Al = 13), which implies that for ZSM-5 (Si/Al = 13) a value close to that obtained for USY can be expected. Consequently, for all zeolites the dominant part of the reaction seems to occur on the more external surface acid sites.

The true reaction rate constants $k_1$ and $k_2$ obtained for the mineral acids ($k_1^* = k_1 K_{MPDA}[H_2O]$ and $k_2^* = k_2 K_{MAP}[H_2O]$) can be compared to the true reaction rate constants $k_1$ and $k_2$ obtained for the aluminosilicates acids ($k_1^{**} = k_1 K_{Water}^{phys}[H_2O]$ and $k_2^{**} = k_2 K_{Water}^{phys}[H_2O]/R$). Judging from the decrease in the ionisation constants of mineral acid (see Table 4.15) when raising the temperature from 25°C to 225°C ($pK_{HA,25℃} - pK_{HA,225℃}$ = -1.7±0.8) and 275°C ($pK_{HA,25℃} - pK_{HA,275℃}$ = -2.3±0.9), it follows that $K_{MPDA,,225℃} \sim 10^{+3.4}$, $K_{MPDA,275℃} \sim 10^{+2.8}$, $K_{MAP,,225℃} \sim 10^{+2.7}$ and $K_{MAP,275℃} \sim 10^{+2.1}$. The water concentration in the bulk solution is regarded as being constant. Since all concentrations are related to the density of water at **ambient temperatures**, $[H_2O]$ = 55.6mol/L. $K_{Water}^{phys}$ is less than unity since the strong adsorption behaviour of MAP and MPDA on the aluminosilcates would result in less water adsorbed on the aluminosilicate surface. Arbitrarily setting $K_{Water}^{phys}$ = 0.5 and $R = (K_{MPDA}^{phys} K_{MPDA}) / (K_{MAP}^{phys} K_{MAP})$ = 2 allows for a rough estimation of the true rate constants $k_1$ and $k_2$ (see Table 4.21).

**Table 4.21 Comparison of true rate constants $k_1$ and $k_2$ in the presence of $H_3PO_4$ with reactions conducted in the presence of aluminosilicates**

| Run No. | Acid[1] | Temp. (°C) | $[AS_l]$ (mol/L) | $k_1$[1] (L/mol/h) | $k_2$[2] (L/mol/h) | No. Data Points | Range (hours) |
|---|---|---|---|---|---|---|---|
| 4 | $H_3PO_4$ | 225 | 6.1E-3 | 2E-4 | 7E-3 | 6 | 0 - 24 |
| 8 | USY | 225 | 5.7E-2 | 9E-4 | 1E-3 | 3 | 0 - 5 |
| 11 | Beta | 225 | 2.9E-2 | 4E-4 | 7E-3 | 5 | 0 - 11 |
| 15 | ZM(13) | 225 | 2.6E-2 | 3E-5 | 3E-4 | 7 | 0 - 36 |
| 5 | $H_3PO_4$ | 275 | 3.2E-3 | 1E-2 | 5E-1 | 5 | 0 - 25 |
| 9 | USY | 275 | 5.7E-2 | 4E-3 | 9E-3 | 3 | 0 - 2 |
| 13 | Beta | 275 | 2.9E-2 | 9E-2 | 1E-1 | 2 | 0 - 1 |
| 16 | ZM(13) | 275 | 2.6E-2 | 1E-4 | 8E-4 | 5 | 0 - 24 |

[1] Values calculated from $k_1^*$ and $k_1^{**}$ with the assumption of $K_{MPDA,,225℃} \sim 10^{+3.4}$, $K_{MPDA,275℃} \sim 10^{+2.8}$, $[H_2O]$ = 55.6mol/L, $K_{Water}^{phys}$ = 0.5 and $R$ = 2.
[2] Values calculated from $k_2^*$ and $k_2^{**}$ with the assumption of $K_{MAP,,225℃} \sim 10^{+2.7}$, $K_{MAP,275℃} \sim 10^{+2.1}$, $[H_2O]$ = 55.6mol/L, $K_{Water}^{phys}$ = 0.5 and $R$ = 2.

Although it needs to be acknowledged that the prediction of the equilibrium constants is quite crude and the values given for $k_1$ and $k_2$ may differ by few orders of magnitude, some type of comparison can be made. The rate constants for the conversion of MPDA to MAP ($k_1$) are generally smaller than the rate constants for the conversion of MAP to resorcinol ($k_2$). The rate constants $k_1$ and $k_2$ for $H_3PO_4$ are on average equal (although there are exceptions) to those for Beta (if the predicted unknowns are correct), which in turn are larger than those obtained for USY and ZSM-5 (Si/Al = 13). This can be explained based on the observations made regarding the number of acid sites on the external surface versus the number of acid sites inside the zeolite pore structure. According to the rate constants in Table 4.21, all the acid sites on H-Beta are equally accessible to the MPDA and MAP molecules as is the case with homogeneous acids. The larger crystallites of H-USY and H-ZSM-5 (Si/Al = 13), to a large extent, only make the more exterior Brønsted acid sites accessible to the incoming reactants, thus reducing the values calculated for the rate constants since not all the Brønsted acid sites are utilised to the same extent.

## 4.6.4 AQUEOUS ACIDS VERSUS ZIRCONIUM PHOSPHATES

The equations derived for the aluminosilicates are also applied to characterise the reactions in the presence of the zirconium phosphates. Only the simplified, 2 parameter rate equations, i.e., Equations 4.24 and 4.25, are considered with the rate constants being defined as $k_1^{**} = k_1 K_{Water}^{phys}[H_2O]$ and $k_2^{**} = k_2 K_{Water}^{phys}[H_2O]/R$. As already mentioned in Section 4.6.3, Equations 4.24 and 4.25 are only applicable when the MPDA conversion is low.

**Table 4.22 Rough evaluation of rate constants for the conversion of MPDA to resorcinol in the presence zirconium phosphates α-ZrP, α-ZrP400, γ-ZrP and γ-ZrP400**

| Run No. | Zirconium Phosphate | Temp. °C | $[AS_i]$ mol/L | $k_1^{**(1)}$ L/mol/h | $k_2^{**(1)}$ L/mol/h | No. Pts. | Range hours | Remarks |
|---|---|---|---|---|---|---|---|---|
| 20 | α-ZrP | 225 | 1.9E-1 | 3.9E-3 | 1.4E-2 | 4 | 0 - 9 | – |
| 21 | α-ZrP400 | 225 | 1.6E-1 | 8.4E-3 | 2.1E-2 | 4 | 0 - 9 | – |
| 22 | α-ZrP400 | 275 | 1.6E-1 | 3.8E-2 | 3.2E-1 | 2 | 0 - 1 | – |
| 23 | γ-ZrP | 225 | 9.0E-2 | 2.4E-1 | 1.0E-1 | 2 | 0 - 1 | – |
| 24 | γ-ZrP | 225 | 9.0E-2 | 2.7E-1 | 1.2E-1 | 2 | 0 - 1 | – |
| 25 | γ-ZrP | 275 | 9.0E-2 | 5.4E-1 | 7.2E-1 | 2 | 0 - 1 | – |
| 26 | γ-ZrP400 | 225 | 5.3E-2 | 8.5E-2 | 9.9E-2 | 3 | 0 - 5 | increase in reaction rate |
| 27 | γ-ZrP400 | 275 | 5.3E-2 | 7.9E-2 | 9.0E-1 | 2 | 0 - 1 | increase in reaction rate |

(1) For heterogeneous systems, $k_1^{**} = k_1 K_{Water}^{phys}[H_2O]$ and $k_2^{**} = k_2 K_{Water}^{phys}[H_2O]/R$.

The α-zirconium phosphates may resemble the homogeneous reactions more closely than the aluminosilicates. The more open architecture that the layered solids provide allows the MPDA greater mobility and access to the active sites. Since the fixed ionogenic phosphate groups on the layered zirconium phosphate macromolecular planes are essentially constituents of mineral ortho-phosphoric acid, the general interaction of the Brønsted acids with the surrounding aqueous solution would also resemble that of the homogeneous reactions more closely. Further, leaching of phosphates into solution does not necessarily involve the

destruction of acid sites as is the case with aluminosilicate since the leached phosphate-amine salt in solution can undergo a subsequent substitution reaction as suggested by Clearfield *et al.* [1984] (see Section 4.5.2). The presence of previously adsorbed amines also encourages the leaching of amine-phosphate into solution as well as the transformation of α-ZrP and α-ZrP400 into $(NH_4)Zr_2(PO_4)_3$ [Clearfield *et al.*, 1984; Herzog-Cance *et al.*, 1992]. The rate constants $k_1^{**}$ and $k_2^{**}$ for α-ZrP400 at 225°C are twice the ones obtained for α-ZrP. This can be explained on the basis that the Brønsted acid sites on α-ZrP400 are stronger than on α-ZrP [Clearfield and Thakur, 1980]. Therefore, an amine compound interacts more rapidly with an acid site on α-ZrP400. In comparison to α-ZrP, the few P-O-P bonds existing between the α-ZrP400 layers seem to have a minor effect in preventing the layers to spread. The XRD patterns after the reactions at 225°C (see Figure 4.48) also confirms that formation of $(NH_4)Zr_2(PO_4)_3$ occurs more readily with α-ZrP400 than with α-ZrP. This implies an increased reaction rate for α-ZrP400, since the leaching of phosphate-salts into solution occurs more quickly.

The reaction rate constants $k_1^{**}$ and $k_2^{**}$ calculated for the γ-ZrP and γ-ZrP400 are considerably larger than the ones calculated for the α-ZrP and α-ZrP400 (see Table 4.22). It is generally accepted that the Brønsted acid sites on γ-ZrP are stronger than the ones on α-ZrP [Espina *et al.*, 1998; Herzog-Cance *et al.*, 1992; La Ginestra and Patrono, 1987]. Since the interlayer distance of γ-ZrP (12.20Å) are larger than the ones of α-ZrP (7.55Å), the driving force required for spreading the layers of γ-ZrP are reduced considerably. Therefore, the adsorption rate constants for MPDA on γ-ZrP are expected to be large. The reaction rate constants observed for γ-ZrP400 tend to increase with reaction time. This can be explained on the basis that large amounts of P-O-P bonds do exist between the individual γ-ZrP400 layers. Also the interlayer distance is considerably less (8.26Å). After an initial induction period (ca. 2hours), the reaction rate increases

considerably since a drastic increase in the rate constants is observed when all data points of a particular reaction are included as opposed to only the first two.

Similarly to the aluminosilicates, the zirconium phosphates can act as concentrating 'vessel', where a large amount of MPDA is previously adsorbed on the macromolecular plains. This would lead to a large concentration of protonated MPDA species, which upon reaching a certain temperature would react with water and result in the relatively quick observed formation of MAP and/or resorcinol. The true reaction rate constants $k_1$ and $k_2$ for the zirconium phosphate can again be compared to those of the mineral acids by assuming that: $K_{MPDA,,225℃} \sim 10^{+3.4}$, $K_{MPDA,275℃} \sim 10^{+2.8}$, $K_{MAP,,225℃} \sim 10^{+2.7}$, $K_{MAP,275℃} \sim 10^{+2.1}$, $K_{Water}^{phys} = 0.5$ and $R = (K_{MPDA}^{phys} K_{MPDA}) / (K_{MAP}^{phys} K_{MAP}) = 2$.

**Table 4.23 Comparison of true rate constants $k_1$ and $k_2$ in the presence of $H_3PO_4$ with reactions conducted in the presence of zirconium phosphates**

| Run No. | Acid[(1)] | Temp. (°C) | $[AS_i]$ (mol/L) | $k_1$[(1)] (L/mol/h) | $k_2$[(2)] (L/mol/h) | No. Data Points | Range (hours) |
|---|---|---|---|---|---|---|---|
| 4 | $H_3PO_4$ | 225 | 6.1E-3 | 2E-4 | 7E-3 | 6 | 0 - 24 |
| 20 | α-ZrP | 225 | 1.9E-1 | 1E-4 | 1E-3 | 4 | 0 - 9 |
| 21 | α-ZrP400 | 225 | 1.6E-1 | 3E-4 | 2E-3 | 4 | 0 - 9 |
| 23 | γ-ZrP | 225 | 9.0E-2 | 9E-3 | 7E-3 | 2 | 0 - 1 |
| 26 | γ-ZrP400 | 225 | 5.3E-2 | 3E-3 | 7E-3 | 3 | 0 - 5 |
| 5 | $H_3PO_4$ | 275 | 3.2E-3 | 1E-2 | 5E-1 | 5 | 0 - 25 |
| 9 | α-ZrP400 | 275 | 1.6E-1 | 1E-3 | 2E-2 | 2 | 0 - 1 |
| 13 | γ-ZrP | 275 | 9.0E-2 | 2E-2 | 7E-3 | 2 | 0 - 1 |
| 16 | γ-ZrP400 | 275 | 5.3E-2 | 3E-3 | 6E-2 | 2 | 0 - 1 |

(1) Values calculated from $k_1^*$ and $k_1^{**}$ with the assumption of $K_{MPDA,,225℃} \sim 10^{+3.4}$, $K_{MPDA,275℃} \sim 10^{+2.8}$, $[H_2O] = 55.6$mol/L, $K_{Water}^{phys} = 0.5$ and $R = 2$.
(2) Values calculated from $k_2^*$ and $k_2^{**}$ with the assumption of $K_{MAP,,225℃} \sim 10^{+2.7}$, $K_{MAP,275℃} \sim 10^{+2.1}$, $[H_2O] = 55.6$mol/L, $K_{Water}^{phys} = 0.5$ and $R = 2$.

The rate constants obtained in the presence of α-ZrP and α-ZrP400 (see Table 4.23) are less than the rate constants obtained for reactions with phosphoric acid. Since the true rate constants for α-ZrP400 is greater then α-ZrP, it can be

concluded that the slow / partial splitting of the layers results in less acid sites being utilised by the incoming MPDA and MAP molecules, especially during the initial reaction period. This is furthered by the observation that the rate constants for $\gamma$-ZrP with a basal spacing 1.6 times that of $\alpha$-ZrP approach those obtained for $H_3PO_4$.

# 4.7 OUTLOOK FOR REPLACEMENT OF HOMOGENEOUS ACIDS WITH HETEROGENEOUS ANALOGUES

Resorcinol can be produced in high yields and selectivity from MPDA in the presence of homogeneous and heterogeneous acids. However, the economic factor is the largest determinant regarding the replacement of homogenous acids by heterogeneous solids.

## 4.7.1 REACTIONS WITH HOMOGENEOUS ACIDS

The mineral acids as reactants are cheap. However, the mineral acids tend to be highly corrosive at the required reaction temperature, thus making the process very capital intensive due to construction and maintenance costs. The separation of the mineral salt product from the reaction mixture as well as the subsequent drying of the salt requires additional separation / drying units and is also very energy intensive. The produced mineral salt has a low commercial value. Apart for the production of fertilisers, the formed ammonium salts can be regarded as waste products.



## 4.7.2 REACTIONS WITH ALUMINOSILICATES

If the conversion of MPDA to resorcinol is carried out in the presence of aluminosilicates, the reactor maintenance costs are reduced considerably since the acid sites on the aluminosilicates have a minute effect on the corrosion of the reactor walls. Also the separation costs in terms of energy required to separate the aluminosilicates from the bulk mixture are reduced considerably. The process in the presence of aluminosilicates would also be more environmentally friendly since the amount of waste produced in terms of mass of ammonium is reduced

considerably. Further, the safety in the work environment is enhanced since in the event of spillage the solids are essentially harmless. The disposal of the used aluminosilicates is also less hazardous with the waste being easily stored.

The disadvantage with the aluminosilicates is that they are relatively expensive (see Table 4.24). The cheaper aluminosilicates, i.e. H-USY and silica-alumina, are unsuitable for the conversion of MPDA to resorcinol as shown by their loss in activity and surface area after one reaction at 300°C. Although reactions with H-Beta give turnover numbers ($NH_3$ produced per number of Brønsted acid sites) greater than 1, the zeolite is relatively expensive with full framework destruction likely to occur after 2-3 reaction cycles. The regeneration of the aluminosilicates is also quite energy intensive.



**Table 4.24 Cost of selected aluminosilicates**

| Aluminosilicate | Cost ($/kg)[1] |
|---|---|
| Silica-alumina | – |
| H-USY | 2 - 4 |
| H-Beta | ca. 70 |
| HZSM-5 (untemplated synthesis) | ca. 10 |
| H-ZSM-5 (templated synthesis) | ca. 50 |

[1] J.C.Q. Fletcher, personal communication [2001]

The H-ZSM-5 synthesis tends to be very stable under the reaction conditions and is relatively cheap if its production occurs via the untemplated synthesis. Since the resorcinol selectivity in the presence of aluminosilicates remains unaffected, whether H-ZSM-5 is produced by means of a template is unimportant, as long as the untemplated synthesised H-ZSM-5 remains stable under the reaction conditions. The activity of H-ZSM-5 can be improved if the H-ZSM-5 crystal size is small and the temperature is raised above that of the present investigation. With a suitable reactor design, the removal of ammonia that collects in the

headspace could increase the turnover number and thereby reduce the number of regeneration cycles.

### 4.7.3 REACTIONS WITH ZIRCONIUM PHOSPHATES

The conversion of MPDA to resorcinol in the presence of the zirconium phosphate needs to be conducted at lower temperature to prevent the leaching of phosphates into solution and also its subsequent transformation to $(NH_4)Zr_2(PO_4)_3$. At the lower temperatures, i.e. 225°C, the turnover numbers ($NH_3$ produced per number of Brønsted acid sites) for the conversion of MPDA to resorcinol are likely to remain below one and thus the reaction can hardly be classified as catalytic. The zirconium phosphates do show some degree of regenerability as observed for γ-ZrP400, which after 3 cycles still leads to good resorcinol yields (>70%). No commercial prices for zirconium phosphates are available. Since these compounds are less stable than H-ZSM-5, the use of zirconium phosphates for the present process is not viable. However, the regeneration of zirconium phosphates by means of aqueous HCL at ambient temperature [Alberti *et al.*, 1989] as a possible regeneration step has not been considered in the present investigation. Thereby, the framework structure of the zirconium phosphates may not be destroyed as quickly as observed for the kiln treated zirconium phosphates.

# Chapter 5

## Conclusions and Recommendations



In teaching man, experimental science results in lessening his pride more and more by proving to him every day that primary causes, like the objective reality of things, will be hidden from him forever and that he can only know relations
(Thomas Henry)

# 5. CONCLUSIONS AND RECOMMENDATIONS

The conversion of MPDA to resorcinol in the presence of an acid reagent is a consecutive reaction with the intermediate product being MAP. The reaction MPDA → MAP → resorcinol in the presence of an acid can be regarded as irreversible. Under the dilute reaction conditions (initial MPDA concentration = 26.4mmol/L and mineral acid < 200mmol/L), resorcinol is attainable in high yield and with high selectivity (resorcinol yield > 95mole-% for $H_2SO_4$ and $H_3PO_4$) at reaction temperatures between 225°C and 275°C. No conversion of MPDA is detected in the absence of an acid. From studies using mineral acids, it is deduced that the rate of reaction is directly proportional to the hydronium ion concentration. Kinetic analyses reveal that the protonation of MPDA or MAP molecules occurs quickly and that substitution of the protonated amine group by *ipso* attack of a hydroxyl group is the rate limiting step. The purpose of the mineral acid is thus to both provide hydronium ions and neutralise the ammonia produced in order to drive the reaction towards the production of resorcinol. This is also confirmed by means of a thermodynamic study where it is shown that the equilibrium conversion of MPDA in the absence of a mineral acid is poor.

Mole-balances over all sample points reveal that under all conditions a maximum of 5% of MPDA remains unaccountable. This can be due to the formation of polyethers, but may also be due to some additional interaction / adsorption of the MPDA with the stainless steel walls of the autoclave. The reaction studies with mineral acids confirm that the mineral acid ionisation constant and the acid concentration inside the reactor determines the extent of the production of polymeric ethers. Mineral acids having an ionisation constant greater than that of hydronium ions are hygroscopic at high concentrations and lead to the production of ethers once resorcinol is formed.

Other possibilities for the loss of MPDA can be the formation of low concentrations of di- or poly-phenylamines (other than 3,3'-diamino-

diphenylamine and 3-hydroxy,3'-amino-diphenylamine) that remain undetected by HPLC. These poly-phenylamines do break up as observed for 3,3'-diamino-diphenylamine and 3-hydroxy,3'-amino-diphenylamine. Since the initial rate of change of 3,3'-diamino-diphenylamine production is greater than zero, mechanistically the compound must be produced from 2 MPDA molecules. The initial rate of production observed for 3-hydroxy-3'-amino-diphenylamine suggests that it is produced consecutively. 3-Hydroxy-3'-amino-diphenylamine is most likely produced by the reaction of the amine group on a MAP molecule with one amine function group on the MPDA molecule. After prolonged reaction time the concentration of 3-hydroxy-3'-amino-diphenylamine tends to zero. Due to the presence of acid sites (homogeneous or heterogeneous) and water, the cleavage of the dimers, i.e., 3,3'-diamino-diphenylamine and 3-hydroxy,3'-amino-diphenylamine, is more likely to occur via acid hydrolysis of the –NH– group bridging the two phenyl rings. Therefore, the breaking up of 3,3'-diamino-diphenylamine would lead to the formation of 2 MAP molecules. The cleavage of 3-hydroxy,3'-amino-diphenylamine would lead to the formation of 1 resorcinol and 1 MAP molecule. It is, however, also feasible that the formation of the dimers is reversible due to a reaction equilibrium existing between the monomers and dimers (see, for example, the conversion of aniline to diphenylamine over partially metal-exchanged H-zeolites; Warawdekar and Rajadhyaksha, 1987).

Replacement of the mineral acids by aluminosilicates is possible, albeit at higher temperatures (275°C and above). The requirement for the higher temperature is due to the strong adsorption of MPDA on the surface of the aluminosilicate. The activity is found to be a function of the Brønsted acid site concentration, crystal diameter, and the aluminosilicate framework stability. The use of zeolites instead of mineral acids for the synthesis of resorcinol does not suppress the formation of 3,3'-diamino-phenylenediamine and 3-hydroxy,3'-amino-diphenylamine.

Although H-USY (Akzo Nobel, Si/Al = 5.6, $S_{BET}$ = 607$m^2$/g, $d_{crystal}$ = 0.4-0.6μm) and H-silica-alumina (Kalichemie, Si/Al = 6.9, $S_{BET}$ = 367$m^2$/g) have a high

concentration of Brønsted acid sites and show good activity during the initial reaction period, these aluminosilicates are very unstable and deactivate quite rapidly. From XRD it is concluded that the framework structure of H-USY is fully destroyed during the reaction, and BET-analyses on H-USY and silica-alumina show a 90% reduction in surface area. The dealumination of the framework aluminium with the ensuing destruction of Brønsted acid sites results in an incomplete reaction. The turnover number in terms of ammonia produced per Brønsted acid site is below 0.5.

H-Beta (Südchemie AG, Si/Al = 14.4, $S_{BET}$ = 557$m^2$/g, $d_{crystal}$ < 0.3μm) shows the highest activity of all the tested aluminosilicates (turnover number at 300°C = 1.6 mole $NH_3$ produced per mole Brønsted acid sites). Under the reaction conditions, however, the framework structure of H-Beta collapses partially with both XRD and $N_2$–BET analyses showing that the crystallinity of H-Beta after the reaction at 300°C is reduced to ca. 30% - 40% compared too that before the reaction. Therefore, the reusability of the regenerated (kiln treated) H-Beta is limited. The economic viability of using H-Beta as a reagent is slim since it is rather expensive.

The use of H-ZSM-5 zeolites with low silica / alumina ratios is more economically viable since the zeolites remain stable under the reaction conditions required for the conversion of MPDA to resorcinol. The activity of H-ZSM-5 (Südchemie AG, Si/Al = 22, $S_{BET}$ = 312$m^2$/g, $d_{crystal}$ = 0.5μm) is considerably greater than the activity of H-ZSM-5 (Südchemie AG, Si/Al = 13, $S_{BET}$ = 303$m^2$/g, $d_{crystal}$ = 1 - 5μm). This is despite the fact that H-ZSM-5 (Si/Al = 13) (turnover number at 300°C = 0.1 mole $NH_3$ per mole acid sites) has more Brønsted acid sites than H-ZSM-5 (Si/Al = 22) (turnover number at 300°C = 1.1 mole $NH_3$ per mole Brønsted acid sites). However, the activity of the zeolite is strongly dependent on the crystallite size. This is confirmed by means of a kinetic analysis.

Considering that the ammonia produced is greater than the number of Brønsted acid sites on some of the zeolites an equilibrium must exist between the ammonia adsorbed on the zeolite, the aqueous ammonia in bulk solution and the gaseous ammonia in reactor headspace. Therefore, the turnover number over a zeolite could be increased if the ammonia produced during the conversion of MPDA to resorcinol is removed from the bulk solution and the headspace, and this would be the easiest technique to drive the reaction towards the production of resorcinol. Since ammonia is volatile, an increase in the reaction temperature would result in more ammonia accumulating in the headspace. The reactor temperature has to be optimised by taking into account the construction and energy costs as well as the stability of the H-ZSM-5 zeolite, which is by far the most stable zeolite.

The method used to predict the equilibrium adsorption constants of MPDA, MAP and resorcinol by means of conducting adsorption studies at low temperatures (30°C, 50°C, 70°C) is flawed. The reason is simply that aluminosilicates act as 'concentrating vessels' that result in determining the heats of physisorption rather than chemisorption. As a recommendation, the heat of adsorption could be evaluated by means of a calorimeter in order to distinguish between the physisorbed and chemisorbed material.

Since the conversion of MPDA to resorcinol seems to proceed only on the more external region of the zeolites, the use of layered compounds such as zirconium phosphates are investigated as an attractive alternative. The swelling property of these layered materials would increase the utilisation of the total number of acid sites. Further, the ionogenic phosphate groups fixed onto the macromolecular zirconium phosphate plane would resemble the mineral phosphoric acid quite closely. These compounds are, however, not as stable as zeolite ZSM-5. The conversion of MPDA to resorcinol over the zirconium phosphate needs to be conducted at a lower reaction temperature (225°C or less) to minimise the leaching of phosphates into solution. Although, the turnover number calculated

for the hydrolysis of MPDA to resorcinol is ~0.6 moles $NH_3$ produced per mole acid sites, the resorcinol yield and selectivity is high, as with mineral phosphoric acid. The reaction in the presence of zirconium phosphates, however, cannot be classified as being catalytic, but the use of zirconium phosphates presents an opportunity to use a heterogeneous process as opposed to the traditional homogeneous routes.

The thermal stability of zirconium phosphates if compared to the aluminosilicates after being kiln treated at 400°C is relatively poor. As a recommendation, the zirconium phosphates could be regenerated chemically at ambient temperature in the presence of HCl [Alberti *et al.*, 1989].

# References

**Adrien, A. and Serjeant, E.P.**, *The Determination of Ionization Constants: a laboratory manual 3rd Ed.*, Chapman and Hall Inc., London, 1989.

**Akerlof, G.C. and Oshry, H.I.**, "The dielectric constant of water at high temperature and in equilibrium with its vapor", *J. Am. Chem. Soc.*, 72 (1950) 2844.

**Alberti, G. and Torracca, E.**, "Crystalline insoluble salts of polybasic metals – II. Synthesis of crystalline zirconium or titanium phosphate by direct precipitation", *J. Inorg. Nucl. Chem.*, 30 (1968) 317.

**Alberti, G. and Costantino, U.**, "Recent progress in the field of synthetic inorganic exchangers having a layered or fibrous structure", *J. Chromatogr.*, 102 (1974) 5-29.

**Alberti, G. and Costantino. U.**,"Recent progress in the intercalation chemistry of layered α-zirconium phosphate and its derivatives, and future perspectives for their use in catalysis", *J. Mol. Catal.*, 27 (1984) 235.

**Alberti, G., Casciola, M. and Costantino, U.**, "Inorganic ion-exchange pellicles obtained by delamination of α-zirconium phosphate crystals", *J. Colloid Interface Sci.*, 107 (1985) 256.

**Alberti, G., Bernasconi, M.G. and Casciola, M.**, "Preparation of γ-zirconium phosphate microcrystals with high degree of crystallinity and proton conductivity of their hydrogen and ammonium forms", *React. Polym.*, 11 (1989) 245.

**Alberti, G. and Costantino, U.**, "Layered solids and their intercalation chemistry" in *Two- and Three-Dimensional Inorganic Networks* (G. Alberti and T. Bein), *Compr. Supramol. Chem.*, Vol. 7, Chap. 1, Pergamon Press, Oxford, UK, 1996.

**Alberti, G., Dionigi, C., Giontella, E., Murcia-Mascaros, S. and Vivani, R.**, "Formation of colloidal dispersions of layered γ-zirconium phosphate in water/acetone mixtures", *J. Colloid Interface Sci.*, 188 (1997) 27.

**Albertsson, J.**, "Inorganic ion exchangers", *Acta Chem. Scand.*, 20 (1966) 1689.

**Allen, F.L.**, "New resorcinol plant benefits from better processing techniques", *Chem. Eng. (NY)*, Sept. 25 (1967) 118.

**Barrer, R.M.**, *Hydrothermal Chemistry of Zeolites*, p. 251, Academic Press, London, 1982.

**Barthomeuf, D.**, "Topology and maximum content of isolated species (Al, Ga, Fe, B, Si, ...) in a zeolite framework. An approach to acid catalysis", *J. Phys. Chem.*, 97 (1993) 10092.

**Beyerlein, R.A., Choi-Feng, C., Hall, J.B., Huggins, B.J. and Ray, G.J.**, "Effect of steaming on the defect structure and acid catalysis of protonated zeolites", *Top. Catal*, 4 (1997) 27.

**Breck, D.W.**, *Zeolite Molecular Sieves: Structure, Chemistry and Use*, Robert E. Krieger Publishing Company, Inc., Malabar, Florida, USA, 1974.

**Brunner, E., Ernst, H., Freude, D., Hunger, M., Krause, C.B., Prager, D., Reschetilowski, W., Schwieger, W. and Bergk, K.-H.**, "Solid-state n.m.r. and catalytic studies of mildly hydrothermally dealuminated HZSM-5", *Zeolites*, 9 (1989) 282.

**Cabani, S. and Gianni, P.**, *Thermodynamic Data for Biochemistry and Biotechnology* (H.-J. Hinz, Ed.), Springer-Verlag, Berlin, 1986.

**Camblor, M.A. and Pérez-Pariente**, "Crystallization of zeolite beta: effect of Na and K ions", *Zeolites*, 11 (1991) 202.

**Campbell, S.M., Bibby, D.M., Coddington, J.M., Howe, R.F. and Meinhold, R.H.**, "Dealumination of HZSM-5 zeolites: I. Calcination and hydrothermal treatment", *J. Catal.*, 161 (1996) 338.

**Chen, N.Y.**, "Hydrophobic Properties of Zeolites", *J. Phys. Chem.*, 80 (1976) 60.

**Chiou, C.C.T. and Manes, M.**, "Application of the Polanyi Adsorption potential theory to adsorption from solutes on activated carbon. V. Adsorption from water of some solids and their melts, and a comparison of bulk and adsorbate melting points", *J. Phys. Chem.*, 78 (1974) 622.

**Christensen, A.N., Andersen, E.K., Andersen, I.G.K., Alberti, G., Nielsen, M and Lehmann, M.S.**, "X-ray powder diffraction study of layer compounds. The crystal structure of α-$Ti(HPO_4)_2 \cdot H_2O$ and a proposed structure for γ-$Ti(PO_4)(H_2PO_4) \cdot 2H_2O$", *Acta Chem. Scand.*, 44 (1990) 865.

**Chu, C.T-W. and Chang, C.D.**, "Isomorphous substitution in zeolite frameworks. 1. Acidity of surface hydroxyls in [B]-, [Fe]-, [Ga]-, and [Al]-ZSM-5", *J. Phys. Chem.*, 89 (1985) 1569.

**Clayden, N.J.**, "Solid-state nuclear magnetic resonance spectroscopic study of γ-zirconium phosphate", *J. Chem. Soc., Dalton Trans.*, (1987) 1877.

**Clearfield, A. and Stynes, J.A.**, "The preparation of crystalline zirconium phosphate and some observations on its ion exchange behaviour", *J. Inorg. Nucl. Chem.*, 26 (1964) 117.

**Clearfield, A., Blessing, R.H. and Stynes, J.A.** "New crystalline phases of zirconium phosphate possessing ion-exchange properties", *J. Inorg. Nucl. Chem.*, 30 (1968) 2249.

**Clearfield, A. and Smith, G.D.**, "The crystallography and structure of α-zirconium bis(monohydrogen orthophosphate) monohydrate", *Inorg. Chem.*, 8 (1969) 431.

**Clearfield, A. and Pack, S.P.**, "Factors determining ion exchange selectivity-I. High temperature phases formed by α-zirconium phosphate and its sodium and potassium exchanged forms", *J. Inorg. Nucl. Chem.*, 37 (1975) 1283.

**Clearfield, A. and Hunter, R.A.**, "On the mechanism of ion exchange in zirconium phosphates. XIV. The effect of crystallinity on $NH_4^+/H^+$ exchange of α-zirconium phosphate", *J. Inorg. Nucl. Chem.*, 38 (1976) 1085.

**Clearfield, A. and Djuric, Z.**, "On the mechanism of ion exchange in zirconium phosphate-XXV. Exchange of surface protons with ammonium ion", *J. Inorg. Nucl. Chem.*, 41 (1978) 903.

**Clearfield, A. and Tindwa, R.M.**, "On the mechanism of ion exchange in zirconium phosphates-XXI", *J. Inorg. Nucl. Chem.* 41 (1979) 871.

**Clearfield, A. and Thakur, D.S.**, "The acidity of zirconium phosphates in relation to their activity in the dehydration of cyclohexanol", *J. Catal.*, 65 (1980) 185.

**Clearfield, A.**," Group IV phosphates as catalysts and catalyst supports", *J. Mol. Catal.*, 27 (1984) 251.

**Clearfield, A., Roberts, B.D. and Subramanian, M.A.**, "Preparation of $(NH_4)Zr_2(PO_4)_3$ and $HZr_2(PO_4)_3$", *Mater. Res. Bull.*, 19 (1984) 219.

**Clearfield, A.**, "Ion exchange and adsorption in layered phosphates", *Mater. Chem. Phys.*, 35 (1993) 257.

**Clearfield, A. and Costantino, U.**, "Layered metal phosphates and their intercalation chemistry" in *Two- and Three-Dimensional Inorganic Networks* (G. Alberti and T. Bein, Eds.), *Compr. Supramol. Chem.*, Vol. 7, Chap. 4, Pergamon Press, Oxford, UK, 1996.

**Costantino, U.**, "Intercalation of Alkanols and Glocols into zirconium(IV) hydrogenphosphate monohydrate", *J. Chem. Soc., Dalton Trans.*, (1979) 402.

**Costantino, U.**, "Intercalation of alkanols and alkylamines in insoluble acid salts of tetravalent metals having layered structure of γ-type", *J. Inorg. Nucl. Chem.*, 41 (1981) 1895.

**Costantino, U. and La Ginestra, A.**, "On the existance of pyrophosphates of tetravalent metals having a layered structure", *Thermochim. Acta*, 58 (1982) 179.

**Costantino, U., Massucci, M.A., La Ginestra, A., Tarola, M. and Zampa, L.**, "Intercalation of Heterocyclic Compounds in α-Zriconium Phosphate: Imidazole, Benzimidazole, Histamine and Histidine", *J. Inclusion Phenom.*, 4 (1986) 147.

**Costantino, U., Vivani, R., Zima, V. and Cernoskova, E.**, "Thermo-analytical study, phase transitions, and dimensional changes of α-$Zr(HPO_4)_2 \cdot H_2O$ large crystals", *J. Solid State Chem.*, 132 (1997) 17.

**Cvetanovic, R.J. and Amenomiya, Y., 1967**, "Application of a temperature-programmed desorption technique to catalyst studies", *Adv. Catal.*, 17 (1967) 103.

**Cvetanovic, R.J. and Amenomiya, Y.**, "A temperature programmed desorption technique for investigation of practical catalysis", *Catal. Rev.*, 6 (1973) 21.

**Dabrowski, A. and Jaroniec, M.**, "Theoretical foundations of physical adsorption from binary non-electrolytic liquid mixtures on solid surfaces: present and future", *Adv. Colloid Interface Sci.*, 27 (1987) 211.

**Dabrowski, A., Jaroniec, M. and Oscik, J.**, "Multilayer and monolayer adsorption from liquid mixtures of nonelectrolytes on solid surface" in *Surf. Colloid Sci.* (E. Matijevic, Ed.) Vol. 14, p. 83, Plenum Press, NY, 1987.

**Daubert, T.E. and Danner, R.P.**, *Physical and Thermodynamic Properties of Pure Chemicals: Data Compilation*, Hemisphere Pub. Corp., NY, 1989.

**Dékány, I. And Szirtes, L.**, "Adsorption and microcalorimetric investigations of n-butylamine intercalation in $\alpha$- and $\gamma$-zirconium phosphates", *J. Radioanal. Nucl. Chem., Articles*, 190 (1995) 167.

**De Koning, A.J. and Mol, T.**, "A convenient method for the accurate determination of phosphorus in fish oils", *Fat Sci. Technol.*, 91 (1989) 36.

**Demmin, R.A. and Gorte, R.J.**, "Influence of adsorption and mass transfer effects on temperature-programmed desorption from porous catalysts", *J. Catal.*, 90 (1984) 32.

**Dempsey, E.**, "Acid strength and aluminium site reactivity of Y zeolites" *J. Catal.*, 33 (1974) 497.

**Derouane, E.G.**, "New aspects of molecular shape-selectivity: catalysis by zeolite ZSM-5" in *Catalysis by Zeolites* (B. Imelik, C. Naccache, Y. Ben Taarit, J.C. Vedrine, G. Coudurier and H. Praliaud, Eds.), *Stud. Surf. Sci. Catal.*, Vol 5, p. 5, Elsevier, Amsterdam, 1980.

**Derouane, E.G. and Vedrine, J.C.**, "On the role of shape selectivity in the catalytic conversion of alcohols and simple hydrocarbon molecules on zeolite ZSM-5", *J. Mol. Catal.*, 8 (1980) 479.

**Derouane, E.G., Andre, J.-M. and Lucas, A.A.**, "Surface curvature effects in physisorption and catalysis by microporous solids and molecular sieves", *J. Catal.*, 110 (1988) 58.

**Derylo-Marczewska, A. and Jaroniec, M.**, "Adsorption of organic solutes from dilute solutions on solids" in *Surf. Colloid Sci.* (E. Matijevic, Ed.), Vol. 14, p. 301, Plenum Press, NY, 1987.

**Dessau, R.M.**, "Selective Sorption Properties of Zeolites" in *Adsorption and Ion Exchange with Synthetic Zeolites: Principles and Practice: based on a Symposium sponsored by the Division of Industrial and Engineering Chemistry at the 180th meeting of the American Chemical Society, San Francisco, California, August 25-26, 1980* (W.H. Flank, Ed.), *ACS Symp. Ser.*, Vol. 135, p. 123, American Chemical Society, Washington D.C., 1980.

**De Vos Burchart, E., van Bekkum, H. and van de Graaf, B.**, "Molecular mechanics studies on MFI-type zeolites: Part 3. The monoclinic-orthorhombic phase transition", *Zeolites*, 13 (1993) 212.

**Dressler, H.**, *Resorcinol: Its Uses and Derivatives*, Plenum Press, New York, 1994.

**Dyer, A. and Leigh, D.**, "Comments on the structure of zirconium phosphate", *J. Inorg. Nucl. Chem.*, 34 (1972) 369.

**Eckert, C.A., Chandler, K., Deng, F., Dillow, A.K. and Liotta, C.I.**, "Alkylation reactions of near-critical water in the absence of acid catalysts", *Ind. Eng. Chem. Res.*, 36 (1997) 5175.

**Einicke, W.-D., Heuchel, M., v.Szombathely, M., Bräuer, P., Schöllner, R., and Rademacher, O.**, "Liquid-phase adsorption of binary ethanol-water mixtures on NaZSM-5 zeolites with different silicon/aluminium ratios", *J. Chem. Soc., Faraday Trans. I*, 85 (1989) 4277.

**Engelhardt, G., Lohse, U., Patzelova, V., Mägi, M. and Lippmaa, E.**, "High resolution $^{29}Si$ n.m.r. of dealuminated Y-zeolites. 1. The dependence of the extent of dealumination on the degree of ammonium exchange and the temperature and water vapour pressure of the thermochemical treatment", *Zeolites*, 3 (1983) 233.

**Espina, A., Garcia, J.R., Guil, J.M., Jaimez, E., Parra, J.B. and Rodriguez, J.**, "Calorimetric study of amine adsorption in α- and γ-titanium phosphate", *J. Phys. Chem. B*, 102 (1998) 1713.

**Everett D.H.**, "Thermodynamics of adsorption from solution", *J. Chem. Soc., Faraday Trans.*, 61 (1965) 2478.

**Feast, S. and Lercher, J.A.**, "Synthesis of Intermediates and Fine Chemicals using Molecular Sieve Catalysts" in *Recent Advances and new Horizons in Zeolite Science and Technology* (H. Chon, S.I. Woo and S.-E. Park, Eds.), *Stud. Surf. Sci. Catal.*, Vol. 102, p. 363, Elsevier, Amsterdam, 1996.

**Feldkamp, J.R. and Stauffer, T.R.**, "Interaction of binary solvents with charged exandable clays. 1. Theory", *J. Phys. Chem.*, 98 (1994) 13594.

**Fellmann, J.D., Saxton, R.J. and Tung, P.**, "Process for manufacture of resorcinol", *US Pat. 5 233 095* (1991).

**Flanigen, E.M.**, "Zeolites and molecular sieves. An historical perspective" in *Introduction to Zeolite Science and Practice* (H. van Bekkum, E.M. Flanigen, J.C. Jansen, Eds.), *Stud. Surf. Sci. Catal.*, Vol. 58, p. 13, Elsevier, Amsterdam, 1991.

**Freeman, J.J. and Unland, M.L., 1978**, "Laser Raman Study of Benzene Adsorption on Alkali Metal X and Y Zeolites", *J. Catal.*, 54 (1978) 183.

**Fyfe, C.A., Goddi, G.C. and Kennedy, G.J.**, "Investigation of the conversion (dealumination) of ZSM-5 into silicalite by high-resolution solid-state $^{29}Si$ and $^{27}Al$ mass nmr spectroscopy", *J. Phys. Chem.*, 88 (1984) 3248.

**Gaffney, T.R., Pierantozzi, T, Seger, M.R.**, "Isomorphous substitution of boron in mordenite and zeolite Y", in *Zeolite Synthesis* (M.L. Occelli and H.E. Robson, Eds.), *ACS Symp. Ser.*, Vol. 398, p. 374, American Chemical Society, Washington D.C., 1989.

**Gorte, R.J.**, "Design parameters for temperature programmed desorption from porous catalysts", *J. Catal.*, 75 (1982) 164.

**Granquist, W.T., and McAtee, J.L.**, "The Gelation of Hydrocarbons by Montmorillonite Organic Complexes", *J. Colloid Sci.*, 18 (1963) 409.

**Greco, N.P.**, "Verfahren zur Herstellung von Resorcin", *Ger. Pat. 1 808* 389 (1968).

**Greco, N.P.**, "Resorcinol manufacture", *US Pat. 3 462 497* (1969).

**Greco, N.P.**, "Resorcinol preparation", *US Pat. 3 862 245* (1972).

**Greco, N.P.**, "Hydrolysis of meta-phenylenediamine", *US Pat. 3 862 246* (1972).

**Greco, N.P.**, "Preparation of resorcinol and substituted resorcinols by liquid-phase dehydrogenation of 1,3-cyclic diones derived by vapor-phase cyclization of delta-keto carboxylic acid esters", *US Pat. 4 431 848* (1982).

**Haag, W.O. and Chen, N.Y.**, "Catalyst design with zeolites" in *Catalyst Design: Progress and Perspectives* (L.L. Hegedus, Ed.), p. 163, John Wiley and Sons, New York, 1987.

**Haase, F. and Sauer, J.**, "$^{1}$H NMR Chemical Shifts of Ammonia, Methanol and Water Molecules Interacting with Brønsted Acid Sites of Zeolite Catalysts: Ab-Initio Calculations", *J. Phys. Chem.*, 98 (1994) 3083.

**Haber, J.**, "Crystallography of Catalyst Types" in *Catal. Sci. Technol.* (J.R. Anderson and M. Boudart, Eds.) Vol. 2, p. 69, Springer-Verlag, Berlin, 1981.

**Hardenberg, T.A.J., Mertens, L., Mesman, P., Muller, H.C. and Nicolaides, C.P.**, "A catalytic method for the quantitative evaluation of crystallinities of ZSM-5 zeolite preparations", *Zeolites*, 12 (1992) 685.

**Hattori, T., Ishiguro, A. and Murakami, Y.**, "Acidity of crystalline zirconium-phosphate", *J. Inorg. Nucl. Chem.*, 40 (1977) 1107.

**Hedge, S.G., Kumar, R., Bhat, R.N. and Ratnasamy, P**, "Characterisation of the acidity of zeolite Beta by FTIR spectroscopy and TPD of $NH_3$", *Zeolites*, 9 (1989) 231.

**Herzog-Cance, M.-H., Jones, D.J., El Mejjad, R., Rozière, J. and Tomkinson, J.**, "Study of ion exchange and intercalation of organic bases in layered substrates by vibrational spectroscopy", *J. Chem. Soc., Faraday Trans.*, 88 (1992) 2275.

**Hidaglo, C.V., Itoh, H., Hattori, T., Niwa, M. and Murakami, Y.** "Measurement of the acidity of various zeolites by temperature-programmed desorption of ammonia", *J. Catal.*, 85 (1984) 362.

**Higgins, J.B., LaPierre, R.B., Schlenker, J.I., Rohrman, A.C., Wood, J.D., Kerr, G.T. and Rohrbaugh, W.J., 1988**, "The framework topology of zeolite beta", *Zeolites*, 8 (1988) 446.

**Hong, H. Y-P.**, "Crystal structures and crystal chemistry in the system $Na_{1+x}Zr_2Si_xP_{3-x}O_{12}$", *Mater. Res. Bull.*, 11 (1976) 173.

**Hopkins, P.D.**, "Adsorption of Hydrocarbons on Sodium and Demetallated Synthetic Faujasites", *J. Catal.*, 29 (1973) 112.

**Hoppe, R., Alberti, G., Costantino, U., Dionigi, C., Schulz-Ekloff, G. and Vivani, R.**, "Intercalation of dyes in layered zirconium phosphates. 1. Preparation and spectroscopic characterisation of α-zirconium phosphate crystal violet compounds", *Langmuir*, 13 (1997) 7252.

**Horsley, S.E., Nowell, D.V. and Stewart, D.T.**, "The infrared and Raman spectra of α-zirconium phosphate", *Spectrochim. Acta, Part A: Mol. Spectrosc.*, 30 (1974) 535.

**Jaroniec, M., Marczewski, A.W., Einicke, W.D., Herden, H. and Schöllner, R., 1983**, "Adsorption of 1-tetradecene / dodecane mixtures on different types of zeolites", *Monatsh. Chem.*, 114 (1983) 857.

**Jones, D.M. and Griffin, G.L.**, "Saturation effects in temperature-programmed desorption spectra obtained from porous catalysts", *J. Catal.*, 80 (1983) 40.

**Kaeding, W.W.**, "Production of para-diisopropylbenzene and use of same in the production of hydroquinone", *EU Pat. 148 584* (1984).

**Katada, N., Iijima, S., Igi, H. and Niwa, M.**, "Synthesis of aniline from phenol and ammonia over zeolite Beta" in *Progress in Zeolite and Microporous Materials* (H. Chon, S.-K. Ihm and Y.S. Uh, Eds.), *Stud. Surf. Sci. Catal.*, Vol. 105B, Elsevier, Amsterdam, 1997.

**Kazansky, V.B.**, "The nature of adsorbed carbenium ions as active intermediates in catalysis by solid acids", *Acc. Chem. Res.*, 24 (1991) 379.

**Kazansky, V.B.**, "The catalytic site from a chemical point of view" in *Advanced Zeolite Science and Applications* (J.C. Jansen, M. Stöcker, H.G. Karge and J. Weitkamp, Eds.), *Stud. Surf. Sci. Catal.*, Vol. 85, p. 251, Elsevier, Amsterdam, 1994.

**Kijima, T.**, "Intercalation of 2-aminopropylamino-substituted β-cyclodextrin by α- and γ-zirconium phosphates", *J. Chem. Soc., Dalton Trans.*, (1990) 425.

**Knacke, O., Kubaschewski, O. and Hesselmann, K.**, *Thermochemical Properties of Inorganic Substances 2nd Ed.*, Springer-Verlag, Berlin Heidelberg, 1991.

**Krossner, M. and Sauer, J.**, "Interaction of Water with Brønsted Acidic Sites of Zeolite Catalysts. Ab Initio Study of 1:1 and 2:1 Surface Complexes", *J. Phys. Chem.*, 100 (1996) 6199.

**Krumenacker, L., Costantini, M., Pontal, P. and Sentenac, J.**, "Hydroquinone, Resorcinol and Catechol" in *Kirk-Othmer Encycl. Chem. Technol. 4th Ed.* (J.I. Kroschwitz, M. Howe-Grant, C.A. Treacy, L.J. Humphreys, C. Punzo and L. Altieri, Eds.), Vol. 13, p. 996, John Wiley and Sons, New York, 1995.

**Kuhlmann, B., Arnett, E.M. and Siskin, M.**, "Classical organic reactions in pure superheated water", *J. Org. Chem.*, 59 (1994) 3098.

**La Ginestra, A. and Patrono, P.**, "Acidic properties of Ge, Ti, Zr and Sn phosphates and arsenates", *Mater. Chem. Phys.*, 17 (1987) 161.

**La Ginestra, A., Patrono, P., Berardelli, M.L., Galli, P., Ferragina, C. and Massucci, M.A.**, "Catalytic activity of zirconium phosphate and some derived phases in the dehydration of alcohols and isomerization of butenes", *J. Catal.*, 103 (1987) 346.

**Lok, B.M., Marcus, B.K. and Angell, C.L.**, "Characterisation of zeolite acidity. II. Measurement of zeolite acidity by ammonia temperature programmed desorption and FTIR spectroscopy techniques", *Zeolites*, 6 (1986) 185.

**Maijanen, A., Derouane, E.G. and Nagy, J.B.**, "Ft-ir and solid-state nmr investigation of surface hydroxyl-groups on dealuminated ZSM-5", *Appl. Surf. Sci.*, 75 (1994) 204.

**Marchese, L., Chen, J., Wright, P.A. and Thomas, J.M.**, "Formation of $H_3O^+$ at the Brønsted Site in SAPO-34 Catalysts", *J. Phys. Chem.*, 97 (1993) 8109.

**Marshall W.L. and Jones, E.V.**, "Second dissociation constant of sulfuric acid from 25 to 350° evaluated from solubilities of calcium sulfate in sulfuric acid solutions", *J. Phys. Chem.*, 70 (1966) 4028.

**Marshall, W.L. and Franck, E.U.**, "Ion product of water substance, 0-1000°C, 1-10000bar; new international formulation and its background", *J. Phys. Chem. Ref. Data*, 10 (1981) 295.

**McMurry, J., 1992**, *Organic Chemistry 3rd Ed.*, p. 560, Brooks/Cole Publishing Company, California, 1992.

**Meier, W.M., Kokotailo, G.T. and Olson, D.H.**, "Structure of synthetic zeolite ZSM-5", *Nature (London)*, Vol. 272 (1978) 437.

**Meier, W.M., Olson, D.H. and Baerlocher, Ch.**, *Atlas of Zeolite Structure Types, revised 4th Ed.*, Structure Commision of the IZA, Elsevier, Singapore, 1996.

**Mesmer, R.E. and Baes Jr., C.F.**, "Phosphoric acid dissociation equilibria in aqueous solutions to 300°C", *J. Solution Chem.*, 3 (1974) 307

**Meyer, P.J.N., Penders, J.M. and Stamicarbon, B.V.**, "Process for the preparation of delta keto-acids and derivatives thereof", *US Pat. 4 267 362* (1979).

**Müller, W.H., Mack, K.E. and Hey, H.**, "Process for the manufacture of resorcinols from delta-carboxylic acid esters" *US Pat. 4 250 336* (1979).

**Musso, H.**, "Phenol Coupling" in *Oxidative Coupling of Phenols* (W.I. Taylor and A.R. Battersby, Eds.), *Org. Subst. Nat. Origin*, Vol. 1, p. 1, Edward Arnold, London, 1967.

**Myers, A.L. and Sircar, S.**, "Statistical thermodynamics of adsorption from liquid mixtures on solids. I. Ideal adsorbed phase", *J. Phys. Chem.*, 74 (1970) 2828.

**Myers, A.L. and Sircar, S.**, "A thermodynamic consistency test for adsorption of liquids and vapors on solids", *J. Phys. Chem.*, 76 (1972) 3412.

**Narita, E., Horiguchi, N. and Okabe, T.**, "Adsorption of phenol, cresols, and benzyl alcohol from aqueous solution by silicalite", *Chem. Lett.*, (1985) 787.

**n.n.**, *Chem. Market Reporter*, 23 November 2000.

**Pelmenschikov, A.G. and Van Santen, R.A.**, "Water adsorption on Zeolites: Ab-initio Interpretation of IR Data", *J. Phys. Chem.*, 97 (1993) 10678.

**Perry, R.H., Green, D.W. and Maloney, J.O.**, *Perry's Chemical Engineers' Handbook*, 6th Ed., McGraw-Hill, Malaysia, 1984.

**Parton, R.F., Jacobs, J.M., Huybrechts, D.R and Jacobs, P.A.**, "Shape-selective catalysis in zeolites with organic substrates containing oxygen" in *Zeolites as Catalysts, Sorbents, and Detergent Builders: Applications and Innovations, 1988* (H.G. Karge and J. Weitkamp, Eds.), *Stud. Surf. Sci. Catal.*, Vol. 46, p. 163, Elsevier, Amsterdam, 1989.

**Poojary, D.M., Zhang, B., Dong, Y., Peng, G. and Clearfield, A.**, "X-ray powder structure of monoammonium-exchanged phase of γ-zirconium phosphate, $Zr(PO_4)(NH_4HPO_4)$", *J. Phys. Chem.*, 98 (1994) 13616.

**Poojary, D.M., Sheizer, B. and Clearfield, A.**, "X-ray powder structure and Rietveld refinement of γ-zirconium phosphate, $Zr(PO_4)(H_2PO_4)\cdot 2H_2O$", *J. Chem. Soc., Dalton Trans.*, (1995) 111.

**Quist, A.S., Marshall, W.L. and Jolley, H.R.**, "Electrical conductance of aqueous solutions at high temperature and presser. II. The conductance and ionization constants of sulfuric acid-water solutions from 0 to 800° and at pressures up to 4000 bars", *J. Phys. Chem.*, 69 (1965) 2726.

**Ratnasamy, P., Bhat, R.N., Pokhiriyal, S.K., Hedge, S.G. and Kumar, R.**, "Reactions of Aromatic Hydrocarbons over Zeolite β", *J. Catal.*, 119 (1989) 65.

**Ramis, G., Busca, G., Lorenzelli, V., La Ginestra, A., Galli, P. and Massucci, M.A.**, "Surface acidity of the layered pyrophosphates of quadrivalent Ti, Zr, Ge, and Sn and their activity in some acid-catalysed reactions", *J. Chem. Soc., Dalton Trans.*, (1988) 881.

**Ravi, V.P., Jasra, R.V. and Bhat, T.S.G.**, "Adsorption of phenol, cresol isomers and benzyl alcohol from aqueous solutions on activated carbon at 278, 298 and 323K", *J. Chem. Technol. Biotechnol.*, 71 (1998) 173.

**Reynolds Jr., R.C.**, "Principles of powder diffraction" in *Modern Powder Diffraction* (D.L. Bish and J.E. Post, Eds.), *Rev. Mineral.*, Vol. 20, p. 1, Mineralogical Society of America, Washington, 1989.

**Rollmann, L.D.**, "Selective poisoning of ZSM-5 by nitrogen heterocyclics" in *Catalyst Deactivation* (C.H. Bartholomew and J.B. Butt, Eds.), *Stud. Surf. Sci. Catal.*, Vol. 68, p. 791, Elsevier, Amsterdam, 1991.

**Romano, U, Esposito, A., Maspero, F., Neri, C. and Clerici, M.G., 1990**, "Selective oxidation with Ti-silicate" in *New Developments in Selective Oxidation* (G. Centi and F. Trifiro, Eds.), *Stud. Surf. Sci. Catal.*, Vol. 55, p. 33, Elsevier, Amsterdam, 1990.

**Ruthven, D.M.**, *Principles of Adsorption and Adsorption Processes*, p. 62, John Wiley and Sons, New York, NY, 1984.

**Sandler, S.I.**, *Chemical and Engineering Thermodynaimcs 2nd Ed.*, John Wiley & Sons Inc., Singapore, 1989.

**Sauer, J.**, "Acidic sites in heterogeneous catalysis: structure, properties and acidity", *J. Mol. Catal.*, 54 (1989) 312.

**Schay, G. and Nagy, L.G.**, "Nouveaux aspects de i'interprétation des isothermes d'absorption de mélanges liquides binaires sur des surfaces solids", *J. Chim. Phys.*, 58 (1961) 149.

**Sheldon, R.A.**, "Selective catalytic synthesis of fine chemicals: opportunities and trends", *J. Mol. Catal., A: Chem.*, 107 (1996) 75.

**Shriver, D.F., Atkins, P.W. and Langford, C.H.**, *Inorganic Chemistry 2nd Ed*, University Press Oxford, Oxford, 1994.

**Sidgwick, N.V. and Callow, R.K.**, "The solubility of aminophenols", *J. Chem. Soc.*, 125 (1924) 522.

**Simon, M.W., Nam, S.S., Xu, W-Q., Suib, S.L., Edwards, J.C. and O'Young, C-L.**, "Effects of $B^{3+}$ content of B-ZSM-11 and B-ZSM-5 on acidity and chemical and thermal stability", *J. Phys. Chem.*, 96 (1992) 6381.

**Sircar, S. and Myers, A.L.**, "Prediction of adsorption at liquid-solid interface from adsorption isotherms of pure unsaturated vapors", *AIChE J.*, 19 (1973) 159.

**Smith, L., Cheetham, A.K., Morris, R.E., Marchese, L., Thomas, J.M., Wright, P.A. and Chen, J.**, "On the Nature of Water Bound to a Solid Acid Catalyst", *Science (Washington, D.C.)*, 271 (1996) 799.

**Subramanian, M.A., Roberts, B.D. and Clearfield, A.**, "On the proton conductor $(H_3O)Zr_2(PO_4)_3$", *Mater. Res. Bull.*, 19 (1984) 1471.

**Sykes. P.**, *A Guidebook to Mechanism in Organic Chemistry 6th Ed.*, Longman Scientific & Technical, Singapore, 1992.

**Szirtes, L. and Raieh, A.O.**, "Preparation of some intercalation compounds of layered γ-zirconium phosphate and zirconium phosphate-phosphite", *Solid State Ion.*, 46 (1991) 69.

**Theissen, R.J.,**, "A new method for the preparation of α-β-unsaturated carbonyl compounds", *J. Org. Chem.*, 36 (1971) 752.

**Topsoe, N.Y., Pedersen, K. and Derouane, E.G.**, "Infrared and temperature-programmed desorption study of the acidic properties of ZSM-5-type zeolites", *J. Catal.*, 70 (1981) 41.

**Treacy, M.M.J. and Newsam, J.M.**, "Two new three-dimensional twelve-ring zeolite frameworks of which zeolite beta is a disordered intergrowth", *Nature (London)*, 332 (1988) 249.

**Treacy, M.M.J., Higgins, J.B. and von Ballmoos, R.**, in *Collection of Simulated XRD Powder Patterns for Zeolites 3rd revised Ed.* (L.V.C. Rees and R. von Ballmoos, Eds.), Elsevier, New York, 1996.

**Troup, J.M. and Clearfield, A.**, "On the mechanism of ion exchange in zirconium phosphates 20. Refinement of the crystal structure of α-zirconium phosphate", *Inorg. Chem.*, 16 (1977) 3311.

**Van de Mond, T.J. and Delahaye, H.J.A.**, "Process for the preparation of cyclohexanone", *US Pat. 4 250 118* (1981).

**Van Krevelen, D.W. and Chermin, H.A.G.**, "Estimation of the free enthalpy (Gibbs free energy) of formation of organic compounds from group contributions", *Chem. Eng. Sci.*, 1 (1952) 66.

**Van Santen, R.A.**, "Theory of Brønsted Acidity in Zeolites" in *Advanced Zeolite Science and Applications* (J.C. Jansen, M. Stöcker, H.G. Karge and J. Weitkamp, Eds.), *Stud. Surf. Sci. Catal.*, Vol. 85, p. 273, Elsevier, Amsterdam, 1994.

**Varagnat, J.**, "Hydroquinone, Resorcinol and Catechol" in *Kirk Othmer Encycl. Chem. Technol. 3rd Ed.* (M. Grayson, D. Eckroth, H.F. Mark, D.F. Othmer, C.G. Overberger and G.T. Seaborg, Eds.), Vol. 13, p. 39, John Wiley and Sons, New York, 1981.

**Vassena, D., Malossa, D., Kogelbauer, A. and Prins, R.**, "Zeolites as catalysts for the selective para-nitration of toluene" in *Proceedings of the 12th International Zeolite Conference* (Treacy, M.M.J, Marcus, B.K., Bisher, M.E. and Higgins, J.B., Eds.), Vol. II, p. 1471, Material Research Society, Warrendale, Pennsylvania, 1999.

**Venuto, P.B. and Wu, E.L.**, "Sorption and exchange patterns of benzene-phenolic mixtures over faujasite catalysts: relevance to phenol ethylation", *J. Catal.*, 15 (1969) 205.

**Venuto, P.B.**, "Organic catalysis over zeolites: a perspective on reaction paths within micropores", *Microporous Mater.*, 2 (1994) 297.

**Vesely, V., Pekarek, V. and Ruvarac, A.**, "Correlation of sorption properties and hydrolysis behaviour for various types of zirconium phosphates", *Bull. Soc. Chim. Fr.*, (1968) 1832.

**Vidic, R.D., Suidan, M.T., Traegner, U.K. and Nakhla, G.F.**, "Adsorption isotherms: illusive capacity and role of oxygen", *Water Res.*, 24 (1990) 1187.

**Viljava T.-R. and Krause, A.O.I.**, "Hydrogenolysis reactions in a batch reactor: Effect of mass balance inaccuracies on the kinetic parameters", *Appl. Catal A: Gen.*, 135 (1996) 317.

**Von Ballmoos, R. and Meier, W.M.**, "Oxygen-18 exchange between zeolite ZSM-5 and water", *J. Phys. Chem.*, 86 (1982) 2698.

**Wang, Q.L., Giannetto, G., Torrealba, M., Perot, G., Kappenstein, C. and Guisnet, M.**, "Dealumination of Zeolites: II. Kinetic Study of Dealumination by Hydrothermal Treatment of a $NH_4NaY$ Zeolite", *J. Catal.*, 130 (1991) 459.

**Wang, Q.L., Giannetto, G. and Guisnet, M.**, "Dealumination of Zeolites: III. Effect of Extra-Framework Aluminium Species on the Activity, Selectivity of Y Zeolites in n-Heptane Cracking", *J. Catal.*, 130 (1991) 471.

**Warawdekar, M.G. and Rajadhyaksha, R.A.**, "Aromatic nucleophilic substitutions on zeolites. I. Amination of anisole and phenol", *Zeolites*, 7 (1987) 574.

**Warawdekar, M.G. and Rajadhyaksha, R.A., 1987**, "Aromatic nucleophilic substitutions on zeolites. II. Conversion of aniline to diphenylamine", *Zeolites*, 7 (1987) 579.

**Weast, R.C., Astile, M.J. and Beyer, W.E.**, *CRC Handbook of Chemistry and Physics 67th Ed.*, CRC Press Inc., Boca Raton, 1986-1987.

**Weber, R.W.**, *The inertisation of the zeolites ZSM-5, mordenite and beta by chemical vapour deposition using tetraethoxysilane*, PhD Thesis, University of Cape Town, 1998.

**Wittrock, C., and Kohler, H.-H.**, "Thermodynamic relations for the noncalorimetrical determination of the Heat of Adsorption in multicomponent systems", *J. Phys. Chem.*, 97 (1993) 7730.

**Woolery, G.L., Alemany, L.B., Dessau, R.M. and Chester, A.W.**, "Spectroscopic evidence for the presence of interanl silanols in highly siliceous ZSM-5", *Zeolites*, 6 (1986) 14.

**Wu, C-Y.**, "Process for preparation of resorcinol", *US Pat. 4 849 549* (1987).

**Young, R.D.**, "Ammonium Compounds" in *Kirk-Othmer Encycl. Chem. Technol. 3rd Ed.* (M. Grayson, D. Eckroth, H.F. Mark, D.F. Othmer, C.G. Overberger and G.T. Seaborg, Eds.), Vol. 2, p. 533, Wiley and Sons, New York, 1978.

# Appendices

# APPENDIX - A

## Adsorption from Solution

The adsorption study is important for establishing the adsorption behaviour of aqueous MPDA, MAP and resorcinol onto the aluminosilicates and zirconium phosphates. The information obtained is also useful for kinetic reaction study, which includes establishing the adsorption equilibrium constants for the liquid-solid interaction at reaction temperature. The adsorption equilibrium constants for a two component system have to be determined indirectly, i.e., at conditions where no chemical transformation can occur [Dabrowski *et al.*, 1987]. These conditions are met by carrying out the adsorption isotherms at lower temperatures and then predicting the isotherm at reaction temperature using the Clausius-Clapeyron equation [Whittrock and Kohler, 1993].

The thermodynamic system consists of a liquid phase in contact with a solid phase (the adsorbent) with the portion of the liquid phase in close proximity to the adsorbent being termed the adsorbed phase. The boundary between the surface and bulk phases, however, cannot be determined explicitly. The adsorption of a liquid mixture is measured by the adsorption excess $\Gamma_2^e$ with

$$\Gamma_2^e = n_2^{\sigma(n)} / m = n^o (x_2^o - x_2^l) / m \qquad \textbf{A.1}$$

where $n^o$ is the total number of moles in the original solution, $n_2^{\sigma(n)}$ represents the reduced excess adsorption and $(x_2^o - x_2^l)$ is the change in the mole fraction of bulk liquid caused by an adsorption process on an adsorbent of mass $m$. The derivation of Equation A.1 requires the assumption that all molecules in solution must have equal access to the surface adsorbent, generally not entirely applicable to porous adsorbents such as zeolites with molecules (MPDA, MAP and resorcinol) considerably larger than water.

## A.1 ISOSTERIC ADSORPTION HEATS

For the case of an ideal dilute solution, the molar heat of adsorption, $\Delta h^{ad}$, of a single substance 2 dissolved in a solvent 1 can be determined from the temperature dependence of the adsorption isotherm by use of the Clausius-Clapeyron equation:

$$\Delta h^{ad} = -RT^2 \frac{\partial \ln x_2^l}{\partial T}\Big|_{p,\Gamma_2^e} \qquad \text{A.2}$$

where $x_2^l$ denotes the mole fraction of solute in the bulk phase and $\Gamma_2^e$ represents the surface excess given by Equation A.1. Plotting the isosteres for the compounds at various $\Gamma_2^e$ yields the adsorption enthalpy. However, the prediction of the adsorption isotherms at reaction temperature from the data gathered at lower temperatures requires some major assumptions. Although a change in the available solid surface area and the pressure can be assumed negligible, the enthalpy remains a strong function of the temperature as well as the amounts of substances present in the active bulk phase and in the surface phase [Wittrock and Kohler, 1993]. The extrapolation of the available data necessitates the assumption that the averaged $\Delta h^{ad}$ is independent of temperature. Additionally, the adsorption process has also been shown to be non-stoichiometric, with the amounts of the adsorbing substances exchanged between the bulk phase and the adsorbed phase not being coupled by constant ratios [Wittrock and Kohler, 1993]. The effect that temperature has on the densities of the compounds and thus the amounts present in the adsorbed phase tends to suggest that the exchange stoichiometry likewise is affected by a change in temperature.

Significant variations in the experimentally determined adsorption isotherms have been reported in literature [Vidic *et al.*, 1990] of which the allowed equilibration time and the solution pH of the aqueous solution were the dominant causes for discrepancies. The pH plays a major part during the adsorption of organic compounds from the aqueous solution since the alteration in the solute-solvent

interaction parameters caused by variations of the pH influences the amount adsorbed onto the solid as observed by Narita *et al.* [1985] studying the adsorption of phenol, cresols and benzyl alcohol from aqueous solution by silicalite. The time allocated for the equilibration is important in allowing enough time for an adsorbate-solid, solute-solvent equilibrium without the occurrence of possible side-reaction due to polymerisation or oxidation, which are commonly observed after prolonged periods [Vidic *et al.*, 1990]. Generally, the molar volume, functional groups, polarity and solubility of the solute in water determine the adsorption capacity [Derylo-Marczewska and Jaroniec, 1987].



### A.1.1 ADSORPTION ISOTHERM EQUATIONS

Adsorption from solution involves an exchange process in which the solvent molecules, i.e., water, are replaced from the solid surface by the adsorbate molecules, i.e., MPDA, MAP or resorcinol. The adsorption isotherm at a constant temperature is determined by the following parameters: (1) molecular interaction in the bulk phase; (2) molecular interaction in the surface phase; (3) interactions between the bulk and surface phases; and (4) molecular interaction at the solid/solution interface which is also a function of the structural and chemical heterogeneity of the solid surface. Dabrowski and Jaroniec [1987] extensively reviewed theoretical foundations for the adsorption of binary liquid mixtures on solid surfaces. However, the theoretical models described in this thesis are based on very simplistic but realistic models, describing the adsorption processes from dilute solutions. The assumed exchange process between the liquid and the adsorbed phases can be represented by a quasi-chemical equation:

$$(2)^l + r(1)^s \rightleftharpoons (2)^s + r(1)^l \qquad \textbf{A.3}$$

Variable $r$ represents the ratio of the limiting values of adsorption for both components. For a binary system, the change in the Gibbs adsorption energy is:

$$\Delta G_a \text{ at equilibrium} = G_2^s + r * G_1^l - G_2^l - r * G_1^s = 0 \qquad \textbf{A.4}$$

where $G_2^l$ partial molar Gibbs energy of compound in solution
$G_1^s$ partial molar Gibbs energy of solvent at surface
$G_2^s$ partial molar Gibbs energy of compound at surface
$G_1^l$ partial molar Gibbs energy of solvent in solution

The partial molar Gibbs energy for the sorbed components [Everett, 1965] may be written

$$G_i^s = G_{i*}^s + RT \ln x_i^s \gamma_i^s + (\sigma_{i,o} - \sigma) w_i \qquad \textbf{A.5}$$

where $G_{i*}^s$ is the partial molar Gibbs energy of pure $i$ in contact with solid and $\sigma_{i,o}$ is the interfacial tension of this surface. The interfacial tension at the solid/solution interface is denoted as $\sigma$, and $w_i$ is the partial molar area occupied by the $i$-th component. The full derivation of Equation A.5 in terms of a two-dimensional spreading pressure, $\pi$, is described in Ruthven [1984], with $\pi$ being defined as the difference between the interfacial tension of the pure solvent-solid interface and that of the solution-solid interface at the same temperature. For the case of layered zirconium phosphates, Equation A.5 would have to include an additional work term due to expansions required to allow molecules to diffuse into the interlayer region, as explained in Section 2.3 (Chapter 2). For layered aluminosilicates and charged expandable clays, Feldkamp and Stauffer [1994] associated the additional work term with the polarisation of the dielectric solution within the interlayer distance. Analogous to the partial molar Gibbs energy of the $i$-th component in the sorbed phase, that of the bulk phase is usually defined as

$$G_i^l = G_{i*}^l + RT \ln(x_i^l \gamma_i^s) + (p - p_{i,o}) V_i \qquad \textbf{A.6}$$

with the symbols $p$, $p_{i,o}$ and $V_i$ respectively denoting the vapour pressure of the solution, the vapour pressure of the $i$-th pure component and its molar volume. In contrast to Equation 2.42, the last term in Equation 2.43 is normally neglected.

Nevertheless, the partial molar Gibbs energy for both phases can be specified as

$$G_i^{\alpha} = G_{i*}^{\alpha}(T,p) + RT\ln(x_i^{\alpha}) + RT\ln(\gamma_i^{\alpha}); \mathrm{i} = 1,2; \alpha = \mathrm{l,s} \qquad \textbf{A.7}$$

with the term $(\sigma_{i,o} - \sigma)w_i$ in Equation A.5 assumed to be incorporated within the activity coefficients $\gamma_i^s$. Assuming a phase equilibrium between the adsorbed phase on the solid and the bulk phase not disturbed by the solid, an equilibrium constant $K_a$ for an energetically homogeneous surface is given by:

$$K_a = \frac{a_2^s * \left(a_1^l\right)^r}{a_2^l * \left(a_1^s\right)^r} = \frac{x_2^s \gamma_2^s}{x_2 \gamma_2^l} * \left[\frac{x_1 \gamma_1^l}{x_1^s \gamma_1^s}\right]^r \qquad \textbf{A.8}$$

Parameters $a_i^l$ and $a_i^s$ represent an activity in solution and an activity at the surface, respectively; $\gamma_i^l$ and $\gamma_i^s$ an activity coefficient in solution and at the surface. Usually a parallel-layer model, in which all molecules are in the parallel orientation towards the flat surface of the adsorbent, is used to represent the surface phase composed of molecules of different sizes [Dabrowski and Jaroniec, 1987]. In the case of zeolites it is supposed that the adsorbed phase is represented by the volume of the channel system [Einicke *et al.*, 1989]. In this respect, the Flory-Huggins theory is often applied to adsorption and solution mixtures of molecules of different sizes. Consequently, the mole fractions ($x_i^l$ and $x_i^s$) used in Equation A.8 are replaced by volume fractions $\phi_i^{\alpha}$, $\alpha$ = *l,s*, where for the adsorbed phase

$$\phi_1^s = \frac{x_1^s}{x_1^s + rx_2^s} \quad \text{and} \quad \phi_2^s = 1 - \phi_1^s = \frac{rx_2^s}{x_1^s + rx_2^s} \qquad \textbf{A.9}$$

and for the liquid phase,

$$\phi_1^l = \frac{x_1^l}{x_1^l + rx_2^l} \quad \text{and} \quad \phi_2^l = 1 - \phi_1^l = \frac{rx_2^l}{x_1^l + rx_2^l} \qquad \textbf{A.10}$$

According to Equation A.3, the term $r$ is equal to $v_2/v_1$, with $v_i$ being some measure of the volume of species $i$ [Sandler, 1987]. However, equalling the ratio $r$ to the ratio of the partial molar areas of components (1) and (2), i.e., $r = w_2/w_1$ tends to be preferred when dealing with adsorption because of Equation A.5 [Dabrowski and Jaroniec, 1987]. Alternatively, $r$ may also be determined experimentally by individual gas component adsorption of pure component $i$, carried out at the same temperature and the same adsorbent as the isotherm derived by the adsorption from solution. These limiting values of adsorption of component $i$ are represented by $n_{i,o}^s$, and $r$ thus equals $n_{1,o}^s/n_{2,o}^s$. Since water may occupy zeolite spaces that are not accessible to the aromatic compounds, it may be useful to determine $n_{2,o}^s$ (2 representing the larger molecule) using gas phase adsorption and to take $r$ as being equal to the ratio of the molar volumes of pure liquids.

The surface excess, given by Equation A.1, may also be expressed in terms of the concentration profile of the $i$'th component, i.e., $x_i = x_i(z)$, with $z$ denoting the distance from the Gibbs surface:

$$\Gamma_2^e = \frac{n_2^e}{m} = \frac{1}{m}\int_{z_0}^{\infty} \frac{x_2(z) - x_2^l}{x_2(z) + x_1(z)/r} dz \qquad \text{A.11}$$

where $z_0$, the distance of the Gibbs surface from the adsorbent surface, is assumed to be equal to zero [Dabrowski and Jaroniec, 1987]. Approximating the unknown concentration profile, $x_i(z)$, by a step function results in a clear distinction between the molecules forming the surface phase and the molecules forming the bulk phase. Referring to Figure A.1, The excess number of moles of compound (2) adsorbed, i.e., $n_2^e = \Gamma_2^e * m$, is represented by area I, whereas the total number of moles (2) adsorbed, or area I plus area II, is represented by $n_2^s$.

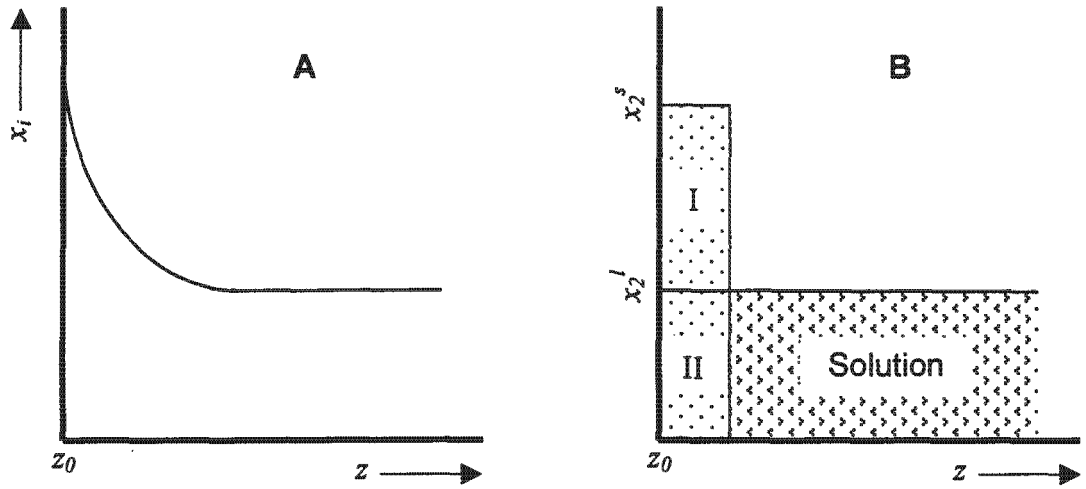


**Figure A.1** Concentration profile $x_i = x_i(z)$ representing real (part A) and step function adsorption systems [Dabrowski and Jaroniec, 1987].



The material balance equates $n_2^e$ to $n_2^s * (x_2^s - x_2^l)/x_2^s$ and since $x_2^s = n_2^s/(n_2^s + n_1^s)$, the following expression is obtained:

$$n_2^e = n_2^s x_1^l + n_1^s x_2^l \qquad \textbf{A.12}$$

Denoting $A_s$ as the total surface area of the adsorbent, and since $(n_1^s + n_2^s)/A_s$ equals $(\sum_i x_i^s w_i)^{-1}$, or $n_1^s/n_{1,o}^s + n_2^s/n_{2,o}^s = 1$ for microporous adsorbents [Dabrowski *et al.*, 1987], an expression for $x_2^s$ in terms of the surface excess is given by:

$$x_2^s = \frac{r(n_{2,o}^s/m)x_2^l + \Gamma_2^e}{r(n_{2,o}^s/m) + (1-r)\Gamma_2^e} \qquad \text{[Schay and Nagy, 1961]} \qquad \textbf{A.13}$$

Use of Equation A.13 allows for the evaluation of $x_2^s$ or $\phi_1^s$ and $\phi_2^s$ in Equation A.8. The equilibrium constant, $K_a$, is related to the molar heat of adsorption, $\Delta h^{ad}$, of a single substance 2 dissolved in a solvent 1 via the van't Hoff equation:

$$\frac{\partial \ln K_a}{\partial T}\Big|_{p,\sigma} = \frac{\Delta h^{ad}}{RT^2} \qquad \textbf{A.14}$$

where the molar heat of adsorption, $\Delta h^{ad}$, is assumed to remain independent of temperature. However, the use of Equation A.14 necessitates for the ratio of limiting values, $r$, in Equation A.8 to remain constant since $r$ is affected by the change in variable $n_{1,o}^{s}$ and $n_{2,o}^{s}$ due a change in their relative densities with temperature. Consequently, $n_{1,o}^{s}$ and $n_{2,o}^{s}$ have to remain independent of temperature.

### A.1.2 SIMPLIFICATIONS TO ISOTHERM EQUATIONS

Since only adsorption from very dilute solvent systems will be analysed, $\phi_1^{l}\gamma_1^{l}$ remains close to unity. Additionally, the variable $r$ in Equation A.3 could be set equal to 1, considering that the adsorbate molecule replaces a cluster of previously sorbed solvent molecules. Since the mole fraction of solvent in the adsorbed phase equals $1 - x_2^{s}$, Equation A.8 can be rewritten as:

$$K_a = \frac{x_2^{s}}{x_2^{l}(1-x_2^{s})} * \frac{\gamma_2^{s}}{\gamma_2^{l}\gamma_1^{s}} \qquad \textbf{A.15}$$

or

$$x_2^{s} = \frac{K_a x_2^{l}\gamma_2^{l}/b}{1 + K_a x_2^{l}\gamma_2^{l}/b} \qquad \textbf{A.16}$$

where $b = \gamma_2^{s}/\gamma_1^{s}$ is a function of temperature, interfacial tension and coverage, $x_i^{s}$. The UNIFAC group contribution model [Sandler, 1989] could be used to estimate $\gamma_2^{l}$, although the solutes MPDA, MAP and resorcinol are solids at 25°C and 1atm. The regular solution theory [Sandler, 1989] is another useful method for determining activity coefficients. The narrow concentration range of $x_2^{l}$ enables $\ln(\gamma_2^{l})$ to be represented by an arbitrary linear function $\alpha x_2^{l} + \beta$. The $b$ term must remain a function of coverage since the concentration of the adsorbed phase

varies considerably. The Flory-Huggins model would provide the best correlative activity coefficients since it is meant to apply to mixtures of molecules of different sizes. Also the number of parameters will be kept at a minimum. The Flory interaction parameter, $\chi^s$, originates by expressing the excess molar enthalpy on mixing as

$$\underline{H}^{ex} = \chi^s RT(x_1^s + rx_2^s)\phi_1^s\phi_2^s \qquad \textbf{A.17}$$

where $\phi_I^s$ are the volume fractions given by Equation A.9 [Sandler, 1989]. Since mixing two components results in part of the homogeneous contacts being replaced by inhomogeneous contacts, $\chi^s$ represents a ratio that relates the excess molar enthalpy due to ideal mixing to that of the real system. Including the entropic contribution in the excess molar Gibbs free energy [Sandler, 1987] allows for the activity coefficients to be expressed in terms of $\chi^s$

$$\ln\gamma_1^s = \ln\frac{\phi_1^s}{x_1^s} + \left(1 - \frac{1}{r}\right)\phi_2^s + \chi^s\left(\phi_2^s\right)^2 \qquad \textbf{A.18}$$

and

$$\ln\gamma_2^s = \ln\frac{\phi_2^s}{x_2^s} + (r-1)\phi_1^s + \chi^s\left(\phi_1^s\right)^2 \qquad \textbf{A.19}$$

On assumption that one adsorbate molecule replaces a cluster of previously sorbed solvent molecules and thus setting $r$ = 1 simplifies Equations A.18 and A.19, giving an expression for $b$ in terms of $\chi^s$

$$\ln b = \chi^s(1 - 2x_2^s) \qquad \textbf{A.20}$$

Due to the derivation of the Flory interaction parameter, only energetic interactions are considered. The Flory interaction parameter between components 1 and 2 in the adsorbed may also be written as

$$\chi^s = \frac{N_A Z^s}{RT}\left[\varepsilon_{12}^s - \frac{\varepsilon_{11}^s + \varepsilon_{22}^s}{2}\right] \qquad \textbf{A.21}$$

where $Z^s$ denotes the number of nearest neighbours of one molecule and $N_A$ the Avogadro's number. The molecular pair interactions between $i$ and $j$, $i$ and $i$, $j$ and $j$ are represented by the binary interaction energies $\varepsilon_{ij}^s$, $\varepsilon_{ii}^s$ and $\varepsilon_{jj}^s$. Consequently, if $ij$ contacts are preferred $\chi^s$ is negative, whereas a positive value suggest that $ii$ and $jj$ contacts a favoured. Therefore, positive values of $\chi^s$ would indicate that the adsorption of the solute is promoted whereas a negative $\chi^s$ implies that the adsorption is inhibited. Nevertheless, $\chi^s$ should not be too positive, since the derivation of the excess molar Gibbs free energy requires that the interaction of the compounds must not obstruct the random mixing of the components. However, the adsorption of basic solutes $MPDA_{(aq)}$ and $MAP_{(aq)}$ on acidic surfaces would suggest large positive values for $\chi^s$, allowing zeolites to serve as reactant concentrating "vessel" as suggested by Venuto [1994].

$K_a$ and $\chi^s$ are determined by least square fit of Equations A.16 and A.20 to the experimentally obtained adsorption isotherms with $x_2^s$ obtained by Equation A.13, setting $r$ = 1. Similar to the extrapolation of the equilibrium constant, $K_a$, to reaction temperature, $b(T, \sigma, x_i^s)$ may also be extrapolated assuming a constant interfacial tension and coverage [Sandler, 1989]:

$$\left(\frac{\partial \ln b(T,\sigma,x_2^s)}{\partial T}\right)_{\sigma,x_2^s} = -\frac{\overline{H}^{ex}(T,\sigma,x_2^s)}{RT^2} \qquad \textbf{A.22}$$

where, for the sake of simplicity, the excess partial molar enthalpy, $H^{ex}$, is assumed independent of temperature and coverage. Incorporating Equation A.18 in the above equation, yields:

$$\left(\frac{\partial \chi^s(T,\sigma)}{\partial T}\right)_{\sigma} = -\frac{\overline{H}^{ex}}{RT^2(1-2x_2^s)} \qquad \textbf{A.23}$$

### A.1.3 INCLUSION OF SURFACE HETEROGENEITY

The previous section considers surfaces that are energetically homogeneous rather than heterogeneous. On heterogeneous surfaces the affinity of an adsorbate for the surface strongly depends on the position and the energetic distribution of the surface [Dabrowski and Jaroniec, 1987]. Another contributing factor to the surface heterogeneity is the adsorption of aromatic molecules onto the pore walls inside the zeolitic micro-pores. Due to the molecules being attracted by all the pore walls, the interaction is larger than on a flat surface [Derouane *et al.*, 1988]. The Flory-Huggins theory of solution as explained above is generally applied. The presence of different types of adsorption sites therefore requires a limited number of different isotherms with corresponding $K_a$ values. For a continuous distribution of $ln(K_a)$, the following equation applies [Dabrowski and Jaroniec, 1987]

$$\phi_{1,t}^{s}(\phi_i^l) = \int_0^{\infty} \phi_{i,loc}^{s} * F[\ln(K_a)]\ d[\ln(K_a)] \qquad \textbf{A.24}$$

where the total volume fraction of the i-th component is given by $\phi_{i,s}^{s}$, with $\phi_{i,loc}$ representing the individual local isotherms characterised by $ln(K_a)$, and $F[(ln(K_a)]$ being a normalised distribution function of $ln(K_a)$. Application of a quasi-Gaussian distribution to Equation A.23 transforms Equation A.8 to

$$\tilde{K}_a = \frac{(\phi_{2,t}^{s})^{1/\pi}\gamma_2^{s}[\phi_1^{l}\gamma_1^{l}]^{r}}{[(\phi_{1,t}^{s})^{1/\pi}\gamma_1^{s}]^{r}\phi_2^{l}\gamma_2^{l}} \qquad \textbf{A.25}$$

where $\tilde{K}_a$ and $\pi$ characterise the distribution function, with $\tilde{K}_a$ denoting the peak position and $\pi$ the width of the distribution. The heterogeneity parameter $\pi$ can be assumed to be temperature dependent [Dabrowski and Jaroniec, 1987]; i.e.,

$$\pi = \pi_0 RT \qquad \textbf{A.26}$$

For the case of $r$ = 1, the overall isotherm reduces to the Langmuir-Freundlich equation [Dabrowski and Jaroniec, 1987], which if the same assumptions were made as in Section A.1.3, Equation A.16 is altered to:

$$x_2^s = \frac{[\tilde{K}_a x_2^l \gamma_2^l / b]^\pi}{1 + [\tilde{K}_a x_2^l \gamma_2^l / b]^\pi} \qquad \textbf{A.27}$$

The bulk phase activity coefficient, $\gamma_2^l$, and $b$ are calculated as illustrated above. The Flory parameter, $\chi^s$, and consequently $b$ will differ to the one calculated in Section A.1.2, since, in the previous section, the heterogeneous surface energies are effectively included in the Flory parameter. Consequently, an alternative equation has been proposed by Rudzinski *et al.* [Jaroniec *et al.*, 1983], by combining the surface activity coefficients with the heterogeneity parameter $\pi$ to form $\xi$, thus

$$K_a = \left(\frac{\phi_2^s}{\phi_1^s}\right)^{1/\xi} \frac{(\phi_1^l \gamma_1^l)^r}{\phi_2^l \gamma_2^l} \qquad \textbf{A.28}$$

### A.1.4 DISSOCIATION EFFECTS IN SOLUTE ADSORPTION

Apart from the surface heterogeneity of the previously assumed adsorption of nonelectrolytes onto solid surface, the effect of pH on the adsorption equilibrium should be taken into consideration. The pH effects on adsorption of weak organic electrolytes may be considered as a complex phenomenon of changing the nature of the solid surface as well as the nature of the different adsorption mechanisms of neutral and ionised solute forms [Derylo-Marczewska and Jaroniec, 1987]. The complexity of modelling the adsorption isotherms of zirconium phosphates is enhanced due to leaching of phosphate groups into solution, resulting in a dependency of the ionic to neutral compositional ratio on the amount of phosphates in solution that predominantly dictates the solution pH.

The simplest method of incorporating the adsorption of ionised species into the previously described single solute isotherm equation includes treating the system as a two-solute adsorption system using the single-component isotherms for each solute form, i.e., ionic and neutral. Although the activity coefficients of the ionic species in the bulk solution is obtained using the Debye-Hückel limiting law [Sandler, 1989] and the ions in solution are determined by pH measurements and knowledge of the dissociation constants, this method will lead to a number of unknown variables that could fit the model well at the low temperatures. However, this may not be suitable for extrapolation to reaction temperature. Complications also arise due to the changing properties of water at near critical temperatures, since the dielectric constants of water given by Akerlof and Oshry [1950] shifts from 78.5 at 25°C down to 19.66 at 300°C, implying a marked decrease in the dissociation constants of the organic solutes. However, the ionisation constant of water increases by 2.7 orders of magnitude during the same temperature range [Marshall and Franck, 1981]. Consequently, the best approach for predicting the adsorption isotherms at reaction temperature includes using Equation A.27 and assuming that all complex changes due to pH effects are incorporated into the Flory parameter.

One theoretical consideration that requires some mentioning was presented by Müller *et al.* [Derylo-Marczewska and Jaroniec, 1987]. Since the adsorption of ionic species and/or dissociation of adsorbed species lead to an alteration of the surface charge, the immediate vicinity of the surface could contain counter-ion species that adsorb to from multilayered adsorption and/or repelling co-ion components. Consequently, the adsorbent surface charge is affected by the hydrogen ion concentration, measured by the pH, and the solution ionic strength. The model of Müller *et al.* is based on the diffuse double-layer theory of Gouy and Chapman, later improved by Stern, yielding a relationship between the surface charge density per unit area and the surface potential, where the electric double-layer represents the region given by the charged interface and the

solution regions in which the surface charge is counterbalanced [Derylo-Marczewska and Jaroniec, 1987].

## A.2 PREDICTING LIQUID-SOLID ISOTHERMS FROM PURE VAPOURS

Myers and Sircar [1972] showed that the liquid-solid adsorption isotherms can be predicted from the adsorption isotherms of the pure unsaturated vapour, measured at the desired temperature for each component of the liquid mixture. The adsorbents are assumed to be crystalline solids having fixed surface areas and pore volumes, e.g., aluminosilicates. Starting with the Gibbs-Duhem equation for the adsorbed phase, with the isothermal thermodynamic system consisting of a solid adsorbent and a mixture of two gases, which were later taken to be in equilibrium with their saturated vapours, Myers and Sircar [1972] derived at the following equation:

$$\frac{A_s(\sigma_{2,o}-\sigma_{1,o})}{mRT}=\int_{p=0}^{p_2^{vap}}\frac{n_2^s}{p}dp-\int_{p=0}^{p_1^{vap}}\frac{n_1^s}{p}dp=\int_{x_2^l=0}^{1}\frac{\Gamma_2^e}{x_2^l(1-x_2^l)}\left[1+x_2^l\left(\frac{\partial\gamma_2^l}{\partial x_2^l}\right)_{T,p}\right]dx_2^l \qquad \textbf{A.29}$$

The first two integrals would refer to the pure, unsaturated vapour adsorption isotherms and the last integral refers to the isotherm for adsorption from liquid mixtures. $p_1^{vap}$ and $p_2^{vap}$ denote the vapour pressure of components 1 and 2, respectively and $A_s$ is the surface area [Sircar and Myers, 1970], [Myers and Sircar, 1972].

Using Equations A.5 and A.6 in A.4 and assuming that the $Vdp$ term for the bulk phase is negligible, the expression

$$RT\ln K_a=-w_2(\sigma_{2,o}-\sigma_{1,o}) \qquad \textbf{A.30}$$

is derived if $K_a$ is assumed to be purely given by Equation A.8. Nevertheless, it must be stated that the adsorbed phase activity coefficients for the method outlined in this section yields the true values and are not identical to those in Section A.1, where the interfacial surface tensions were ignored.

Since the activity coefficients for the adsorbed phase are unknown, it must be assumed that the adsorbed solution is ideal and thus $\gamma_i^s$ = 1. A more detailed theoretical and practical discussion regarding this topic is given in Sircar and Myers [1973].

The method outline in this section is not suitable for determining the adsorption isotherms for zirconium phosphates since their layers would contract at the desired temperatures (225°C < T < 300°C), thus disallowing any gaseous components diffusing into its interlayer region. Also, attention would have to be given on the effect that steaming has on the aluminosilicates since the morphology and surface area may be affected, which has been reviewed in Section 2.2 (Chapter 2).

# APPENDIX - B

## Chemical and Physical Data of Reaction Compounds

Important thermodynamic and physical properties on meta-phenylenediamine (MPDA), resorcinol, meta-aminophenol (MAP), water, ammonia, $H_3PO_4$ and $(NH_4)H_2PO_4$ are given under their corresponding sectional titles. Most of the data regarding MPDA, water, resorcinol and ammonia are obtained from Daubert and Danner [1989]. The absence of reliable experimental data on MAP necessitates some estimation techniques in determining its physical properties. Most data on MAP is obtained by averaging the properties of MPDA and resorcinol due to their structural similarities as well as MAP containing one functional group of both MPDA and resorcinol. Where possible, the error associated with the data is given.

The heat capacity constants found in literature for the ideal gas phase fit to a different equation than the one given below. Applying the least square method, the data is refitted to Equation B.1 in order to ease the integration of the formula. Some liquid phase heat capacity coefficients are also refitted to a four-parameter heat capacity equation instead of five parameters.

$$C_p = A + B*T + C*T^2 + D*T^3 \qquad \textbf{B.1}$$

Constants for determining the heat of vapourisation ($\Delta h^{vap}$) of the relevant compounds are fitted to Equation B.2.

$$h^{vap} = A*(1-T_r)^{(B+C*T_r+D*T_r^2)} \qquad \textbf{B.2}$$

$T_r$ is the reduced temperature

## B.1 Meta-phenylenediamine

**Table B.1 Physical and Chemical Property Constants for MPDA**

| Property | MPDA [108-45-2] | Error | Reference |
|---|---|---|---|
| Molecular Weight, g/mol | 108.143 | | [PTPC] |
| Critical Temperature, K | 824.00 | <5% | [PTPC] |
| Critical Pressure, bar | 51.80 | <10% | [PTPC] |
| Melting Point, K | 334.00 | <3% | [PTPC] |
| Boiling Point (@1atm), K | 560.00 | <5% | [PTPC] |
| Acentric Factor | 0.5432 | | [PTPC] |
| Dissociation Constant at 20°C | | | |
| $pKa_1$ ($MPDA^+$) | 5.11 | | [IC] |
| $pKa_2$ ($MPDA^{2+}$) | 2.50 | | [IC] |
| IG $\Delta h_f^o$ @ 25°C, J/mol | 91200 | <3% | [PTPC] |
| IG $\Delta G_f^o$ @ 25°C, J/mol | 207000 | <25% | [PTPC] |

**Table B.2 Thermodynamic Equation Coefficients: MPDA [PTPC]**

| Property | Error | Coefficients | | | |
|---|---|---|---|---|---|
| | | A | B | C | D |
| IG Heat Capacity, J/mol/K (300 < Temp(K) < 600) | <25% | -1.97E+1 | 6.26E-1 | -3.80E-4 | 3.02E-8 |
| Liquid Heat Capacity, J/mol/K (412 < Temp(K) < 612) | <10% | 8.54E+1 | 3.31E-1 | | |
| Heat of Vapourisation, J/mol (334 < Temp(K) < 824) | <5% | 7.76E+4 | 2.89E-1 | | |

**[PTPC]** Daubert, T.E. and Danner, R.P., *Physical and Thermodynamic Properties of Pure Chemicals: Data Compilation*, Hemisphere Pub. Corp., New York, 1989.
**[IC]** Adrien, A. and Serjeant, E.P., *The Determination of Ionization Constants: a laboratory manual 3rd Ed.*, Chapman and Hall Inc., London New York, 1981.

## B.2 Resorcinol

**Table B.3 Physical and Chemical Property Constants for Resorcinol**

| Property | Resorcinol [108-46-3] | Error | Reference |
|---|---|---|---|
| Molecular Weight, g/mol | 110.112 | | [PTPC] |
| Critical Temperature, K | 810.00 | <10% | [PTPC] |
| Critical Pressure, bar | 74.90 | <10% | [PTPC] |
| Melting Point, K | 382.00 | <1% | [PTPC] |
| Boiling Point (@1atm), K | 549.65 | <3% | [PTPC] |
| Acentric Factor | 0.6767 | | [PTPC] |
| Dissociation Constant at 25°C | | | |
| $pKa_1$ [Resorcinol] | 9.32 | | [IC] |
| $pKa_2$ [Resorcinol$^-$] | 11.10 | | [IC] |
| IG $\Delta h_f^o$ @ 25°C, J/mol | -274700 | <5% | [PTPC] |
| IG $\Delta G_f^o$ @ 25°C, J/mol | -181300 | <10% | [PTPC] |

**Table B.4 Thermodynamic Equation Coefficients: Resorcinol [PTPC]**

| Property | Error | Coefficients A | B | C | D |
|---|---|---|---|---|---|
| IG Heat Capacity, J/mol/K (298 < Temp(K) < 600) | <1% | -6.60E+1 | 9.05E-1 | -1.05E-3 | 4.99E-7 |
| Liquid Heat Capacity, J/mol/K (405 < Temp(K) < 605) | <25% | 8.32E+1 | 3.72E-1 | | |
| Heat of Vapourisation, J/mol (382 < Temp(K) < 810) | <10% | 1.01E+5 | 3.97E-1 | | |

**[PTPC]** Daubert, T.E. and Danner, R.P., *Physical and Thermodynamic Properties of Pure Chemicals: Data Compilation*, Hemisphere Pub. Corp., New York, 1989.
**[IC]** Adrien, A. and Serjeant, E.P., *The Determination of Ionization Constants: a laboratory manual 3rd Ed.*, Chapman and Hall Inc., London New York, 1981.

## B.3 Meta-aminophenol

**Table B.5 Physical and Chemical Property Constants for MAP**

| Property | MAP [591-27-5] | Error | Reference |
|---|---|---|---|
| Molecular Weight, g/mol | 109.127 | | |
| Critical Temperature, K | 817.00 | | estimate |
| Critical Pressure, bar | 63.35 | | estimate |
| Melting Point, K | 358.00 | | estimate |
| Boiling Point (@1atm), K | 554.83 | | estimate |
| Acentric Factor | 0.6100 | | estimate |
| Dissociation Constant at 20°C | | | |
| $pKa_1$ (proton gained) | 4.37 | | [IC] |
| $pKa_1$ (proton lost) | 9.82 | | [IC] |
| IG $\Delta h_f^o$ @ 25°C, J/mol | -91750 | | estimate |
| IG $\Delta G_f^o$ @ 25°C, J/mol | 12850 | | estimate |

**Table B.6 Thermodynamic Equation Coefficients: MAP**

| Property | Error | Coefficients A | B | C | D |
|---|---|---|---|---|---|
| IG Heat Capacity, J/mol/K (298 < Temp(K) < 600) | | -3.63E+1 | 7.19E-1 | -6.09E-4 | 1.85E-7 |
| Liquid Heat Capacity, J/mol/K (405 < Temp(K) < 605) | | 8.43E+1 | 3.31E-1 | | |
| Heat of Vapourisation, J/mol (382 < Temp(K) < 810) | | 8.91E+4 | 3.49E-1 | | |



[IC] Adrien, A. and Serjeant, E.P., *The Determination of Ionization Constants: a laboratory manual 3rd Ed.*, Chapman and Hall Inc., London New York, 1981.

## B.4 Water

**Table B.7 Physical and Chemical Property Constants for Water**

| Property | Water [7732-18-5] | Error | Reference |
|---|---|---|---|
| Molecular Weight, g/mol | 18.015 | | [PTPC] |
| Critical Temperature, K | 647.13 | <0.2% | [PTPC] |
| Critical Pressure, bar | 220.55 | <0.2% | [PTPC] |
| Melting Point, K | 273.15 | <0.2% | [PTPC] |
| Boiling Point (@1atm), K | 373.15 | <0.2% | [PTPC] |
| Acentric Factor | 0.3448 | | [PTPC] |
| Ion product (Sat'd Vapour) at | | | |
| 200°C | 11.289 | | [CRC67] |
| 250°C | 11.191 | | [CRC67] |
| 300°C | 11.406 | | [CRC67] |
| IG $\Delta h_f^o$ @ 25°C, J/mol | -241810 | <0.2% | [PTPC] |
| IG $\Delta G_f^o$ @ 25°C, J/mol | -228590 | <0.2% | [PTPC] |

**Table B.8 Thermodynamic Equation Coefficients: Water [PTPC]**

| Property | Error | Coefficients | | | |
|---|---|---|---|---|---|
| | | A | B | C | D |
| IG Heat Capacity, J/mol/K (298 < Temp(K) < 600) | <1% | 3.52E+1 | -1.81E-2 | 5.12E-5 | -2.98E-8 |
| Liquid Heat Capacity, J/mol/K (273 < Temp(K) < 533) | <1% | -6.14E+1 | 1.09E0 | -2.92E-3 | 2.63E-6 |
| Heat of Vapourisation, J/mol (273 < Temp(K) < 647) | <1% | 5.21E+4 | 3.20E-1 | | |



**[PTPC]** Daubert, T.E. and Danner, R.P., *Physical and Thermodynamic Properties of Pure Chemicals: Data Compilation*, Hemisphere Pub. Corp., New York, 1989.
**[CRC67]** Weast, R.C., Astle, M.J. and Beyer, W.H., *CRC Handbook of Chemistry and Physics 67th Ed.*, CRC Press Inc., Boca Raton, 1986-1987.

## B.5 Ammonia

**Table B.9 Physical and Chemical Property Constants for Ammonia**

| Property | Ammonia [7664-41-7] | Error | Reference |
|---|---|---|---|
| Molecular Weight, g/mol | 17.031 | | [PTPC] |
| Critical Temperature, K | 405.65 | <3% | [PTPC] |
| Critical Pressure, bar | 112.78 | <5% | [PTPC] |
| Melting Point, K | 195.41 | <1% | [PTPC] |
| Boiling Point (@1atm), K | 239.72 | <1% | [PTPC] |
| Acentric Factor | 0.2520 | | [PTPC] |
| Dissociation Constant (pKa) at | | | |
| 20°C [$NH_4^+$] | 9.40 | | [CRC67] |
| 30°C [$NH_4^+$] | 9.09 | | [CRC67] |
| 50°C [$NH_4^+$] | 8.54 | | [CRC67] |
| IG $\Delta h_f^o$ @ 25°C, J/mol | -45898 | <1% | [PTPC] |
| $\Delta h_f^o$ of $NH_{3\,(aq)}$ @ 25°C, J/mol | -80290 | | [TPIS] |
| IG $\Delta G_f^o$ @ 25°C, J/mol | -16401 | <3% | [PTPC] |

**Table B.10 Thermodynamic Equation Coefficients: Ammonia [PTPC]**

| Property | Error | Coefficients | | | |
|---|---|---|---|---|---|
| | | A | B | C | D |
| IG Heat Capacity, J/mol/K (298 < Temp(K) < 600) | <1% | 2.94E+1 | 6.38E-3 | 6.20E-5 | -4.78E-8 |
| Heat of Vapourisation, J/mol (195 < Temp(K) < 406) | <3% | 3.15E+4 | 3.91E-1 | -2.29E-1 | 2.31E-1 |



**[PTPC]** Daubert, T.E. and Danner, R.P., *Physical and Thermodynamic Properties of Pure Chemicals: Data Compilation*, Hemisphere Pub. Corp., New York, 1989.
**[CRC67]** Weast, R.C., Astle, M.J. and Beyer, W.H., *CRC Handbook of Chemistry and Physics 67th Ed.*, CRC Press Inc., Boca Raton, 1986-1987.
**[TPIS]** Knacke, O., Kubaschewski, O. and Hesselmann, K., *Thermochemical Properties of Inorganic Substances 2nd Ed.*, Springer-Verlag, Berlin Heidelberg, 1991.

The solubility of ammonia at fixed partial pressure of 1.013bar is correlated as a function of temperature [TDBB] in the form

$$\ln(x) = A + \frac{B}{T} + C * \ln(T) + D * T \qquad \textbf{B.3}$$

where $T$ is the temperature given in Kelvin

$x$ is the gas mole fraction in the liquid

$A$ = -81.7466; $B$ = 1096.82; $C$ = 16.5603; $D$ = -0.0602469

The experimental data is not corrected for non-ideality of the gas phase and chemical reactions with the solvents. The quoted coefficients are valid in the temperature range of 273 to 373 Kelvin.

## B.6 Hydrolysed Ammonia ($NH_4OH$)

**Table B.11 Physical and Chemical Property Constants for $NH_4OH$**

| Property | $NH_4OH$ [1336-21-6] | Error | Reference |
|---|---|---|---|
| Molecular Weight, g/mol | 35.046 | | [PTPC] |
| Liquid $C_p$ @ 25°C, J/mol | 154.89 | <3% | [PTPC] |
| Liquid state $\Delta h_f^o$ @ 25°C, J/mol | -361200 | <3% | [PTPC] |
| Liquid state $\Delta G_f^o$ @ 25°C, J/mol | -254020 | <3% | [PTPC] |
| $\Delta h_f^o$ of $NH_4^+{}_{(aq)}$ @ 25°C, J/mol | -132800 | | [CET] |
| $\Delta h_f^o$ of $OH^-{}_{(aq)}$ @ 25°C, J/mol | -229940 | | [CET] |
| $\Delta G_f^o$ of $NH_4^+{}_{(aq)}$ @ 25°C, J/mol | -79496 | | [CET] |
| $\Delta G_f^o$ of $OH^-{}_{(aq)}$ @ 25°C, J/mol | -157297 | | [CET] |



**[TDBB]** Cabani, S., Gianni, P. in Hinz, H-J, editor, *Thermodynamic Data for Biochemistry and Biotechnology*, Springer-Verlag, Berlin, 1986.
**[PTPC]** Daubert, T.E. and Danner, R.P., *Physical and Thermodynamic Properties of Pure Chemicals: Data Compilation*, Hemisphere Pub. Corp., New York, 1989.
**[CET]** Sandler, S.I., *Chemical and Engineering Thermodynamics 2nd Ed.*, John Wiley & Sons Inc., Singapore, 1989.

## B.7 Phosphoric Acid

**Table B.12 Physical and Chemical Property Constants for $H_3PO_4$**

| Property | $H_3PO_4$ [7664-38-2] | Error | Reference |
|---|---|---|---|
| Molecular Weight, g/mol | 97.995 | | [PTPC] |
| Solid State $\Delta h_f^o$ @ 25°C, J/mol | -1124300 | | [CRC73] |
| Solid state $\Delta G_f^o$ @ 25°C, J/mol | -1284400 | | [CRC73] |
| Liquid state $\Delta h_f^o$ @ 25°C, J/mol | -1271700 | | [CRC73] |
| Liquid State $\Delta G_f^o$ @ 25°C, J/mol | -1123600 | | [CRC73] |
| $\Delta h_f^o$ of $H_2PO_4^-{}_{(aq)}$ @ 25°C, J/mol | -1296290 | | [TPIS] |
| $\Delta h_f^o$ of $H^+{}_{(aq)}$ @ 25°C, J/mol | 0 | | [TPIS] |

**Table B.13 Physical and Chemical Property Constants for $NH_4H_2PO_4$**

| Property | $NH_4H_2PO_4$ [7722-76-1] | Error | Reference |
|---|---|---|---|
| Molecular Weight, g/mol | 115.110 | | [PTPC] |
| Solid State $\Delta h_f^o$ @ 25°C, J/mol | -1027000 | | [PTPC] |
| Solid state $\Delta G_f^o$ @ 25°C, J/mol | -813990 | | [PTPC] |
| $\Delta h_f^o$ of $H_2PO_4^-{}_{(aq)}$ @ 25°C, J/mol | -1296290 | | [TPIS] |
| $\Delta h_f^o$ of $NH_4^+{}_{(aq)}$ @ 25°C, J/mol | -132800 | | [CET] |
| $\Delta G_f^o$ of $NH_4^+{}_{(aq)}$ @ 25°C, J/mol | -79496 | | [CET] |

**[PTPC]** Daubert, T.E. and Danner, R.P., *Physical and Thermodynamic Properties of Pure Chemicals: Data Compilation*, Hemisphere Pub. Corp., New York, 1989.
**[CRC73]** Lide, D.R., *CRC Handbook of Chemistry and Physics 73rd Ed.*, CRC Press, Boca Raton, Florida, 1992-1993.
**[TPIS]** Knacke, O., Kubaschewski, O. and Hesselmann, K., *Thermochemical Properties of Inorganic Substances 2nd Ed.*, Springer-Verlag, Berlin Heidelberg, 1991.
**[CET]** Sandler, S.I., *Chemical and Engineering Thermodynamics 2nd Ed.*, John Wiley & Sons Inc., Singapore, 1989.

# APPENDIX – C

## Derivation of Response Factors

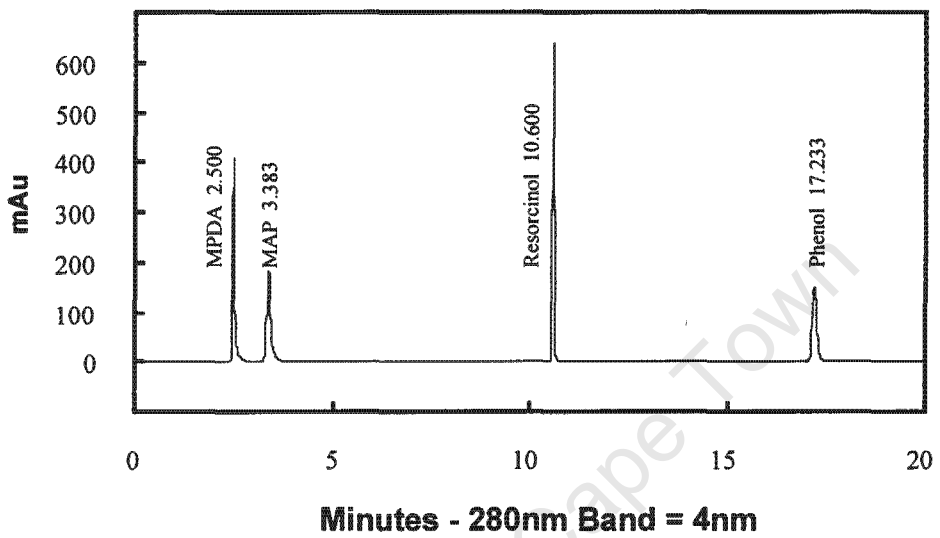


| Peak | Time | Area | Area% |
|---|---|---|---|
| 1 | 2.50 | 1484109 | 24.441 |
| 2 | 3.83 | 1277506 | 21.038 |
| 3 | 10.60 | 2049233 | 33.747 |
| 4 | 17.23 | 1261444 | 20.774 |
| Total | | 6072292 | 100.000 |

**Figure C.1** HPLC chromatogram trace for determining response factors.

A solution of MPDA (2.8112g/L), MAP (2.7032g/L) and resorcinol (3.0328g/L) is made up in a volumetric flask. The second solution contains the internal standard, phenol. For this case, the phenol concentration is 3.0172g/L. It is of great importance to know the concentration of each organic solution as accurately as possible. A number of test-solutions are made up, varying the volumetric ratio of the first flask (2.00ml) to the phenol solution (0.50ml to 3.00ml). The resulting mixtures are then diluted to 50ml before being analysed by

the HPLC. The calculations of the response factors of MPDA, MAP and resorcinol relative to phenol will be explained based on the HPLC trace illustrated in Figure C.1.

**Table C.1 Determination of Response Factors: Illustration based on one Data Point**

| Compound | 50ml Flask Conc. (g/L) | Conc. Ratio | HPLC Area | Area Ratio |
|---|---|---|---|---|
| MPDA | 0.1124 | 0.9317 | 1484109 | 1.1765 |
| MAP | 0.1081 | 0.8959 | 1277506 | 1.0127 |
| Resorcinol | 0.1185 | 1.0052 | 2049233 | 1.6245 |
| Phenol | 0.1207 | - | 1261444 | - |

The 50ml flask concentrations in Table C.1 are obtained by combining 2ml of MPDA, MAP and resorcinol mixture with 2ml phenol-solution and diluting it to the 50ml mark. Concentration ratios are then simply calculated by dividing the MPDA, MAP and resorcinol concentrations by the phenol concentration. The area ratio is evaluated by dividing the HPLC determined area counts of a particular compound by the area of phenol. After repeating the above procedure using a number of different concentration ratios, a plot of the area ratio (x) versus the concentration ratio ($y$) gives a straight line $y=m*x$ for each compound, MPDA, MAP and resorcinol. The response factor ($m$) after injecting more than 20samples is determined by regression analysis or by least sum squared errors and 95% confidence to be:

| | |
|---|---|
| MPDA | 0.8023 ± 0.0124 |
| MAP | 0.8907 ± 0.0095 |
| Resorcinol | 0.6203 ± 0.0054 |

Conversely, the response factors can be used to evaluate the concentration of the relevant compounds if the phenol concentration is known. See APPENDIX-D for a worked example.

It needs to be mentioned that the response factors have to be checked regularly since significant changes in the response factors are noticed during the duration of the study. Deactivation of the packing inside the column is also evident since the retention time required for each compound to traverse through the column reduced incrementally. This effect manifested itself strongly towards the end of the study.

# APPENDIX - D

## Worked Example for evaluating Adsorbed Concentration

The following data is recorded during the adsorption study of $MPDA_{(aq)}$ onto the zeolite H-Beta to evaluate the adsorbed concentration (mmol/g):

**Information gathered before adsorption**

| | |
|---|---|
| Adsorption temperature: | 70°C |
| Dehydrated mass H-Beta: | 0.3499g |
| Initial MPDA concentration: | 1.9640g/L |
| Volume of MPDA solution: | 15ml |

**Information gathered after the adsorption (after 6days)**

| | |
|---|---|
| Previously determined response factor: | 0.8121 |
| Internal standard (Phenol) conc.: | 2.9816g/L |
| Volume MPDA solution added to 50ml flask: | 2.00ml |
| Volume Phenol solution added to 50ml flask: | 2.00ml |
| HPLC determined area ratio (MPDA/Phenol): | 0.0488 |

**Calculation of $MPDA_{(aq)}$ concentration after adsorption**

Given above is the response factor for MPDA calculated by the method described in APPENDIX-C. These response factors are always determined on the same day as the MPDA concentration.

$$\frac{x * \frac{2ml}{50ml}}{2.9816 \frac{g}{L} * \frac{2ml}{50ml}} = 0.8121 * 0.0488 \qquad \textbf{D.1}$$

Solving for $x$ returns a MPDA concentration of 0.1182g/L

Therefore, the mass of MPDA that adsorbs onto the H-Beta at equilibrium is: (1.9640- 0.1182)*0.015 = 0.02769g.

The moles of MPDA adsorbed per gram of dehydrated H-Beta is then calculated by determining the number of moles of MPDA adsorbed divided by the mass of dehydrated zeolite or:

$$\text{MPDA adsorbed} = \frac{0.02769}{108.14406 * 0.3499} * 1000 \frac{mmol}{g} = 0.7316 \frac{mmol}{g}$$

The mole-fractions of MPDA in solution at equilibrium adsorption is calculated using the HPLC determined MPDA concentration:

$$\text{MPDA}_{(aq)} \text{ mole fraction} = \frac{\frac{0.1182 g/L * 0.015 L}{108.14406 g/mol}}{\frac{0.1182 g/L * 0.015 L}{108.14406 g/mol} + \frac{0.015 L * 997 g/L}{18.0154 g/mol}} = 1.975E-5$$

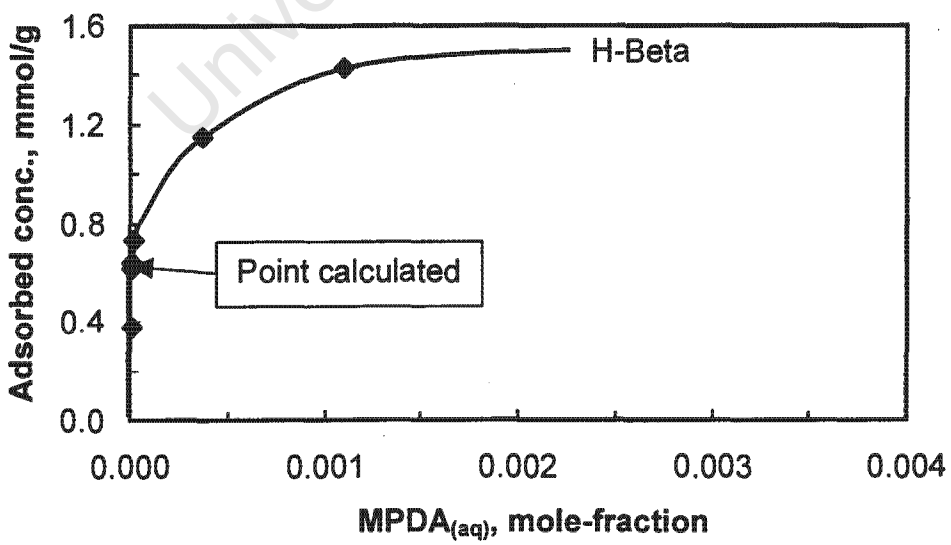


**Figure D.1** Adsorption-equilibrium data of $MPDA_{(aq)}$ on H-Beta at 70°C.

# APPENDIX - E

## Determination of Response Factors for 3,3'-Diamino-Diphenyl-amine and 3-Hydroxy,3'-Amino-Diphenylamine

3,3'-Diamino-diphenylamine and 3-hydroxy,3'-amino-diphenylamine are identified by means of the HPLC-MS at AECI.Ltd(Modderfontein). An identical HPLC column and the same analysis method as described in Section 3.3.2 is used in order to determine the corresponding retention times for the two compounds to traverse through the spherisorb ODS2 column. As illustrated in Figure E.1, the retention times for 3,3'-diamino-diphenylamine and 3-hydroxy,3'-amino-diphenylamine are around 7.42minutes and 12.23minutes, respectively. Depending on the sensitivity of the integrator, two peaks could be detected for 3,3'-diamino-diphenylamine. The area under these two peaks is added together.

The compounds cannot be bought and therefore their retention times are evaluated by first producing them under condition favourable for their production and then estimating their response factors simultaneously. It is generally assumed that the overall mass balance accounts for MPDA, MAP, resorcinol, 3,3'-diamino-diphenylamine and 3-hydroxy,3'-amino-diphenylamine. By using phosphoric acid in a number of reactions ($150^{o}C$ < Temp. < $215^{o}C$) as the reaction promoter, it is further assumed that no polyethers and any other solid ethers could be formed. Adsorption of any organic compounds onto the reactor walls is also considered negligible. Since this method introduces a lot of errors and only a small amount of these diamines could be produced at any given time, the final response factors are only an approximation of their true response factors.

The number of moles MPDA lost due to the formation of the dimers is calculated by subtracting the number of moles of MPDA, MAP and resorcinol remaining

inside the reactor (after say 2hours at 200°C) from the initial number of moles MPDA used. Since two moles of MPDA are required for the formation of one mole of dimers, the subtracted value is divided by 2. The reactor concentration of 'Compound-**A+B**' (termed as such, since the individual concentrations of 3,3'-diamino-diphenylamine and 3-hydroxy,3'-amino-diphenylamine are not known) is subsequently calculated.

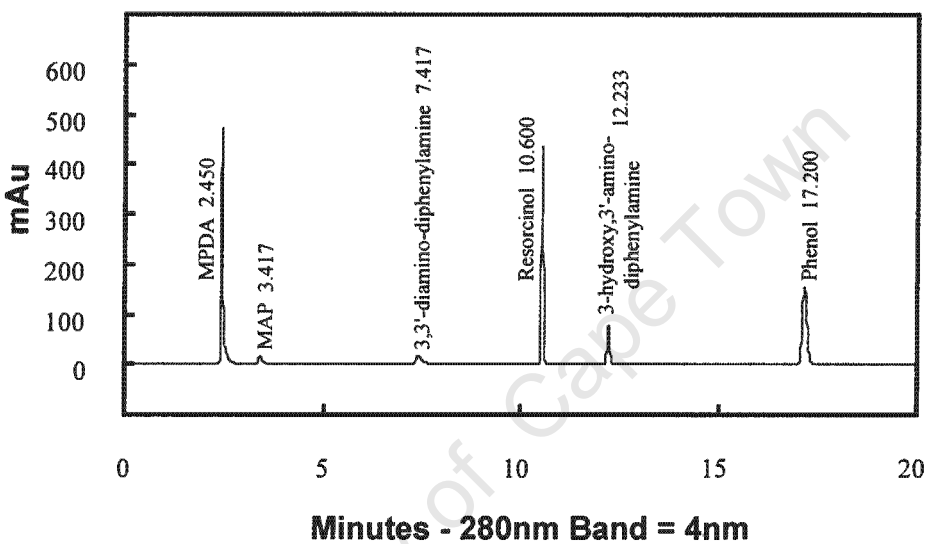




| Peak | Time | Area | Area% |
|---|---|---|---|
| 1 | 2.45 | 953426 | 33.851 |
| 2 | 3.42 | 70658 | 2.509 |
| 3 | 7.42 | 94780 | 3.365 |
| 4 | 7.63 | 18438 | 0.655 |
| 5 | 10.60 | 766037 | 27.198 |
| 6 | 12.23 | 206215 | 7.322 |
| 7 | 17.20 | 706979 | 25.101 |
| Total | | 2816533 | 100.000 |

**Figure E.1** HPLC chromatogram trace for determining response factors of 3,3'-diamino-diphenylamine and 3-hydroxy,3'-amino-diphenylamine.

Varying the volumetric ratio of the internal standard to the sample solution (see APPENDIX-C), the concentrations ratio of 'Compound-**A+B**' are determined and fitted to $y_{A+B} = x_A{*}m_A + x_B{*}m_B$. The variables $x_A$ and $x_B$ are the respective area ratios of 3,3'-diamino-diphenylamine and 3-hydroxy,3'-amino-diphenylamine with respect to phenol. The corresponding concentration ratios of 'Compound-**A+B**' (mmol/L) with respect to phenol (mmol/L) are given by the variable $y_{A+B}$. Response factors of 3,3'-diamino-diphenylamine ($m_A$) and 3-hydroxy,3'-amino-diphenylamine ($m_B$) are optimised by minimising the sum of all the squared errors. Applying statistical analyses, the possible response factors for 3,3'-diamino-diphenylamine and 3-hydroxy,3'-amino-diphenylamine are illustrated in Figure E.2. These response factors apply to molar concentrations.

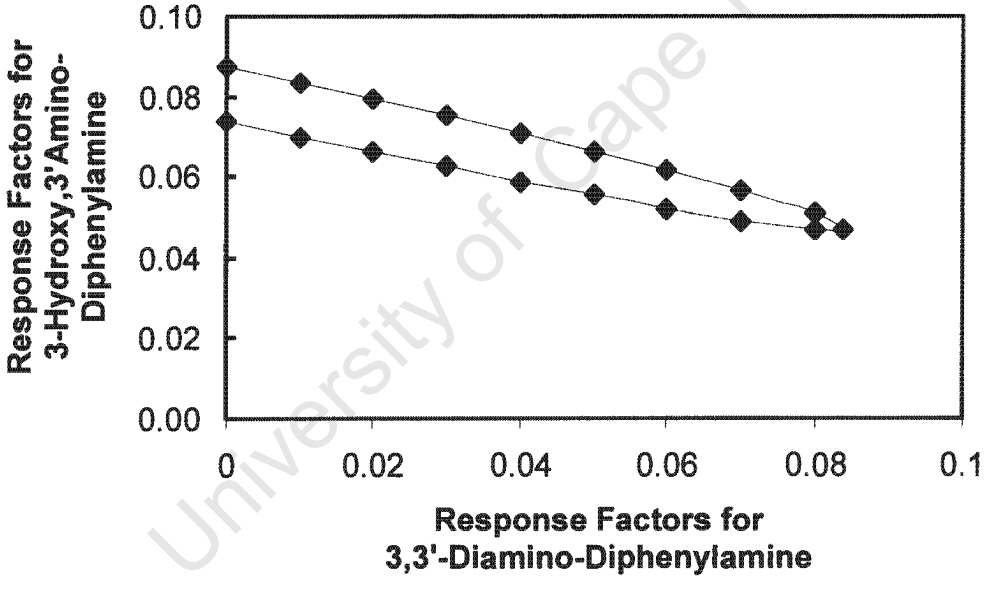




**Figure E.2** Response Factors ((mol/L of compound) per (mol/L of phenol)) for 3,3'diamino-diphenylamine and 3-hydroxy,3'-amino-diphenylamine with 95% confidence.

Response factor for 3,3'diamino-diphenylamine is thus set to 0.04 and that of 3-hydroxy,3'-amino-diphenylamine is taken at 0.07. The response factors evaluating the concentration ratio in terms of g/L instead of mmol/L is thus

determined by multiplying the response factor with the molar mass of the compound divided by the molar mass of phenol.

**Response Factors to determine Concentration Ratios in terms of Mass**

| | | |
|---|---|---|
| 3,3'diamino-diphenylamine | = 0.04*199.26/94.11 | = 0.085 |
| 3-hydroxy,3'-amino-diphenylamine | = 0.07*200.24/94.11 | = 0.149 |

# APPENDIX - F

## Correction of observed Sample Concentration

### F.1 Mineral or Aqueous Acids

Inside a closed vessel, heating water from ambient temperature to reaction temperature (>200°C) results in water evaporating until its corresponding vapour pressure is attained. With the reasonable assumption that all the organic compounds remain in liquid solution, the concentration of the components should change upon heating water from ambient temperature to above 200°C inside an autoclave. Consequently, less water remains in contact with the organic compounds as initially assumed at room temperature. The same rule applies to the aqueous mineral acids. Nevertheless, the sum of the mass of water in the liquid and vapour phase is conserved during the temperature change since no sampling has yet occurred.

$$V_{L,25} * \rho_{L,25} + V_{V,25} * \rho_{V,25} = V_{L,T} * \rho_{L,T} + V_{V,T} * \rho_{V,T} \qquad \textbf{F.1}$$

where $V_{L,25}$ = liquid volume at room temperature (L)
$V_{V,25}$ = vapour volume at room temperature (L)
$V_{L,T}$ = liquid volume at reaction temperature (L)
$V_{V,T}$ = vapour volume at reaction temperature (L)
$\rho_{L,25}$ = liquid density at room temperature (g/L)
$\rho_{V,25}$ = vapour density at room temperature (g/L)
$\rho_{L,T}$ = liquid density at reaction temperature (g/L)
$\rho_{V,T}$ = vapour density at reaction temperature (g/L)

Knowing that the reactor volume is 0.60L, it follows that $V_{L,T}$ = 0.60 – $V_{V,T}$ (in Litres), and Equation F.1 can be rearranged to:

$$V_{L,T} * \rho_{L,T} = \frac{V_{L,25} * \rho_{L,25} + V_{V,25} * \rho_{L,25} - 0.60 * \rho_{V,T}}{\rho_{L,T} - \rho_{V,T}} * \rho_{L,T} \qquad \text{F.2}$$

Densities for ρ are easily obtained from steam tables. Applying Equation F.2, the true initial concentration is altered by dividing the initial number of moles of MPDA by $V_{L,T} * \rho_{L,T} / \rho_{L,25}$ instead of $V_{L,25}$. The purpose of multiplying the mass of water in the liquid phase by the density of water at 25°C instead of the density at reaction temperature is because the HPLC analysis is carried out at ambient temperatures.

Upon sampling, however, the withdrawal of liquid results in the liquid level inside the reactor to drop, thereby creating more space for water to evaporate until a new liquid-vapour equilibrium is reached. This is illustrated in the following figure, where $M_G$ and $M_L$ are the corresponding mass of water in the liquid and vapour phase; $m$ is the cumulative mass of liquid sampled; and $C_{HPLC}$ resembles the HPLC determined concentration (mmol/L) of sample $i$. The term *init* refers to the initial conditions inside the reactor (at reaction temperature) before the removal of any liquid from the reactor system.

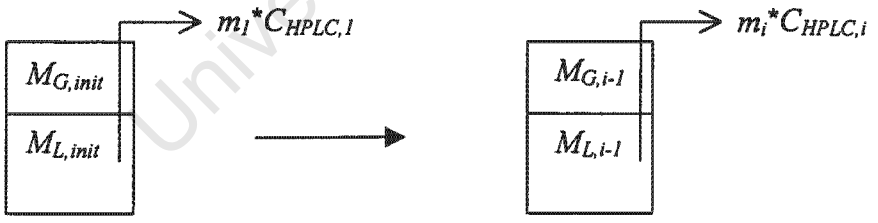


**Figure F.1** Schematic of the effect of sampling on the concentration.

Assuming the formation of the new vapour-liquid equilibrium occurs only after an individual sample is taken, the following formula is derived:

$$C_{CORR,i} = C_{HPLC,i} * \frac{M_{L,init} - \sum_{0}^{i-1} m_i - (M_{G,i-1} - M_{G,init})}{M_{L,init} - \sum_{0}^{i-1} m_i} \quad \text{F.3}$$

where $C_{CORR,i}$ represents the corrected concentration of sample i

**Example F.1:** The MPDA concentrations (mmol/L) determined by HPLC analysis is given in Table F.1. Included in Table F.2 is the corrected concentration for which a sample calculation will follow. The corrected concentration of the reactor sample shows an increase in the concentration. The reason being that the water which is previously in the vapour phase will now be present in the liquid form since the sample is taken when the reactor itself is at 25°C.

**Table F.1 Experimental Data obtained**

| Sample Number | Time (h) | Temperature (°C) | HPLC det. Conc. (mmol/L) | Cumulative Sample mass (g) |
|---|---|---|---|---|
| 0 | 0.00 | 25 | 26.422 | 0.0 |
| 0 | ? | 275 | | 0.0 |
| 1 | 1.00 | 275 | 15.977 | 19.4 |
| 2 | 5.12 | 275 | 2.939 | 38.6 |
| 3 | 9.27 | 275 | 0.570 | 59.9 |
| 4 | 25.00 | 275 | 0.236 | 79.8 |
| Reactor | 25.20 | 25 | 0.216 | 79.8 |

**Table F.2 Calculation of the corrected Concentration**

| Sample Number | $M_L$ (g) | $M_G$ (g) | Corrected Conc. or $C_{CORR}$ (mmol/L) | Ratio of $C_{CORR}/C_{HPLC}$ |
|---|---|---|---|---|
| 0 | 349.0 | 0.006 | | |
| 0 | 344.5 | 4.46 | 26.764 | 1.013 |
| 1 | 324.3 | 5.27 | 15.977 | 1.000 |
| 2 | 304.3 | 6.08 | 2.932 | 0.998 |
| 3 | 282.1 | 6.97 | 0.567 | 0.995 |
| 4 | 261.4 | 7.80 | 0.224 | 0.991 |
| Reactor | 269.2 | 0.007 | 0.219 | 1.017 |

$M_L$ and $M_G$ are determined by Equation F.2, however, the cumulative sample mass would have to be included in the numerator of Equation F.2.

Taking sample number 2:

$$C_{CORR,2} = 2.939 * \frac{344.5 - 19.4 - (5.27 - 4.46)}{344.5 - 19.4} = 2.932 mmol/L$$

## F.2 Solid Acids

For solid acids the same procedure applies as outline in Section F.1 above for aqueous mineral acids. However, since the solids remain with the reaction mixture a corresponding correction has to be made by using Formula F.4. Due to the increase of the mass of solids relative to the total moles of the relevant compounds in the reaction mixture, the overall mass balance over the organic compounds would not seem to balance. The effect is illustrated in Example F.2 where the ratio of $C_{CORR,i}$ / $C_{DET}$ deviates considerably from 1. Another method would be to define the number of acid sites available on the solid material in terms of the liquid volume inside the reactor, i.e., mmols of solid acid sites available per litre of liquid; the concentration of the organic materials would also be defined in mmol/L. The second approach is preferred since it prevented the huge alteration in the concentration of the organic compounds, rather than affecting the concentration of the acid sites.

$$C_{SOLID,i} = \frac{C_{ACT,i} * M_{L,i-1}}{M_S} \qquad \textbf{F.4}$$

where $C_{SOLID,i}$ is the organic concentration based on the mass of solid

$M_S$ represents the initial calcined mass of solid used in reaction.

**Example F.2:** This example is a continuation of Example F.1 where Equation F.4 is applied assuming that this time 10g of zeolite was initially used in the reaction given above. The result is illustrated in Table F.3.

**Table F.3 Determining Concentration based on 10g of Zeolites**

| Sample Number | $M_L$ (g) | Det. Conc. (mmol/g) | Corrected Conc. or $C_{CORR}$ (mmol/g) | Ratio of $C_{CORR}/C_{HPLC}$ |
|---|---|---|---|---|
| 0 | 349.0 | 0.9248 | 0.9248 | 1.000 |
| 0 | 344.5 | 0.9248 | 0.9248 | 1.000 |
| 1 | 324.3 | 0.5521 | 0.5521 | 1.000 |
| 2 | 304.3 | 0.1013 | 0.0954 | 0.941 |
| 3 | 282.1 | 0.0196 | 0.0173 | 0.883 |
| 4 | 261.4 | 0.0078 | 0.0063 | 0.819 |
| Reactor | 269.2 | 0.0076 | 0.0058 | 0.759 |

# APPENDIX - G

## Reaction Data using Mineral Acids

The method used for calculating the **corrected mole concentration** is illustrated in Appendix-F. The **mole balances** given in the last column of each table are calculated by the addition of the mole concentrations of MPDA, MAP, resorcinol and two times 3,3'-diamino-diphenylamine (denoted as Comp. **A**) and 3-hydroxy,3'-amino-diphenylamine (denoted as Comp. **B**) with the summations then being divided by the initial concentration of MPDA.

### G.1 Sulphuric Acid

**Table G.1 Reaction Data at 225°C with the initial $H_2SO_4$/MPDA mole ratio equaling 3.39**

| Time (h) Sample | pH | Corrected Mole Concentration (mmol/L) | | | | | Mole Balance |
|---|---|---|---|---|---|---|---|
| | | MPDA | MAP | Comp.A[1] | Resorc. | Comp.B[2] | |
| 0.0 | | 26.43 | 0.00 | 0.00 | 0.00 | 0.00 | 100.0% |
| 1.0 Sample1 | 1.42 | 21.65 | 3.21 | 0.01 | 0.39 | 0.01 | 95.7% |
| 2.0 Sample2 | 1.34 | 16.75 | 5.59 | 0.03 | 2.75 | 0.05 | 95.5% |
| 3.0 Sample3 | 1.38 | 14.05 | 5.32 | 0.04 | 5.68 | 0.10 | 95.9% |
| 5.2 Sample4 | 1.37 | 9.52 | 3.88 | 0.06 | 11.81 | 0.21 | 97.4% |
| 22.8 Sample5 | 1.25 | 1.83 | 0.28 | 0.04 | 24.57 | 0.24 | 103.0% |
| Reactor Sample | | 1.78 | 0.25 | 0.04 | 23.57 | 0.21 | 98.7% |

**Table G.2 Reaction Data at 225°C with the initial $H_2SO_4$/MPDA mole ratio equaling 6.77**

| Time (h) Sample | pH | Corrected Mole Concentration (mmol/L) | | | | | Mole Balance |
|---|---|---|---|---|---|---|---|
| | | MPDA | MAP | Comp.A[1] | Resorc. | Comp.B[2] | |
| 0.0 | | 26.44 | 0.00 | 0.00 | 0.00 | 0.00 | 100.0% |
| 1.0 Sample1 | 1.15 | 16.76 | 5.28 | 0.01 | 0.62 | 0.01 | 85.8% |
| 2.0 Sample2 | 1.16 | 12.54 | 8.22 | 0.03 | 4.22 | 0.05 | 95.0% |
| 3.0 Sample3 | 1.12 | 10.19 | 7.40 | 0.04 | 9.10 | 0.13 | 102.1% |
| 5.0 Sample4 | 1.21 | 5.30 | 3.52 | 0.04 | 15.92 | 0.18 | 95.2% |
| 8.2 Sample5 | 1.22 | 2.79 | 1.44 | 0.03 | 21.08 | 0.15 | 97.0% |
| 24.0 Sample6 | 1.29 | 0.22 | 0.00 | 0.01 | 25.45 | 0.01 | 97.2% |
| Reactor Sample | | 0.09 | 0.00 | 0.00 | 24.49 | 0.01 | 93.0% |

[1] Comp. **A** denotes 3,3'-diamino-diphenylamine
[2] Comp. **B** denotes 3-hydroxy,3'-amino-diphenylamine

**Table G.3 Reaction Data at 275°C with the initial $H_2SO_4$/MPDA mole ratio equaling 3.38**

| Time (h) | Sample | pH | Corrected Mole Concentration (mmol/L) | | | | | Mole |
|---|---|---|---|---|---|---|---|---|
| | | | MPDA | MAP | Comp.A[1] | Resorc. | Comp.B[2] | Balance |
| 0.0 | | | 26.46 | 0.00 | 0.00 | 0.00 | 0.00 | 100.0% |
| 1.0 | Sample1 | 1.93 | 13.86 | 3.48 | 0.04 | 8.81 | 0.12 | 100.0% |
| 2.5 | Sample2 | 1.09 | 4.68 | 0.66 | 0.04 | 20.99 | 0.29 | 101.9% |
| 5.2 | Sample3 | 1.36 | 2.59 | 0.24 | 0.03 | 23.55 | 0.24 | 101.7% |
| 10.0 | Sample4 | 2.26 | 1.12 | 0.18 | 0.01 | 24.39 | 0.16 | 98.4% |
| 24.0 | Sample5 | 0.82 | 0.17 | 0.15 | 0.01 | 25.10 | 0.03 | 96 3% |
| Reactor Sample | | | 0.22 | 0.00 | 0.01 | 24.92 | 0.02 | 95 2% |

## G.2 Phosphoric Acid

**Table G.4 Reaction Data at 225°C with the initial $H_3PO_4$/MPDA mole ratio equaling 6.77**

| Time (h) | Sample | pH | Corrected Mole Concentration (mmol/L) | | | | | Mo e |
|---|---|---|---|---|---|---|---|---|
| | | | MPDA | MAP | Comp.A[1] | Resorc. | Comp.B[2] | Balance |
| 0.0 | | | 26.48 | 0.00 | 0.00 | 0.00 | 0.00 | 100.0% |
| 1.0 | Sample1 | 1.70 | 24.20 | 1.68 | 0.02 | 0.54 | 0.01 | 100.0% |
| 2.0 | Sample2 | 1.73 | 19.98 | 2.64 | 0.04 | 3.08 | 0.10 | 98.1% |
| 3.2 | Sample3 | 1.73 | 16.83 | 2.61 | 0.07 | 7.05 | 0.23 | 102.3% |
| 7.5 | Sample4 | 1.71 | 8.76 | 1.21 | 0.10 | 15.11 | 0.44 | 98.8% |
| 26.9 | Sample5 | 1.73 | 1.14 | 0.16 | 0.03 | 24.59 | 0.17 | 99.3% |
| Reactor Sample | | | 0.37 | 0.00 | 0.01 | 24.59 | 0.08 | 94.9% |

**Table G.5 Reaction Data at 275°C with the initial $H_3PO_4$/MPDA mole ratio equaling 6.77**

| Time (h) | Sample | pH | Corrected Mole Concentration (mmol/L) | | | | | Mole |
|---|---|---|---|---|---|---|---|---|
| | | | MPDA | MAP | Comp.A[1] | Resorc. | Comp.B[2] | Balance |
| 0.0 | | | 26.42 | 0.00 | 0.00 | 0.00 | 0.00 | 100.0% |
| 1.0 | Sample1 | 2.02 | 18.30 | 2.04 | 0.07 | 5.17 | 0.17 | 98.4% |
| 5.1 | Sample2 | 1.99 | 3.05 | 0.98 | 0.03 | 21.99 | 0.22 | 100.4% |
| 9.3 | Sample3 | 2.08 | 0.60 | 0.21 | 0.02 | 25.60 | 0.05 | 100.4% |
| 25.0 | Sample4 | 2.13 | 0.17 | 0.16 | 0.00 | 25.80 | 0.01 | 99.0% |
| Reactor Sample | | | 0.26 | 0.26 | 0.00 | 25.58 | 0.01 | 98.9% |

[1] Comp. **A** denotes 3,3'-diamino-diphenylamine
[2] Comp. **B** denotes 3-hydroxy,3'-amino-diphenylamine

## G.3 Ammonium Dihydrogen Phosphate

**Table G.6 Reaction Data at 225°C with the initial $NH_4H_2PO_4$/MPDA mole ratio equaling 6.76**

| Time (h) | Sample | pH | Corrected Mole Concentration (mmol/L) | | | | | Mole Balance |
|---|---|---|---|---|---|---|---|---|
| | | | MPDA | MAP | Comp.A[1] | Resorc. | Comp.B[2] | |
| 0.0 | | | 26.44 | 0.00 | 0.00 | 0.00 | 0.00 | 100.0% |
| 1.2 | Sample1 | 5.34 | 25.13 | 0.00 | 0.00 | 0.01 | 0.00 | 95.1% |
| 3.1 | Sample2 | 5.25 | 26.39 | 0.28 | 0.00 | 0.01 | 0.00 | 101.0% |
| 6.1 | Sample3 | 5.23 | 26.70 | 0.55 | 0.01 | 0.20 | 0.01 | 104.0% |
| 11.0 | Sample4 | 5.24 | 25.64 | 0.68 | 0.02 | 0.54 | 0.04 | 102.1% |
| 26.5 | Sample5 | 5.23 | 23.19 | 0.98 | 0.05 | 1.78 | 0.14 | 99.6% |
| Reactor Sample | | | 21.74 | 0.89 | 0.05 | 1.79 | 0.14 | 93.8% |

**Table G.7 Reaction Data at 275°C with the initial $NH_4H_2PO_4$/MPDA mole ratio equaling 6.63**

| Time (h) | Sample | pH | Corrected Mole Concentration (mmol/L) | | | | | Mole Balance |
|---|---|---|---|---|---|---|---|---|
| | | | MPDA | MAP | Comp.A[1] | Resorc. | Comp.B[2] | |
| 0.0 | | | 26.44 | 0.00 | 0.00 | 0.00 | 0.00 | 100.0% |
| 1.0 | Sample1 | 5.81 | 25.25 | 0.34 | 0.00 | 0.12 | 0.01 | 97.3% |
| 5.0 | Sample2 | 5.83 | 20.94 | 1.08 | 0.06 | 3.72 | 0.27 | 99.8% |
| 24.0 | Sample3 | 6.21 | 7.03 | 2.45 | 0.05 | 15.21 | 0.54 | 97.9% |
| 48.0 | Sample4 | 6.42 | 2.05 | 3.36 | 0.01 | 20.59 | 0.21 | 100.0% |
| Reactor Sample | | 6.37 | 1.50 | 3.44 | 0.01 | 20.63 | 0.17 | 98.0% |



[1] Comp. **A** denotes 3,3'-diamino-diphenylamine
[2] Comp. **B** denotes 3-hydroxy,3'-amino-diphenylamine

# APPENDIX - H

## Adsorption Data of Solutes onto Zeolites

The following tables provide the adsorption data of solutes MPDA, MAP, resorcinol and ammonia onto zeolites USY, Beta and ZSM-5 (Si/Al = 13). The respective adsorption temperatures are given either in table titles or headings.

### H.1 Adsorption of aqueous MPDA

**Table H.1 Adsorption of MPDA onto USY**

| 30°C | | 50°C | | 70°C | | 90°C | |
|---|---|---|---|---|---|---|---|
| Bulk Conc. (mole-frac.) | Ads. Conc. (mmol/g) | Bulk Conc. (mole-frac.) | Ads. Conc. (mmol/g) | Bulk Conc. (mole-frac.) | Ads. Conc. (mmol/g) | Bulk Conc. (mole-frac.) | Ads. Conc. (mmol/g) |
| 1.014E-04 | 0.2251 | 7.416E-05 | 0.1654 | 4.435E-05 | 0.2906 | 5.774E-06 | 0.2719 |
| 2.888E-04 | 0.4947 | 1.927E-04 | 0.4234 | 1.573E-04 | 0.4637 | 1.151E-04 | 0.4821 |
| 8.913E-04 | 0.7883 | 5.540E-04 | 0.7164 | 5.683E-04 | 0.7111 | 5.237E-04 | 0.6779 |
| 2.009E-04 | 0.3582 | 1.077E-04 | 0.2853 | 1.325E-04 | 0.4607 | | |
| 3.109E-04 | 0.5028 | 1.630E-04 | 0.4003 | 1.272E-04 | 0.4327 | | |
| 1.762E-03 | 1.1063 | 1.318E-03 | 0.9533 | 1.389E-03 | 0.8220 | | |



**Table H.2 Adsorption of MPDA onto Beta**

| 30°C | | 50°C | | 70°C | | 90°C | |
|---|---|---|---|---|---|---|---|
| Bulk Conc. (mole-frac.) | Ads. Conc. (mmol/g) | Bulk Conc. (mole-frac.) | Ads. Conc. (mmol/g) | Bulk Conc. (mole-frac.) | Ads. Conc. (mmol/g) | Bulk Conc. (mole-frac.) | Ads. Conc. (mmol/g) |
| 2.652E-05 | 0.3916 | 1.963E-05 | 0.2902 | 7.570E-06 | 0.3759 | 3.273E-06 | 0.2653 |
| 1.052E-04 | 0.9415 | 3.611E-05 | 0.7510 | 2.007E-05 | 0.7316 | 1.549E-05 | 0.6557 |
| 6.257E-04 | 1.3218 | 3.234E-04 | 1.1640 | 3.738E-04 | 1.1468 | 2.923E-04 | 1.1661 |
| 5.846E-05 | 0.8364 | 1.337E-05 | 0.5863 | 1.231E-05 | 0.6428 | | |
| 7.950E-05 | 0.8718 | 1.351E-05 | 0.6376 | 8.744E-06 | 0.6160 | | |
| 1.477E-03 | 1.7048 | 1.124E-03 | 1.4054 | 1.126E-03 | 1.4284 | | |

**Table H.3 Adsorption of MPDA onto ZSM-5 (Si/Al = 13)**

| 30°C | | 50°C | | 70°C | | 90°C | |
|---|---|---|---|---|---|---|---|
| Bulk Conc. (mole-frac.) | Ads. Conc. (mmol/g) | Bulk Conc. (mole-frac.) | Ads. Conc. (mmol/g) | Bulk Conc. (mole-frac.) | Ads. Conc. (mmol/g) | Bulk Conc. (mole-frac.) | Ads. Conc. (mmol/g) |
| 1.830E-04 | 0.0157 | 9.063E-05 | 0.1139 | 1.114E-04 | 0.0998 | 7.181E-05 | 0.0824 |
| 4.080E-04 | 0.2045 | 2.554E-04 | 0.2143 | 1.300E-04 | 0.1131 | 2.637E-04 | 0.2172 |
| 1.060E-03 | 0.3044 | 7.597E-04 | 0.2066 | 6.612E-04 | 0.2537 | 6.928E-04 | 0.2567 |
| 2.749E-04 | 0.0541 | 1.411E-04 | 0.1638 | 5.168E-04 | 0.2314 | 1.638E-03 | 0.4560 |
| 4.774E-04 | 0.1753 | 2.683E-04 | 0.1885 | 2.655E-04 | 0.1684 | | |
| 2.055E-03 | 0.3434 | 1.643E-03 | 0.1927 | 1.589E-03 | 0.3324 | | |

## H.2 Adsorption of aqueous MAP

**Table H.4 Adsorption of MAP onto USY**

| 30°C | | 70°C | |
|---|---|---|---|
| Bulk Conc. (mole-frac.) | Ads. Conc. (mmol/g) | Bulk Conc. (mole-frac.) | Ads. Conc. (mmol/g) |
| 1.099E-04 | 0.0336 | 1.334E-04 | 0.1036 |
| 3.548E-04 | 0.1497 | 4.026E-04 | 0.2097 |
| 7.268E-04 | 0.1856 | 7.718E-04 | 0.2856 |
| 1.596E-03 | 0.4250 | 1.836E-03 | 0.4050 |
| 3.052E-03 | 0.4649 | 3.185E-03 | 0.4149 |
| 4.346E-03 | 1.6365 | 4.387E-03 | 0.4349 |

**Table H.5 Adsorption of MAP onto Beta**

| 30°C | | 70°C | |
|---|---|---|---|
| Bulk Conc. (mole-frac.) | Ads. Conc. (mmol/g) | Bulk Conc. (mole-frac.) | Ads. Conc. (mmol/g) |
| 3.054E-06 | 0.2772 | 9.168E-07 | 0.1759 |
| 1.274E-04 | 0.6341 | 3.460E-06 | 0.3201 |
| 4.653E-04 | 0.7572 | 1.069E-04 | 0.5891 |
| 1.295E-03 | 1.0533 | 1.175E-03 | 1.0971 |
| 2.718E-03 | 1.1411 | 3.067E-04 | 0.7349 |
| 4.055E-03 | 1.9504 | 2.884E-03 | 1.2209 |

**Table H.6 Adsorption of MAP onto ZSM-5 (Si/Al = 13)**

| 70°C | |
|---|---|
| **Bulk Conc.** (mole-frac.) | **Ads. Conc.** (mmol/g) |
| 7.416E-04 | 0.1961 |
| 1.139E-04 | 0.0252 |
| 3.138E-04 | 0.0538 |
| 1.539E-03 | 0.2875 |
| 3.375E-03 | 0.4014 |
| 2.478E-03 | 0.3573 |

## H.3 Adsorption of aqueous Resorcinol

**Table H.7 Adsorption of Resorcinol at 70°C onto zeolites**

| USY | | Beta | | ZSM-5 (Si/Al = 13) | |
|---|---|---|---|---|---|
| **Bulk Conc.** (mole-frac.) | **Ads. Conc.** (mmol/g) | **Bulk Conc.** (mole-frac.) | **Ads. Conc.** (mmol/g) | **Bulk Conc.** (mole-frac.) | **Ads. Conc.** (mmol/g) |
| 1.166E-04 | 0.0126 | 1.081E-04 | 0.0309 | 1.198E-04 | 0.0044 |
| 4.224E-04 | 0.0288 | 7.828E-04 | 0.2364 | 8.692E-04 | 0.0477 |
| 3.374E-03 | 0.3937 | 3.913E-04 | 0.0954 | 4.166E-04 | 0.0393 |
| 1.791E-03 | 0.2244 | 3.285E-03 | 0.5704 | 3.414E-03 | 0.2883 |
| 8.777E-05 | 0.0126 | 1.746E-03 | 0.3572 | 1.803E-03 | 0.1836 |
| 1.556E-04 | 0.0250 | 7.921E-05 | 0.0301 | 8.498E-05 | 0.0169 |
| 3.311E-04 | 0.0405 | 1.353E-04 | 0.0651 | 1.520E-04 | 0.0288 |
| 1.701E-03 | 0.2541 | 2.978E-04 | 0.1119 | 3.292E-04 | 0.0396 |
| 7.011E-04 | 0.0455 | 1.624E-03 | 0.4086 | 1.701E-03 | 0.2286 |
| 3.467E-03 | 0.3523 | 6.523E-04 | 0.1474 | 7.046E-04 | 0.0347 |
| | | 3.366E-03 | 0.5065 | 3.479E-03 | 0.2587 |

## H.4 Adsorption of aqueous Ammonia

All adsorption of aqueous ammonia is carried out at 70°C. The presence of ammonia in the headspace of the sample flask has been accounted for by estimating the ammonia in the vapour phase using [Sandler, 1989].

**Table H.8 Adsorption of Ammonia at 70°C onto zeolites**

| USY | | Beta | | ZSM-5 (Si/Al = 13) | |
|---|---|---|---|---|---|
| **Bulk Conc.** (mole-frac.) | **Ads. Conc.** (mmol/g) | **Bulk Conc.** (mole-frac.) | **Ads. Conc.** (mmol/g) | **Bulk Conc.** (mole-frac.) | **Ads. Conc.** (mmol/g) |
| 4.246E-04 | 1.7322 | 5.174E-04 | 1.1980 | 1.011E-03 | 0.3263 |
| 1.316E-03 | 2.3003 | 1.338E-03 | 1.6742 | 1.946E-03 | 0.6363 |
| 2.315E-03 | 2.5696 | 4.022E-03 | 2.6506 | 2.796E-03 | 1.2394 |
| 4.105E-03 | 3.6579 | 2.326E-03 | 1.7947 | 4.859E-03 | 1.5915 |
| 9.431E-03 | 4.2366 | 9.292E-03 | 2.7225 | 1.035E-02 | 1.7349 |

# APPENDIX - I

## Reaction Data using Aluminosilicates

Reaction data for USY, Beta and ZSM-5 (Si/Al = 13) are given for reaction temperatures 225°C, 275°C and 300°C. A reproducibility check for zeolite Beta at 275°C is included. Reaction data for the ZSM-5 (Si/Al = 22) and Silica-Alumina solids at 300°C are given. One reaction performed with plain Alumina (<200 mesh) is also included. The following tables all use 1.0000 ± 0.0100g MPDA, 350ml water and 10.000 ± 0.100g uncalcined fresh solids. The dehydrated solid mass is obtained by making use of Table 4.1. The mass of liquid withdrawn during sampling is included. The mole balance column denotes the percentage of accountable organic molecules relative to the initial quantity of MPDA.



### I.1 Reactions with USY

**Table I.1 Fresh USY (10g) at 225°C in 350ml water**

| Time (h) | Sample | Sample Weight (g) | pH | Corrected Mole Concentration (mmol/L) MPDA | MAP | Comp.A[1] | Resorc. | Comp.B[2] | Mole Balance |
|---|---|---|---|---|---|---|---|---|---|
| 0.0 | | | | 26.44 | 0.00 | 0.00 | 0.00 | 0.00 | 100.0% |
| 0.6 | Sample1 | 9.84 | 6.30 | 20.84 | 0.51 | 0.01 | 0.34 | 0.01 | 82.2% |
| 4.6 | Sample2 | 13.54 | 6.65 | 18.23 | 5.20 | 0.01 | 0.47 | 0.04 | 90.8% |
| 8.6 | Sample3 | 8.40 | 7.07 | 17.34 | 6.56 | 0.02 | 0.96 | 0.02 | 94.3% |
| 24.6 | Sample4 | 6.54 | 7.61 | 14.06 | 6.69 | 0.01 | 2.24 | 0.15 | 88.1% |

**Unaccounted Weight Loss = (-0.20 g)**

**Table I.2 Fresh USY (10g) at 275°C in 350ml water**

| Time (h) | Sample | Sample Weight (g) | pH | Corrected Mole Concentration (mmol/L) MPDA | MAP | Comp.A[1] | Resorc. | Comp.B[2] | Mole Balance |
|---|---|---|---|---|---|---|---|---|---|
| 0.0 | | | | 26.46 | 0.00 | 0.00 | 0.00 | 0.00 | 100.0% |
| 1.0 | Sample1 | 14.52 | 7.74 | 18.45 | 3.09 | 0.24 | 0.19 | 0.02 | 84.1% |
| 2.0 | Sample2 | 9.18 | 8.75 | 18.91 | 5.89 | 0.05 | 1.29 | 0.01 | 99.1% |
| 5.0 | Sample3 | 16.67 | 8.09 | 16.91 | 5.85 | 0.21 | 2.26 | 0.05 | 96.5% |
| 25.4 | Sample4 | 16.59 | 8.73 | 15.58 | 4.69 | 0.23 | 4.95 | 0.08 | 97.7% |
| 49.0 | Sample5 | 18.20 | 8.82 | 13.72 | 3.90 | 0.10 | 6.26 | 0.03 | 91.3% |

**Unaccounted Weight Loss = 3.49 g**

[1] Comp.**A** denotes 3,3'-diamino-diphenylamine
[2] Comp.**B** denotes 3-hydroxy,3'-amino-diphenylamine

**Table I.3 Fresh USY (10g) at 300°C in 350ml water**

| Time (h) | Sample | Sample Weight (g) | pH | Corrected Mole Concentration (mmol/L) MPDA | MAP | Comp.A[1] | Resorc. | Comp.B[2] | Mole Balance |
|---|---|---|---|---|---|---|---|---|---|
| 0.0 | | | | 26.47 | 0.00 | 0.00 | 0.00 | 0.00 | 100.0% |
| 1.0 | Sample1 | 24.48 | 7.75 | 16.87 | 6.11 | 0.04 | 0.64 | 0.00 | 89.6% |
| 5.1 | Sample2 | 18.76 | 8.12 | 16.63 | 6.63 | 0.09 | 2.73 | 0.00 | 98.8% |
| 9.3 | Sample3 | 25.51 | 8.48 | 16.80 | 6.26 | 0.05 | 4.14 | 0.00 | 103.1% |
| 25.0 | Sample4 | 34.02 | 8.56 | 12.84 | 3.77 | 0.16 | 6.08 | 0.03 | 87.2% |
| Reactor Sample | | | | 13.12 | 3.85 | 0.16 | 6.08 | 0.03 | 88.5% |

**Unaccounted Weight Loss = 0.37 g**

## I.2 Reactions with Beta

**Table I.4 Fresh Beta (10g) at 225°C in 350ml water**

| Time (h) | Sample | Sample Weight (g) | pH | Corrected Mol Concentration (mmol/L) MPDA | MAP | Comp.A[1] | Resorc. | Comp.B[2] | Mole Balance |
|---|---|---|---|---|---|---|---|---|---|
| 0.0 | | | | 26.44 | 0.00 | 0.00 | 0.00 | 0.00 | 100.0% |
| 0.5 | Sample1 | 12.94 | 7.68 | 5.23 | 0.28 | 0.00 | 0.01 | 0.02 | 21.1% |
| 4.8 | Sample2 | 9.53 | 8.22 | 7.78 | 1.70 | 0.02 | 0.51 | 0.30 | 40.3% |
| 8.8 | Sample3 | 13.86 | 8.72 | 7.39 | 1.83 | 0.06 | 0.88 | 0.67 | 43.7% |
| 10.8 | Sample4 | 11.63 | 9.00 | 7.29 | 1.88 | 0.08 | 1.19 | 0.78 | 45.7% |
| 24.8 | Sample5 | 10.34 | | 7.24 | 1.58 | 0.17 | 1.53 | 1.05 | 48.3% |

**Unaccounted Weight Loss =** unknown

**Table I.5 Fresh Beta (10g) at 275°C in 350ml water**

| Time (h) | Sample | Sample Weight (g) | pH | Corrected Mole Concentration (mmol/L) MPDA | MAP | Comp.A[1] | Resorc. | Comp.B[2] | Mole Balance |
|---|---|---|---|---|---|---|---|---|---|
| 0.0 | | | | 26.44 | 0.00 | 0.00 | 0.00 | 0.00 | 100.0% |
| 0.7 | Sample1 | 18.34 | | 2.84 | 2.01 | 0.19 | 0.36 | 0.10 | 21.9% |
| 1.1 | Sample2 | 20.32 | 7.34 | 5.14 | 12.02 | 0.12 | 3.08 | 0.11 | 78.4% |
| 2.0 | Sample3 | 20.10 | | 3.77 | 10.72 | 0.05 | 6.31 | 0.07 | 79.6% |
| 5.2 | Sample4 | 19.18 | 9.73 | 2.68 | 8.04 | 0.08 | 12.30 | 0.08 | 88.3% |
| 9.0 | Sample5 | 19.29 | 9.86 | 2.19 | 5.34 | 0.00 | 16.20 | 0.01 | 89.9% |
| 25.0 | Sample6 | 20.39 | 9.84 | 1.09 | 3.29 | 0.00 | 21.91 | 0.04 | 99.7% |
| Reactor Sample | | | | 1.04 | 3.25 | 0.00 | 20.44 | 0.04 | 93.8% |

**Unaccounted Weight Loss = 3.73 g**

[1] Comp.**A** denotes 3,3'-diamino-diphenylamine
[2] Comp.**B** denotes 3-hydroxy,3'-amino-diphenylamine

**Table I.6 Fresh Beta (10g) at 275°C in 350ml water (repeated)**

| Time (h) | Sample | Sample Weight (g) | pH | Corrected Mole Concentration (mmol/L) | | | | | Mole Balance |
|---|---|---|---|---|---|---|---|---|---|
| | | | | MPDA | MAP | Comp.A[1] | Resorc. | Comp.B[2] | |
| 0.0 | | | | 26.46 | 0.00 | 0.00 | 0.00 | 0.00 | 100.0% |
| 1.0 | Sample1 | 22.73 | 5.45 | 5.33 | 11.43 | 0.10 | 2.91 | 0.08 | 75.7% |
| 5.0 | Sample2 | 23.68 | 9.08 | 2.89 | 7.45 | 0.18 | 13.55 | 0.21 | 93.3% |
| 9.0 | Sample3 | 26.52 | 9.25 | 1.87 | 4.84 | 0.13 | 16.18 | 0.21 | 89.1% |
| 25.0 | Sample4 | 26.95 | 9.43 | 0.70 | 2.54 | 0.06 | 21.95 | 0.21 | 97.2% |
| Reactor Sample | | | | 0.42 | 2.09 | 0.00 | 19.91 | 0.03 | 85.0% |

**Unaccounted Weight Loss = 3.62 g**

**Table I.7 Fresh Beta (10g) at 300°C in 350ml water**

| Time (h) | Sample | Sample Weight (g) | pH | Corrected Mole Concentration (mmol/L) | | | | | Mole Balance |
|---|---|---|---|---|---|---|---|---|---|
| | | | | MPDA | MAP | Comp.A[1] | Resorc. | Comp.B[2] | |
| 0.0 | | | | 26.43 | 0.00 | 0.00 | 0.00 | 0.00 | 100.0% |
| 1.0 | Sample1 | 10.49 | | 5.48 | 11.66 | 0.07 | 3.73 | 0.07 | 80.0% |
| 4.0 | Sample2 | 12.07 | | 1.47 | 7.21 | 0.08 | 16.46 | 0.27 | 97.8% |
| 7.0 | Sample3 | 16.63 | | 1.53 | 4.73 | 0.04 | 19.73 | 0.05 | 99.1% |
| 24.0 | Sample4 | 16.25 | 9.74 | 0.23 | 1.82 | 0.13 | 23.10 | 0.07 | 96.7% |
| Reactor Sample | | | | 0.19 | 1.66 | 0.07 | 22.04 | 0.14 | 91.9% |

**Unaccounted Weight Loss = (-2.55 g)**

## I.3 Reactions with ZSM-5 (Si/Al = 13)

**Table I.8 Fresh ZSM-5 (Si/Al = 13) (10g) at 225°C in 350ml water**

| Time (h) | Sample | Sample Weight (g) | pH | Corrected Mole Concentration (mmol/L) | | | | | Mole Balance |
|---|---|---|---|---|---|---|---|---|---|
| | | | | MPDA | MAP | Comp.A[1] | Resorc. | Comp.B[2] | |
| 0.0 | | | | 26.58 | 0.00 | 0.00 | 0.00 | 0.00 | 100.0% |
| 0.6 | Sample1 | 10.61 | 7.46 | 26.26 | 0.05 | 0.02 | 0.00 | 0.07 | 99.6% |
| 4.6 | Sample2 | 12.90 | 8.38 | 25.27 | 0.03 | 0.04 | 0.02 | 0.17 | 96.8% |
| 8.6 | Sample3 | 12.56 | 7.83 | 24.90 | 0.13 | 0.04 | 0.24 | 0.14 | 96.4% |
| 11.3 | Sample4 | 8.65 | 7.38 | 24.94 | 0.17 | 0.06 | 0.22 | 0.15 | 96.9% |
| 24.6 | Sample5 | 9.75 | 7.94 | 23.78 | 0.28 | 0.03 | 0.24 | 0.12 | 92.5% |
| 35.6 | Sample6 | 15.68 | 7.99 | 25.25 | 0.51 | 0.03 | 0.28 | 0.12 | 99.1% |

**Unaccounted Weight Loss = 12.54 g**

[1] Comp.**A** denotes 3,3'-diamino-diphenylamine
[2] Comp.**B** denotes 3-hydroxy,3'-amino-diphenylamine

**Table I.9 Fresh ZSM-5 (Si/Al = 13) (10g) at 275°C in 350ml water**

| Time (h) | Sample | Sample Weight (g) | pH | Corrected Mole Concentration (mmol/L) | | | | | Mole Balance |
|---|---|---|---|---|---|---|---|---|---|
| | | | | MPDA | MAP | Comp.-A | Resorc. | Comp.-B | |
| 0.0 | | | | 26.44 | 0.00 | 0.00 | 0.00 | 0.00 | 100.0% |
| 1.1 | Sample1 | 17.28 | 8.58 | 24.73 | 0.00 | 0.00 | 0.00 | 0.00 | 93.5% |
| 5.0 | Sample2 | 20.11 | 8.82 | 23.54 | 0.30 | 0.00 | 0.02 | 0.00 | 90.2% |
| 9.0 | Sample3 | 20.70 | 8.68 | 23.30 | 0.68 | 0.00 | 0.04 | 0.00 | 90.9% |
| 24.0 | Sample4 | 23.06 | 8.72 | 23.71 | 1.95 | 0.00 | 0.25 | 0.00 | 98.0% |
| Reactor Sample | | | | 23.32 | 1.78 | 0.00 | 0.12 | 0.00 | 95.4% |

**Unaccounted Weight Loss = 2.36 g**

**Table I.10 Fresh ZSM-5 (Si/Al = 13) (10g) at 300°C in 350ml water**

| Time (h) | Sample | Sample Weight (g) | pH | Corrected Mole Concentration (mmol/L) | | | | | Mole Balance |
|---|---|---|---|---|---|---|---|---|---|
| | | | | MPDA | MAP | Comp.-A | Resorc. | Comp.-B | |
| 0.0 | | | | 26.43 | 0.00 | 0.00 | 0.00 | 0.00 | 100.0% |
| 1.0 | Sample1 | 15.71 | 8.54 | 26.99 | 0.13 | 0.00 | 0.06 | 0.00 | 102.9% |
| 3.0 | Sample2 | 12.92 | 8.65 | 25.38 | 0.45 | 0.00 | 0.06 | 0.00 | 98.0% |
| 5.5 | Sample3 | 18.73 | 8.25 | 26.36 | 0.87 | 0.00 | 0.08 | 0.00 | 103.4% |
| 24.0 | Sample4 | 27.54 | 8.86 | 22.47 | 2.60 | 0.00 | 0.48 | 0.00 | 96.7% |
| Reactor Sample | | | | 21.26 | 2.46 | 0.00 | 0.44 | 0.00 | 91.5% |

**Unaccounted Weight Loss = 2.30 g**

## I.4 Reactions with ZSM-5 (Si/Al = 22)

**Table I.11 Fresh ZSM-5 (Si/Al = 22) (10g) at 300°C in 350ml water**

| Time (h) | Sample | Sample Weight (g) | pH | Corrected Mole Concentration (mmol/L) | | | | | Mole Balance |
|---|---|---|---|---|---|---|---|---|---|
| | | | | MPDA | MAP | Comp.-A | Resorc. | Comp.-B | |
| 0.0 | | | | 26.43 | 0.00 | 0.00 | 0.00 | 0.00 | 100.0% |
| 1.0 | Sample1 | 17.42 | 8.69 | 14.74 | 5.59 | 0.00 | 0.66 | 0.00 | 79.5% |
| 3.1 | Sample2 | 24.90 | 8.58 | 10.62 | 8.11 | 0.00 | 3.94 | 0.00 | 85.8% |
| 9.1 | Sample3 | 25.92 | 8.85 | 5.66 | 6.80 | 0.00 | 9.56 | 0.06 | 83.8% |
| 25.0 | Sample4 | 25.27 | | 1.89 | 3.32 | 0.00 | 12.91 | 0.26 | 70.6% |
| Reactor Sample | | | | 1.93 | 3.40 | 0.00 | 12.91 | 0.26 | 71.0% |

**Unaccounted Weight Loss = 1.71 g**

[1] Comp.**A** denotes 3,3'-diamino-diphenylamine
[2] Comp.**B** denotes 3-hydroxy,3'-amino-diphenylamine

## I.5 Reactions with Silica-Alumina

### Table I.12 Fresh Silica-Alumina (10g) at 300°C in 350ml water

| Time (h) | Sample | Sample Weight (g) | pH | Corrected Mole Concentration (mmol/L) | | | | | Mole Balance |
|---|---|---|---|---|---|---|---|---|---|
| | | | | MPDA | MAP | Comp.-A | Resorc. | Comp.-B | |
| 0.0 | | | | 26.43 | 0.00 | 0.00 | 0.00 | 0.00 | 100.0% |
| 1.0 | Sample1 | 13.07 | 6.79 | 20.80 | 3.43 | 0.05 | 0.40 | 0.11 | 94.4% |
| 5.0 | Sample2 | 17.91 | 7.35 | 16.85 | 5.11 | 0.11 | 4.05 | 0.07 | 99.8% |
| 10.0 | Sample3 | 24.67 | 8.42 | 10.63 | 2.80 | 0.03 | 10.75 | 0.15 | 92.9% |
| 24.4 | Sample4 | 20.89 | 9.04 | 9.99 | 2.62 | 0.11 | 10.44 | 0.27 | 90.1% |
| Reactor Sample | | | | 10.20 | 2.68 | 0.11 | 10.44 | 0.27 | 91.1% |

**Unaccounted Weight Loss = 3.50 g**

## I.6 Reactions with Alumina (<200 mesh)

### Table I.13 Fresh Alumina (10g) at 300°C in 350ml water

| Time (h) | Sample | Sample Weight (g) | pH | Corrected Mole Concentration (mmol/L) | | | | | Mole Balance |
|---|---|---|---|---|---|---|---|---|---|
| | | | | MPDA | MAP | Comp.-A | Resorc. | Comp.-B | |
| 0.0 | | | | 26.61 | 0.00 | 0.00 | 0.00 | 0.00 | 100.0% |
| 0.7 | Sample1 | 8.24 | 8.17 | 25.96 | 0.00 | 0.00 | 0.00 | 0.00 | 97.6% |
| 4.8 | Sample2 | 7.62 | 9.05 | 26.17 | 0.03 | 0.00 | 0.00 | 0.00 | 98.5% |
| 8.8 | Sample3 | 13.49 | 9.02 | 26.26 | 0.04 | 0.00 | 0.01 | 0.00 | 98.9% |
| 24.6 | Sample4 | 10.65 | 9.02 | 26.33 | 0.03 | 0.00 | 0.06 | 0.00 | 99.3% |
| 31.8 | Sample5 | 15.26 | 8.60 | 25.79 | 0.04 | 0.00 | 0.03 | 0.00 | 97.2% |

**Unaccounted Weight Loss = (-2.87 g)**



[1] Comp.**A** denotes 3,3'-diamino-diphenylamine
[2] Comp.**B** denotes 3-hydroxy,3'-amino-diphenylamine

# APPENDIX - J

## Adsorption Data of Solutes onto Zirconium Phosphates

The following tables provide the adsorption data of solutes MPDA, MAP, resorcinol and ammonia onto zirconium phosphates α-ZrP, α-ZrP400, γ-ZrP and γ-ZrP400. The solution pH after the 6days adsorption period is included. The respective adsorption temperatures are given in table titles or sectional headings.

### J.1 Adsorption of aqueous MPDA

**Table J.1 Adsorption of MPDA onto α-ZrP**

| 30°C | | | 50°C | | | 70°C | | |
|---|---|---|---|---|---|---|---|---|
| **Bulk Conc.** mole-frac. | **Ads. Conc.** mol/(mol Zr) | **pH** | **Bulk Conc.** mole-frac. | **Ads. Conc.** mol/(mol Zr) | **pH** | **Bulk Conc.** mole-frac. | **Ads. Conc.** mol/(mol Zr) | **pH** |
| 4.779E-06 | 0.1155 | 2.50 | 5.343E-06 | 0.1612 | n.a. | 7.998E-06 | 0.0970 | 2.08 |
| 5.624E-06 | 0.2590 | 2.91 | 6.433E-06 | 0.1653 | n.a. | 8.389E-06 | 0.1601 | 2.05 |
| 5.959E-06 | 0.2540 | 2.34 | 7.224E-06 | 0.2115 | n.a. | 8.511E-06 | 0.1903 | 2.08 |
| 7.393E-06 | 0.2833 | 2.68 | 7.544E-06 | 0.4833 | n.a. | 8.710E-06 | 0.1648 | 2.12 |
| 7.047E-05 | 0.6832 | 4.76 | 2.240E-05 | 0.0725 | n.a. | 2.118E-05 | 0.5130 | 3.23 |
| 1.013E-03 | 0.7338 | 5.69 | 5.260E-04 | 0.6818 | n.a. | 5.924E-04 | 0.7166 | 5.36 |

**Table J.2 Adsorption of MPDA onto α-ZrP400**

| 70°C | | |
|---|---|---|
| **Bulk Conc.** mole-frac. | **Ads. Conc.** mol/(mol Zr) | **pH** |
| 6.144E-06 | 0.0588 | 2.05 |
| 9.131E-06 | 0.1234 | 2.16 |
| 1.300E-05 | 0.1910 | 2.30 |
| 3.316E-05 | 0.3987 | 3.67 |
| 7.755E-04 | 0.5519 | 5.33 |
| 3.803E-03 | 0.6312 | 6.00 |

**Table J.3 Adsorption of MPDA onto γ-ZrP**

| 30°C | | | 70°C | | |
|---|---|---|---|---|---|
| **Bulk Conc.** mole-frac. | **Ads. Conc.** mol/(mol Zr) | **pH** | **Bulk Conc.** mole-frac. | **Ads. Conc.** mol/(mol Zr) | **pH** |
| 1.445E-06 | 0.1055 | 2.31 | 4.748E-08 | 0.0881 | 1.87 |
| 9.094E-06 | 0.3018 | 3.14 | 5.612E-08 | 0.1423 | 1.97 |
| 1.114E-05 | 0.2942 | 2.96 | 2.561E-06 | 0.2220 | 2.37 |
| 1.787E-05 | 0.3086 | 2.95 | 7.757E-05 | 0.4233 | 4.15 |
| 3.338E-04 | 0.5604 | 5.16 | 9.745E-04 | 0.5788 | 5.24 |
| 2.243E-03 | 0.7513 | 5.88 | 3.445E-03 | 0.7243 | 5.88 |

**Table J.4 Adsorption of MPDA onto γ-ZrP400**

| 30°C | | | 50°C | | | 70°C | | |
|---|---|---|---|---|---|---|---|---|
| **Bulk Conc.** mole-frac. | **Ads. Conc.** mol/(mol Zr) | **pH** | **Bulk Conc.** mole-frac. | **Ads. Conc.** mol/(mol Zr) | **pH** | **Bulk Conc.** mole-frac. | **Ads. Conc.** mol/(mol Zr) | **pH** |
| 1.451E-04 | 0.0109 | 4.44 | 6.644E-05 | 0.0136 | 4.05 | 6.886E-05 | 0.0283 | 3.93 |
| 2.539E-04 | 0.0338 | 4.91 | 2.024E-04 | 0.0425 | 4.83 | 1.809E-04 | 0.0747 | 4.65 |
| 4.162E-04 | 0.0312 | 4.98 | 2.152E-04 | 0.0652 | 4.88 | 7.189E-04 | 0.0564 | 5.46 |
| 4.798E-04 | 0.0398 | 4.98 | 6.539E-04 | 0.0839 | 5.37 | 1.527E-03 | 0.1662 | 5.78 |
| 1.062E-03 | 0.0755 | 5.49 | 1.558E-03 | 0.1204 | 5.77 | 3.199E-03 | 0.2450 | 6.03 |
| 2.843E-03 | 0.3426 | 6.45 | 4.994E-03 | 0.3289 | 6.29 | 4.549E-03 | 0.3427 | 6.11 |



## J.2 Adsorption of aqueous MAP

**Table J.5 Adsorption of MAP at 70°C onto α-ZrP and α-ZrP400**

| α-ZrP | | | α-ZrP400 | | |
|---|---|---|---|---|---|
| **Bulk Conc.** mole-frac. | **Ads. Conc.** mol/(mol Zr) | **pH** | **Bulk Conc.** mole-frac. | **Ads. Conc.** mol/(mol Zr) | **pH** |
| 1.145E-04 | 0.0064 | n.a. | 1.280E-04 | 0.0099 | 2.55 |
| 2.872E-04 | 0.0309 | n.a. | 2.204E-04 | 0.0660 | 3.02 |
| 5.083E-04 | 0.1941 | n.a. | 3.229E-04 | 0.2831 | 2.62 |
| 1.071E-03 | 0.3559 | n.a. | 6.127E-04 | 0.6354 | 3.33 |
| 1.694E-03 | 0.5469 | n.a. | 7.945E-04 | 0.5931 | 3.81 |
| 2.580E-03 | 0.5720 | n.a. | 1.842E-03 | 0.7431 | 3.88 |

**Table J.6 Adsorption of MAP at 70°C onto γ-ZrP and γ-ZrP400**

| γ-ZrP | | | γ-ZrP400 | | |
|---|---|---|---|---|---|
| **Bulk Conc.** mole-frac. | **Ads. Conc.** mol/(mol Zr) | **pH** | **Bulk Conc.** mole-frac. | **Ads. Conc.** mol/(mol Zr) | **pH** |
| 3.821E-05 | 0.0562 | n.a. | 1.059E-04 | 0.0213 | 3.05 |
| 5.452E-05 | 0.1806 | n.a. | 2.900E-04 | 0.0261 | 2.75 |
| 1.293E-04 | 0.4526 | n.a. | 7.454E-04 | 0.0474 | 4.18 |
| 6.179E-04 | 0.6630 | n.a. | 1.617E-03 | 0.0573 | 3.81 |
| 1.434E-03 | 0.7732 | n.a. | 1.761E-03 | 0.0510 | 4.08 |
| 2.230E-03 | 0.8234 | n.a. | 2.971E-03 | 0.0979 | 5.28 |

## J.3 Adsorption of aqueous Resorcinol

**Table J.7 Adsorption of Resorcinol at 70°C onto α-ZrP and α-ZrP400**

| α-ZrP | | | α-ZrP400 | | |
|---|---|---|---|---|---|
| **Bulk Conc.** mole-frac. | **Ads. Conc.** mol/(mol Zr) | **pH** | **Bulk Conc.** mole-frac. | **Ads. Conc.** mol/(mol Zr) | **pH** |
| 8.980E-05 | 0.0013 | n.a. | 1.485E-04 | - | 1.75 |
| 9.177E-05 | 0.0002 | 1.86 | 3.380E-04 | 0.0014 | 1.80 |
| 2.154E-04 | 0.0029 | 1.78 | 6.372E-04 | 0.0080 | 1.92 |
| 2.172E-04 | 0.0018 | n.a. | 9.950E-04 | 0.0017 | 2.09 |
| 4.121E-04 | 0.0036 | 2.02 | 1.847E-03 | 0.0112 | 1.75 |
| 4.145E-04 | 0.0022 | n.a. | 3.783E-03 | 0.0054 | 2.15 |
| 7.559E-04 | 0.0273 | 2.10 | | | |
| 7.743E-04 | 0.0165 | n.a. | | | |
| 1.471E-03 | 0.0244 | n.a. | | | |
| 1.476E-03 | 0.0208 | 2.01 | | | |
| 3.494E-03 | 0.0932 | n.a. | | | |
| 3.531E-03 | 0.0708 | 2.09 | | | |

**Table J.8 Adsorption of Resorcinol at 70°C onto γ-ZrP and γ-ZrP400**

| γ-ZrP | | | γ-ZrP400 | | |
|---|---|---|---|---|---|
| **Bulk Conc.** mole-frac. | **Ads. Conc.** mol/(mol Zr) | **pH** | **Bulk Conc.** mole-frac. | **Ads. Conc.** mol/(mol Zr) | **pH** |
| 1.192E-04 | 0.0016 | 2.65 | 1.348E-04 | 0.0072 | 2.25 |
| 4.165E-04 | 0.0107 | 2.43 | 3.408E-04 | - | 2.28 |
| 8.917E-04 | 0.0139 | 2.60 | 6.415E-04 | 0.0054 | 2.23 |
| 1.803E-03 | 0.0407 | 2.56 | 9.885E-04 | 0.0019 | 2.21 |
| 4.607E-03 | 0.1584 | 2.62 | 1.832E-03 | 0.0194 | |
| | | | 3.782E-03 | 0.0047 | 2.32 |

## J.4 Adsorption of aqueous Ammonia

All adsorption of aqueous ammonia is carried out at 70°C. The presence of ammonia in the headspace of the sample flask has been accounted for by estimating the ammonia in the vapour phase using [Sandler, 1989].

**Table J.9 Adsorption of Ammonia at 70°C onto α-ZrP and γ-ZrP**

| α-ZrP | | | γ-ZrP | | |
|---|---|---|---|---|---|
| **Bulk Conc.** mole-frac. | **Ads. Conc.** mol/(mol Zr) | **pH** | **Bulk Conc.** mole-frac. | **Ads. Conc.** mol/(mol Zr) | **pH** |
| 0.000E+00 | 0.3386 | n.a. | 0.000E+00 | 0.3601 | n.a. |
| 0.000E+00 | 0.6723 | n.a. | 0.000E+00 | 0.7243 | n.a. |
| 0.000E+00 | 1.0328 | n.a. | 0.000E+00 | 1.0786 | n.a. |
| 2.705E-05 | 1.7092 | n.a. | 6.594E-05 | 1.7422 | n.a. |
| 2.331E-03 | 2.0499 | n.a. | 2.577E-03 | 1.9516 | n.a. |
| 7.531E-03 | 2.2633 | n.a. | 7.785E-03 | 2.3010 | n.a. |

# APPENDIX - K

## Reaction Data using Zirconium Phosphates

Reaction data for the conversion of MPDA over α-ZrP, α-ZrP400, γ-ZrP and γ-ZrP400 are given for the reactions carried out at 225°C and 275°C. The reaction tables all use 1.0000 ± 0.0100g MPDA, 350ml water and 10.000 ± 0.100g of the uncalcined fresh solids. According to the method outline in Section 3.3.1.2, the recovered zirconium phosphates (α-ZrP400, γ-ZrP and γ-ZrP400) are regenerated and reused in the second reaction with the reaction temperature corresponding to the temperature used during the first reaction. The zirconium phosphate to MPDA mole ratios (mol Zr)/(mol MPDA) for the second set of reactions (regenerated samples) are roughly identical to the first set of reactions by means of the method stated in Section 3.3.1.3.



### K.1 Reactions with α-ZrP

**Table K.1 Fresh α-ZrP (10g) at 225°C in 350ml water and 1g MPDA**

| Time (h) | Sample | Sample Weight (g) | pH | Corrected Mole Concentration (mmol/L) MPDA | MAP | Comp.A[1] | Resorc. | Comp.B[2] | Mole Balance |
|---|---|---|---|---|---|---|---|---|---|
| 0.0 | | | | 27.50 | 0.00 | 0.00 | 0.00 | 0.00 | 100.0% |
| 0.7 | Sample1 | 17.41 | 5.44 | 25.16 | 0.40 | 0.00 | 0.00 | 0.08 | 93.5% |
| 4.7 | Sample2 | 16.54 | 5.01 | 20.07 | 2.75 | 0.03 | 0.77 | 0.13 | 87.0% |
| 8.7 | Sample3 | 15.75 | 5.00 | 17.64 | 3.68 | 0.02 | 1.99 | 0.18 | 86.3% |
| 24.7 | Sample4 | 19.64 | 4.96 | 11.83 | 3.35 | 0.05 | 7.55 | 0.40 | 85.9% |
| 32.7 | Sample5 | 15.95 | 4.95 | 9.51 | 4.02 | 0.04 | 9.35 | 0.38 | 86.3% |

**Unaccounted Weight Loss =** unknown

**Table K.2 Fresh α-ZrP (10g) at 275°C in 350ml water and 4g MPDA**

| Time (h) | Sample | Sample Weight (g) | pH | Corrected Mole Concentration (mmol/L) MPDA | MAP | Comp.A[1] | Resorc. | Comp.B[2] | Mole Balance |
|---|---|---|---|---|---|---|---|---|---|
| 0.0 | | | | 105.78 | 0.00 | 0.00 | 0.00 | 0.00 | 100.0% |
| 72.0 | Sample1 | | | 28.03 | 10.15 | 3.29 | 36.11 | 12.36 | 99.8% |

[1] Comp.**A** denotes 3,3'-diamino-diphenylamine
[2] Comp.**B** denotes 3-hydroxy,3'-amino-diphenylamine

## K.2 Reactions with α-ZrP400

10g of the original α-ZrP weighs ca. 9.3g after calcination at 400°C (see Table 4.11 in Section 4.5).

**Table K.3 Fresh α-ZrP400 (9.3g) at 225°C in 350ml water and 1g MPDA**

| Time (h) | Sample | Sample Weight (g) | pH | Corrected Mole Concentration (mmol/L) | | | | | Mole Balance |
|---|---|---|---|---|---|---|---|---|---|
| | | | | MPDA | MAP | Comp.A[1] | Resorc. | Comp.B[2] | |
| 0.0 | | | | 26.44 | 0.00 | 0.00 | 0.00 | 0.00 | 100.0% |
| 1.0 | Sample1 | 20.07 | 5.38 | 22.55 | 1.28 | 0.14 | 0.29 | 0.01 | 92.3% |
| 5.0 | Sample2 | 16.06 | 5.47 | 18.37 | 4.76 | 0.38 | 1.97 | 0.09 | 98.5% |
| 9.0 | Sample3 | 15.23 | 5.67 | 14.91 | 5.43 | 0.48 | 4.80 | 0.16 | 100.0% |
| 24.0 | Sample4 | 17.17 | 5.38 | 8.78 | 2.64 | 0.51 | 13.26 | 0.35 | 99.9% |
| Reactor Sample | | | | 7.31 | 2.76 | 0.19 | 14.75 | 0.35 | 97.9% |

**Unaccounted Weight Loss = 3.0 g**

**Table K.4 Regenerated α-ZrP400 (89w/w% original α-ZrP400) at 225°C in 350ml water and corresponding mass of MPDA**

| Time (h) | Sample | Sample Weight (g) | pH | Corrected Mole Concentration (mmol/L) | | | | | Mole Balance |
|---|---|---|---|---|---|---|---|---|---|
| | | | | MPDA | MAP | Comp.A[1] | Resorc. | Comp.B[2] | |
| 0.0 | | | | 23.63 | 0.00 | 0.00 | 0.00 | 0.00 | 100.0% |
| 1.0 | Sample1 | 18.30 | 5.54 | 21.01 | 0.77 | 0.05 | 0.15 | 0.01 | 93.3% |
| 5.0 | Sample2 | 16.50 | 5.33 | 18.01 | 3.18 | 0.22 | 1.36 | 0.04 | 97.7% |
| 9.0 | Sample3 | 16.10 | 5.61 | 15.39 | 3.77 | 0.31 | 3.51 | 0.09 | 99.3% |
| 25.0 | Sample4 | 16.23 | 4.68 | 8.21 | 2.02 | 0.37 | 11.84 | 0.29 | 99.0% |
| Reactor Sample | | | | 7.62 | 2.11 | 0.08 | 12.58 | 0.28 | 97.5% |

**Unaccounted Weight Loss = 7.7 g**

**Table K.5 Fresh α-ZrP400 (9.3g) at 275°C in 350ml water and 1g MPDA**

| Time (h) | Sample | Sample Weight (g) | pH | Corrected Mole Concentration (mmol/L) | | | | | Mole Balance |
|---|---|---|---|---|---|---|---|---|---|
| | | | | MPDA | MAP | Comp.A[1] | Resorc. | Comp.B[2] | |
| 0.0 | | | | 26.44 | 0.00 | 0.00 | 0.00 | 0.00 | 100.0% |
| 1.1 | Sample1 | 14.66 | 5.33 | 20.71 | 1.59 | 0.06 | 0.69 | 0.01 | 87.5% |
| 5.3 | Sample2 | 14.16 | 4.93 | 14.58 | 2.04 | 0.13 | 7.53 | 0.15 | 93.5% |
| 9.0 | Sample3 | 16.49 | 4.05 | 7.52 | 1.22 | 0.12 | 15.94 | 0.33 | 96.8% |
| 25.1 | Sample4 | 17.50 | 2.02 | 0.13 | 0.00 | 0.02 | 26.79 | 0.01 | 102.0% |

**Unaccounted Weight Loss = 2.1 g**

[1] Comp.**A** denotes 3,3'-diamino-diphenylamine
[2] Comp.**B** denotes 3-hydroxy,3'-amino-diphenylamine

## K.3 Reactions with γ-ZrP

Reactions are conducted with γ-ZrP (batch no.: G05-7) and γ-ZrP (batch no.: E0906). Apart for γ-ZrP (batch no.: G05-7) containing small amounts of solid $H_3PO_4$ (0.05mmol/g γ-ZrP), the structural and chemical properties of the two γ-ZrP samples are identical.

**Table K.6 Fresh γ-ZrP (batch no.: G05-7) (10g) at 225°C in 350ml water and 1g MPDA**

| Time (h) | Sample | Sample Weight (g) | pH | Corrected Mole Concentration (mmol/L) | | | | | Mole Balance |
|---|---|---|---|---|---|---|---|---|---|
| | | | | MPDA | MAP | Comp.A[1] | Resorc. | Comp.B[2] | |
| 0.0 | | | | 26.47 | 0.00 | 0.00 | 0.00 | 0.00 | 100.0% |
| 1.0 | Sample1 | 13.58 | 4.88 | 9.60 | 8.30 | 0.17 | 0.85 | 0.03 | 72.3% |
| 5.0 | Sample2 | 15.73 | 4.28 | 3.82 | 8.11 | 0.29 | 10.26 | 0.19 | 87.5% |
| 9.0 | Sample3 | 18.64 | 3.94 | 1.99 | 4.39 | 0.24 | 16.01 | 0.22 | 88.1% |
| 25.0 | Sample4 | 13.75 | 3.85 | 0.54 | 0.59 | 0.15 | 21.91 | 0.19 | 89.6% |
| Reactor Sample | | | | 0.10 | 0.45 | 0.01 | 20.90 | 0.17 | 82.4% |

**Unaccounted Weight Loss = 5.8 g**

**Table K.7 Reuse γ-ZrP (batch no.: G05-7) (80w/w% original γ-ZrP) at 225°C in 350ml water and 1g MPDA**

| Time (h) | Sample | Sample Weight (g) | pH | Corrected Mole Concentration (mmol/L) | | | | | Mole Balance |
|---|---|---|---|---|---|---|---|---|---|
| | | | | MPDA | MAP | Comp.A[1] | Resorc. | Comp.B[2] | |
| 0.0 | | | | 21.27 | 0.00 | 0.00 | 0.00 | 0.00 | 100.0% |
| 1.0 | Sample1 | n.a. | 6.45 | 20.65 | 0.50 | 0.03 | 0.25 | 0.01 | 101.0% |
| 5.0 | Sample2 | n.a. | 6.90 | 19.78 | 1.87 | 0.04 | 0.37 | 0.03 | 104.2% |
| 9.0 | Sample3 | n.a. | | 18.08 | 2.60 | 0.06 | 0.89 | 0.03 | 102.3% |
| 25.2 | Sample4 | n.a. | 7.62 | 14.79 | 3.52 | 0.10 | 3.62 | 0.09 | 104.8% |
| Reactor Sample | | n.a. | | 13.49 | 3.35 | 0.06 | 3.01 | 0.07 | 94.5% |

**Unaccounted Weight Loss =** unknown

[1] Comp.**A** denotes 3,3'-diamino-diphenylamine
[2] Comp.**B** denotes 3-hydroxy,3'-amino-diphenylamine

**Table K.8 Fresh γ-ZrP (batch no.: E0906) (10g) at 225°C in 350ml water and 1g MPDA**

| Time (h) | Sample | Sample Weight (g) | pH | Corrected Mole Concentration (mmol/L) | | | | | Mole Balance |
|---|---|---|---|---|---|---|---|---|---|
| | | | | MPDA | MAP | Comp.A[1] | Resorc. | Comp.B[2] | |
| 0.0 | | | | 26.40 | 0.00 | 0.00 | 0.00 | 0.00 | 100.0% |
| 1.0 | Sample1 | 16.41 | 6.85 | 8.37 | 9.08 | 0.22 | 1.08 | 0.03 | 72.1% |
| 5.0 | Sample2 | 11.54 | 7.40 | 2.70 | 7.73 | 0.27 | 11.07 | 0.17 | 84.7% |
| 9.0 | Sample3 | 21.37 | 8.72 | 1.40 | 4.01 | 0.25 | 17.07 | 0.19 | 88.5% |
| 25.0 | Sample4 | 13.75 | 8.46 | 0.36 | 0.45 | 0.17 | 22.26 | 0.14 | 89.8% |
| Reactor Sample | | | | 0.05 | 0.30 | 0.05 | 21.69 | 0.12 | 84.7% |

**Unaccounted Weight Loss = (-1.5 g)**

**Table K.9 Reuse γ-ZrP (batch no.: E0906) (86w/w% original γ-ZrP) at 225°C in 350ml water and corresponding mass of MPDA**

| Time (h) | Sample | Sample Weight (g) | pH | Corrected Mole Concentration (mmol/L) | | | | | Mole Balance |
|---|---|---|---|---|---|---|---|---|---|
| | | | | MPDA | MAP | Comp.A[1] | Resorc. | Comp.B[2] | |
| 0.0 | | | | 22.64 | 0.00 | 0.00 | 0.00 | 0.00 | 100.0% |
| 1.0 | Sample1 | 14.54 | 6.69 | 22.83 | 0.60 | 0.06 | 0.18 | 0.00 | 104.8% |
| 5.1 | Sample2 | 18.87 | 8.08 | 20.59 | 2.50 | 0.10 | 0.64 | 0.02 | 105.9% |
| 9.0 | Sample3 | 17.65 | 8.75 | 18.81 | 3.45 | 0.12 | 1.34 | 0.04 | 105.6% |
| 24.0 | Sample4 | 16.34 | 8.32 | 15.19 | 3.68 | 0.15 | 3.83 | 0.09 | 102.3% |

**Unaccounted Weight Loss = 0.3 g**

**Table K.10 Fresh γ-ZrP (batch no.: G05-7) (10g) at 275°C in 350ml water and 1g MPDA**

| Time (h) | Sample | Sample Weight (g) | pH | Corrected Mole Concentration (mmol/L) | | | | | Mole Balance |
|---|---|---|---|---|---|---|---|---|---|
| | | | | MPDA | MAP | Comp.A[1] | Resorc. | Comp.B[2] | |
| 0.0 | | | | 26.44 | 0.00 | 0.00 | 0.00 | 0.00 | 100.0% |
| 1.0 | Sample1 | 19.48 | 4.67 | 8.50 | 7.97 | 0.21 | 4.35 | 0.08 | 81.0% |
| 5.0 | Sample2 | 20.43 | 3.31 | 2.52 | 1.10 | 0.16 | 19.12 | 0.18 | 88.6% |
| 9.8 | Sample3 | 18.27 | 3.10 | 1.25 | 0.43 | 0.10 | 22.46 | 0.15 | 93.2% |
| 25.0 | Sample4 | 21.79 | 2.42 | 0.21 | 0.18 | 0.04 | 26.06 | 0.03 | 100.6% |
| Reactor Sample | | | | 0.21 | 0.21 | 0.02 | 22.17 | 0.10 | 86.3% |

**Unaccounted Weight Loss = 11.2 g**

[1] Comp.**A** denotes 3,3'-diamino-diphenylamine
[2] Comp.**B** denotes 3-hydroxy,3'-amino-diphenylamine

## K.4 Reactions with γ-ZrP400

10g of the original γ-ZrP weighs ca. 8.4g after calcination at 400°C (see Table 4.11 in Section 4.5). Only γ-ZrP with batch no. G05-7 is used.

**Table K.11 Fresh γ-ZrP400 (8.4g) at 225°C in 350ml water and 1g MPDA**

| Time (h) | Sample | Sample Weight (g) | pH | Corrected Mole Concentration (mmol/L) MPDA | MAP | Comp.A[1] | Resorc. | Comp.B[2] | Mole Balance |
|---|---|---|---|---|---|---|---|---|---|
| 0.0 | | | | 26.47 | 0.00 | 0.00 | 0.00 | 0.00 | 100.0% |
| 1.1 | Sample1 | 16.25 | 6.01 | 24.11 | 1.06 | 0.07 | 0.36 | 0.00 | 97.0% |
| 5.0 | Sample2 | 17.99 | 4.79 | 5.42 | 9.25 | 0.34 | 6.87 | 0.25 | 85.9% |
| 9.0 | Sample3 | 18.64 | 3.57 | 0.79 | 4.95 | 0.29 | 16.94 | 0.30 | 90.1% |
| 25.0 | Sample4 | 18.64 | 2.64 | 0.07 | 0.22 | 0.11 | 24.64 | 0.15 | 96.2% |
| Reactor Sample | | | | 0.02 | 0.12 | 0.01 | 23.64 | 0.13 | 90.9% |

**Unaccounted Weight Loss = 1.0 g**

**Table K.12 Reuse γ-ZrP400 (89w/w% original γ-ZrP) at 225°C in 350ml water and corresponding mass of MPDA**

| Time (h) | Sample | Sample Weight (g) | pH | Corrected Mole Concentration (mmol/L) MPDA | MAP | Comp.A[1] | Resorc. | Comp.B[2] | Mole Balance |
|---|---|---|---|---|---|---|---|---|---|
| 0.0 | | | | 23.53 | 0.00 | 0.00 | 0.00 | 0.00 | 100.0% |
| 1.0 | Sample1 | 21.00 | 6.05 | 21.52 | 0.24 | 0.00 | 0.57 | 0.01 | 95.0% |
| 5.1 | Sample2 | 22.90 | 4.81 | 8.79 | 3.88 | 0.06 | 3.89 | 0.09 | 71.6% |
| 9.0 | Sample3 | 22.74 | 4.16 | 5.09 | 3.56 | 0.07 | 9.31 | 0.15 | 78.2% |
| 25.0 | Sample4 | 23.39 | 4.20 | 1.48 | 0.78 | 0.07 | 21.59 | 0.21 | 103.8% |
| Reactor Sample | | | | 1.05 | 0.63 | 0.05 | 20.61 | 0.19 | 96.8% |

**Unaccounted Weight Loss = 16.1 g**

**Table K.13 Fresh γ-ZrP400 (8.4g) at 275°C in 350ml water and 1g MPDA**

| Time (h) | Sample | Sample Weight (g) | pH | Corrected Mole Concentration (mmol/L) MPDA | MAP | Comp.A[1] | Resorc. | Comp.B[2] | Mole Balance |
|---|---|---|---|---|---|---|---|---|---|
| 0.0 | | | | 26.67 | 0.00 | 0.00 | 0.00 | 0.00 | 100.0% |
| 1.0 | Sample1 | 23.96 | 5.50 | 22.40 | 0.91 | 0.02 | 0.25 | 0.00 | 88.6% |
| 5.0 | Sample2 | 21.79 | 3.29 | 3.69 | 1.18 | 0.08 | 17.73 | 0.21 | 86.9% |
| 9.0 | Sample3 | 21.13 | 2.49 | 0.93 | 0.29 | 0.05 | 24.07 | 0.14 | 96.3% |
| 25.0 | Sample4 | 21.15 | 2.48 | 0.05 | 0.09 | 0.00 | 24.84 | 0.01 | 93.8% |

**Unaccounted Weight Loss = 5.8 g**

[1] Comp.**A** denotes 3,3'-diamino-diphenylamine
[2] Comp.**B** denotes 3-hydroxy,3'-amino-diphenylamine